FEBIP 2018

Modena (IT), 10–13 July

7TH INTERNATIONAL WORKSHOP ON FOCUSED ELECTRON BEAM INDUCED PROCESSING

BOOK OF ABSTRACTS

Organized by
CNR ISTITUTO NANOSCIENZE
MODENA (IT)

Under the patronage of
Università di Modena e
Reggio Emilia - Modena (IT)

FEBIP 2018

7TH INTERNATIONAL WORKSHOP ON
FOCUSED ELECTRON BEAM-INDUCED PROCESSING

10-13 JULY 2018

SAN GEMINIANO COMPLEX, UNIVERSITY OF MODENA AND REGGIO EMILIA
VIA S. GEMINIANO 3 – MODENA - ITALY

COMMITTEES

LOCAL ORGANIZING COMMITTEE

GIAN CARLO GAZZADI – CHAIRMAN (CNR NANO)
STEFANO FRABBONI – CO-ORGANIZER (UNIVERSITY OF MODENA E REGGIO EMILIA & CNR NANO)

SECRETARIAT

MARIA BARTOLACELLI
LUISA NERI
ANNA GRAZIA STEFANI

FEBIP SCIENTIFIC COMMITTEE

CORNELIS W. HAGEN (DELFT UNIVERSITY OF TECHNOLOGY, THE NETHERLANDS), CHAIRMAN
KLAUS EDINGER (SMT CARL ZEISS, GERMANY)
GIAN CARLO GAZZADI (CNR INSTITUTE NANOSCIENCE MODENA, ITALY)
MICHAEL HUTH (GOETHE UNIVERSITY FRANKFURT, GERMANY)
HARALD PLANK (GRAZ UNIVERSITY OF TECHNOLOGY, AUSTRIA)
PHILIP RACK (UNIVERSITY OF TENNESSEE KNOXVILLE, USA)
MASAYUKI SHIMOJO (SHIBAURA INSTITUTE OF TECHNOLOGY, JAPAN)
JOSÉ MARIA DE TERESA (ICMA ZARAGOZA, SPAIN)
MILOS TOTH (UNIVERSITY OF TECHNOLOGY SIDNEY, AUSTRALIA)
IVO UTKE (EMPA THUN, SWITZERLAND)
HEINZ WANZENBÖCK (VIENNA UNIVERSITY OF TECHNOLOGY, AUSTRIA)

INDEX

INTRODUCTION

Dear FEBIP 2018 participant,

It is a pleasure to welcome you to Modena for the **7th International Workshop on Focused Electron Beam Induced Processing**, organized by the Institute Nanoscience of National Research Council (CNR NANO), and hosted at the San Geminiano Complex, a XVth century cloister in the heart of the city, part of the University of Modena and Reggio Emilia (UNIMORE).

Following the editions in Delft (NL) – 2006, Thun (CH) – 2008, Albany (US) – 2010, Saragoza (ES) – 2012, Frankfurt (D) – 2014, and Vienna (AT) – 2016, the workshop is primarily aimed at the scientific community that employs focused electron beams for direct nanofabrication through gas-assisted deposition and etching, but also covers focused ion beam selected topics. We shall explore the latest advances and applications of the technique, along with more fundamental aspects of the process that still need to be investigated.

The last two editions of the workshop were held under CELINA Cost Action, an EU project connecting the original FEBIP community with those of gas precursor chemistry and electron-induced reactions. This has opened new perspectives and collaborations on various topics, that can be found in a number of works presented here, and that we are challenged to maintain, now that the project is over.

The scientific program of this 7th edition includes 8 invited talks and 28 contributed orals, divided into 9 sessions, and 16 poster presentations. Each session is dedicated to a specific topic. On day 1, we start with *New Gas Precursors*, followed by *Purification*, *Process Basics & Modeling* and *FEBIP Applications*. Day 2 is opened by *3D Deposition*, where we pay tribute to a pioneer of the field (Shinji Matsui), followed by *Magnetism* and *Mechanical Properties*. Finally, on day 3, we have *Nanofabrication & Characterization* and *New Materials & Methods*.

The number of scientific participants is 68 from 17 countries, and, more importantly, about half of them are students, meaning that FEBIP keeps lively and attractive, and, hopefully, with a bright future ahead. In order to ensure this, we have to pursue the long-standing goal of establishing FEBIP as a discipline of its own rather than just a mere nanofabrication tool. Therefore, you are invited to listen, discuss and share your knowledge to contribute to this aim and to spread FEBIP application even more.

The workshop is also an opportunity to visit our city, eager to show you its ancient and modern landmarks: the Cathedral, the *Ghirlandina* tower and *Piazza Grande*, Romanesque architecture masterpieces part of UNESCO world heritage, and *Enzo Ferrari* museum, a tribute to the founder of Ferrari Cars' myth. And when your appetite is calling for rich flavours, enjoy the delicacies Modena is renowned for (the 2018 world's best restaurant is here!), dressed with Balsamic vinegar and washed down with a glass of sparkling Lambrusco.

Finally, let me conclude with some due acknowledgements. I thank the five sponsor and one exhibitor companies for their essential financial support. Thanks to co-organizer Stefano Frabboni and to the FEBIP scientific committee for their help and advices in defining the scientific program, and, last but not least, a special thanks to the workshop secretariat (Luisa Neri, Maria Bartolacelli, Anna Grazia Stefani) and to the technical staff (Davide Calanca), for the everyday support in the past months, and for their assistance now at the meeting.

I wish you a fruitful and pleasant workshop,

Gian Carlo Gazzadi
Chairman

SPONSORS

EXHIBITORS

PROGRAM OVERVIEW

Tuesday 10/07/2018	
17.30 - 20.00	Welcome Reception with Refreshments at the Workshop Venue (*San Geminiano* complex)

Wednesday 11/07/2018	
8.45 - 9.00	Opening Address
Morning Session 1: New Gas Precursors	
9.00 - 9.30 **(Invited)**	**P. Swiderek**: The Diverse Facets of Chemistry Involved in E-Beam Induced Nanofabrication
9.30 - 9.50	**L. McElwee-White**: Au(I) Precursors for FEBID
9.50 - 10.10	**P. Le Gal**: Deposition of Pure and Stable Au Films
10.10 - 10.30	**K. Höflich**: Towards 3D in direct electron beam writing of silver
10.30 - 10.50	**L. Berger**: Exploring New Copper Complexes for FEBID
10.50 - 11.15	Coffee Break
Morning Session 2: Purification	
11.15 - 11.45 **(Invited)**	**J.J.L Mulders**: Review on Deposit Purification Approaches
11.45 - 12.05	**H.D. Wanzenboeck**: Impact of purity and conductivity on plasmonic Au nanostructure
12.05 - 12.25	**J. Pablo-Navarro**: Purification of 3D Co and Fe Nanowires
12.25 - 12.45	**J. Jurczyk**: FEBID and purification of Ru using halogenated compounds
12.45 - 13.45	Buffet Lunch on site
Aft. Session 1: Process Basics & Modeling	
13.45 - 14.05	**D. Sanz-Hernández**: FEBID frequency maps for design of multilayer processes
14.05 - 14.25	**C.W. Hagen**: Fast Monte Carlo Simulator of e-Matter Interaction
14.25 - 14.45	**J. Bishop**: New insights into the basic mechanisms of EBIE and EBID
14.45 - 15.05	**J. T. Hastings**: Models and Process windows for FEBIP of Cu with Liquid Reactants
15.05 - 15.30	Coffee break
Afternoon Session 2: FEBIP Applications	
15.30 - 16.00 **(Invited)**	**M. Huth**: FEBID meets Materials Science
16.00 - 16.20	**G. Di Prima**: Single Electron Transistors (SET) fabricated by FEBID
16.20 - 16.40	**J. E. Fröch**: Photonic Crystal Cavities in hexagonal Boron Nitride by EBIE
16.40 - 17.00	**C. Preischl**: Metal-Organic Frameworks as Resists for sub-10 nm EBL
17.00 - 17.45	Sponsor Presentations: RAITH GETec TESCAN
17.45 - 19.15	Poster Session I (with Refreshments)

Thursday 12/07/2018	
Morning Session 3: 3D Deposition	
9.00 - 9.30 **(Invited)**	**S. Matsui**: 3D Nanostructure Fabrication by Focused-Ion-Beam Chemical-Vapor-Deposition
9.30 - 10.00 **(Invited)**	**R. Winkler**: 3D-Nanoprinting via FEBID: from Growth Fundamentals to Applications
10.00 - 10.20	**L. Keller**: 3D Nanostructures by FEBID:Pattern Generation
10.20 - 10.40	**A. Fernández-Pacheco**: Magnetic information using FEBID 3D nanowires
10.40 - 11.00	Coffee break
Morning Session 4: Magnetism	
11.00 - 11.30 **(Invited)**	**P. Vavassori**: FEBID of magnetic nanostructures and nanoactuated magneto-mechanical systems
11.30 - 11.50	**J. M. De Teresa**: MFM probes by FEBID and their application
11.50 - 12.10	**R. Sachser**: Tuning the Hall resistivity of ferromagnetic FEBID structures
12.10 - 12.30	**M. V. Puydinger dos Santos**: magn.-electr. enhancement of ferromagnetic FEBID
12.30 - 14.00	Buffet Lunch + Poster Session II
Aft. Session 3: Mechanical Properties	
14.00 - 14.30 **(Invited)**	**J. D. Fowlkes**: Nanomechanical Characterization of 3D FEBID Nanostructures
14.30 - 14.50	**J. E. Fröch**: Mechanical Properties of 3D FEBID Nano-Architectures
14.50 - 15.10	**J. Sattelkow**: Fabrication of Electric and Thermal High-Resolution Nano-Probes
15.10 - 15.40	Sponsor Presentations: ZEISS THERMOFISHER
15.40 - 16.00	Coffee break
16.00 - 19.00	Modena Tour: UNESCO site & *Enzo Ferrari* Museum
20.30 - 22.30	Social Dinner at restaurant: *Caffè Concerto*

Friday 13/07/2018	
MS 5: Nanofabrication & Characterization	
9.00 - 9.30 **(Invited)**	**R. Cordoba**: Focused Ion Beam Induced Processing of Nanosuperconductors
9.30 - 9.50	**M. Hanefeld**: Ac response of nano-granular metals prepared via FEBID
9.50 - 10.10	**C. Trummer**: Internal Morphology of FEBID by TEM Tomography
10.10 - 10.30	**A. Mahgoub**: Novel Platinum Precursors
10.30 - 11.00	Coffee break
MS 6: New Materials & Methods	
11.00 - 11.20	**F. Porrati**: Binary Mn-Si nanostructures prepared by the SiH3Mn(CO)5 precursor
11.20 - 11.40	**F. Vollnhals**: Role of Surface and Precursor Chemistry for EBISA
11.40 - 12.00	**P. Gruszka**: Dedicated area-selective-ALD micro-reactor
12.00 - 12.20	**S.S. Choi**: Plasmonic Optical Nanopores by e- Beam Irradiations
12.20 - 13.00	Conclusions & Announcements
13.00 - 14.00	Buffet Lunch on site

Day 0: Tuesday 10/07/2018

17.30 – 20.00	**Welcome Reception with Refreshments at the Workshop Venue (*San Geminiano* complex)**

Day 1: Wednesday 11/07/2018

08.45 – 9.00	**Opening Address**
	Morning Session 1: New Gas Precursors (Chair: Kees Hagen)
9.00 – 9.30 **(Invited)**	**Petra Swiderek** (University of Bremen, Germany) *The Diverse Facets of Chemistry Involved in Electron Beam Induced Nanofabrication (p. 14)*
9.30 – 9.50	**Lisa McElwee-White** (University of Florida, USA) *Au(I) Precursors for FEBID: Volatility and Electron-Induced Reactivity (p. 16)*
9.50 – 10.10	**Pierre Le Gal** (Orsay Physics - TESCAN, France) *Deposition of Pure and Stable Au Films with Inorganic Precursor by Focused Electron Beam Induced Processing (FEBIP) (p. 18)*
10.10 – 10.30	**Katja Höflich** (Helmholtz-Zentrum Berlin, Germany) *Towards the third dimension in direct electron beam writing of silver (p. 20)*
10.30 – 10.50	**Luisa Berger** (EMPA Thun, Switzerland) *Exploring New Copper Complexes for FEBID (p. 22)*
10.50 – 11.15	**Coffee break**
	Morning Session 2: Purification (Chair: Petra Swiderek)
11.15 – 11.45 **(Invited)**	**J.J.L. (Hans) Mulders** (ThermoFisherScientific, The Netherlands) *Review on Deposit Purification Approaches (p. 24)*
11.45 – 12.05	**Heinz D. Wanzenboeck** (TU Wien, Austria) *Impact of purity and conductivity on plasmonic response of FEBID gold nanostructures (p. 26)*
12.05 – 12.25	**Javier Pablo-Navarro** (LMA – INA, Zaragoza, Spain) *Purification and crystallization of 3D Co and Fe Nanowires Grown by Focused Electron Beam Induced Deposition (p. 28)*
12.25 – 12.45	**Jakub Jurczyk** (EMPA Thun, Switzerland) *Focused Electron Beam Induced Deposition and purification of Ru using halogenated organometallic compounds (p. 30)*
12.45 – 13.45	**Buffet Lunch on site**
	Afternoon Session 1: Process Basics & Modeling (Chair: Ivo Utke)
13.45 – 14.05	**Dédalo Sanz-Hernández** (University of Cambridge, UK) *FEBID frequency maps: a new tool for interpretation and design of experiments in FEBID Langmuir and multilayer processes (p. 32)*
14.05 – 14.25	**C.W. (Kees) Hagen** (UT Delft, The Netherlands) *Fast Monte Carlo Simulator of Electron Matter Interaction (p. 34)*
14.25 – 14.45	**James Bishop** (UT Sydney, Australia) *New insights into the basic mechanisms of electron beam induced etching and deposition (p. 36)*
14.45 – 15.05	**J. Todd Hastings** (University of Kentucky, USA) *Predictive Models and Process Windows for FEBIP of Copper with Liquid Reactants (p. 38)*

15.05 – 15.30	**Coffee break**
	Afternoon Session 2: FEBIP Applications (Chair: Heinz Wanzenboeck)
15.30 – 16.00 **(Invited)**	**Michael Huth** (University of Frankfurt, Germany) *FEBID meets Materials Science (p. 40)*
16.00 – 16.20	**Giorgia Di Prima** (University of Frankfurt, Germany) *Single Electron Transistors (SET) fabricated by Focused Electron Beam Induced Deposition (FEBID) (p. 42)*
16.20 – 16.40	**Johannes E. Fröch** (UT Sydney, Australia) *Fabrication and Tuning of Photonic Crystal Cavities in Hexagonal Boron Nitride by Electron Beam Induced Etching (p. 44)*
16.40 – 17.00	**Christian Preischl** (University of Erlangen-Nürnberg, Germany) *Surface-Anchored Metal-Organic Frameworks as Versatile Resists for E-Beam Lithography: Fabrication of sub-10 nm Structures (p. 46)*
	Sponsor Presentations
17.00 – 17.45	**RAITH** **(p. 114)**
	GETec **(p. 115)**
	TESCAN **(p. 117)**
17.45 – 19.15	**POSTER SESSION I** **(with Refreshments)**

Day 2: Thursday 12/07/2018

	Morning Session 3: 3D Deposition (Chair: Harald Plank)
9.00 – 9.30 **(Invited)**	**Shinji Matsui** (University of Hyogo, Japan) *Three-Dimensional Nanostructure Fabrication by Focused-Ion-Beam Chemical-Vapor-Deposition (p. 48)*
9.30 – 10.00 **(Invited)**	**Robert Winkler** (UT Graz, Austria) *3D-Nanoprinting via FEBID – from Growth Fundamentals to Applications (p. 50)*
10.00 – 10.20	**Lukas Keller** (University of Frankfurt, Germany) *Direct Printing of 3D Nano-Structures via Focused Electron Beam Induced Deposition: Pattern Generation (p. 52)*
10.20 – 10.40	**Amalio Fernández-Pacheco** (University of Cambridge, UK) *Three-dimensional injection and motion of magnetic information using FEBID 3D nanowires (p. 54)*
10.40 – 11.00	**Coffee break**
	Morning Session 4: Magnetism (Chair: Michael Huth)
11.00 – 11.30 **(Invited)**	**Paolo Vavassori** (nanoGUNE, San Sebastian, Spain) *FEBID fabrication of individual magnetic nanostructures and nanoactu-ated-magneto-mechanical systems (p. 56)*
11.30 – 11.50	**José Marìa De Teresa** (LMA – INA, Zaragoza, Spain) *Magnetic Force Microscopy (MFM) probes by FEBID and their application (p. 58)*
11.50 – 12.10	**Roland Sachser** (University of Frankfurt, Germany) *Tuning and in-situ monitoring the Hall resistivity of ferromagnetic FEBID structures (p. 60)*
12.10 – 12.30	**Marcos V. Puydinger dos Santos** (University of Campinas, Brazil) *Towards a simple and fast protocol for magneto-electrical properties enhancement of non-noble ferromagnetic nanocomposites grown by focused-electron-beam-induced deposition (p. 62)*
12.30 – 14.00	**Buffet Lunch & POSTER SESSION II**
	Afternoon Session 3: Mechanical Properties (Chair: Josè Maria De Teresa)
14.00 – 14.30 **(Invited)**	**Jason D. Fowlkes** (CNMS - Oak Ridge National Laboratory, USA) *Nanomechanical Characterization of 3D FEBID Nanostructures (p. 64)*
14.30 – 14.50	**Johannes E. Fröch** (UT Sydney, Australia) *Mechanical Properties of 3D Nano-Architectures Fabricated via Focused Electron Beam Induced Deposition (p. 66)*
14.50 – 15.10	**Jürgen Sattelkow** (UT Graz, Austria) *Direct-Write Fabrication of Electric and Thermal High-Resolution Nano-Probes on Self-Sensing AFM Cantilever (p. 68)*
	Sponsor Presentations
15.10 – 15.40	**ZEISS (p.118)**
	THERMOFISHER (p. 119)
15.40 – 16.00	**Coffee break**
16.00 – 19.00	**Modena Tour: UNESCO site & *Enzo Ferrari* Museum**
20.30 – 22.30	**Social Dinner at restaurant *Caffè Concerto***

Day 3: Friday 13/07/2018

	Morning Session 5: Nanofabrication & Characterization (Chair: Stefano Frabboni)
9.00 – 9.30 **(Invited)**	**Rosa Córdoba** (UAM - Madrid & ICMA - Zaragoza, Spain) *Focused Ion Beam Induced Processing of Nanosuperconductors (p. 70)*
9.30 – 9.50	**Marc Hanefeld** (University of Frankfurt, Germany) *Ac response of nano-granular metals prepared via FEBID (p. 72)*
9.50 – 10.10	**Cornelia Trummer** (Graz Centre for Electron Microscopy, Austria) *Accessing the Internal Morphology of Nano-Granular FEBID Materials in 3D Space by Electron Tomography (p. 74)*
10.10 – 10.30	**Aya Mahgoub** (UT Delft, The Netherlands) *Electron Beam Induced Deposition Using Novel Platinum Precursors: $PtC_{l2}(CO)_2$ and $PtB_{r2}(CO)_2$ (p. 76)*
10.30 – 11.00	**Coffee break**
	Morning Session 6: New Materials & Methods (Chair: Gian Carlo Gazzadi)
11.00 - 11.20	**Fabrizio Porrati** (University of Frankfurt, Germany) *Binary Mn-Si nanostructures prepared by the $SiH_3Mn(CO)_5$ precursor (p. 78)*
11.20 - 11.40	**Florian Vollnhals** (University of Erlangen-Nürnberg, Germany) *On the Role of Surface and Precursor Chemistry for Electron Beam Induced Surface Activation (EBISA) (p. 80)*
11.40 - 12.00	**Peter Gruszka** (University of Frankfurt, Germany) *Dedicated area-selective-ALD micro-reactor (p. 82)*
12.00 - 12.20	**Seong Soo Choi** (SunMoon University, South Korea) *Towards the Plasmonic Optical Nanopores for Single Molecule Analysis by Using Electron Beam Irradiations (p. 84)*
12.20 – 13.00	**Conclusions & Announcements**
13.00 – 14.00	**Buffet Lunch on site**

ORAL PRESENTATIONS

The Diverse Facets of Chemistry Involved in Electron Beam Induced Nanofabrication

K. Ahlenhoff, M. Rohdenburg, and P. Swiderek*

University of Bremen, Fachbereich 2 (Chemie/Biologie), Institute of Applied and Physical Chemistry, Leobener Straße 5, PO Box 330440, 28334 Bremen, Germany

* Corresponding author: swiderek@uni-bremen.de

During the last few years, an amazing precision has been achieved in the fabrication of extremely small and complex nanostructures by focused electron beam induced deposition (FEBID). For instance, complex freestanding 3D nanoscale architectures can now be constructed by simulation-guided 3D FEBID [1]. Also, proximity effects can efficiently be suppressed by FEBID on thin molecular adsorbate layers which, in turn, can also be activated by the electron beam to serve as template for autocatalytic growth of pure metallic deposits [2]. Finally, purification protocols have emerged that convert a highly contaminated deposit into pure metal [3] or even prevent the integration of carbon in the deposit [4] and that are, at the same time, capable of preserving the shape of complex 3D structures [1].

However, despite this major progress in nanofabrication by FEBID, much remains to be resolved regarding the underlying chemical processes. In fact, a multitude of different aspects is involved in this chemistry (Fig. 1). This starts with the synthesis of novel precursors and their electron-induced dissociation. Thermal and catalytic surface reactions may assist in the removal of ligands or produce unwanted material that will remain embedded in the deposit. Another level of complexity is added when process gases are applied in purification protocols. Also, molecular adsorbate layers used to control the electron-induced surface chemistry are themselves modified by electron irradiation to produce species that will contribute to the precursor surface chemistry. Understanding and controlling each of these different chemistries poses significant challenges but is the key to ultimate deposit purity, spatial resolution, and deposition speed in FEBID.

Surface science experiments using a combination of different analytical tools can monitor the outcome of the different types of chemical processes involved in FEBID. This contribution gives an overview of such research carried out in our group. The studies focus on the effect of low-energy electrons representative of the numerous secondary electrons released when a high energy electron beam impinges on a dense material. In particular, we apply experiments on electron-stimulated desorption (ESD), isothermal desorption of volatile products upon dosing of process gases, and subsequent thermal desorption spectrometry (TDS). Using these experiments (Fig. 2), in combination with other surface science tools, we obtain insight regarding processes such as deposit purification [5] and electron beam induced surface activation of layer-by-layer grown metal organic materials [6,7]. Furthermore, we investigate electron-induced reactions leading to formation of larger and less volatile species [8,9] that potentially contribute to retention of contaminations in deposits formed by FEBID.

References

[1] R. Winkler, F.-P. Schmidt, U. Haselmann, J.D. Fowlkes, B.B. Lewis, G. Kothleitner, P.D. Rack, H. Plank, *Direct-Write 3D Nanoprinting of Plasmonic Structures*, ACS Appl. Mater. Interfaces 9, 8233 (2017).

[2] M. Drost, F. Tu, F. Vollnhals, I. Szenti, J. Kiss, H. Marbach, *On the Principles of Tweaking Nanostructure Fabrication via Focused Electron Beam Induced Processing Combined with Catalytic Growth Processes*, Small Methods 1, 1700095 (2017).

[3] B. Geier et al., *Rapid and highly compact purification for focused electron beam induced deposits: A low temperature approach using electron stimulated H_2O reactions,* J. Phys. Chem. C 118, 14009 (2014).

[4] M.M. Shawrav et al., *Highly conductive and pure gold nanostructures grown by electron beam induced deposition*, Scientific Reports 6, 34003 (2016).

[5] Z. Warneke, M. Rohdenburg, J. Warneke, J. Kopyra, P. Swiderek, *Electron-driven and thermal chemistry during water-assisted purification of platinum nanomaterials generated by electron beam induced deposition*, Beilstein J. Nanotechnol. 9, 77 (2018).

[6] K. Rückriem et al., *Efficient electron-induced removal of oxalate ions and formation of copper nanoparticles from copper(II) oxalate precursor layers*, Beilstein J. Nanotechnol. 7, 852 (2016).

[7] K. Ahlenhoff, C. Preischl, P. Swiderek, H. Marbach, *Electron beam induced surface activation of metal organic frameworks: Unravelling the underlying chemistry*, in preparation.

[8] J. Warneke, W.F. Van Dorp, P. Rudolf, M. Stano, P. Papp, S. Matejcik, T. Borrmann, P. Swiderek, *Acetone and the precursor ligand acetylacetone: Distinctly different electron beam induced decomposition?,* Phys. Chem. Chem. Phys. 17, 1204 (2015).

[9] E. Böhler, J. Warneke, P. Swiderek, *Control of chemical reactions and synthesis by low-energy electrons*, Chem. Soc. Rev. 42, 9219 (2013).

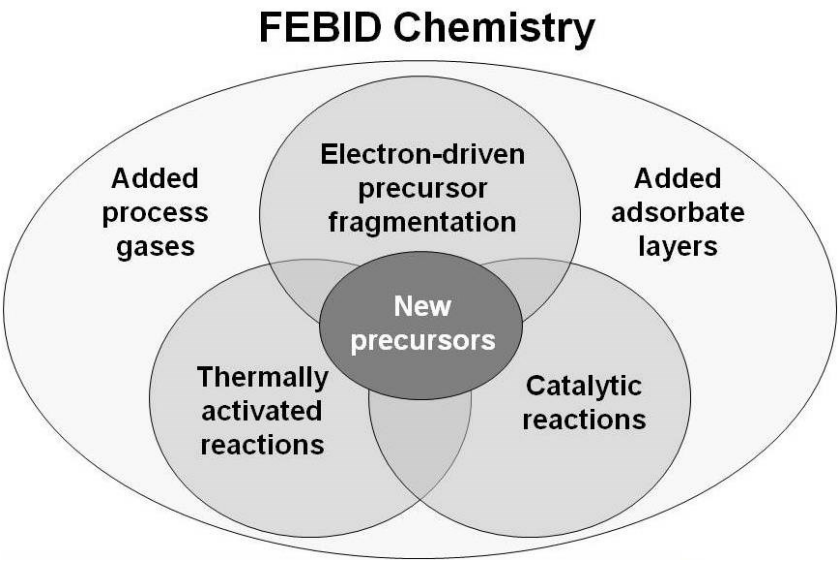

Fig. 1: The diverse aspects of chemistry involved in FEBID processes.

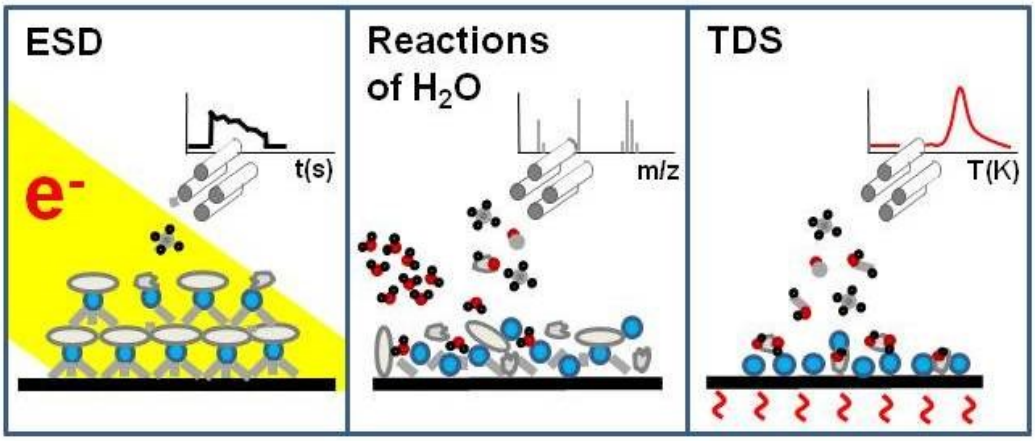

Fig. 2: Mass spectrometric desorption experiments used to obtain insight in the chemical reactions involved in FEBID: Electron-stimulated desorption (ESD) (left), isothermal desorption of volatile products upon dosing of a process gas (middle), and thermal desorption spectrometry (TDS).

Au(I) Precursors for FEBID: Volatility and Electron-Induced Reactivity

W. G. Carden[1], I. Unlu[2], R.M. Thorman[2], J. Pedziwiatr[1], D.H. Fairbrother[2], and L. McElwee-White[1]*

[1] Department of Chemistry, University of Florida, Gainesville, Florida 32611-7200, USA
[2] Department of Chemistry, Johns Hopkins University, Baltimore, Maryland 21218-2685, USA

* Corresponding author: lmwhite@chem.ufl.edu

Gold precursors for FEBID have been of recent interest due to potential applications of nanoscale deposits. Nanostructures of Au have been shown to exhibit high DC conductivity and low ohmic losses, making them an ideal material for plasmonic applications. The ability of FEBID to fabricate nanostructures with 3D control makes gold precursors of interest to enable production of plasmonic structures. We have used gold complexes as a platform to explore ligand effects on precursor volatility and as part of our efforts to identify privileged ligands for the mechanism-based design of FEBID precursors [1].

Volatility studies are motivated by the need to deliver gas phase precursor to the substrate for FEBID. Trends in volatility with changes in the halide ligand were established for gold(I) complexes of the type X-Au-L [X = Cl, Br, I; L = CN^tBu, CNMe, PMe_3, $P(NMe_2)_3$, $P(OCH_2CF_3)_3$] by determining the temperatures for onset of sublimation (T_{sub}) at a fixed pressure [2]. Within each series of isocyanide complexes, T_{sub} decreases with increasing atomic radius of the halide, making the iodide complex the most volatile. For the phosphine and phosphoramidate complexes, the chloride and bromide have similar T_{sub} values with the bromide slightly higher but the iodide complex is again the most volatile of the three. The trends in volatility can be correlated to variation in Au-Au bond distances and aggregation patterns in the solid state structures (Figure 1). For the $P(OCH_2CF_3)_3$ complexes, melting occurred before sublimation, but the iodide complex was still more volatile than the bromide. These trends have implications for the use of these complexes in FEBID, for which precursor volatility is important.

Following initial attempts to create deposits from X-Au-L compounds that were unsuccessful due to insufficient volatility or competitive decomposition, the trifluoromethyl complexes CF_3-Au-CN^tBu and CF_3-Au-CNMe were synthesized (Figure 2). Fluorination of ligands has previously been demonstrated to increase precursor volatility due to the repulsive interactions between the fluorine lone pairs [3]. The isocyanide ligands were chosen because they are isoelectronic with CO, a ligand that has been demonstrated to be labile under FEBID conditions [1]. Gold isocyanide complexes are, however, significantly more thermally robust than gold carbonyl complexes and both CF_3-Au-CN^tBu and CF_3-Au-CNMe can be sublimed without decomposition. Au-containing deposits formed in an Auger spectrometer from both CF_3-Au-CN^tBu and CF_3-Au-CNMe exhibited chemical compositions indicating that all of the carbon and nitrogen atoms but none of the fluorine atoms were retained. The Au-content in deposits created from CF_3-Au-CNMe is comparable to the value obtained when the widely used Au-precursor $Me_2Au(acac)$ was used to create deposits under the same deposition conditions. UHV-surface science studies reveal that electron stimulated decomposition of CF_3-Au-CNMe leads to the reduction of the Au(I) species to a state close to metallic Au(0) but in the absence of any intact ligand desorption, consistent with the observation from deposition experiments that all of the carbon and nitrogen atoms were retained in the deposits. Fluorine was continually lost from the films as a result of electron stimulated C-F bond cleavage. Thus, although isocyanide ligands are isoelectronic with CO they do not appear to exhibit the same lability shown by CO ligands towards desorption in FEBID.

References

[1] W.G. Carden, H. Lu, J.A. Spencer, D.H. Fairbrother, L. McElwee-White, *Mechanism-Based Design of Precursors for Focused Electron Beam Induced Deposition*, MRS Communications, accepted for publication (2018).

[2] W.G. Carden et al., *Halide Effects on the Sublimation Temperature of X–Au–L Complexes: Implications for Their Use as Precursors in Vapor Phase Deposition Methods*, ACS Appl. Mater. Interfaces 9, 40998-41005 (2017).

[3] R.O. Bonsu et al., *Partially fluorinated oxo-alkoxide tungsten(VI) complexes as precursors for deposition of WO_x nanomaterials*, Dalton Trans. 43, 9226-9233 (2014).

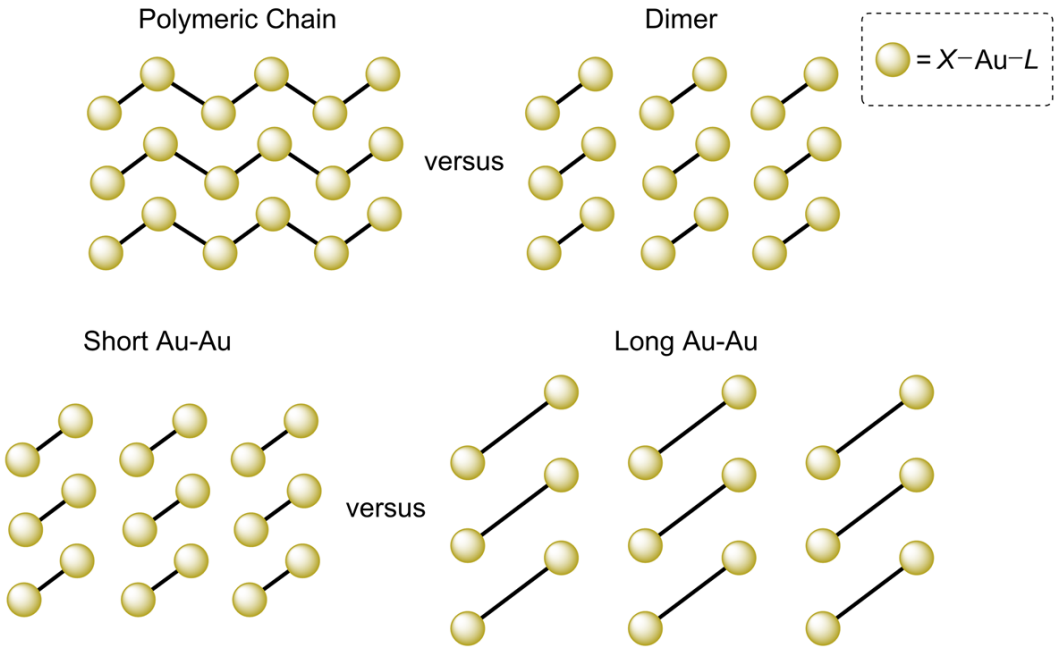

Fig. 1: Relationship between X-Au-L volatility and the nature of aurophilic bonding.

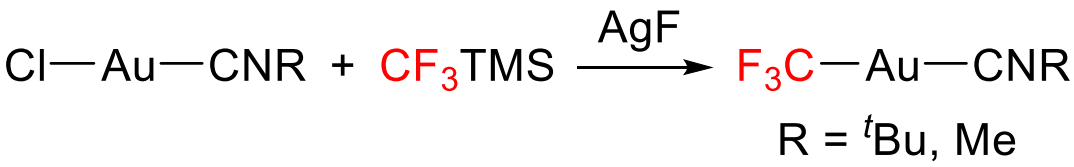

Fig. 2: Synthesis of CF_3AuCNR complexes.

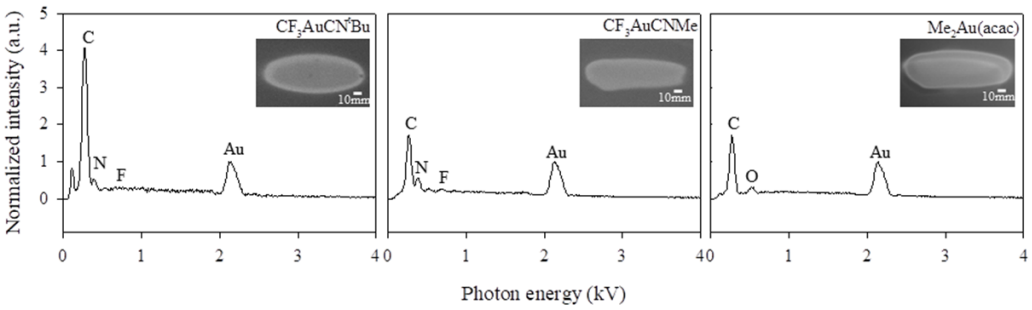

Fig. 3: EDS of deposits made in an Auger spectrometer.

Deposition of Pure and Stable Au Films with Inorganic Precursor by Focused Electron Beam Induced Processing (FEBIP)

P. Le Gal[1]*, D. Markó[2], G. Goupil[1], J. Jiruše[2], M. Kocman[2], and A. Delobbe[1]

[1] Orsay Physics, TESCAN Orsay,95 Avenue des Monts Auréliens – ZA Saint-Charles 13710 Fuveau, France
[2] TESCAN Brno, Libušina tř. 1, 623 00 Brno, Czech Republic

* Corresponding author: pierre.LEGAL@orsayphysics.com

Direct nanofabrication of gold structures using FEBIP process with TESCAN scanning electron microscope **LYRA** and Orsay Physics gas injection system **OptiGIS** was performed. Gold deposition is constantly growing in demand for catalytic and sensor applications. Gold metallization in microelectronic devices is also very interesting due to its high controlled conductivity and its corrosion stability versus oxidation. Purity and stability of the deposition are critical to ensure reliability of the parameters of the as-deposited pattern.

Most of gold precursors commonly used are organometallic compounds [1] to reach a suitable volatility of gold in a reasonable range of temperatures and to stabilize the molecule to the gold intrinsic autocatalytic behavior versus ligands. The main drawback of such molecules is that the more the ligands are carbonated, the more contamination of the deposition. Many suggestions for gold precursors were made [2-5], however, up to now, studies reported gold-based precursors to have a poor short-term stability. Fast decomposition of precursors occurred in a few days or weeks preventing it from a practical use.

In this study, an overview of the results achieved with TESCAN ORSAY **AmazeGold™** precursor (purity, resistivity measurements (Figure 1)) will be introduced. Selected structures, electron beam parameters as well as gas temperature will be shown. An example of deposition patterns is given in Figure 2 using 5 keV electron beam energy, 1000 pA primary beam current, exposure time 100s (top), 300s (middle) and 600s (bottom), dwell time 100 ns, dimensions 25x1 µm and zig-zag scanning strategy to analyze the impact of the beam on the deposition. Parameter as well as instrumentation optimization were carried out. Purity measurements realized over a period of 8 months with the same reservoir and precursor filling have shown a purity of ~ 97% without any alteration in time. This promises a stable precursor for practical purposes.

References

[1] I. Utke, P. Hoffmann, J. Melngailis, *Gas-assisted focused electron beam and ion beam processing and fabrication*, J. Vac. Sci. Technol. B, 26(4), 1197 (2008).

[2] M.M. Shawrav et al., *Highly conductive and pure gold nanostructures grown by electron beam induced deposition*, Nature scientific reports 6, 34003 (2016).

[3] K. Höflich, R.B. Yang, A. Berger, G. Leuchs, S. Christiansen, *The direct writing of plasmonic gold nanostructures by electronbeam-induced deposition,* Advanced Materials 23, 2657–2661 (2011).

[4] K. Höflich, M. Becker, G. Leuchs, S. Christiansen, *Plasmonic dimer antennas for surface enhanced Raman scattering*, Nanotechnology 23 (2012).

[5] W.G. Carden et al., *Effects on the Sublimation Temperature of X–Au–L Complexes: Implications for Their Use as Precursors in Vapor Phase Deposition Methods*, ACS Appl. Mater. Interfaces, 9(46), 40998-41005 (2017).

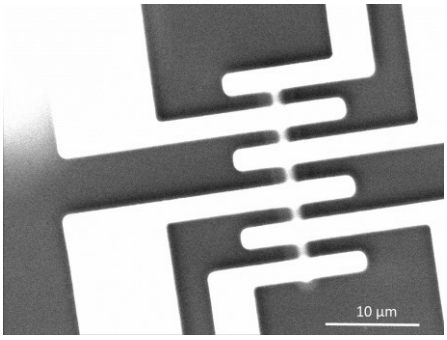

Fig. 1: Image of the pre-pattern substrate used for electrical measurement of the deposition.

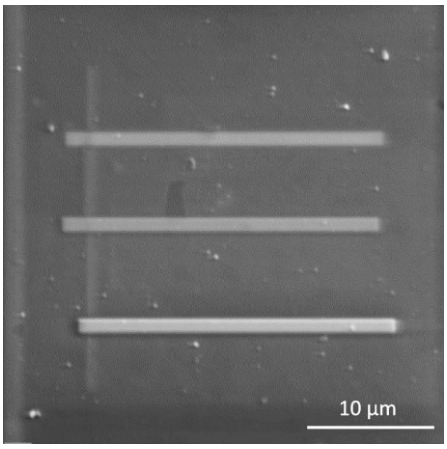

Fig. 2: SEM image of gold deposits by FEBID.

Towards the third dimension in direct electron beam writing of silver

K. Höflich[1,2]*, J.M. Jurczyk[2,3], K. Madajska[4], M. Götz[1], L. Berger[2],
C. Guerra-Nunez[2], C. Haverkamp[1], I. Szymanska[4], and I. Utke[2]

[1] Nanoscale Structures and Microscopic Analysis, Helmholtz-Zentrum Berlin für Materialien und Energie, Hahn-Meitner-Platz 1, 14109 Berlin, Germany
[2] Laboratory for Mechanics of Materials and Nanostructures, Empa - Swiss Federal Laboratories for Materials Science and Technology, Feuerwerkerstrasse 39, 3602 Thun, Switzerland
[3] Faculty of Physics and Applied Computer Sciences, AGH University of Science and Technology, 30-059 Kraków, Poland
[4] Faculty of Chemistry, Nicolaus Copernicus University in Toruń, Gagarina 7, 87-100 Toruń, Poland

* Corresponding author: katja.hoeflichl@helmholtz-berlin.de

Direct writing utilizing a focused electron beam constitutes an interesting alternative to resist-based techniques, as it allows for precise and flexible growth onto any conductive substrate in a single-step process. One important challenge, however, is the identification of appropriate precursors which allow for deposition of the material of choice, e.g., for envisaged applications in nano-optics. In this regard the coinage metal silver is of particular interest since it shows a relatively high plasma frequency and, thus, excellent plasmonic properties in the visible range.

However, the coinage metal silver comes with some technical issues. It tends to react to silver sulfide under ambient conditions and hence requires an encapsulation within the final device. Furthermore, the electron beam induced deposition of silver is challenging. Many potential precursor candidates have to be heated above 100 °C and show extremely low vapor pressures. This is related to the main oxidation state of +1 for silver, which severely limits the possibility to attach appropriate ligands. Even more importantly, the ligands tend to be only weakly bonded and, thus, easily exchange the metal atom. These properties exclude the gas-phase FEBID of silver for conventional gas-injection systems (GIS) that are flanged at the outer chamber walls.

Recently, the first gas-phase silver FEBID could be realized with a fully integrated GIS[1]. The used compound silver 2,2-dimethylbutyrate $[Ag(\mu\text{-}O_2CC(CH_3)_2CH_2CH_3)]_2$ (AgO_2Me_2Bu) is extremely sensitive to electron beam impact. Figure 1 shows an example of deposition and characterization using AgO_2Me_2Bu. Deposition suffers from the low vapor pressure of the precursor compound and a low vertical growth rate. Consequently, no growth of silver nano-structures could be achieved. To address these issues AgO_2Me_2Bu was compared to another carboxylate compound. Silver pentafluoropropionate $[Ag(\mu\text{-}O_2CC_2F_5)]_2$ (AgO_2F_5Prop) provides for a similar evaporation temperature and electron-beam sensitivity but also for slightly higher gas flux and stability leading to deposits of high silver contents [2]. This makes it ideally suited for a comparative study elucidating the deposition behavior of such carboxylate compounds. Depositions varying beam and current and dwell times were investigated concerning their morphology and composition. As depicted in Figure 2, AgO_2Me_2Bu showed a strong depletion in the center of the impinging electron beam profile hindering any vertical growth. In contrast, AgO_2F_5Prop indicated a pronounced dependency of the deposit height on the dwell time. Finally, FEBID of truly three-dimensional silver structures could be realized for the first time under use of AgO_2F_5Prop [3]. The resulting pillars are shown in Figure 3 and exhibit large silver contents of more than 50 atom %.

While the volume growth rate for the fabricated pillars shows reasonable values of around 1 μm^3/hour, achievable lateral dimensions and shape control require significant improvement. One reason may be the complex local precursor dynamics, like an enhanced desorption due to the elevated stage temperature. A further issue is the limitation of the used tungsten cathode in terms of electron beam spot size and local electron density. Hence, the experiment is currently transferred to a field emitter electron microscope. Recent results will be presented.

References

[1] K. Höflich et al., *Direct Electron Beam Writing of Silver-based Nanostructures*, ACS Appl. Mater. Interface 9, 24071–24077 (2017).

[2] L. Berger et al., *Gas-assisted silver deposition with a focused electron beam*, Beilstein J. Nanotechnol. 9, 224–232 (2018).

[3] K. Höflich et al., *Towards the third dimension in direct electron beam writing of silver*, Beilstein J. Nanotechnol. 9, 842–849 (2018).

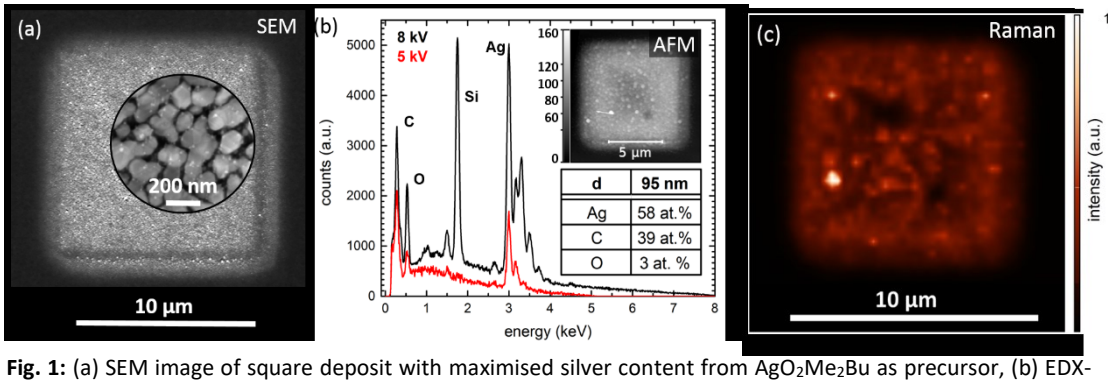

Fig. 1: (a) SEM image of square deposit with maximised silver content from AgO_2Me_2Bu as precursor, (b) EDX-spectra together with thin-film corrected quantification, (c) Raman mapping of the G band of the carbonaceous matrix showing a pronounced signal enhancement due to the embedded silver crystals [P4].

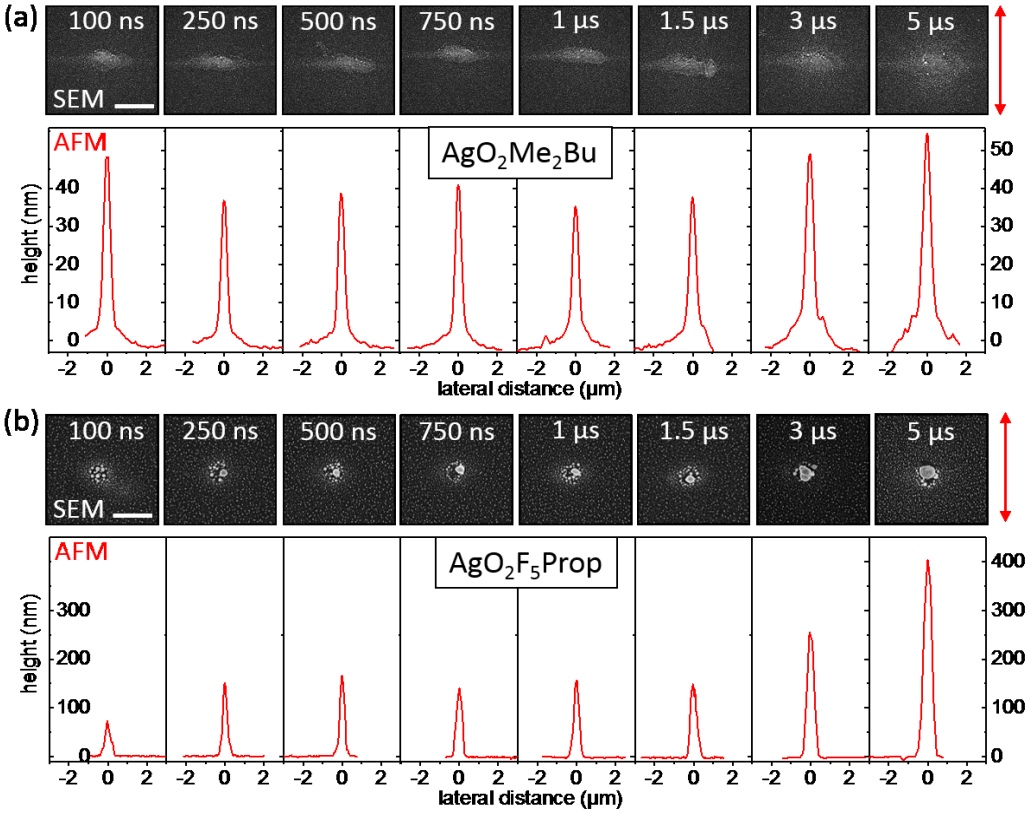

Fig. 2: Dwell time series for a beam current of 150 pA using (a) AgO_2Me_2Bu and (b) AgO_2F_5Prop as precursor compounds. The upper rows of (a) and (b) show scanning electron micrographs of the spot deposits, with the red arrow indicating the direction of taking AFM profiles. Below the SEM images averaged height profiles are displayed. While there is no distinct correlation between dwell time and deposit height for AgO_2Me_2Bu, the deposit height significantly increases for AgO_2F_5Prop.

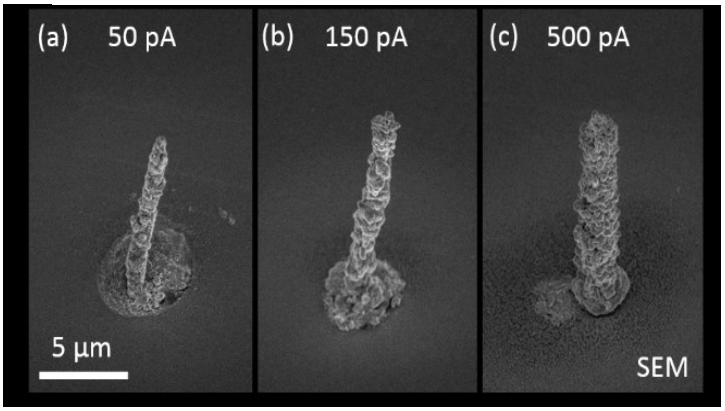

Fig. 3: Scanning electron micrographs of single silver pillars obtained after continuous spot irradiation for (a) 50 pA, (b) 150 pA, and (c) 500 pA beam current using AgO_2F_5Prop as precursor compound.

Exploring New Copper Complexes for FEBID

L. Berger[1], K. Madajska[2], N. Boysen[3], I. Szymànska[2], A. Devi[3], K. Höflich[4], P. Hoffmann[1], and I. Utke[1]*

[1] Empa - Swiss Federal Laboratories for Materials Science and Technology, Feuerwerkerstrasse 39, 3602 Thun, Switzerland
[2] Department of Chemistry, Nicolaus Copernicus University, Gagarina 7, 87100 Toruń, Poland
[3] Inorganic Materials Chemistry, Ruhr-University Bochum, 44801 Bochum, Germany
[4] Nanoscale Structures and Microscopic Analysis, Helmholtz-Zentrum Berlin für Materialien und Energie, Hahn-Meitner-Platz 1, 14109 Berlin, Germany

* Corresponding author: ivo.utke@empa.ch

The deposition of pure copper via FEBID has not been achieved so far and metal contents typically reached 13-25 at.% [1]. By exploring novel copper precursor classes namely, the fluorinated copper carboxylates $[Cu_2(\mu\text{-}O_2CC_2F_5)_4]$ (Fig. 1a) and $[Cu_2(EtNH_2)_2(\mu\text{-}O_2CC_2F_5)_4]$ (Fig. 1b) and the fluorine-free β-diketonate $Cu(tbaoac)_2$ we intend to achieve the deposition of high purity structures.

The latter was employed in FEBID recently [2] while the carboxylates were reported as CVD precursors [3]. The influence of varying deposition parameters on appearance and composition was investigated. First interesting results lead to copper contents of 25 at.%.

The Cu pentafluoro carboxylate (Fig. 1a) is compared to previous results achieved with the silver analogue complex $Ag(\mu\text{-}O_2CC_2F_5)$ (Fig. 1c) [4]. We found granular deposits with increasing metal contents at areas with lower electron densities. Deposition up to the outmost areas of the theoretical exit ranges of backscattered electrons (BSE) [5] indicates high sensitivity of the precursor towards electron induced dissociation (Fig. 2a). Despite structural similarities, the aminated carboxylate does not show such a pronounced sensitivity (Fig. 2 b).

In respect to those preliminary results, we will present the influence of varying deposition parameters on the chemical deposit composition.

References

[1] A. Luisier et al., *Comparative study of Cu-precursors for 3D focused electron beam induced deposition*, J. Electrochem. Soc. 151, C535 (2004).

[2] C. Haverkamp, K. Höflich et al., *A novel copper precursor for electron beam induced deposition,* Beilstein J. Nanotechnol. 9, 1220 (2018).

[3] P. Piszczek and I.B. Szymańska, *Deposition of Thin Copper Layers using Copper (II) Carboxylate Complexes with tert-Butylamine as New CVD Precursors*, Chem. Vap. Deposition 19, 251 (2013).

[4] L. Berger et al., *Gas-assisted silver deposition with a focused electron beam*, Beilstein J. Nanotechnol. 9, 224 (2018).

[5] K. Kanaya and S. Okayama, *Penetration and energy-loss theory of electrons in solid targets*, J. Phys. D: Appl. Phys. 5, 43 (1972).

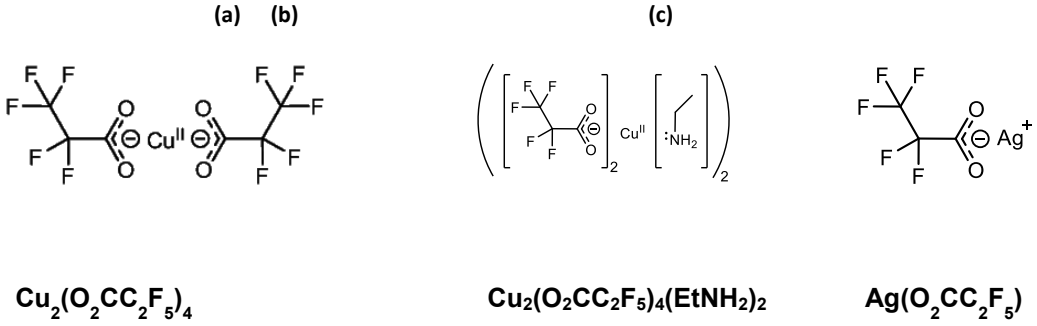

Fig. 1: Structural formula, sum formula and metal-carbon ratio in the molecule of **(a)** the Cu pentafluoro carboxylate, **(b)** the aminated carboxylate and **(c)** the silver analogue of (a). Interestingly, (a) and (b) exhibit similar behavior upon deposition.

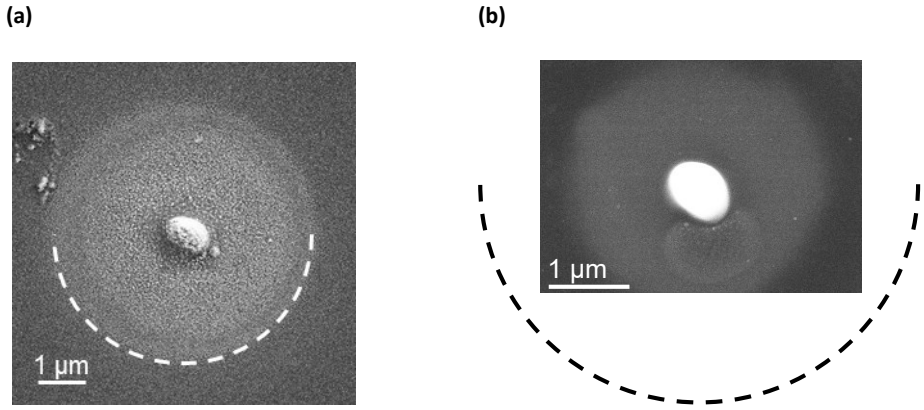

Fig. 2: Spot exposure deposition of **(a)** the pentafluoro carboxylate and **(b)** the aminated carboxylate precursor. The dashed lines indicate the maximum exit ranges for BSE emitted from bulk Si from a 20 keV primary beam. The ranges were calculated according to Kanaya and Okayama [5]. Despite their structural similarities, deposition does not occur with the same sensitivity.

Review on Deposit Purification Approaches

J.J.L. Mulders* and P.H.F. Trompenaars

ThermoFisherScientific, Achtseweg Noord 5, 5651 GG Eindhoven, The Netherlands

* Corresponding author: hans.mulders@thermofisher.com

Precursors that are commonly applied for FEBID can be found in the chemical catalogue for CVD and ALD precursors and a large group is related to the so called organo-metallic precursors, where the metal of interest is present as an atom in a larger organic molecular cluster such as acetonate, allyl, acetyl-acetonate, Cp-ring or CO groups. Ideally the deposition process splits the molecule in a desired non-volatile part (the deposition) and a volatile part (those molecules that are pumped away). Precursors that have this inherent capability can be called pyrolytic precursors and the general reaction mechanism is:

General reaction: $AX(g) + \text{thermal energy} \rightarrow A(s) + X(g)$;

EBID example $Co_2(CO)_8 + e^- \rightarrow 2Co + 8\,CO + e^-$

Examples of FEBID precursors that have this property are $Co_2(CO)_8$, $Fe(CO)_5$, $Fe_2(CO)_9$, $Fe_3(CO)_{12}$, $W(CO)_6$ where the volatile part is formed by the CO molecule. In addition there are precursors that have volatile non-organic ligand groups such as $Pt(PF_3)_4$, $AuCl(PF_3)$ and WF_6. A precursor with both a carbonyl and a halogen groups is Au(CO)Cl. If a precursor has a halogen group, then this is released during deposition and as a consequence the process can induce an unwanted etching behavior towards the sample surface. The group of pyrolytic precursors with CO ligands indeed has shown the ideal split behavior in FEBID reactions, although in many cases there still is a small contamination part with either C and/or O that induces impurity in the deposition. As an example the Co content in decomposition of $Co_2(CO)_8$ can easily be > 90 at% (Fig 1), while $W(CO)_6$ has a maximum of around 55 at% W, even with the process at elevated temperature to facilitate the release of the ligands (Fig 2), see also [1]. This group of precursors has been examined extensively by many researchers optimizing deposition parameters as beam energy, beam current, patterning strategy and local gas flux. The Au(CO)Cl precursor has directly produced a high purity gold deposition, but unfortunately the life-time of the precursor is too low (Fig 3).

Another class of precursors cannot directly split into pure metal and volatile parts, but they require an additional molecule for reduction or oxidation reaction. Examples of these very stable precursors are: $MePtCpMe_3$, Auacac, $Au(tfac)_2$, Pd(hfac)2, CpPd(allyl). These precursors can produce volatile components from the release of ligand groups, but the non-volatile part is a mix of metal and residual molecule. As a consequence, the deposition has low purity. The classical example is the Pt deposition using $MePtCpMe_3$, where the Pt content is roughly 16 at%, corresponding to a ratio 1:5 of Pt and C. For this group of precursors a third particle in the chemical reaction may help to promote the formation of volatile species during the deposition. These particles can for example be O_2 [2,3], H_2 or H_2O [4] to assist the removal of carbon during the deposition (for example by formation of CO or CO_2)

General reaction: $2AX(g) + H_2\,(g) \rightarrow 2A(s) + 2HX(g)$;

EBID example $Si\,(C_2H_5O)_4 + 2\,H_2O + e^- \rightarrow SiO_2 + 4\,(C_2H_5OH) + e^-$

Generally, H_2 is not favorable because of its flammability, very short sample surface residence time and poor pumping behavior in the microscope. In all cases, the particle reactions have to balance the local reaction speeds and generally the flux of additional particles must be much higher than the precursor flux. Post irradiation in the presence of the additional particle is one way to achieve cleaning (purification) of the deposition but a simultaneous supply of both precursor and, for example, O_2 can also be applied. Simultaneous supply can be arranged by a dedicated nozzle (Fig 5) making it a one step process as all regular FEBID. The precursors that require a third particle have been examined by various groups, for example at TFS (ex-FEI), KTH Stockholm, TU Vienna, Graz University, Goethe University Frankfurt. The process has a great potential to provide high purity depositions, both as isolators such as SiO_2 and TiO_2 (Fig 4) and pure metals such as Au (Fig 5), Pd and Pt (Fig 6). Of course a less-noble metal such as Ni from $Ni(Cp)_2$ will oxidize during the deposition process and hence instead of O_2 a reducing particle such as H_2, ammonia or hydrazine could be investigated as a future challenge.

References

[1] S. Rosenberg et al., Phys. Chem. Chem. Phys. 15, 4002-4015 (2013).

[2] S. Mehendale et al., NanoTechnology 24, 145303 (2013).

[3] B. Lewis et al., Beilstein J. Nanotechnology 6, 907-918 (2015).

[4] M.M. Shawrav et al., Scientific Reports 6, 34003 (2016).

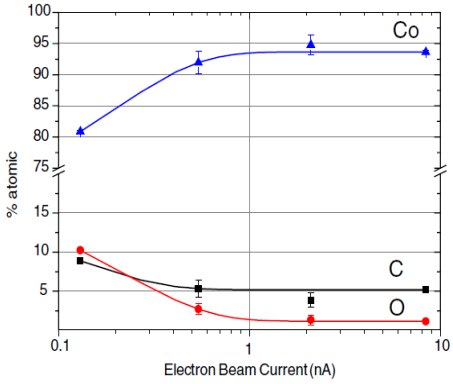

Fig. 1: Co, C and O content from deposition of the $Co_2(CO)_8$ precursor. A. Fernandez-Pacheo et al., J. Phys. D: Appl. Phys. 42 (2009) 055005.

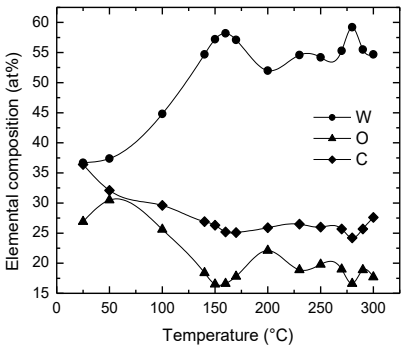

Fig. 2: W deposition made with $W(CO)_6$ as a function of the substrate temperature. J. Mulders et al., Nanotechnology 22 (2011) 055302.

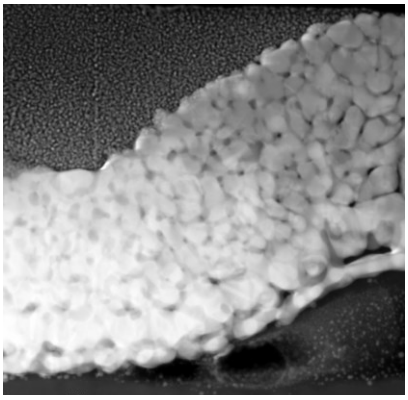

Fig. 3: TEM image of a direct (> 95 at% purity) Au deposition using Au(CO)Cl – a precursor with both a halogen and a CO group. The poor precursor stability however is a major issue that needs to be solved. J. Mulders et al., J. Phys. D Appl. Phys 45 (2012) 475301.

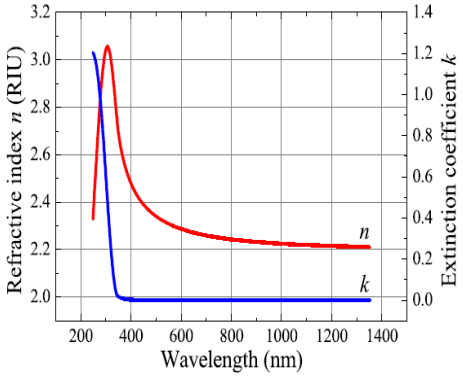

Fig. 4: Optical properties of a TiO_2 reveal its purity. Deposition made with simultaneous precursor and O_2 supply. Resistivity 10 – 40 GΩ.cm, breakdown voltage 10 – 70 V/µm. A. Riazanova et al., Nanotechnology 27 (2016) 115304.

Method	C/Au ratio	ρ (µΩ·cm)
a - Deposited without O_2	0.45	3.1×10^4
b - Deposited with O_2	0.1	5.3×10^3
c = b with e^- irradiation	0.083	1.7×10^1
d = c with e^- irradiation + O_2	0.062	4.8
e = b with e^- irradiation + O_2	0.068	3.5×10^1

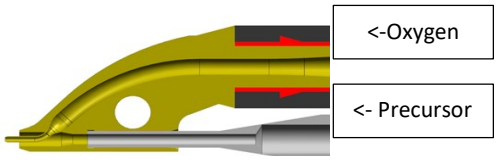

Fig. 5: Au deposition using direct deposit, simultaneous with O_2 and/or combined with post irradiation w/wo O_2. A variety of process combinations producing very low resistivity ρ (2.4 = bulk Au value). Dedicated concentric nozzle for simultaneous supply. C. Manisilla et al, Nanotechnology 27, 415301 (2016).

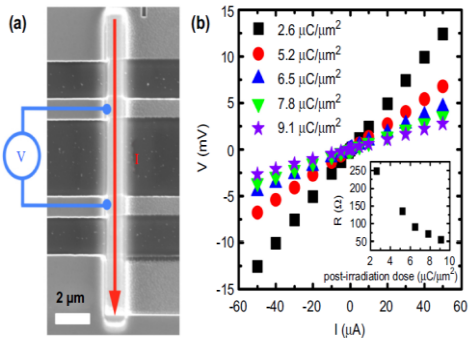

Fig. 6: Post irradiated Pt deposition under O_2. Resistivity improvement as a function of the dose. E. Villamor et al., Nanotechnology 26 (2015) 9095303.

Impact of purity and conductivity on plasmonic response of FEBID gold nanostructures

M.M. Shawrav[1]*, M-H Chien[1], S. Schmid[1], and H.D. Wanzenboeck[2]

[1] Micro & Nanosensors group, Institute of Sensors & Actuator System, TU Wien, Gusshausstrasse 27-29/ E 366, 1040 Vienna, Austria
[2] Bionanobeam group, Institute of Solid Sate Electronics, TU Wien, Floragasse 7, 1040 Vienna, Austria

* Corresponding author: mostafa.shawrav@tuwien.ac.at

Recently, plasmonics has received great attention due to its applications biomedical engineering, solar cells, chemical sensing and metamaterials. Focused Electron Beam Induced Deposition (FEBID) already has shown its potential for fabrication of complex plasmonic nanostructures. However, low carbon contamination originated from organometallic precursors are the major barrier of the wider application of this technique. This work will show various purification strategies and the impact of purification on plasmonic response of nanostructures.

Highly sensitive silicon nitride membrane resonators were used as a substrate to produce FEBID nanostructures. Nanodiscs, nanowires and bowtie shaped structures were deposited using LEO 1530 VP Scanning Electron Microscope with 3 kV acceleration voltage. The chemical composition of the structures where measured using Energy Dispersive Spectroscopy. The electrical resistivity of the deposited nanowires was measured using 4-point-probe electrical characterization method.

The structures were purified using various water-assisted in-situ deposition [1] and post-deposition purification approaches. Nanomechanical Scanning Absorption microscopy were used to characterize plasmonic properties of the nanostructures [2]. This technique uses a laser Doppler vibrometer to detect the thermal frequency detuning of a nanomechanical resonator as presented in Figure 1. The change of the resonance frequency is than converted into an intensity profile. As shown in Figure 2 and Figure 3, the photothermal analysis of as-deposited nanodiscs and purified nanodiscs showed significant change in absorption due to higher purity.

The conductivity of the structures was calculated from absorption cross section using Mie theory. In addition, a measurement and a theoretical model will be discussed which will give emphasis on the correlation between conductivity and purity of the structures.

Overall, this work will discuss the potential applications of FEBID nanostructures for future plasmonics based nanodevices.

References

[1] M. Shawrav, P. Taus, H. Wanzenboeck, M. Schinnerl, M. Stoeger-Pollach, S. Schwarz. A. Steiger-Thirsfeld, E. Bertganolli, *Highly conductive and pure gold nanostructures grown by electron beam induced deposition,* Sci. Rep 6, 34003 (2016).

[2] S. Schmid, K. Wu, P.E. Larsen, T. Rindzevicius, A. Boisen, *Low-Power Photothermal Probing of Single Plasmonic Nanostructures with Nanomechanical String Resonators*, Nano Lett. 14, 2318–2321 (2014).

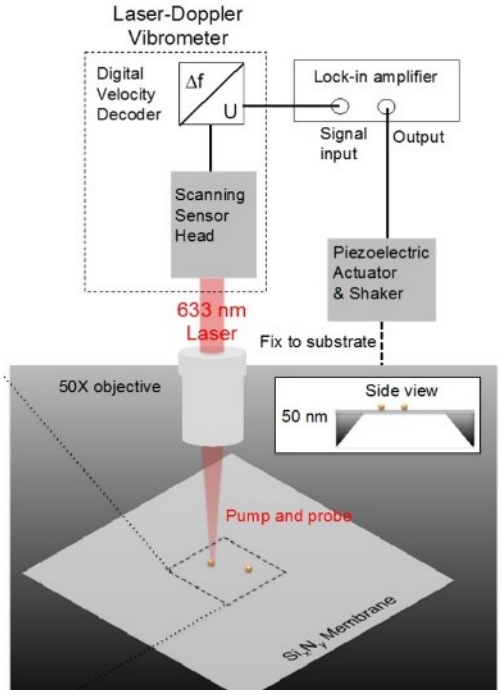

Fig. 1: Schematic process of Nanomechanical Scanning Absorption Microscopy.

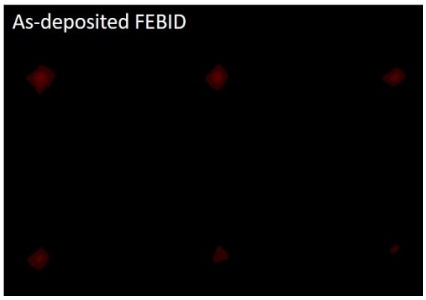

Fig. 2: Photothermal analysis of gold nanodiscs deposited using FEBID process**.**

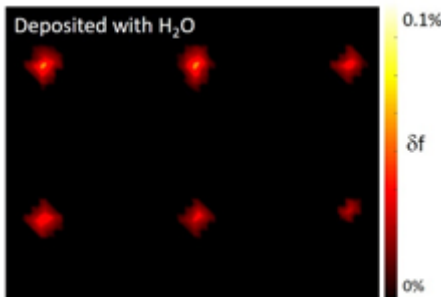

Fig. 3: Photothermal analysis of gold nanodiscs deposited using water-assisted FEBID process.

Purification and crystallization of 3D Co and Fe Nanowires Grown by Focused Electron Beam Induced Deposition

J. Pablo-Navarro[1]*, C. Magén[1,2,3], and J.M. De Teresa[1,2,3]

[1] Laboratorio de Microscopías Avanzadas (LMA), Instituto de Nanociencia de Aragón (INA) - Universidad de Zaragoza, 50018 Zaragoza, Spain

[2] Departamento de Física de la Materia Condensada, Universidad de Zaragoza, 50009 Zaragoza, Spain

[3] Instituto de Ciencia de Materiales de Aragón, Universidad de Zaragoza-CSIC, 50009 Zaragoza, Spain

* Corresponding author: javpablo@unizar.es

Ferromagnetic nanostructures are being investigated for potential application in many electronic devices for magnetic memories, logic and sensing [1]. For this aim, 3D magnetic nanowires (NWs) are considered as extraordinarily promising candidates. Thus, both optimization of nanofabrication processes and post-growth treatments should be refined to obtain NWs with the desired properties and functionalities, enhancing the performance of the futures spintronic devices.

Many efforts have been carried out to improve the magnetic properties of 3D ferromagnetic NWs grown by Focused Electron Beam Induced Deposition (FEBID) [2,3]. Here we report on the nanofabrication of 3D Co and Fe NWs by FEBID and the post-growth ex-situ high-vacuum annealing at different temperatures up to 600 °C for 100 minutes. In addition, High Resolution Transmission Electron Microscopy (HRTEM) imaging, Electron Energy Loss Spectroscopy (EELS) in Scanning Transmission Electron Microscopy (STEM) mode (Fig. 1), and Electron Holography (Fig. 2) have been used to monitor the structural, chemical and magnetic alterations at each annealing temperature. In the case of Co, NWs of 90 nm in diameter with high aspect ratio maintain the original shape after the thermal annealing treatment. The metallic composition increases from 65 at. % to 95 at. %, a recrystallization of the standard nanocrystalline as-deposited nanostructure into hexagonal-closest-packed and face-centered-cubic crystals is produced and the average net magnetic induction of the NWs increases dramatically from 0.8 T to 1.6 T, very close to the bulk Co one [4]. Fe NWs of 45 nm in diameter with high aspect ratio were also grown. In this case, despite increasing the crystallinity under thermal annealing processes above 150 °C, this treatment leads to a clear segregation of the Fe inside the core, giving rise to large, isolated and non-ferromagnetic carbon areas. As a consequence, different annealing conditions need to be used to improve their physical properties while preserving the original architecture [5].

This achievement opens new paths for the fabrication of either individual or arrays of 3D NWs with high purity and crystallinity based on other materials, obtaining nanostructures which could be used for future magnetic devices.

References

[1] A. Fernández-Pacheco et al., *Three dimensional magnetic nanowires grown by focused electron-beam induced deposition*, Sci. Rep. 3, 1492 (2013).

[2] J. Pablo-Navarro et al., *Three-dimensional core-shell ferromagnetic nanowires grown by focused electron beam induced deposition*, Nanotechnology 27, 285302 (2016).

[3] M. V. Puydinger dos Santos et al., *Annealing-Based Electrical Tuning of Cobalt-Carbon Deposits Grown by Focused-Electron-Beam-Induced Deposition*, ACS Appl. Mater. Interfaces 8, 32496 (2016).

[4] J. Pablo-Navarro et al., *Purified and Crystalline Three-Dimensional Electron-Beam-Induced Deposits: The Successful Case of Cobalt for High-Performance Magnetic Nanowires*, ACS Appl. Nano Mater. 1, 38 (2018).

[5] J. Pablo-Navarro et al., manuscript in preparation.

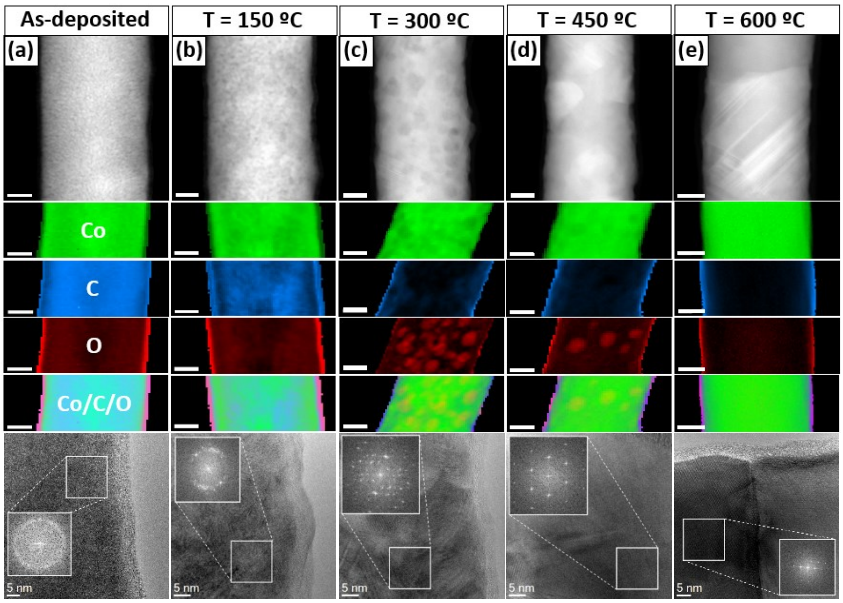

Fig. 1: High-angle annular dark-field STEM images, STEM-EELS maps and HRTEM images of (a) an as-deposited Co-FEBID NW and the ones annealed at (b) 150, (c) 300, (d) 450 and (e) 600 °C. The chemical maps show the spatial distribution of Co, C and O, representing also the three elements at the same time. The undefined scale bars are 20 nm. In the lowest panels, each HRTEM image is accompanied with an inset of the Fast Fourier Transform.

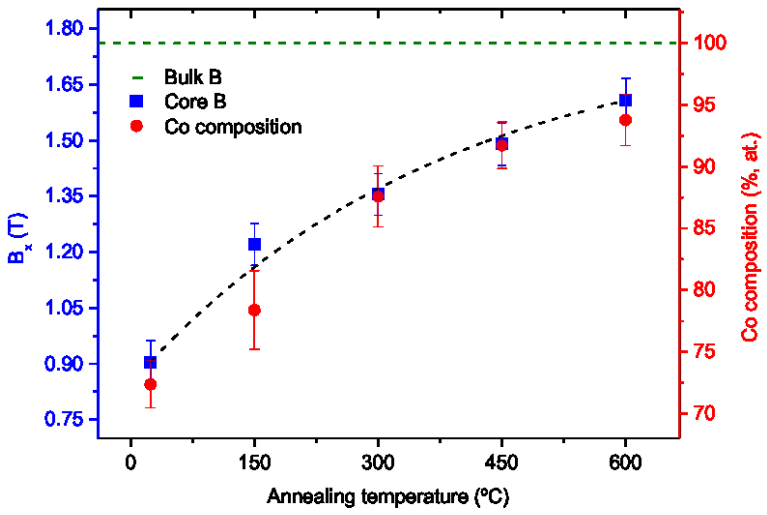

Fig. 2: Average net magnetic induction (square symbol) and Co composition (circle symbol) as a function of the annealing temperature considering the central 20 nm of each NW.

Focused Electron Beam Induced Deposition and purification of Ru using halogenated organometallic compounds

J. Jurczyk[1,2], C. Brewer[3], O. Hawkins[3], M. Polyakov[1], C. Kapusta[2],
L. McElwee-White[3], and I. Utke[1]*

[1] Laboratory of Mechanics of Materials and Nanostructures, Empa – Swiss Federal Laboratories for Materials Science and Technology, Feuerwerkstrasse 39, CH-3602 Thun, Switzerland
[2] Faculty of Physics and Applied Computer Sciences, AGH University of Science and Technology Krakow, Al. Mickiewicza 30, 30-059 Kraków, Poland
[3] Department of Chemistry, University of Florida, Gainesville, Florida 32611-7200, USA

* Corresponding author: ivo.utke@empa.ch

Focused Electron Beam Induced Deposition (FEBID) studies of potential organometallic halogenated ruthenium precursors were performed. FEBID is based on non-thermal electron induced dissociation of adsorbed molecules and has been increasingly investigated in recent years. As a local and direct method of deposition, FEBID is the only technique allowing manufacturing of three dimensional vertical structures on the nano-scale, with nearly every desired shape [1]. Yet there is still only a very limited number of materials which were successfully deposited with close to 100 at.% metal content.

Ruthenium FEBID is one of the processes which still require further investigation. Ruthenium is especially interesting as a material for Extreme Ultraviolet Lithography (EUVL) mask repair. Until now, the best reported FEBID result was achieved using bis(ethylcyclopentyldienyl) ruthenium(II) giving a C:Ru ratio of 9:1 (i.e. 10 at.% Ru) in as deposited material [2]. In this contribution we present three compounds that were specially designed to investigate interactions of electrons with different types of functional groups under real electron beam induced deposition process conditions: η^3-allyl-$Ru(CO)_3Cl$, η^3-allyl-$Ru(CO)_3Br$ and η^3-allyl-$Ru(CO)_3I$. All of them have structures similar to the one shown in Figure 1, but with different halogens. As they are volatile at room temperature and have a low initial C:Ru ratio of 6:1, those compounds are promising FEBID precursors. Recent gas phase [3] and surface science studies [4] confirmed that at least 2 CO groups are dissociated and desorbed due to interaction between low energy electrons and the molecule.

In our studies, we investigated the metal content obtained in FEBID material as a function of growth regime and writing strategy (dwell time) for vertical and planar structures. Preliminary promising results of up to 20 at.% of Ru in as deposited material were achieved, already doubling previous ratios obtained from bis(ethylcyclopentadienyl) ruthenium(II). A post growth purification procedure by a two-step annealing process was developed. During the initial step, heating up in oxygen atmosphere significantly reduced the amounts of halogen and carbon, but caused oxidation of Ru to RuO_2. During the second step, by using forming gas (98% of N_2 and 2% of H_2), ruthenium dioxide was reduced back to the pure metallic form.

To better understand both electrical conductivity and the dissociation processes leading to deposit formation, inner structure was investigated using Transmission Electron Microscopy. In Figure 2 we can observe the TEM image of 2-3 nm size grains in non-purified material. The inset presents the diffraction pattern, matching the one of pure, metallic Ru. These results suggest higher probability of co-deposition of ligands rather than incomplete dissociation of precursor. Figure 3a presents the line deposit, made between Pt electrodes on the Si substrate covered with 200nm of SiO_2. Figure 3b shows voltage – current characteristics measured with 4-point probe method on one of the lines. High resistivity value (5 orders of magnitude higher than for pure bulk Ru) of as deposited structures can be explained by the granular structure shown in Figure 2. In the contribution we will show the influence of described dissociation process on the metal content and electrical properties of the deposit on every stage of annealing.

References

[1] M. Huth et al., *Focused electron beam induced deposition meets materials science,* Microelectronic Engineering 185-186, 9-28 (2018).

[2] J.H. Noh et al., *Nanoscale electron beam-induced deposition and purification of ruthenium for extreme ultraviolet lithography mask repair*, App. Phys. A 117, 1705-1713 (2014).

[3] R.M. Thorman et al., *Low energy electron-induced decomposition of (n3-C3H5)Ru(CO)3Br, a potential focused electron beam induced deposition precursor with a heteroleptic ligand set*, Phys. Chem. Chem. Phys 19, 13264-13271 (2017).

[4] J.A. Spencer et al., *Electron-Induced Surface Reactions of η3-Allyl Ruthenium Tricarbonyl Bromide [(η3-C3H5)Ru(CO)3Br]: Contrasting the Behavior of Different Ligands,* J. Phys. Chem. C 119, 15349-15359 (2015).

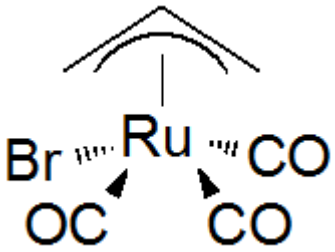

Fig. 1: Structural formula of η^3-allyl-Ru(CO)$_3$Br.

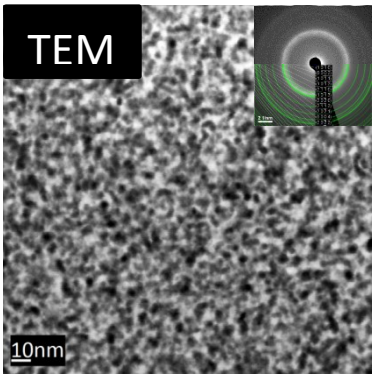

Fig. 2: TEM image of pillar deposit. Inset: Diffraction pattern of this deposit.

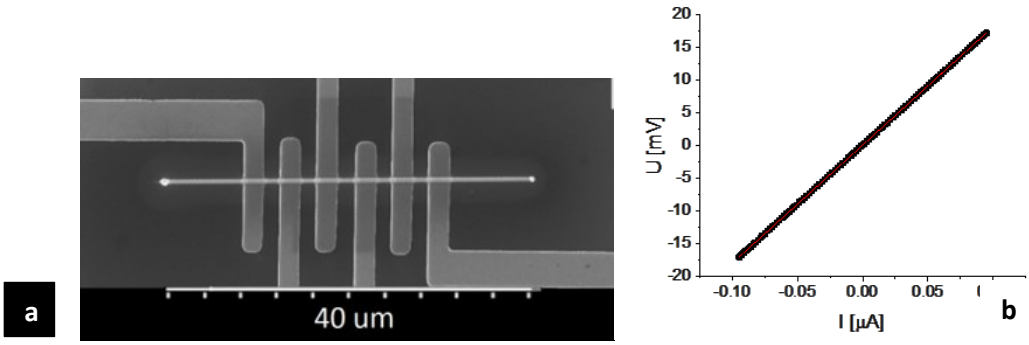

Fig. 3: One pixel line deposit made on Si substrate with 200nm SiO_2 layer, between Pt electrodes (a), Voltage current characteristics of ine deposit measured with a 4 point probe method (b).

FEBID frequency maps: a new tool for interpretation and design of experiments in FEBID Langmuir and multilayer processes

D. Sanz-Hernández[1]* and A. Fernández-Pacheco[1]

[1] Cavendish Laboratory - University of Cambridge, JJ Thomson Avenue, CB3 0HE, Cambridge, United Kingdom

* Corresponding author: dsh41@cam.ac.uk

The FEBID continuum model has long been a key ingredient in the ongoing efforts to enhance the predictability of FEBID processes [1]. Using the continuum model, the time evolution of adsorbate concentration on a substrate as a function of the various processes comprising FEBID can be modelled. This provides fundamental knowledge about the different regimes to be expected during experiments, and enables the development of FEBID 3D nano-printing computational tools [2].

A better understanding of FEBID underlying processes demands for new frameworks which describe this growth technique more generally and under a wide range of experimental conditions [3]. In the work presented in this talk [4], we generalize the FEBID continuum model, going beyond Langmuir adsorption, that is, allowing the system to form adsorbate coverages above one monolayer. Using this model, we have investigated what conditions are necessary for either mono- or multi-layer adsorption, by analytically calculating the stationary state of the system under no diffusion.

In this new approach, we have simulated FEBID processes involving both chemi- and physi-adsoption, using the BET model (see Figure 1), i.e. introducing two types of adsorption energies: one accounting for molecule–substrate interaction and a second for molecule–molecule interaction in upper monolayers. This generalizes the range of applicability of the FEBID continuum model by including processes involving multilayer formation, which are typical at low temperatures and for heterogeneous substrates [5]. It also enables the modelling of FEBID processes occurring on activated deposit surfaces, where both chemisorption and physisorption processes are relevant, opening a new route to interpret results where autocatalytic-mediated high purity deposits have been reported [6,7]. The approximations followed by the model presented here, and next steps for further generalization, will be discussed during the talk.

As a core part of this work, we also present a new tool to the FEBID community, the "FEBID frequency maps" (Figure 2). These diagrams, where adsorbate concentration and growth rates are plotted as a function of the fundamental frequencies present in a FEBID process, have been designed to compare theoretical results and experimental data, and as an aid to identify different possible steady states and transitions between growth regimes. By applying this new way of representing FEBID processes to pre-existing results available in the literature [8], we can trace the different regimes observed in an experiment, and e.g. determine if multilayer formation is physi- or chemi-adsorption dominated. Furthermore, the use of these maps emphasizes the presence of a desorption-dominated regime, coexisting with traditionally considered (mass-transport and reaction-limited) regimes. It also makes clear the need for investigating and reporting FEBID processes as a function of multiple experimental conditions to fully determine the growth regime in a particular experiment. Finally, we will present a frequency calculator tool to facilitate the use of FEBID frequency maps to the community.

References

[1] M. Toth, C. Lobo, V. Friedli, A. Szkudlarek, I. Utke, *Continuum models of focused electron beam induced processing*, Beilstein Journal of nanotechnology 6, 1518 (2015).

[2] J.D. Fowlkes et al., *High-Fidelity 3D-Nanoprinting via Focused Electron Beams: Computer-Aided Design (3BID)*, ACS Applied Nano Materials (2018).

[3] J.D. Wnuk, S.G. Rosenberg, J.M. Gorham, W.F. Van Dorp, C.W. Hagen, D.H. Fairbrother, *Electron beam deposition for nanofabrication: insights from surface science*, Surface Science 605(3-4), 257-266 (2011).

[4] D. Sanz-Hernández, A. Fernández-Pacheco, *Modelling focused electron beam induced deposition beyond Langmuir adsorption*, Beilstein Journal of Nanotechnology 8, 2151 (2017).

[5] D.H. Everett, *Colloid science*, Royal Society of Chemistry: London Vol. 4 (1983).

[6] M.M. Walz et al., *Electrons as "Invisible Ink": Fabrication of Nanostructures by Local Electron Beam Induced Activation of SiOx*, Angew. Chem. Int. Ed. Engl. 49, 4669-73 (2010).

[7] K. Muthukumar et al., *Spontaneous dissociation of $Co_2(CO)_8$ and autocatalytic growth of Co on SiO_2: A combined experimental and theoretical investigation,* Beilstein J. Nanotechnol 3, 546–555 (2012).

[8] M. Bresin, M. Toth, K.A. Dunn, *Direct-write 3D nanolithography at cryogenic temperatures,* Nanotechnology, 24(3), 035301 (2012).

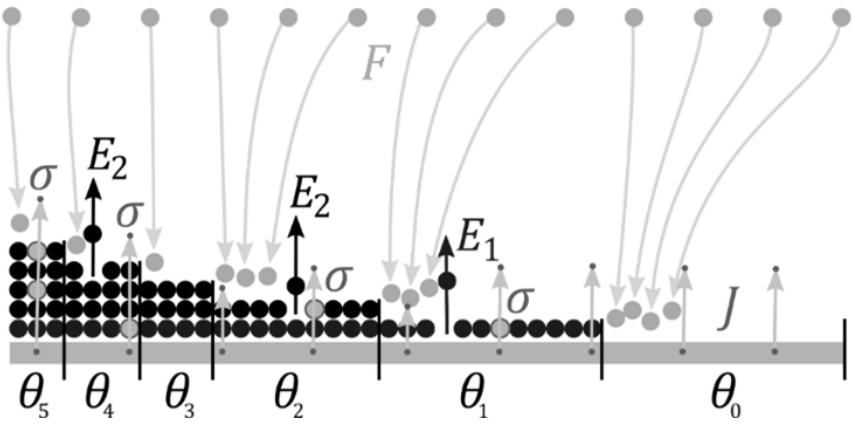

Fig. 1: FEBID multilayer model. Incoming precursor molecules with flux F onto the substrate. Molecules are adsorbed with energy E_1 in the lowest monolayer and upper monolayers are adsorbed with energy E_2. Electrons responsible for dissociation with current density J and dissociation probability σ, are represented by the uprising arrows. Molecules dissociated by electrons are shown as grey spheres with dark outline. The fraction of empty sites is θ_0, and fraction of occupied sites with one, two, three, etc. adsorbed monolayers, is θ_1, θ_2, θ_3, etc.

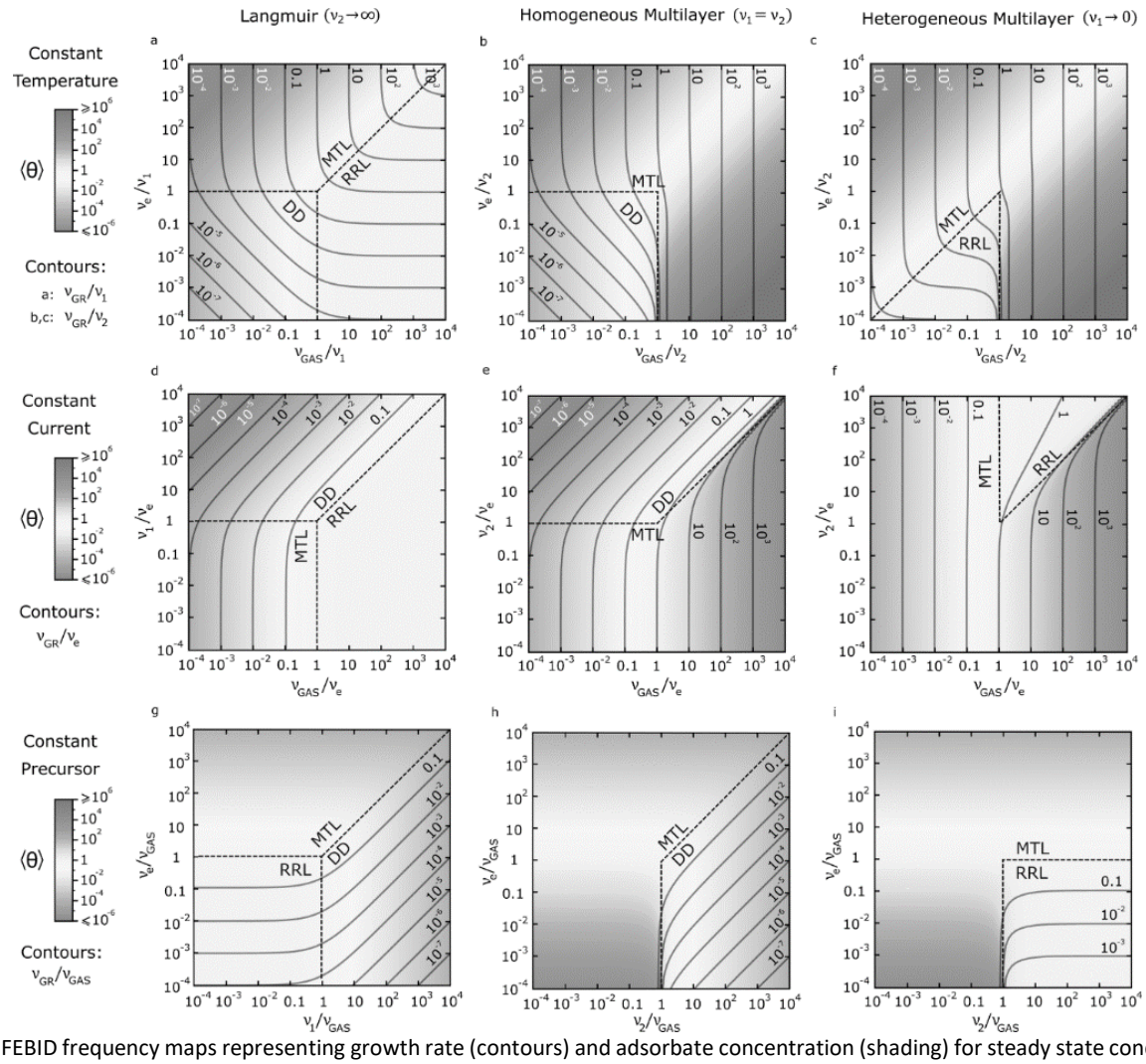

Fig. 2: FEBID frequency maps representing growth rate (contours) and adsorbate concentration (shading) for steady state conditions, as a function of the characteristic frequencies ruling a FEBID process. Different growth regimes are indicated for each region: Mass Transport Limited (MTL), Reaction Rate Limited (RRL) and Desorption Dominated (DD). Maps for constant temperature (a–c), current (d–f) and precursor flux (g–i) conditions are given.

Fast Monte Carlo Simulator of Electron Matter Interaction

C.W. Hagen*, T. Verduin, L.C.P.M. van Kessel, K.T. Arat, A. Mahgoub, and P. Kruit

Department of Imaging Physics – Delft University of Technology, Lorentzweg 1, 2628CJ Delft, The Netherlands

* Corresponding author: c.w.hagen@tudelft.nl

In many different fields in science and industry, electron beams are directed onto solid materials, after which either scattered particles are detected or electron-induced reactions occur. Examples are electron microscopes, electron beam lithography machines, and electron multiplier tubes. But also high-energetic photon beams may generate electrons such as in EUV-lithography machines, or X-ray photo-electron spectrometers. The incident electron energies involved are usually below 30 keV, or at most 100 keV (e-beam lithography). In all cases accurate knowledge of the electron-matter interaction would enable the prediction of secondary electron yields (SEY), backscattered electron yields, electron-induced reaction rates, counting rates, etc. Such knowledge is best obtained from Monte Carlo (MC) simulations.

We are developing a *fast* MC-scattering simulator based on first principle physics models, including Mott cross sections for elastic scattering, electron-phonon scattering, inelastic scattering based on the dielectric function, and quantum mechanical boundary crossing [1,2]. Furthermore, samples with complex geometries, such as rough surfaces, can be simulated (see Figures 1 and 2). Currently, we work on including charging effects, surface plasmons, and other dynamic effects, such as the evolution of structures grown by Electron Beam Induced Deposition (EBID). Our program runs on Graphics Processing Units (GPU), as well as on Central Processing Units (CPU). The MC-program provides reliable values for the SEY compared to experimental values and is faster than any existing electron scattering simulation program, as far as we know. As an example the total simulation time of an isolated Silicon line, with rough sidewalls, on a Si substrate is shorter by a factor of 387 to 894 (depending on the incident energy) when calculated with the GeForce GTX480 from NVIDIA than when calculated on a single threaded Intel X5650 CPU [1].

Our fields of application are lithography, metrology and imaging with electron microscopes. For instance, using the MC-simulator we can expose lithographically-defined patterns in resist (Figure 1) and construct electron images of those patterns (Figure 3), through which we can study the shot-noise limit in resist-based lithography. This may have a great impact on the throughput of critical dimension (CD) analysis, using dedicated Scanning Electron Microscopes (CD-SEM), in the wafer inspection industry.

Furthermore, the simulator can help in characterizing the EBID growth process, providing accurate spatial and energy distributions of scattered electrons. It may lead to a better understanding of broadening and proximity effects that occur during EBID and how to minimize such effects.

We will present the simulator, the physics models used, and some applications.

References

[1] T. Verduin, S.R. Lokhorst, C.W. Hagen, *GPU accelerated Monte-Carlo simulation of SEM images for metrology*, Proc. SPIE 9778, 97780D (2016).

[2] T. Verduin, *Quantum noise effects in e-beam lithography and metrology*, Thesis, TU-Delft (2016).

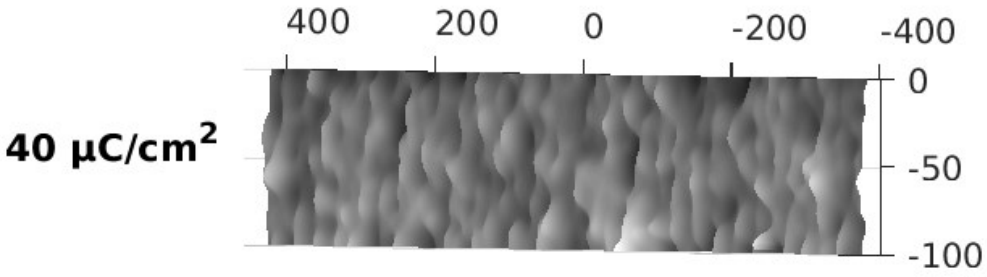

Fig. 1: Simulated sidewall of a chemically amplified resist line exposed with 40 µC/cm², after development.

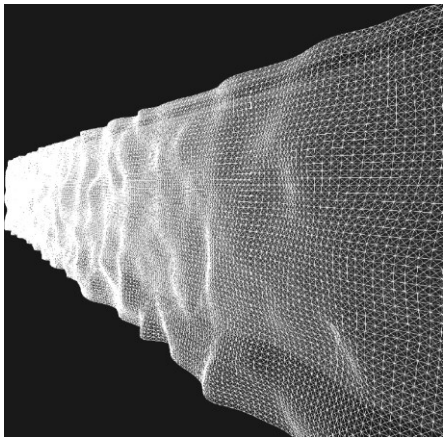

Fig. 2: Typical example of complex geometry: a triangulated rough sidewall (not the same one as in Figure 1).

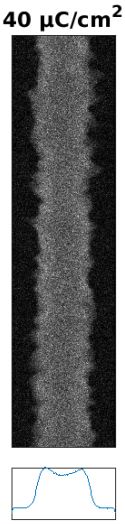

Fig. 3: Top-down SEM image of the chemically amplified resist line in Figure 1. The bottom graph shows the integrated intensity profile of the line.

New insights into the basic mechanisms of electron beam induced etching and deposition

J. Bishop[1]*, M. Fronzi[1], A. Bahm[2], A. Martin[3], J. Fröch[1], C. Elbadawi[1], N. Duong[1], C. Lobo[1], and M. Toth[1]

[1] School of mathematical and physical sciences, University of Technology, Sydney, New South Wales, Australia.
[2] FEI company, Hillsboro, Oregon, USA.
[3] Lawrence Livermore national laboratory, San Francisco, USA

* Corresponding author: jamesdbishop1@gmail.com

The primary factors that determine growth and etch rates as well as the morphologies of structures fabricated by electron beam induced etching (EBIE) and deposition (EBID), have been described in detail [1,2]. However, abnormal behaviors that cannot be explained by existing models have been documented for a number of systems, suggesting that current understanding of the basic mechanisms is incomplete [3,4,5]. Here we describe two such mechanisms that explain anisotropic EBIE of diamond and extreme electron beam induced heating during 3D EBID – namely, preferential passivation and stabilization of specific diamond crystal planes by hydrogen, and resistive heating caused by a charge compensation current flowing through self-supporting nanostructures grown by high-resolution 3D EBID.

We previously demonstrated that EBIE of single crystal (SC) diamond using H_2O results in anisotropic etching and crystallographic pattern formation [6]. We have now extended our investigation so as to explain the cause of the anisotropy by characterizing the EBIE kinetics when using H_2, O_2 and $H_2 + O_2$ as the precursor gases [7]. We find that isotropic EBIE of single crystal diamond is possible using pure, anhydrous O_2 as the precursor gas. Addition of H_2 makes EBIE anisotropic, with the ratio of etch rates on the different crystal planes evolving with the H_2:O_2 partial pressure ratio (fig. 1). The experiments and density functional theory calculations reveal that H serves to inhibit EBIE. The simulations also show that the extent of H adsorption depends on the diamond crystal plane, and that these variations explain the observed anisotropy. Furthermore, our experiments reveal how a remote plasma generator can be used during EBIE to increase the reactivity of precursor gases such as H_2, and to substantially suppress the concentration of residual water at the sample surface [8]. These findings can be used to broaden the range of precursors that can be used for EBIE, and to realize highly anisotropic diamond dry etching, enabling formation of symmetrical structures composed of smooth {110} planes or high rate isotropic etching with morphologies dictated only by the electron beam scan pattern and/or mask used.

Electron beam induced heating (EBIH) has long been hypothesized to play a role in EBID, particularly during 3D EBID [9]. Here we report the causal mechanisms and significance of EBIH during 3D EBID using a range of precursors and beam conditions. Extensive experiments and simulations indicate that EBIH is inherent to 3D EBID due to restricted heat dissipation. Two mechanisms are considered: electron energy loss via scattering (#1) and Joule heating (#2). Mechanism #1 is typically the dominant contributor to EBIH. However, mechanism #2 can cause significant EBIH for nanostructures of high resistivity (> 10 Ω.m) or thin cross section (< 100 nm). This is the result of “charge compensation currents”, which travel the length of 3D EBID structures during deposition to prevent charge-imbalance caused by secondary electron (SE) emission. We measure this experimentally and show that these currents can exceed the incident electron beam current (fig. 3). The electron beam energy is demonstrated to be the most convenient control parameter for EBIH. Beam pulsing enables further control. The results indicate that EBIH is a fundamental process in 3D EBID and highlight a mechanism that was overlooked in the literature whilst demonstrating the necessity of controlling EBIH for predictable results and providing means to achieve this control.

References

[1] I. Utke, S. Moshkalev, P. Russell, *Nanofabrication Using Focused Ion and Electron Beams*, OUP USA (2012).

[2] J.D. Fowlkes an PD. Rack, *Fundamental Electron-Precursor-Solid interactions […],* ACS Nano 4, 1619 (2010).

[3] J. Bishop et al., Phys. Rev. Lett. 109, 146103 (2012).

[4] A. Martin et al., ACS Appl. Mater. Interfaces 5, 8002 (2013).

[5] D. Belić et al., ACS Appl. Mater. Interfaces 7, 2467 (2015).

[6] A. Martin et al., Phys. Rev. Lett. 115, 255501 (2015).

[7] J. Bishop et al., ACS Nano 12, 2873 (2018).

[8] A. Martin and M. Toth, *Electron beam induced etching of carbon*. Appl. Phys. Lett. 107, 041603 (2015).

[9] S. Randolph, P. Rack et al., *Effects of heat generation during electron […]*, J. Appl. Phys. 97, 124312 (2005).

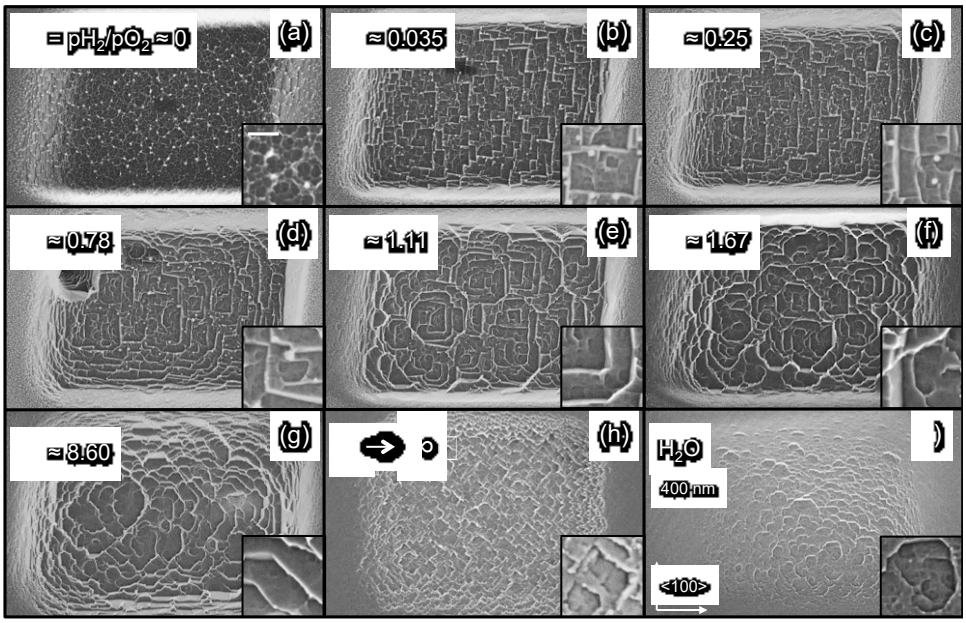

Fig. 1: EBIE of {100} SC diamond using different ratios of H_2 and O_2 precursor gases. A remote plasma was used during EBIE for precursor radicalization and residual water reduction. The partial pressure ratio of hydrogen to oxygen (R_p) used for each etch is indicated. Insets (all at same scale, scale bar = 100 nm) show close-ups of key surface morphologies. We observe a "sponge-like" texture and lack of crystallographic patterns with pure O_2 indicating an isotropic etch (a). As R_p is increased, we see rectangular {110} basis patterns (b - c), and then increasing contributions from {111} planes (d - g), resulting in octagonal patterns. Pure H_2 results in {111} basis patterns (h). EBIE with H_2O also gives rise to octagonal patterns (i). Etch times and conditions were equal for all pits. The etch rate with H_2O or H_2 is lower than with O_2 or $O_2 + H_2$. Etch pit sidewalls are aligned with <100> directions, indicated in (i). Edges aligned with pit sidewalls are formed by {110} planes and those at 45° by {111} planes. All main images are at the same scale indicated by the scale bar in (i).

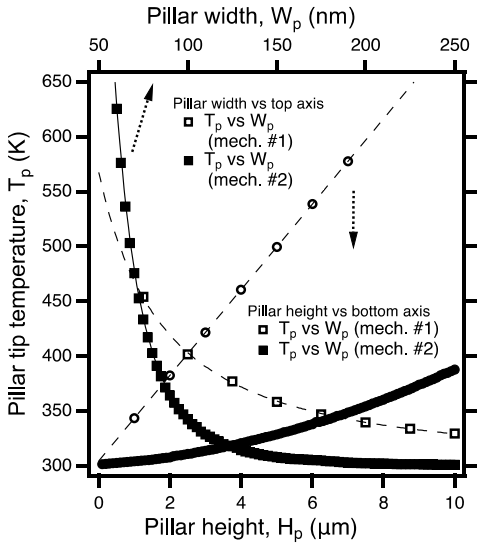

Fig. 2: Simulations of EBIH for a nanopillar structure. The beam current is 0.72 nA and the default height and width are 4.2 µm and 120 nm respectively. Two EBIH mechanisms are considered: electron energy loss via scattering (mech. #1) and joule heating (mech. #2). Pillar tip temperature, T_p due to EBIH by mech. #1 (open markers) and mech. #2 (filled markers) as a function of pillar height (bottom axis) and width (top axis). EBIH due to joule heating is $\alpha\ W_p^{-4}$ and should be significant for high resolution 3D EBID. EBIH by mech. #1 is dominant for wider structures.

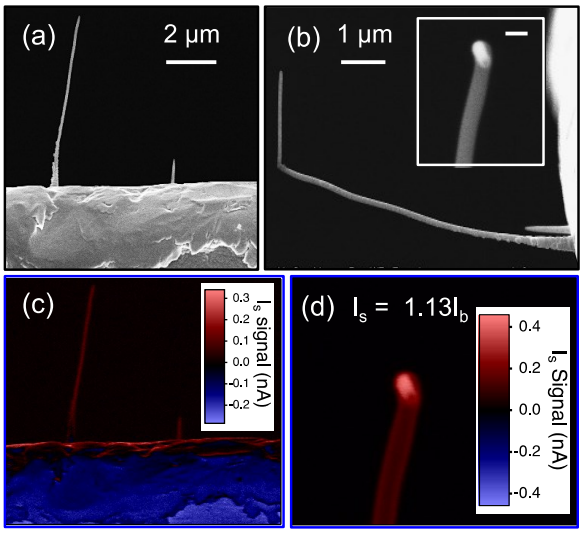

Fig. 3: Measurement of positive specimen currents in EBID pillars suspended from the edge of a TEM grid. (a-b): SEM images of nanopillar before (a) and after (b) deposition of a vertical pillar at the tip (inset scale bar = 100 nm). (c-d): Specimen current, I_s images of the pillar before (c) and after (d) deposition of the secondary pillar. Positive I_s occurs in regions where SE emission exceeds current injection. A 5 keV, 0.4 nA beam was used. We measure a current exceeding the incident beam current, travelling the length of the pillar (d). This is caused by high SE emission from the vertical pillar sidewalls.

Predictive Models and Process Windows for FEBIP of Copper with Liquid Reactants

S.K. Lami, G. Smith, S. Esfandiarpour, and J.T. Hastings[1]*

[1] Department of Electrical and Computer Engineering - University of Kentucky, Lexington, KY USA

* Corresponding author: todd.hastings@uky.edu

Integrated circuit editing is a key industrial driver for charged-particle beam induced processing. Currently, ion-beam induced processing is used to etch copper interconnects and either ion- or electron- beam induced deposition of other metals is used to add new interconnects. However, these processes have significant limitations. Ion-beam induced etching is challenging, but effective, for the lowest level interconnects (i.e. the smallest metal lines) where the lack of volatile etch products, redeposition, low etch rates, and low selectivity are less problematic. (See, for example, references [1, 2]). However, at higher interconnect levels where larger volumes of copper must be removed, these limitations are more severe. We have previously shown that electron beam induced etching of copper in thin layers of sulfuric acid (aq) provides efficient etching with excellent selectivity to underlying layers [3]. Because the etch product, $CuSO_4$, is soluble, redeposition is less problematic.

Nevertheless, there has been limited ability to predict the details of the etch process. Here we show that a hybrid Monte Carlo and finite element model can provide semi-quantitative predictions of etch rates and etch geometry for e-beam induced etching of copper in sulfuric acid. We use NIST's JMONSEL [4] code for Monte Carlo modeling of electron scattering and energy loss and COMSOL for modeling radiation-chemistry [5], subsequent reactions, mass transport, and the moving boundary at the Cu-liquid interface. Figure 1 shows an overlay of a simulated cross-section and a feature etched in electroplated copper. Figure 2 plots the relationship between the etch rate of eletrodeposited copper and the beam current for large features and shows good agreement between simulation and experiment. Both simulation and experiment show that the etch rate increases sub-linearly with beam current as the local concentration of the etch products increases.

One would also prefer to perform circuit edit by depositing copper similar to the electrodeposited copper used in the original fabrication process. However, FEBID of copper from metaorganic precursors yields low purity and low conductivity materials with resistivities of $10^4\ \Omega \cdot \mathrm{cm}$ as deposited and $1\ \Omega \cdot \mathrm{cm}$ after annealing [6]. As a result, circuit edit is usually performed with other metals. Copper deposited by FEBID from aqueous solutions of copper sulfate and sulfuric acid offers much higher purity [7]. However, we have observed great variability in conductivity depending on process conditions. Here we show that holding the total linear dose constant for the deposition of a copper nanowire while increasing the number of exposure loops (and thus reducing the dwell time) resulted in a transition from highly conductive wires ($< 500\ \Omega$, including contact resistance) to nearly insulating wires ($> 2\ M\Omega$) for linear dose/pass exceeding $20\ \mu\mathrm{C/cm}$. Four point probe measurements showed that the resistivity of the copper under favorable conditions was as low as $7 \times 10^{-6}\ \Omega \cdot \mathrm{cm}$ which is within a factor of 4 of bulk copper. Cross-sections, shown in Figure 3, revealed that short dwell times produced dense copper (low resistivity) while longer dwell times produced porous copper (high resistivity). We speculate that the porosity is the result of formation of copper oxides, hydroxides, or sulfides that subsequently dissolve in the sulfuric acid or the result of hydrogen bubble formation from the irradiation of sulfuric acid.

References

[1] N. Usami et al., *An arrayed test structure for transistor damage assessment induced by circuit analysis and repairing processes […]*, International Conference of Microelectronic Test Structures (ICMTS) 1-4 (2017).

[2] R. Timilsina et al. *Monte Carlo simulations of nanoscale focused neon ion beam sputtering of copper: elucidating resolution limits and sub-surface damage*, Nanotechnology 485704 (2014).

[3] L. Boehme et al., *Focused electron beam induced etching of copper […],* Nanotechnology 495301 (2015).

[4] J. S. Villarrubia et al. *Scanning electron microscope measurement of width and shape of 10nm patterned lines using a JMONSEL-modeled library*, Ultramicroscopy 15-28 (2015).

[5] P.-Y. Jiang et al. *Pulse radiolysis study of concentrated sulfuric acid solutions. Formation mechanism, yield and reactivity of sulfate radicals*, Journal of the Chemical Society, Faraday Transactions 1653-1658 (1992).

[6] A. Szkudlarek et al. *Formation of pure Cu nanocrystals upon post-growth annealing of Cu-C material obtained from focused electron beam induced deposition…*, Beilstein Journal of Nanotechnology 1508-1517 (2015).

[7] S. Esfandiarpour et al., *Focused electron beam induced deposition of copper with high resolution and purity from aqueous solutions*, Nanotechnology 125301 (2017).

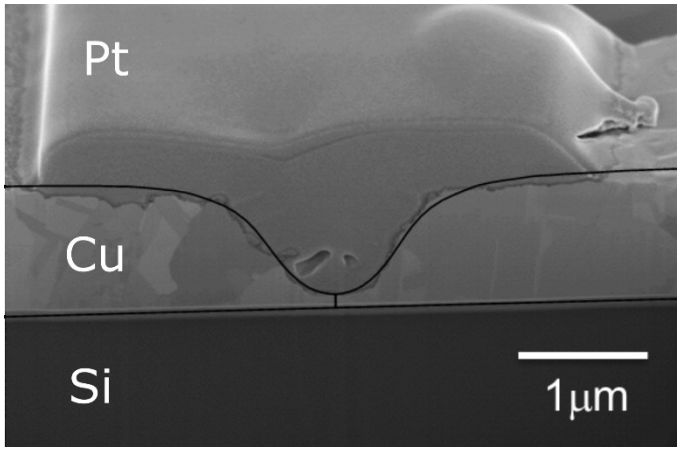

Fig. 1: Simulated cross-section (black line) overlaid on a FIB cross section of an etched feature in an electroplated copper film. Sulfuric acid (aq) was used as the etchant, and a point electron dose of approximately 10 nC reached the sample through a ~5 torr water vapor ambient. The SiO_2/TaN/Ta barrier layer is faintly visible at the Si-Cu interface. The Pt capping layer was added for protection during cross-sectioning.

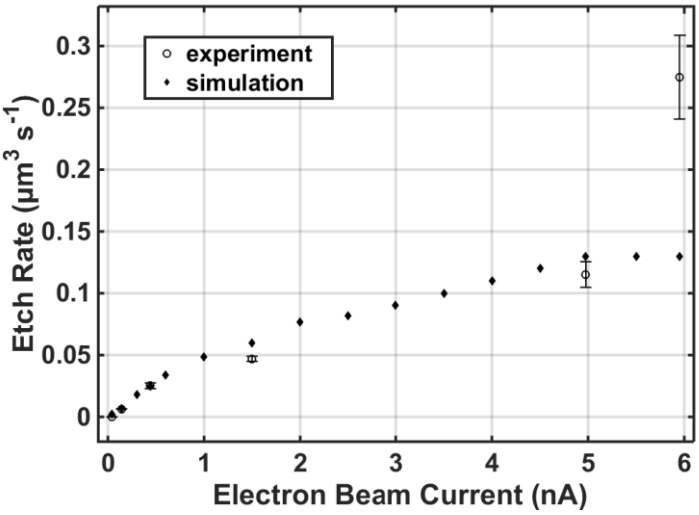

Fig. 2: Experimentally measured and simulated etch rates as a function of beam current. Etching was conducted in sulfuric acid (aq) with a liquid layer thickness of ~330 nm (measured interferometrically) at six different beam currents. At lower beam currents the variation in etch rate is small and agrees well with simulation. At the highest beam current, variability increases and there is a large deviation from simulation.

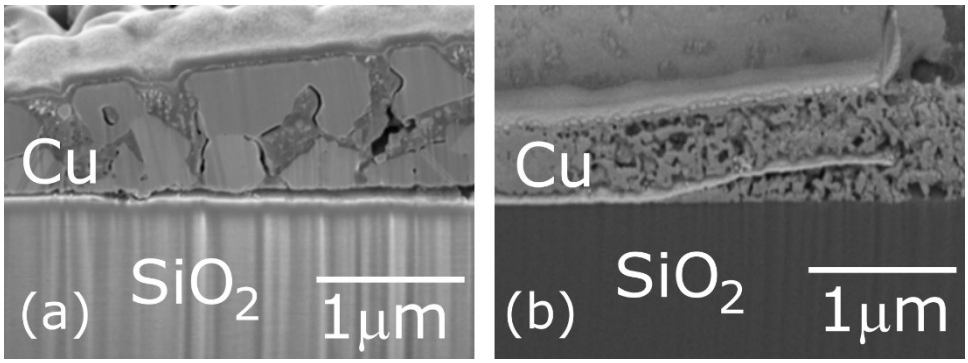

Fig. 3: Cross-sections of copper wires deposited from solutions containing copper sulfate and sulfuric acid. (a) At lower linear dose per pass ($\approx \mathbf{20\ \mu C/cm}$) larger copper grains are deposited in a dense network yielding highly conductive structures. (b) At higher dose per pass (i.e. longer dwell times) porous material is deposited yielding low conductivity structures.

FEBID meets Materials Science

M. Huth*

Physikalisches Institut - Goethe University, Max-von-Laue-Str. 1, 60438 Frankfurt am Main, Germany

* Corresponding author: michael.huth@physik.uni-frankfurt.de

Focused electron beam induced deposition (FEBID) is a direct-write method for the fabrication of nanostructures whose lateral resolution rivals that of advanced electron beam lithography but is in addition capable of creating complex three-dimensional nano-architectures (see Figs. 1 & 2). Over the last decade several new developments in FEBID and focused electron beam induced processing (FEBIP) have led to a growing number of scientific contributions in solid state physics and materials science based on FEBID-specific materials and particular shapes and arrangements of the employed nanostructures, see [1,2] for recent reviews.

In this talk an attempt is made to give a broad overview of these developments and the resulting contributions in various research fields encompassing mesoscopic physics with nano-structured metals at low temperatures, direct-write of superconductors and nano-granular alloys or intermetallic compounds and their applications, the contributions of FEBID to the field of metamaterials, and the application of FEBID structures for sensing of force or strain, dielectric changes or magnetic stray fields. The very recent development of FEBID towards simulation-assisted growth of complex three-dimensional nano-architectures is also covered. Of course, with such a broad focus on materials science and condensed matter physics this overview naturally cannot address all recent developments in FEBID.

Despite of all these exciting and scientifically interesting developments one may rightfully ask: Is there a broad recognition of FEBID and its capabilities for contribution to the various research areas within condensed matter physics and material science? Do condensed matter physicists and materials scientists know what processes and materials are already available with direct relevance for their research field? Can they, consequently, be active in inspiring new directions in driving FEBID development to ever more application fields? The answer is most probably “No”. On the other hand, with regard to what is already possible today with FEBID, developed by a small community of certainly less than 100 scientists worldwide, and what could be developed in a few years, the answer should be “Yes”. In the talk I will therefore briefly address the following questions: What can scientists, actively involved in FEBID development, and industry, providing instrumentation for FEBID, do to fundamentally change the perception of FEBID as a niche application for mask repair and TEM sample fabrication towards a core nanofabrication methodology with the broadest application range? In this context, I will briefly go into three important “action points” to be addressed by our community. **Materials basis**: A core requirement for a broader adoption of FEBID will be the availability of a larger material base of FEBID structures. From the scientist’s point of view, the task is threefold: (1) The fabrication technology has to be developed. (2) The materials have to be used with advantage in different research fields of broader interest. (3) The processes have to be optimized for high yield and ease-of-use. **Process adaption**: New FEBID processes developed in different scientific laboratories should be critically evaluated with regard to their potential use as “customer solutions” for extended use of FEBID with SEMs. Here scientists and industry have to work in close collaboration. Immediately relevant fields are “pure metallic FEBID structures”, “patterning strategies for metallic 3D structures”, “processes for magnetic and superconducting nanostructures”, and “algorithmic FEBID process self-optimization”, to name a few. **Outreach**: Presentations of FEBID-related technologies, materials and materials’ properties have to be brought to a broader audience by attending dedicated large-scale conferences. As an example may serve the LT-conference series (low-temperature physics), the international conference on magnetism series (ICM), the spring and autumn meetings of physics and materials science societies (DPG, MRS, APS etc.).

References

[1] J.M. De Teresa et al., *Review of magnetic nanostructures grown by focused electron beam induced deposition (FEBID)*, J. Phys. D Appl. Phys. 49, 243003 (2016).

[2] M. Huth, F. Porrati, O.V. Dobrovolskiy, *Focused electron beam induced deposition meets materials science*, Microelectronic Engineering 9, 185-186 (2018).

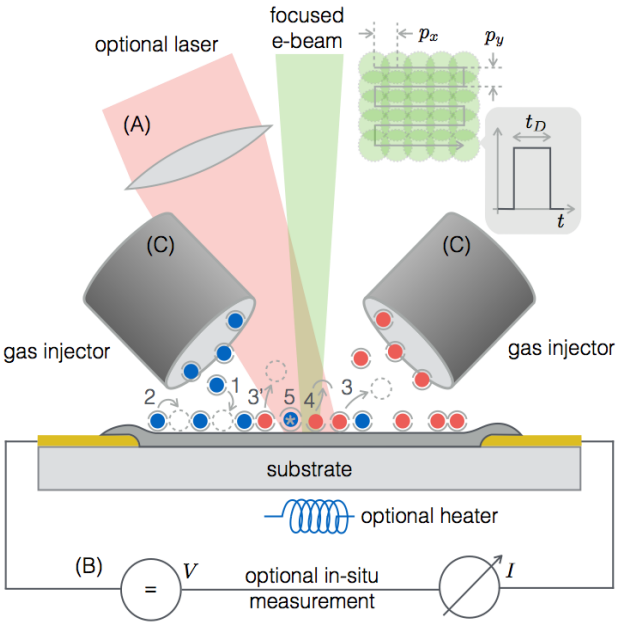

Fig. 1: Schematic of a SEM adapted for FEBIP with additional process equipment. Illustration of the FEBID process with two different precursor species. Taken from [2].

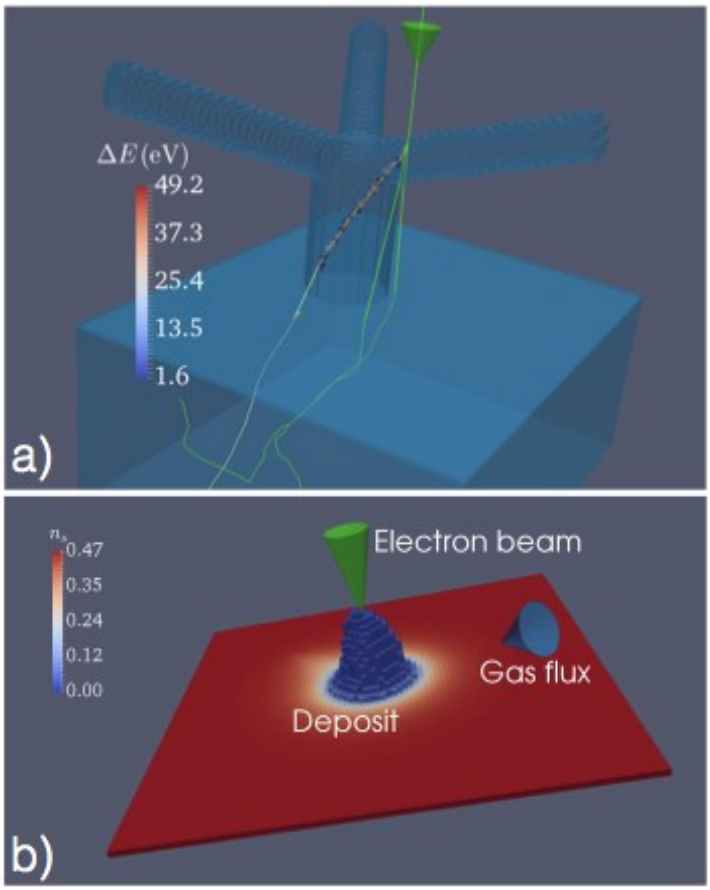

Fig. 2: Schematic of FEBID growth process based on Monte Carlo simulation of the electron trajectory and energy loss and numerical solution of the reaction-diffusion equation for the precursor density n_s. Taken from [2].

Single Electron Transistors (SET) fabricated by Focused Electron Beam Induced Deposition (FEBID)

G. Di Prima* and M. Huth

Physikalisches Institut, Goethe University, D-60438 Frankfurt am Main, Germany

* Corresponding author: diprima@physik.uni-frankfurt.de

Focused Electron Beam Induced Deposition (FEBID) is commonly applied in Semiconductor Industry for circuit modifications and mask repairs [1]. Thanks to the versatility of the technique additional applications have been found in fields such as magnetism, superconductivity, nano-optics, sensing, nano-electronics, etc.

In this contribution, the attention will be drawn towards the unconventional use of FEBID for nanodevice fabrication. In particular, we demonstrate that the FEBID is suitable for the realization of electronic key-elements for single electron transport effects in coupled nanostructures. In order to clearly detect single-electron phenomena, we fabricated Single Electron Transistors (SET).

A SET consists of a metallic nano-island that is connected by tunnel junctions to two electrodes (source and drain) and capacitively to a voltage source as gate (a schematic and a SEM picture of a fabricated SET appears in Fig. 1). However, with minimum feature sizes <10 nm, increasingly challenging fabrication barriers concerning the island and the tunnel junctions have to be taken into account. In this scenario, the direct-write capabilities of FEBID are advantageous.

The SETs are realized using pre-patterned contacts in a cross configuration and which are milled with a Focused Ga-Ion Beam in order to obtain a SET device geometry with two gate electrodes. Afterwards, a Pt-C island is placed between the milled electrodes using FEBID and subsequently subjected to a localized Ar-etching [3] in order to erase the Pt-codeposit. The Pt-C island itself is a system of Pt-grains (2-3 nm in size) embedded in a carbonaceous matrix [2]. When an electron charges the island, it will tunnel across the tunnel junctions hopping among the Pt-grains through the carbon. Finally, the electron will escape from the island tunneling to the drain electrode. In this way, co-tunneling processes, in which an electron can tunnel simultaneously over the distance of two junctions, will not disturb the observation of the single-electron-tunneling through the island. The sub-granular microstructure of the Pt-C islands therefor represents an advantage.

These structures showed that single electron transport is taking place through the Pt-FEBID island and it can be tuned applying voltage to the gate electrode. The clear evidence of the hopping of a single electron through one of the fabricated device is visible in Fig. 2 where the defined blockade regions have the characteristic diamond shape. Moreover, in Fig. 3 periodic Coulomb oscillations are shown for different drain-source voltages, proving the “pumping” action of the gate voltage in the sequential passage of single-electrons through the island. Lastly, current-voltage characteristics of the same device for different temperatures are reported in Fig. 4. The Coulomb blockade vanishes between 50K and 77K demonstrating a large temperature operation regime of the device.

References

[1] T. Bret, T. Hofmann, K. Edinger, *Industrial perspective on focused electron beam-induced processes*, Appl. Phys. A 11, 1607 (2014).

[2] J.M. De Teresa et al., *Origin of the Difference in the Resistivity of As-Grown Focused-Ion- and Focused-Electron-Beam-Induced Pt Nanodeposits*, Journal of Nanomaterials, 936863 (2009).

[3] In situ Ar-etching instrumentation provided by Hans Mulders and Piet Trompenaars, ThermoFischer Scientific.

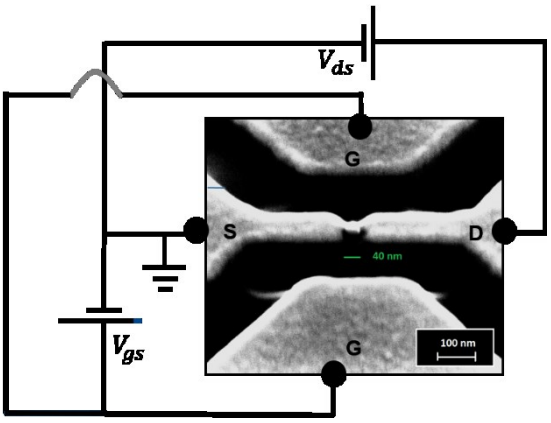

Fig. 1: Schematic of the SET circuit and SEM picture of a fabricated structures.

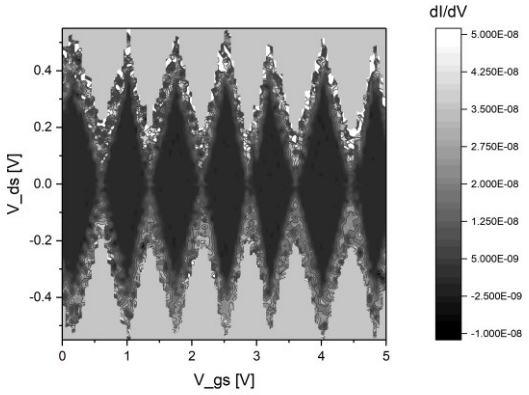

Fig. 2: Stability diagram of a fabricated SET. The diamonds show the presence of one electron in the island for well-defined voltage regions.

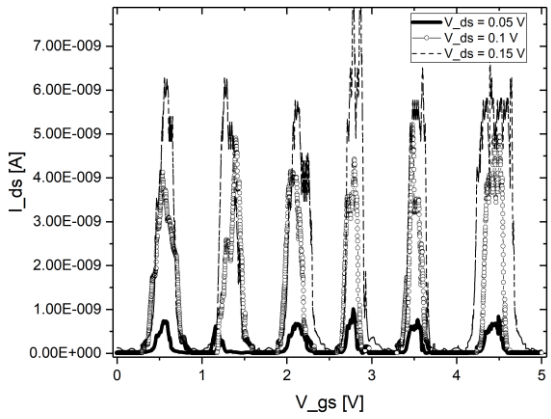

Fig. 3: Periodic Coulomb oscillations for different drain-source voltages show the tunability of the single-electron transport by the gate voltage.

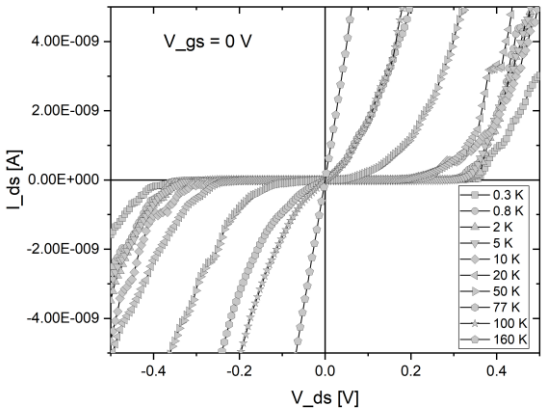

Fig. 4: Current-voltage characteristics of a SET for different temperatures. The SET operation regime is 0.3-50K.

Fabrication and Tuning of Photonic Crystal Cavities in Hexagonal Boron Nitride by Electron Beam Induced Etching

J.E. Fröch[1], S. Kim[1], J. Christian[2], M. Straw[2], J. Bishop[1], D. Totonjian[1], K. Watanabe[3], T. Taniguchi[3], M. Toth[1]*, and I. Aharonovich[1]

[1] Institute of Biomedical Materials and Devices (IBMD), Faculty of Science, University of Technology Sydney, Ultimo, NSW, 2007, Australia

[2] Thermo Fisher Scientific, 5350 NE Dawson Creek Drive, Hillsboro, OR 97214 - 5793 USA

[3] National Institute for Materials Science, 1 - 1 Namiki Tsukuba Ibaraki 305 - 0044 Japan

* Corresponding author: milos.toth@uts.edu.au

Exceptional efforts have been undertaken in recent years to identify suitable platforms for solid state quantum photonic technologies [1] and to develop new fabrication schemes to exploit the full potential of these materials. Ideally, such a material hosts on-demand single photon emitters and can be easily processed in a robust and reliable manner to yield functional nanostructures on a large scale. While the first criterion is fulfilled for hexagonal Boron Nitride (hBN) due to the discovery of room-temperature, stable, ultra-bright quantum emitters [2], the second remains a challenge as, until recently, fabrication of complex hBN geometries was not viable. As hBN is a layered van der Waals crystal, several established processing steps, such as vapor release techniques, or angled bulk etching neither tackle the weaknesses nor exploit the advantages of this material. Yet, the intriguing characteristics of this materials necessitate a robust fabrication scheme to exploit it in quantum photonic devices that have applications in quantum information processing. Here, we demonstrate a new processing approach for the fabrication of complex photonic nanostructrues in suspended hBN [3]. Using the technique of Electron Beam Induced Etching (EBIE) [4] we demonstrate photonic crystal cavities with quality factors of close to 2000 (Fig. 1). The EBIE technique employs an electron beam and a precursor gas – in this case H_2O vapour – to induce dry etching through chemical reactions that volatilize hBN. It is minimally invasive, as evidenced by no changes in Raman spectra obtained before and after processing. A further highlight of our study is the demonstration of cavity tuning using mask-free, direct-write focused electron beam induced etching (Fig. 2). This approach is appealing as it allows iterative, selective tuning of individual devices on a chip. Even more intriguingly, we discovered that electron beam processing of hBN can give rise to the creation (or activation) of single photon emitters. This compelling effect suggests that electron beam processing may provide a pathway for deterministic fabrication of single photon emitters with high spatial resolution.

Overall, our methodology and results set the foundation for cavity quantum electrodynamics experiments to be performed using hBN and other material platforms.

References

[1] J.L. O'brien, A. Furusawa, J. Vučković, *Photonic quantum technologies,* Nature Photonics 3.12, 687 (2009).

[2] T.T. Tran et al., *Quantum emission from hexagonal boron nitride monolayers,* Nature nanotechnology 11.1, 37 (2016).

[3] S. Kim et al., *Photonic Crystal Cavities from Hexagonal Boron Nitride,* arXiv preprint arXiv:1801.04399 (2018).

[4] C. Elbadawi et al., *Electron beam directed etching of hexagonal boron nitride,* Nanoscale 8, 16182 - 16186 (2016).

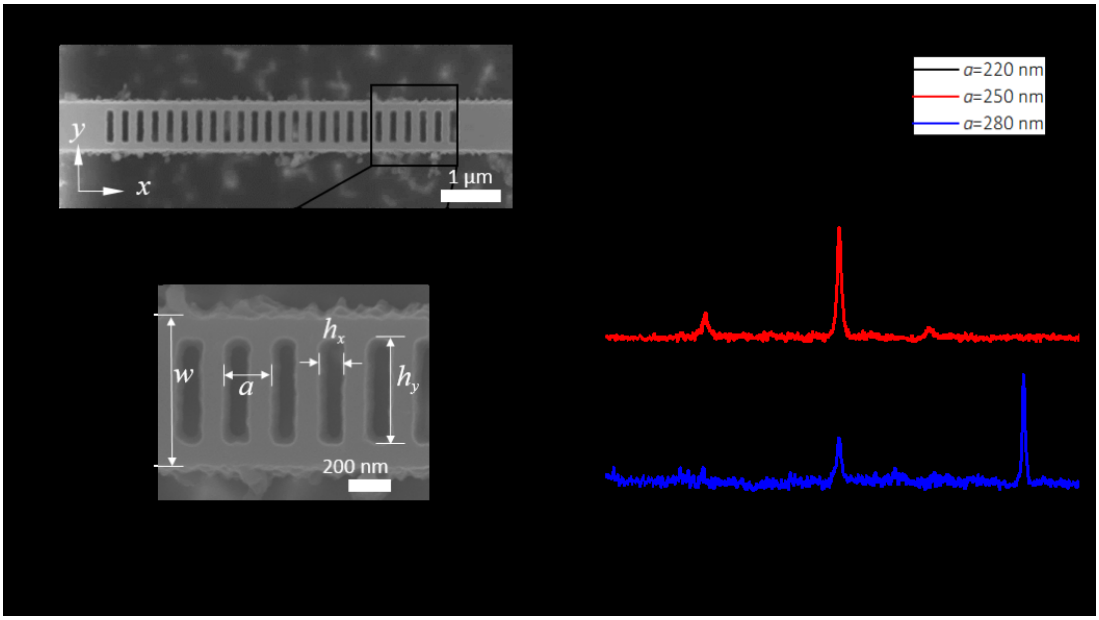

Fig. 1: Photonic Crystal cavity fabricated in hBN. **a,** SEM image of a 1D ladder cavity, showing the geometrical parameters; width (w), lattice constant (a), air hole width (h_x), and air hole height (h_y), whose dimensions determine the resonant wavelength of the cavities. **b,** by using different geometries, various resonances in the cavities were realised.

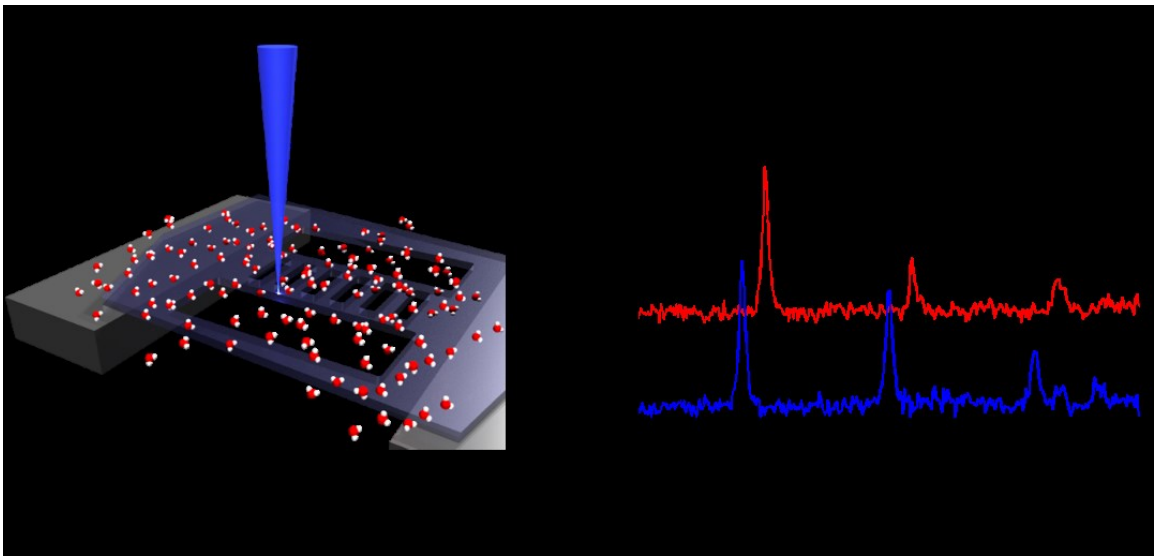

Fig. 2: Direct-write iterative editing of a single cavity using FEBIE. **a,** Schematic depiction of the editing process in which a focused electron beam (blue) etches selected areas of the cavity, resulting in an effective dimension change of the cavity. **b,** the resonant modes of the cavity can be shifted deterministically using this technique.

Surface-Anchored Metal-Organic Frameworks as Versatile Resists for E-Beam Lithography: Fabrication of sub-10 nm Structures

C. Preischl[1], F. Vollnhals[1], E. Bilgilisoy[1], M. Drost[1], L. Berger[1], W. Zhou[3], H. Gliemann[3], C. Wöll[3], and H. Marbach[1]*

[1] Lehrstuhl für Physikalische Chemie II, Universität Erlangen-Nürnberg, Egerlandstr. 3, 91058 Erlangen, Germany,

[2] Institut für Funktionelle Grenzflächen, Karlsruher Institut für Technologie (KIT), Hermann-von-Helmholtz-Platz 1, D-76344 Eggenstein-Leopoldshafen, Germany

*Corresponding author: hubertus.marbach@fau.de

In this contribution we demonstrate the possibility to structure surface-anchored metal-organic frameworks [1] on the nanometer scale by using Focused Electron Beam Induced Processing (FEBIP). The two methods of choice we were using are Electron Beam Induced Deposition (EBID) and Electron Beam Induced Surface Activation (EBISA) (see Fig. 1). In EBID adsorbed precursor molecules are locally dissociated by the impact of the electron beam yielding the deposition of non-volatile dissociation products on the surface [2,3]. On the part of the EBISA process, in a first step, the surface is irradiated with the electron beam without any precursor gas present. In the second step, the surface is exposed to a suitable precursor gas which decomposes at the activated sites [4]. For both processes autocatalytic growth can be observed already at room temperature for certain precursor gases, resulting in very clean deposits. EBISA and the autocatalytic growth process only occur due to our "surface science approach" towards FEBIP, as we are working under ultrahigh vacuum conditions. The precursor molecules to be discussed in this contribution are $Fe(CO)_5$ and $Co(CO)_3NO$ which both show autocatalytic growth behavior. We demonstrate the huge potential of the approach for two different types of SURMOFs (HKUST-1 and ZN-DPDCPP). With the EBID process we obtained well-defined deposits from $Fe(CO)_5$ and $Co(CO)_3NO$ (see Fig. 2), whereas the EBISA process only works for $Fe(CO)_5$ and shows no deposition from $Co(CO)_3NO$ for both SURMOFs [5].This interesting behavior reveals a very specific chemical selectivity of the corresponding EBISA processes. Local Auger Electron Spectroscopy (AES) evidences that deposits from $Fe(CO)_5$ exclusively consist of iron, whereas deposits from $Co(CO)_3NO$ contain cobalt, nitrogen and oxygen. In addition, we demonstrate is the fabrication of "nested-L test structures" with Fe(CO)5 on HKUST-1 with unusually narrow line widths (average FWHM value 9.6 nm, smallest width 7.5 nm, see Fig. 3).[5] Since the actual diameter of the electron beam was larger than 6 nm at the time of the experiments, the resolution is remarkably high. We discuss that reduced electron scattering and quenching of secondary electrons occurs within the SURMOF material, leading to drastically reduced proximity effects.

References

[1] J.X. Liu, C. Wöll, *Surface-supported metal-organic framework thin films: fabrication methods, applications, and challenges,* Chemical Society Reviews 46, 5730 (2017).

[2] W. van Dorp, C.W. Hagen, *A critical literature review of focused electron induced deposition,* Journal of Applied Physics 104, 081301 (2008).

[3] I. Utke et al., *Gas-assisted focused electron beam and ion beam processing and fabrication.* Journal of Vacuum Science & Technology B 26, 1197 (2008).

[4] H. Marbach, *Electron beam induced surface activation: a method for the lithographic fabrication of nanostructures via catalytic processes*, Applied Physics A 117, 987 (2014).

[5] M. Drost, F. Tu, L. Berger, C. Preischl, W. Zhou, H. Gliemann, C. Wöll, H. Marbach, *Surface-Anchored Metal- Organic Frameworks as Versatile Resists for E-Beam Lithography: Fabrication of sub-10 nm Structures,* ACS Nano 12, 3825 (2018).

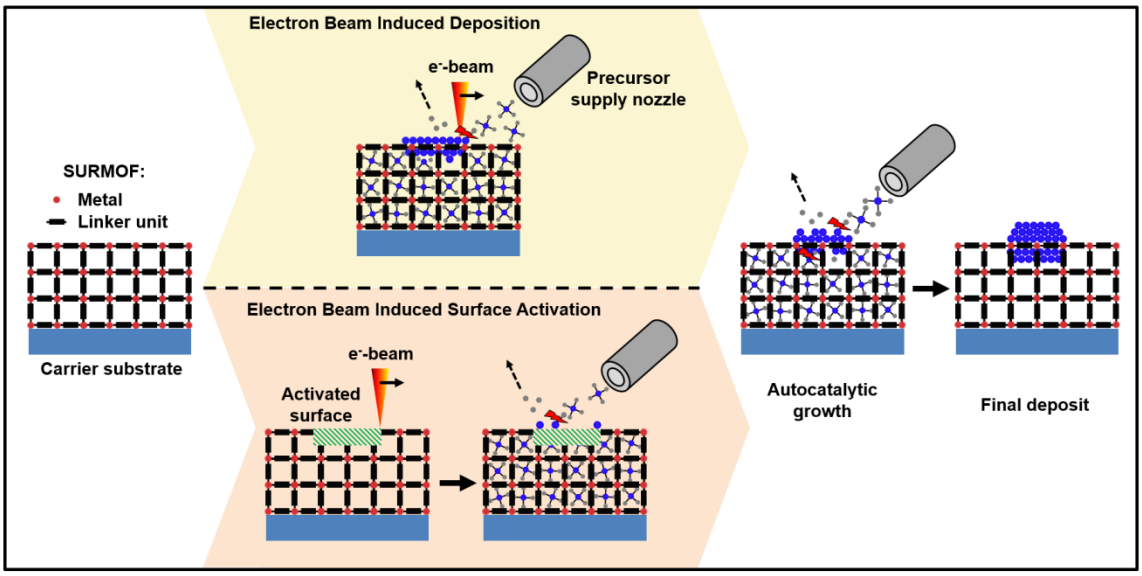

Fig. 1: Schematics of the EBID and EBISA experiments conducted on SURMOFs presented in this work. In EBID (above the dashed line), the electron beam of the scanning electron microscope irradiates the SURMOF in the presence of a precursor gas, leaving behind a deposit. In EBISA (below the dashed line), the SURMOF is irradiated in the absence of a precursor, leading to a chemically modified, activated surface. Subsequently dosed precursor can dissociate at activated sites, also leaving behind a deposit or a seed layer, respectively. In an autocatalytic growth process, the initial deposits fabricated by either method grow in size as long as the precursor is supplied.

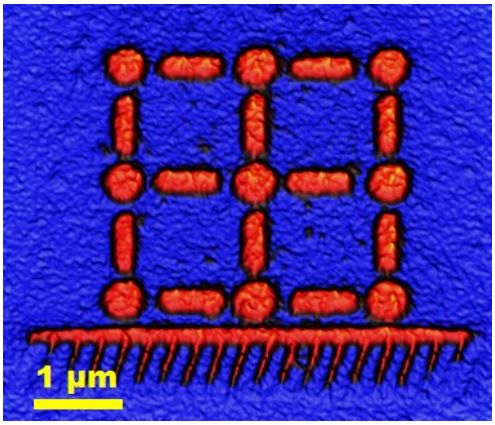

Fig. 2: Processed SEM image of a "SURMOF icon" produced by EBID on HKUST-1 grown on the self-assembled monolayer MUDA on a gold coated silicon wafer.

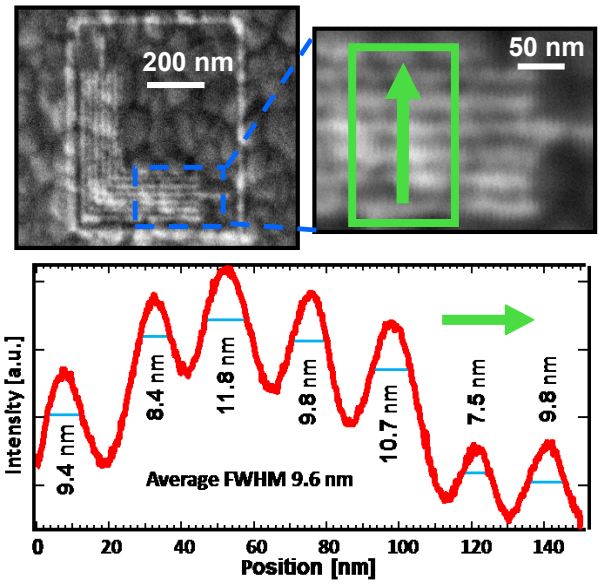

Fig. 3: SEM images of "nested L" as prototype test structure for resolution measurements fabricated with 2.3-33.8 µC/cm, 250 sweeps, t_{AG} = 17 min. The red dashed rectangle indicates the position of the corresponding blow-up. RGB profiles extracted from the green rectangle in b). A minimum FWHM of 7.5 nm was measured, with a pitch of 23.6 nm.

Three-Dimensional Nanostructure Fabrication by Focused-Ion-Beam Chemical-Vapor-Deposition

S. Matsui*

University of Hyogo, 3-1-2 Koto, Ako, Hyogo, Japan

* Corresponding author: shinjimatsui1@gmail.com

Two-dimensional (2D) nanostructure fabrication using electron-beam (EB) and focused-ion-beam (FIB) has been achieved and applied to make various nanostructure devices. Ten-nm structures are able to be formed by using a commercial available EB or FIB system with 5 –10 nm beam diameter and high-resolution resist. In this way, it is considered that the technique of 2D nanostructure fabrication has been established. On the other hand, three-dimensional (3D) nanostructure fabrication has been also studied using both EB and FIB induced deposition (CVD).

In this presentation, we describe 3D nanostructure fabrication techniques using FIB-CVD [1]. We first describe 30 keV Ga^+ FIB-CVD using a *phenanthrene* ($C_{14}H_{10}$) source gas as precursor. A film deposited during such a process is diamond-like amorphous carbon, which has a Young's modulus exceeding 600 GPa, appearing to make it highly desirable for various applications.

The process of fabricating 3D structures by FIB-CVD is illustrated in Fig. 1 [1]. In FIB-CVD processes, the beam is scanned in digital mode. First, a pillar is formed on the substrate by fixing the beam-position (position 1). After that, the beam position is moved to within a diameter of the pillar (position 2) and then fixed until the deposited terrace thickness exceeds the range of the ions (a few ten nm). This process is repeated to make 3D structures. The key point to making 3D structures is to adjust the beam-scan-speed so that the ion-beam remains within the deposited terrace, which means that the terrace thickness always exceeds the range of the ions. The growth in the x- and y-directions are controlled by both beam-deflectors. The growth in the z-direction is determined by the deposition rate; that is, the height of structure is proportional to an irradiation-time when a deposition rate is constant. A 3D pattern generator system has been developed to make arbitrary 3D nanostructures [2].

We consider microstructure plastic art, which is a new field that has been made possibility by beam technology, and we present examples of such art. A "micro-wine-glass" was created on a human hair as a work of microstructure plastic arts as shown in a scanning ion microscope (SIM) image of Fig. 2. A micro wine glass with an external diameter 2.75μm and a height of 12μm was formed [1]. The fabrication time was 600 s at a beam current 16 pA. This beautiful micro wine glass shows the potential of the field of microstructure plastic art. Figure 3 shows a "nano T4 bacteriophage", which is an artificial version of the virus fabricated by FIB-CVD on silicon surface. The size of the artificial nano "T4 bacteriophage" is about ten times as that of the real virus.

Nano-spring [3], nano-manipulator [4], and nano-space-wiring [5] with 0.1μm dimension are demonstrated as parts of nano-mechanical system. The electrical properties of free-space nano-wiring using a mixture of $C_{14}H_{10}$ and $W(CO)_6$ indicates increasing the metal content results in lower resistivity. We have also successfully demonstrated that a *Morpho* butterfly scale quasistructure fabricated by FIB-CVD can give almost the same optical characteristics as real *Morpho* butterfly scale [6].

References

[1] S. Matsui, T. Kaito, J. Fujita, M. Komuro, K. Kanda, Y. Haruyama, *Three-dimensional nanostructure fabrication by focused-ion-beam chemical vapor deposition*, J. Vac. Sci. Technol. B 18, 3181-3184 (2000).

[2] T. Hoshino et al., *Development of three-dimensional pattern-generating system for focused-ion-beam chemical-vapor-deposition*, J. Vac. Sci. Technol. B 21, 2732-2736 (2003).

[3] K. Nakamatsu, M. Nagase, H. Namatsu, S. Matsui, *Mechanical characteristics of diamond-like-carbon nanosprings fabricated by focused-ion-beam chemical vapor deposition*, Jpn. J. Appl. Phys. 44, L1228-L1230 (2005).

[4] R. Kometani et al., *Performance of nanomanipulator fabricated on glass capillary by focused-ion-beam chemical vapor deposition*, J. Vac. Sci. Technol. B23, 298-301 (2005).

[5] T. Morita et al., *Free-space-wiring fabrication in nano-space by focused-ion-beam chemical vapor deposition*, J. Vac. Sci. Technol. B 21, 2737-2741 (2003).

[6] K. Watanabe, T. Hoshino, K. Kanda, Y. Haruyama, S. Matsui, *Brilliant blue observation from a Morpho-butterfly-scale quasi-structure*, Jpn. J. Appl. Phys. 44, L48-L50 (2005).

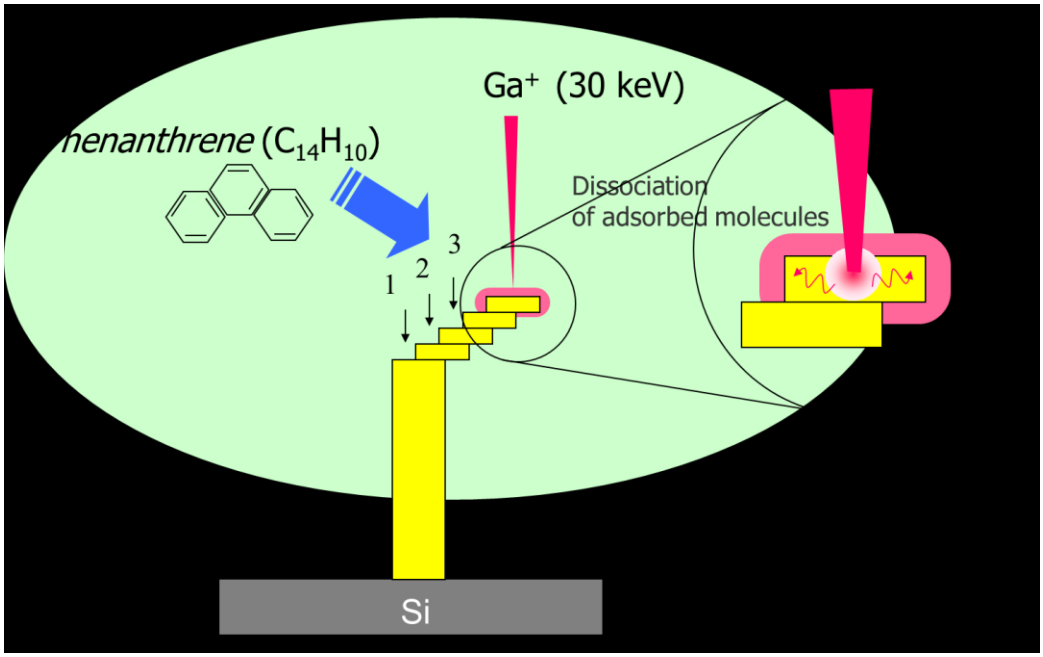

Fig. 1: Fabrication Process for three-dimensional nanostructure by FIB-induced CVD.

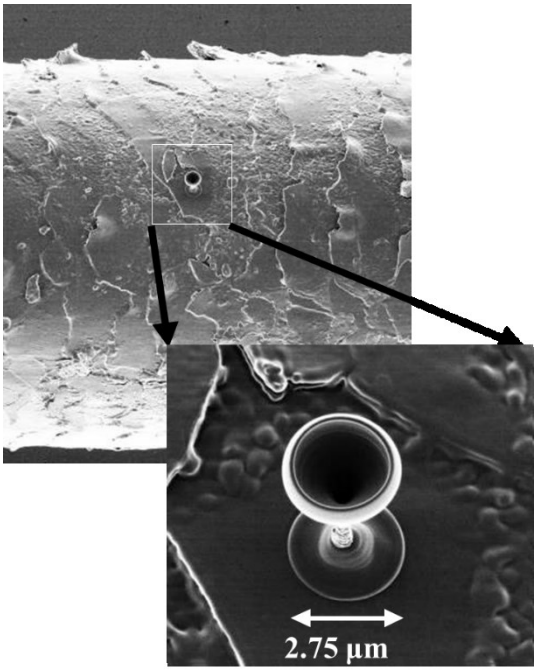

Fig. 2: Micro-wine-glass with an external diameter of 2.75 µm and a height of 12 µm on a human hair.

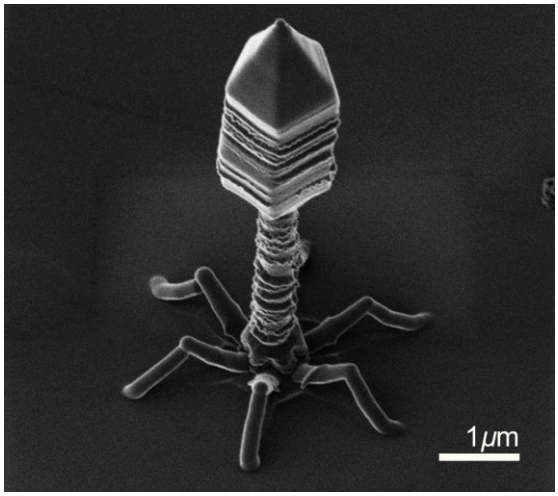

Fig. 3: T-4 Bacteriophage.

3D-Nanoprinting via FEBID – from Growth Fundamentals to Applications

R. Winkler[1,2], J. Sattelkow[1,2], J.D. Fowlkes[3,4], P.D. Rack[3,4], and H. Plank[1,2,5]*

[1] Institute of Electron Microscopy and Nanoanalysis, Graz University of Technology, 8010 Graz, Austria
[2] Christian Doppler Laboratory – DEFINE, Graz University of Technology, 8010 Graz, Austria
[3] Department of Materials Science and Engineering, University of Tennessee, Knoxville, Tennessee 37996, USA
[4] Center for Nanophase Materials Sciences, Oak Ridge National Laboratory, Oak Ridge, Tennessee 37831, USA
[5] Graz Centre for Electron Microscopy, 8010 Graz, Austria

* Corresponding author: harald.plank@felmi-zfe.at

3D-printing of functional structures has become an important technology in research and development. While being reliable on the micro and sub-micron scale, it gets very challenging when aiming for nano-sized geometries. Among the very few direct-write techniques on that scale, Focused Electron Beam Induced Deposition (FEBID) is one of the promising candidates [1] as this technology has recently taken tremendous steps forward. Comprehensive experiments [2] and 3D-simulations [3] have led to a deeper understanding of the growth fundamentals, enabling the reliable and reproducible direct-write fabrication of 3D-geometries with a high degree of complexity (Figure 1).

The contribution starts with a brief overview on the recent progress, which leverages this technology from a scientifically oriented fabrication tool into the status of a reliable and predictable 3D-nanoprinter [2,3]. This also includes the introduction of a user-friendly CAD-design software (3BID) that allows an almost straightforward printing of highly complex architectures [4]. To get a deeper insight in the growth characteristics for 3D-structures, considerations on the most important process parameters, their mutual relationships and the shapes of single elements are discussed (Figure 2a,b) [2]. Furthermore, we evaluate the possibility to tune material properties by using different precursor materials or post-treatment procedures [5] (Figure 2c).

These advances open up new possibilities for applications in research and development. Thus, we present some application examples of this generic fabrication technology in the field of 3D-nano-plasmonics [5], 3D-geometries with magnetic frustration [6, 7] and 3D nano-probe concepts for advanced AFM (Figure 3). Finally, the talk gives an overview of ongoing activities, remaining challenges together with future perspectives.

References

[1] L. Hirt, A. Reiser, R. Spolenak, T. Zambelli, *Additive Manufacturing of Metal Structures at the Micrometer Scale,* Adv. Mater. 29, 1604211 (2017).

[2] R. Winkler, B.B. Lewis, J.D. Fowlkes, P.D. Rack, H. Plank, *High-Fidelity 3D-Nanoprinting via Focused Electron Beams: Growth Fundamentals,* ACS Appl. Nano Mater. 1, 1014-1027 (2018).

[3] J.D. Fowlkes, R. Winkler, B.B. Lewis, M.G. Stanford, H. Plank, P.D. Rack, *Simulation-Guided 3D-Nanomanufacturing via Focused Electron Beam Induced Deposition,* ACS Nano 10, 6163-6172 (2016).

[4] J.D. Fowlkes et al., *High-Fidelity 3D-Nanoprinting via Focused Electron Beams: Computer-Aided Design (3BID),* ACS Appl. Nano Mater. 1, 1028-1041 (2018).

[5] R. Winkler, F.P. Schmidt, U. Haselmann, J.D. Fowlkes, B.B. Lewis, G. Kothleitner, P D. Rack, H. Plank, *Direct-Write 3D Nanoprinting of Plasmonic Structures,* ACS Appl. Mater. Interfaces 9, 8233-8240 (2017).

[6] L. Keller, M. Al Mamoori, J. Pieper, C. Gspan, I. Stockem, C. Schröder, S. Barth, R. Winkler, H. Plank, M. Pohlit, J. Müller, M. Huth, *Direct-write of free-form 3D nanostructures with controlled magnetic frustration*, Sci. Rep. accepted (2018).

[7] M. Al Mamoori, L. Keller, J. Pieper, S. Barth, R. Winkler, H. Plank, J. Müller, M. Huth, *Magnetic Characterization of Direct-Write Free-Form Building Blocks for Artificial Magnetic 3D Lattices,* Materials 11, 289 (2018).

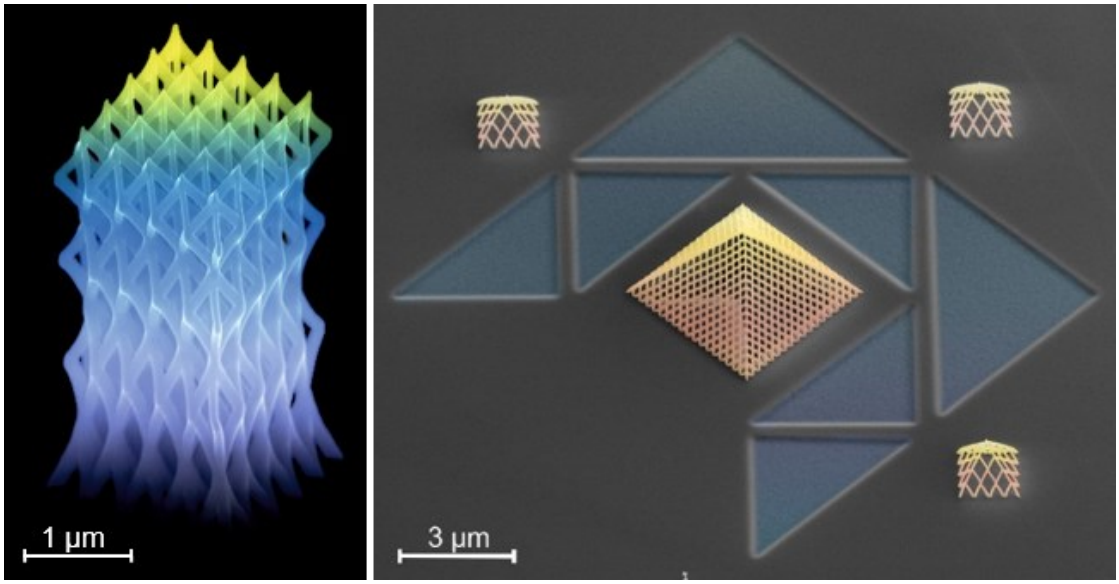

Fig. 1: Representatives for 3D-nanoprinting via FEBID [5]. Sponge fabricated from $MeCpPtMe_3$ (left). Miniature of the glass pyramids of the Louvre, Paris printed on a FIB-pre-structured silicon wafer (right).

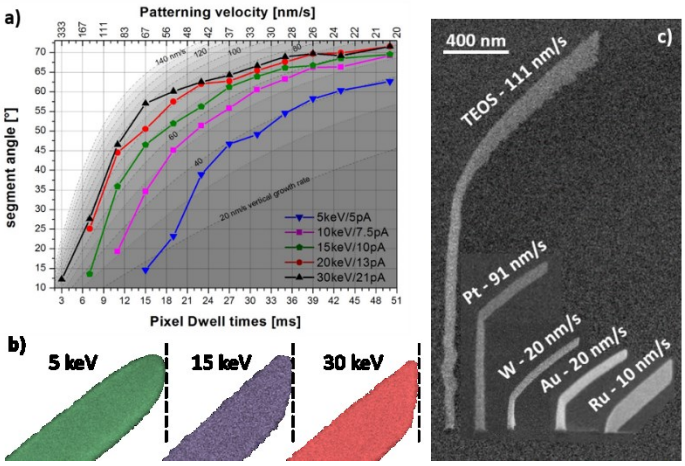

Fig. 2: 3D growth characteristics. a) Segment angles as a function of the Pixel Dwell times at a fixed point pitch of 1 nm [2]. The end cap shapes shown in b) expose influences of the primary energy. c) 3D growth for different precursor materials for diving boards with an inclination angle of about 45° [2].

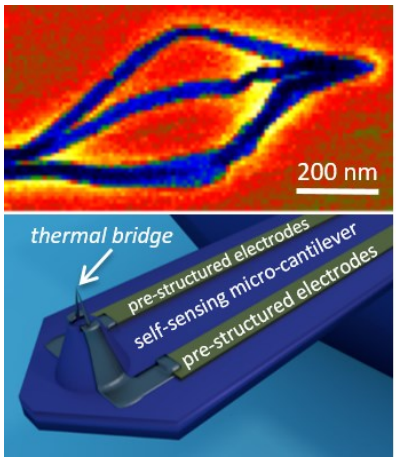

Fig. 3: Top: plasmonic activity of a gold 3D-geometry. STEM-EELS map of a tetragonal-bipyramid fabricated from $Me_2Au(acac)$ and purified in water vapor under electron exposure [5]. Bottom: Concept of a thermal 3D nano-probe deposited on a tip of a self-sensing AFM cantilever for accessing surface temperature properties.

Direct Printing of 3D Nano-Structures via Focused Electron Beam Induced Deposition: Pattern Generation

L. Keller and M. Huth*

Institute of Physics, Goethe University, Max-von-Laue-Str. 1, 60438 Frankfurt am Main, Germany

* Corresponding author: michael.huth@physik.uni-frankfurt.de

Fabrication of three-dimensional (3D) nano-architectures by focused electron beam induced deposition (FEBID) has matured to a level that highly complex and functional deposits are becoming available for nanomagnetics [1,2] and plasmonics [3]. The main issue of generating a desired 3D nano-structure is the control of the electron beam in the x-y-plane. However, the generation of suitable pattern files that define the electron beam deflection at any time during the deposition and reliably map the desired target 3D structure from a purely geometrical description to a shape-conforming 3D deposit is non trivial.

Here we present our implementation of a pattern file generator that handles proximity effects (see Fig. 1), corrects for height-dependent precursor coverage (Fig. 2) and can avoid shadowing effects regarding the directed component of the precursor flux if necessary. Several examples of successful 3D nano-fabrication using different precursors are presented that attest the effectiveness of the implementation. We also demonstrate the possibility to use different precursors for different parts of a 3D nano-structure (Fig. 3).

The implementation of the algorithms is done in C++ for speed, flexibility and independence from other software with no dependencies on non-standard C++ libraries.

References

[1] L. Keller, M.K.I. Al Mamoori, J. Pieper, C. Gspan, I. Stockem, C. Schröder, S. Barth, R. Winkler, H. Plank, M. Pohlit, J. Müller, M. Huth, *Direct-write of free-form building blocks for artificial magnetic 3D lattices*, Scientific Reports 8, 6160 (2018).

[2] M.K.I. Al Mamoori, L. Keller, J. Pieper, S. Barth, R. Winkler, H. Plank, J. Müller, M. Huth, *Magnetic Characterization of Direct-Write Free-Form Building Blocks for Artificial Magnetic 3D Lattices*, Materials 11, 289 (2018).

[3] R. Winkler, F.P. Schmid, U. Haselmann, J.D. Fowlkes, B.B. Lewis, G. Kothleitner, P.D. Rack, H. Plank, *Direct-Write 3D Nanoprinting of Plasmonic Structures*, ACS Appl. Mater. Interfaces 9, 8233−8240 (2017).

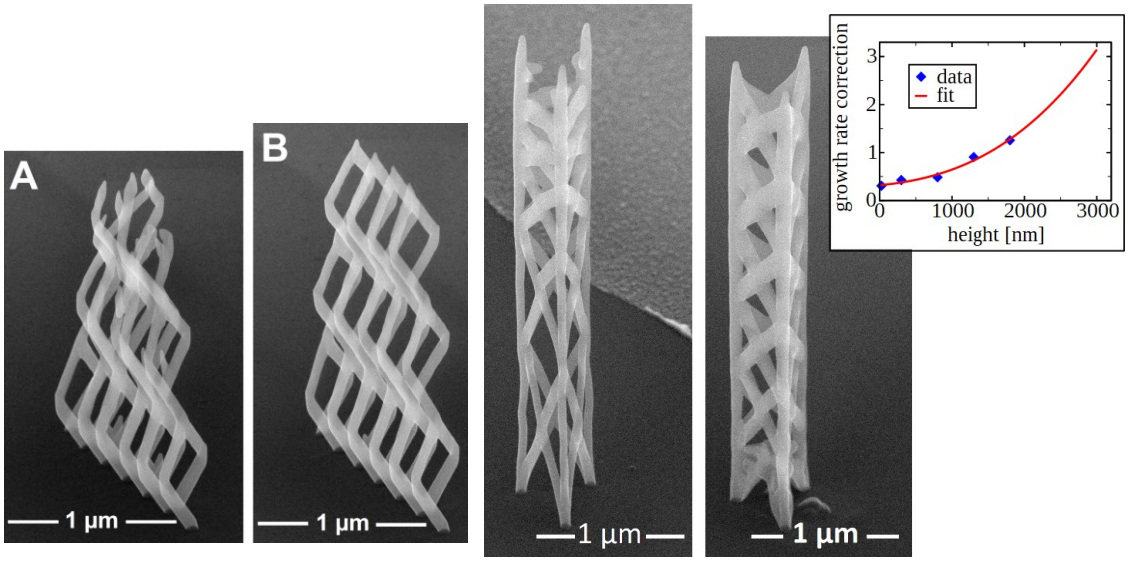

Fig. 1: The order of dwell points meanwhile deposition is crucial due to precursor dynamics. The pattern generator offers different, more or less complex proximity effect avoiding algorithms. The better one provided structure B whereas the cheaper one failed to reproduce the three coils on top of each other in A.

Fig. 2: Meanwhile deposition precursor is consumed in the writing area. For a subsequent deposition step precursor has to replenish. The higher the deposition area is, the slower becomes the precursor replenishment and the growth rate drops. Without correcting this effect deposit A was obtained. By compensating the growth rate with a polynomial of order three, shown on the right, deposit B exhibits equidistant plateaus.

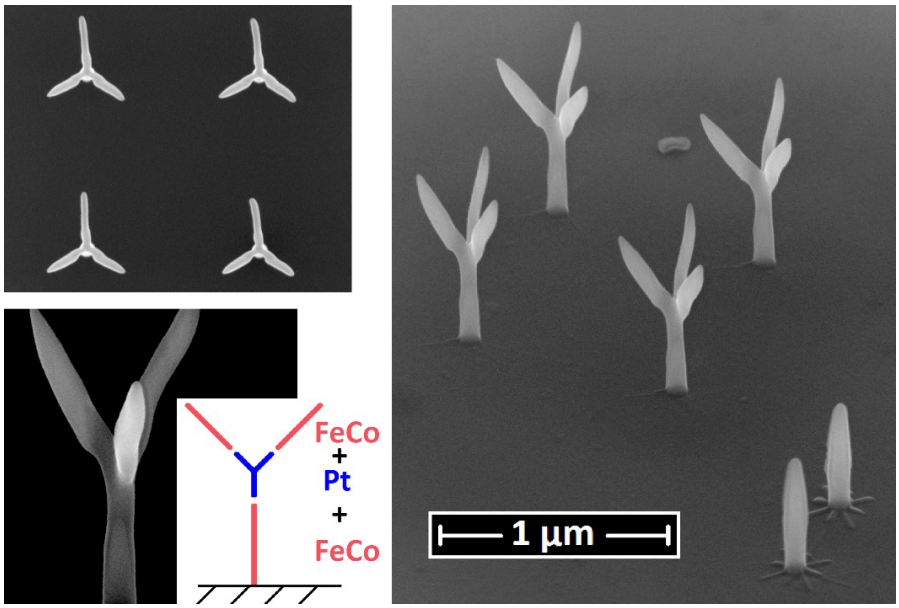

Fig. 3: 2x2-array of trees consisting of a root and branches deposited with the precursor $HCo_3Fe(CO)_{12}$ and a connecting node in the middle of each tree deposited with the precursor $Me_3CpMePt(IV)$. In the bottom right corner two pillars, serving as markers, are visible. On each pillar is a thin star, which was used for aligning the second (Pt) and third (CoFe) deposition. The pillars are part of the first pattern-file. Every star is part of either the second or the third pattern-file. They are available by a single line in the geometry file. The upper left picture shows a top view.

Three-dimensional injection and motion of magnetic information using FEBID 3D nanowires

A. Fernández-Pacheco[1]*, D. Sanz-Hernández[1], L. Skoric[1], A. Welbourne[1], J.W. Liao[1], R. Hamans[2], R. Lavrijsen[2], J.D. Fowlkes[3], and P. Rack[3]

[1] Cavendish Laboratory - University of Cambridge, JJ Thomson Avenue CB3 0HE Cambridge, United Kingdom
[2] Department of Applied Physics, Eindhoven University of Technology, P.O. Box 513, 5600 MB Eindhoven, The Netherlands
[3] Center for Nanophase Materials Sciences, Oak Ridge National Laboratory, Oak Ridge, Tennessee 37831, United States

* Corresponding author: af457@cam.ac.uk

Three-dimensional (3D) nanomagnetism is an exciting new area of research, with potential applications in fields such as data storage, nanoelectronics and biology. In 3D nanomagnets, new physical effects emerge, with geometry, topology and chirality becoming interlinked [1].

Acting as a 3D nano-printer, Focused Electron Beam Induced Deposition (FEBID) is currently the nanofabrication technique most capable of prototyping 3D nanostructures [2]. In particular, the usage of magnetic organo-metallic precursors enables to create 3D magnetic nano-objects for advanced magnetic studies [3].

In this talk, I will present our recent work in this area, where we have created ultra-advanced 3D magnetic devices based on nanowires for spintronic applications [4]. By exploiting a hybrid growth technique comprising FEBID fabrication using $(CH_3)_3(CH_3)CpPt$ as precursor, followed by thermal evaporation (Fig. 1), we have created 3D magnetic nanowires formed by Permalloy. Nanowire networks made of this material can be exploited as memory, logic and sensing devices, with magnetic information transmitted in the form of domain walls [5]. To finely control the wire geometry, a two-pitch scanning strategy has been developed, which enables to define wires of different widths [6]. The two-step lithography method here developed results in high-quality nanowires forming a fixed angle with respect to the substrate plane, which acts as a magnetic domain source. In addition, the FEBID growth of 2D-to-3D nanowire-substrate interconnectors involves a constant gradient SEM scanning speed, favoring a smooth motion of domain walls.

In order to investigate the magnetic properties of such devices, we have developed a new magneto-optical method, the "Dark-Field Kerr effect" [4] (Fig. 1), which exploits the geometry of 3D nanostructures to probe different active magnetic planes. This new technique has allowed us to determine simultaneously and independently the magnetic switching of the substrate and a single nanowire (Fig. 2). By constructing magnetic switching diagrams, the symmetry of the magnetic system during reversal can be directly inferred. We have compared such symmetries for interconnected nanowires and control nanostructures, where nanowire and substrate have been intentionally disconnected using additional shadowing bridges. Thanks to this method, it is possible to infer the reversal mechanism of the wires under external magnetic fields, dominated by magnetostatic interactions, as well as to determine what are the nucleation, propagation and transmission magnetic fields of these devices, which compare well with state-of-the-art 2D Permalloy nanowires. Moreover, and exploiting the 3D susceptibility of these devices to vector (B_x, B_y, B_z) moderate magnetic fields, we have operated these devices under complex magnetic field sequences, leading to advanced 3D motion and gating of magnetic information (Fig. 3).

The fabrication (involving FEBID 3D nano-printing) and optical detection methods presented in this work provide a new and powerful platform for the study of 3D magnetic nanostructures, naturally extensible to more complex materials and geometries.

We acknowledge funding from EPSRC grants EP/M008517/1 and EP/L015978/1, the Winton Program for the Physics of Sustainability, the Royal Society and the CELINA COST EU Action CM1301.

References

[1] A. Fernández-Pacheco et al., *Three dimensional nanomagnetism*, Nature Comm. 8, 15756 (2017).

[2] J. Fowlkes et al., *High-Fidelity 3D-Nanoprinting via Focused Electron Beams: Computer-Aided Design (3BID)*, ACS Appl. Nano Mater. 1, 1028 (2018).

[3] M.K.I. Al Mamoori et al., *Magnetic Characterization of Direct-Write Free-Form Building Blocks for Artificial Magnetic 3D Lattices*, Materials 11, 289 (2018).

[4] D. Sanz-Hernández et al, *Fabrication, detection and operation of a three-dimensional nanomagnetic conduit*, ACS Nano 11, 11066 (2017).

[5] S. Parkin et al., *Memory on the racetrack*, Nature Nanotechnology 10, 195 (2015).

[6] D. Sanz-Hernández et al, *3D nano-printed magnetic nanowires for domain wall motion studies*, Nanomaterials, in preparation (2018).

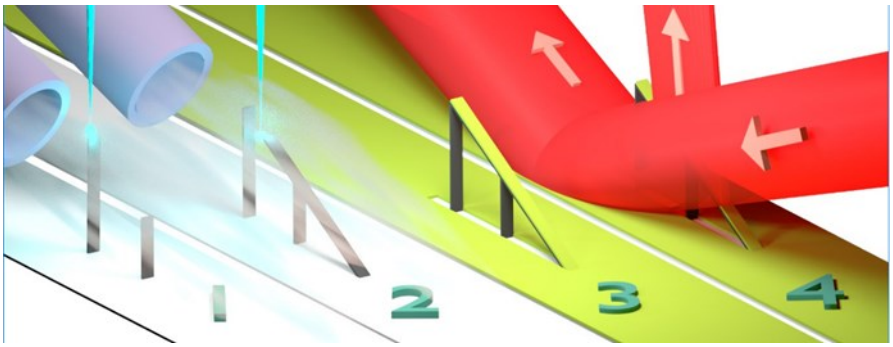

Fig. 1: Four-stage method followed in this work: 3D FEBID nano-printing (steps 1-2), evaporation (step 3) and Dark-Field magneto-optical detection (step 4) of 3D magnetic nanowires.

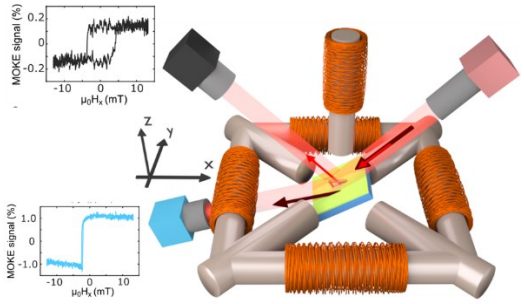

Fig. 2: Dark-Field MOKE technique for advanced magneto-optical probing of 3D nanostructures.

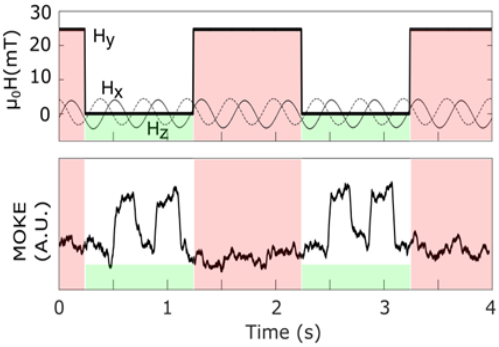

Fig. 3: Magnetic information injection, propagation and gating in a 3D magnetic nanowire, controlled via vector external magnetic fields.

FEBID fabrication of individual magnetic nanostructures and nanoactuated magneto-mechanical systems

P. Vavassori[1,2]*, M. Pancaldi[1], M.J. Perez-Roldan[1], A. Berger[1], and A. Chuvilin[1,2]

[1] CIC nanoGUNE Consolider, 20018 Donostia-San Sebastian, Spain
[2] IKERBASQUE, Basque Foundation for Science, 48013 Bilbao, Spain

* Corresponding author: p.vavassori@nanogune.eu

Besides more traditional applications of nano-magnetism in the field of data storage technologies, new areas of utilization are emerging in recent years [1]. Relevant examples are the areas of nano-sensing, and nano-actuation for bio-medical applications, robotics, and energy harvesting These new avenues of application of nano-magnetism require the development of novel methodologies allowing for 3-dimensional (3D) nano-fabrication together with the combined use of different materials in a well-controlled manner.

This work gives first an illustration of the viability of advanced focused electron-beam induced deposition (FEBID) [2-7] to fabricate magnetic nano- and micro-structures and it demonstrates that by means of a combination of electronic and magneto-optical microscopy, one can analyze the size and shape effects in individual magnetic structures [4,5]. Furthermore, we show the capability of FEBID to fabricate functional and complex 3D magnetic structures [8-14]. Specifically, we explored the utilization of FEBID for the nano-fabrication of heterogeneous [11-13], multi-functional nano-structures (see examples in Fig. 1) that allowed us to demonstrate a novel approach to remote-actuation with sub-nm scale precision, high linearity, and reproducibility [14]. This approach is radically different from generally pursued strategies based upon down-scaling the existing micro-electro-mechanical-systems technology since it relies on a new class of nanoactuated-magneto-mechanical systems remotely addressable by a magnetic external stimulus. As they do not require physical contact to be operated, have the potential to be employed in diverse environments, such as liquids or even inside living organisms, opening new avenues to bio-applications and nano-robotic systems, which are thought to be key technologies for the upcoming decades.

References

[1] D. Sander et al., *The 2017 Magnetism Roadmap*, J. Phys. D: Appl. Phys.50, 363001 (2017).

[2] M. Huth et al., *Focused electron beam induced deposition meets materials science*, Beilstein J. Nanotechnol. 3, 597(2012).

[3] L. Serrano-Ramón et al., *Ultrasmall functional ferromagnetic nanostructures grown by focused electron-beam-induced deposition*, ACS Nano 5, 7781 (2011).

[4] E. Nikulina et al., *Magneto-optical magnetometry of individual 30nm cobalt nanowires grown by electron beam induced deposition*, Appl. Phys. Lett. 100, 142401 (2012).

[5] E. Nikulina et al., *Origin and control of magnetic exchange coupling in between focused electron beam deposited cobalt nanostructures*, Appl. Phys. Lett. 103, 123112 (2013).

[6] O. Idigoras et al., *FEBID fabrication and magnetic characterization of individual nano-scale and micro-scale Co structures*, Nanofabrication 1, 23 (2014).

[7] J.M. De Teresa et al., *Review of magnetic nanostructures grown by focused electron beam induced deposition (FEBID)*, J. Phys. D: Appl. Phys. 49, 243003 (2016).

[8] A. Fernández-Pacheco et al., *Three-dimensional magnetic nanowires grown by focused electro-beam induced deposition*, Sci. Rep. 3, 1492 (2013).

[9] A. Berger, *Viewpoint on 'Tuning shape, composition and magnetization of 3D cobalt nanowires grown by focused electron beam induced deposition (FEBID)*, J. Phys. D: Appl. Phys. 50, 231002 (2017).

[10] J. Pablo-Navarro et al., *Tuning shape, composition and magnetization of 3D cobalt nanowires grown by focused electron beam induced deposition (FEBID)*, J. Phys. D: Appl. Phys. 50, 18LT01 (2017).

[11] M. Winhold et al., *Binary Pt-Si Nanostructures prepared by Focused Electron-Beam-Induced Deposition*, ACS Nano 5, 9675 (2011).

[12] M.J. Perez-Roldan et al., *Segregation of materials in double precursor electron-beam-induced-deposition: a route to functional magnetic nanostructures*, Nanotechnology 26, 375302 (2015).

[13] J. Pablo-Navarro et al., *Three-dimensional core–shell ferromagnetic nanowires grown by focused electron beam induced deposition*, Nanotechnology 27, 285302 (2016).

[14] P. Vavassori et al., *Remote Magnetomechanical Nanoactuation*, Small 12, 1013 (2016).

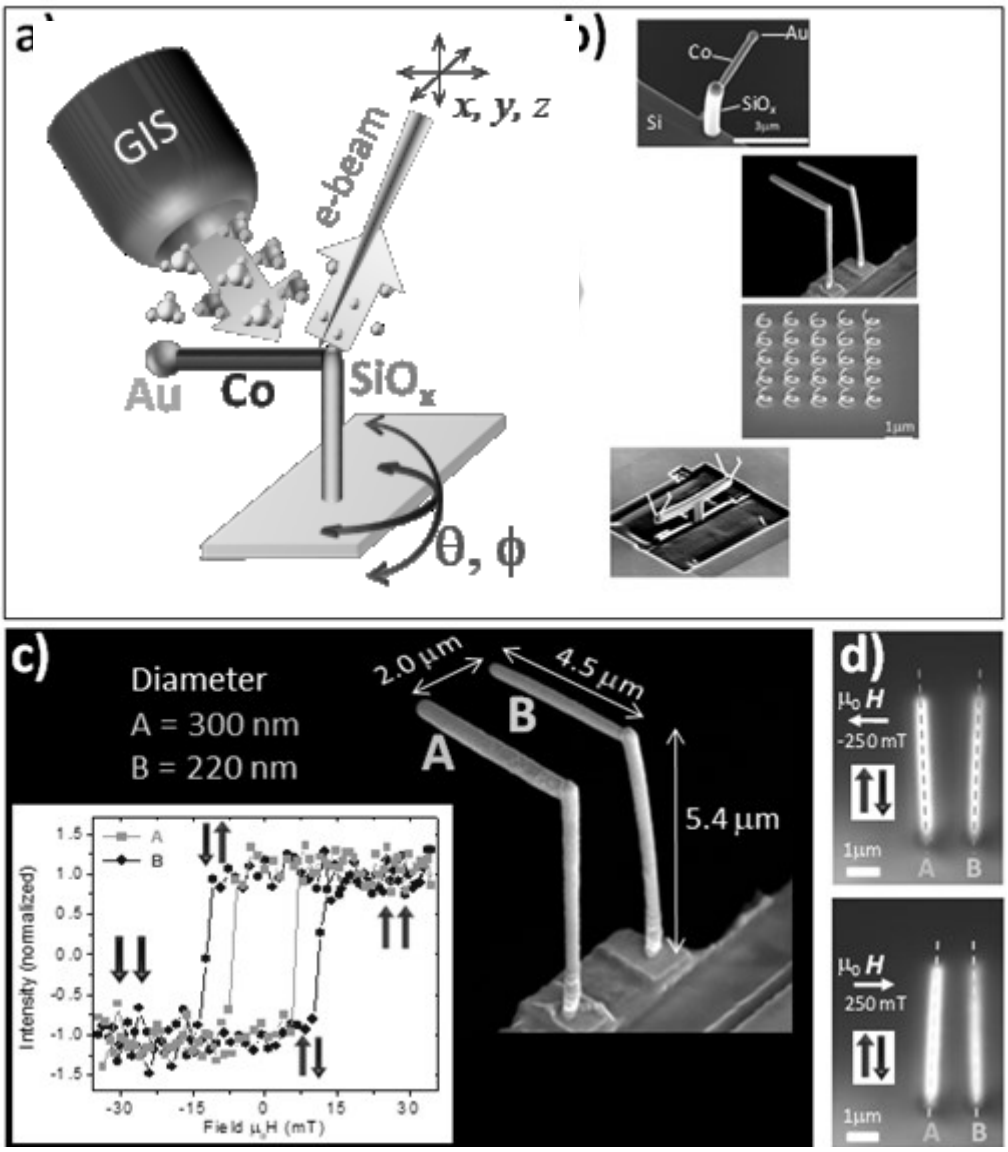

Fig. 1: a) Schematic of advanced 3D FEBID. b) SEM images of 3D nano-actuated-magneto-mechanical devices. c) SEM image of a nano-actuated-magneto-mechanical double-cantilever device with two suspended Co nano-rods: the inset shows micro-MOKE hysteresis loops of the suspended nano-rods. d) Snap-shots of a video showing the remote magnetic activation of the nano-actuated-magneto-mechanical double-cantilever device [14].

Magnetic Force Microscopy (MFM) probes by FEBID and their application

J. Pablo-Navarro[1], C. Magén[1,2], E. Berganza[3], M. Jaafar[3], A. Asenjo[3], and J.M. De Teresa[1,2]*

[1] Laboratorio de Microscopías Avanzadas (LMA) - Instituto de Nanociencia de Aragón (INA), Universidad de Zaragoza, 50018 Zaragoza, Spain

[2] Instituto de Ciencia de Materiales de Aragón (ICMA), Universidad de Zaragoza-CSIC, 50009 Zaragoza, Spain

[3] Instituto de Ciencia de Materiales de Madrid (ICMM), CSIC, 28049 Madrid, Spain

* Corresponding author: deteresa@unizar.es

Focused Electron Beam Induced Deposition (FEBID) was used in the past to grow magnetic tips of width ≈50 nm with potential application in Magnetic Force Microscopy (MFM) [1,2]. In order to show that FEBID tips are superior than standard MFM tips and can give rise to the next-generation commercial MFM tips, dedicated experiments need to be carried out. Here, we report on our efforts to optimize the MFM tips grown by FEBID and we compare their behavior to that of standard MFM tips.

We have grown Co and Fe nanowires on various types of tips and under different growth conditions. The tips have been tested in MFM experiments, in ambient conditions as well as in liquid environment, behaving appropriately in terms of mechanical stability, resolution and sensitivity [3]. In the example shown in Figure 1, using the $Fe_2(CO)_9$ precursor gas and 30 kV electron beam acceleration, it can be noticed that is possible to grow Fe tips with 34 nm in diameter and finalized in a 7 nm-wide sharp end. This is very useful to achieve very high resolution in the MFM experiments as well as relatively low sample-tip magnetic interaction to minimize the influence of the magnetic tip on the magnetic state of small structures [4]. Transmission Electron Microscopy (TEM), Electron-Energy Loss Spectroscopy (EELS) and Electron Holography (EH) have been carried out to characterize the structural, compositional and magnetic properties of these tips, as shown in Figure 2. The Fe content is found to decrease as the tip end is approached, which influences the magnetization value and the magnetic stray fields generated around the tip end. The EH results allow mapping the value of the magnetic stray field as a function of the distance to the tip end [5], which is useful towards quantitative MFM measurements.

References

[1] I. Utke et al., *High-Resolution Magnetic Co Supertips Grown by a Focused Electron Beam*, Appl. Phys. Lett. 80, 4792 (2002).

[2] M. Gavagnin et al., *Free-Standing Magnetic Nanopillars for 3D Nanomagnet Logic*, ACS Appl. Mater. & Inter. 6, 20254 (2014).

[3] M. Jaafar et al., *System for an Atomic Force Microscope*, Spanish patent ES1641.1290, submitted.

[4] E. Berganza et al., *Observation of hedgehog skyrmions in sub-100 nm soft magnetic nanodots*, submitted to Nature Communications. Arxiv.: 1803.08768.

[5] J. Pablo-Navarro et al., manuscript in preparation.

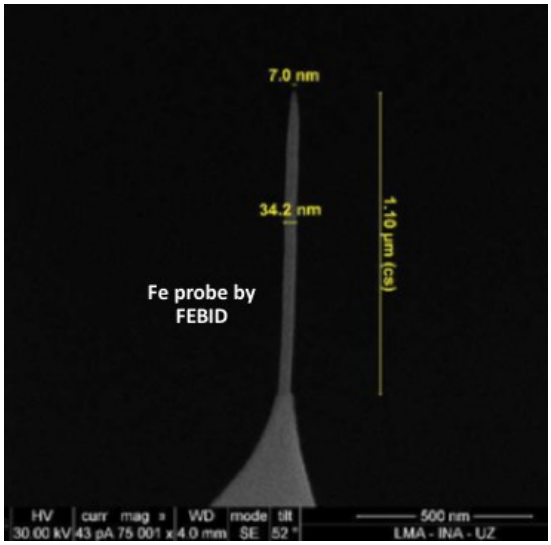

Fig. 1: SEM micrograph of an Fe nanowire grown at the apex of a tip for subsequent MFM experiments. The main nanowire's diameter is 34 nm but the end of the nanowire is only 7 nm.

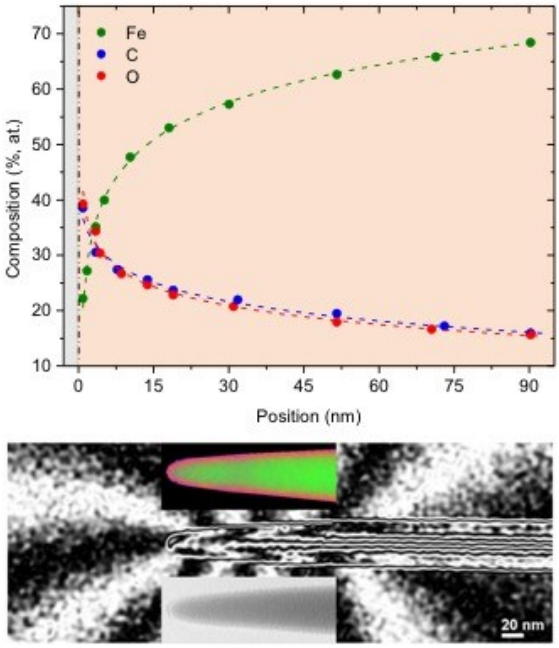

Fig. 2: TEM characterization of one Fe nanowire grown at the apex of a tip. EELS chemical maps indicate that the Fe content (in green colour) grows from very low values at its end up to 70% at a distance of 90 nm inside the nanowire. Electron holography measurements indicate that whereas the magnetization saturation is high in the inner part of the nanowire, it decreases as the end is approached, with the corresponding impact on the distribution of stray fields in the surroundings of the tip.

Tuning and in-situ monitoring the Hall resistivity of ferromagnetic FEBID structures

R. Sachser* and M. Huth

Physikalisches Institut, Goethe-Universität, 60438 Frankfurt am Main, Germany

* Corresponding author: sachser@physik.uni-frankfurt.de

In granular ferromagnetic systems an enhanced anomalous Hall effect was observed by Pakhomov et al. [1]. Conventional ferromagnetic films typically show Hall resistivities below 1μΩcm, whereas in granular systems the effect increases and close to a metal-to-insulator transition values up to 160μΩcm were observed. FEBID seems as an ideal preparation technique for such systems, as for many precursors the resulting deposits have directly an intrinsic granularity. Indeed, Córdoba et al could show an enhanced Hall resistivity in FEBID deposits by use of the precursor $Fe_2(CO)_9$ in conjunction with water vapor via a controllable leak that led to a reduced deposit conductivity [2].

In this contribution we will show our approach to prepare such systems via co-deposition of two precursors: $HFeCo_3(CO)_{12}$ and $(CH_3)_3CH_3C_5H_4Pt$. $HFeCo_3(CO)_{12}$ is an excellent FEBID precursor, which allows the deposition of magnetic and metallic CoFe alloy nanostructures [3]. The resulting deposits show a resistivity of 43μΩcm and are far away from the metal-to-insulator transition in the metallic regime. In contrast, the widely used $(CH_3)_3CH_3C_5H_4Pt$ standard precursor results in insulating deposits, consisting of Pt nanograins embedded in a carbonaceous matrix. Via post electron beam irradiation, the deposits allow for a wide tunability of their transport characteristics from insulating to metallic [4].

We pursued the idea to combine the ferromagnetic properties of FeCo-deposits with the wide tunability of PtC-deposits by co-deposition of both precursors. Varying the deposition conditions, namely the Pt precursor flux, the combined metal content of the deposits can be controlled. The resulting composition measured by EDX for four deposits is shown in Figure 1. Increasing the Pt precursor flux, the metal content can be reduced from about 78 at% to 40 at%. As a result, the resistivity and the Hall resistivity of the samples varies.

In-situ measurements of the Hall resistivity directly inside the SEM are performed using the magnetic field provided by the immersion lens of the instrument. In Figure 2(a) the Hall resistivity at different magnetic fields is shown for samples of different metal content. In Figure 2(b) the Hall resistivity at 150mT is plotted against the resistivity of the samples. For lower metal content, an increase of the resistivity and of the Hall resistivity is observed. It has to be noted, that the maximum field available at the sample position inside the SEM is about 150mT. For comparison with other material systems, the measured values have to be scaled to saturation field. Assuming a saturation field of about 1T, for the lowest metal content the Hall resistivity increases to about 18 μΩcm.

Further characterization of the structures is done via temperature-dependent electrical and magnetotransport measurements. In Figure 3 the normalized temperature dependence of the conductivity is shown. Decreasing the metal content, the transport characteristic is shifted towards a metal-to-insulator transition.

In addition, the co-deposited samples are sensitive to post-growth electron beam irradiation, which influences its electrical transport properties, as it is already known for normal FEBID deposits obtained by the Pt precursor. Using the immersion lens inside the SEM, the change of resistivity and Hall resistivity can be monitored directly during the irradiation.

References

[1] A.B. Pakhomov, X. Yan, Y. Xu, *Observation of giant Hall effect in granular magnetic films*, J. Appl. Phys. 79, 6140 (1996).

[2] R. Córdoba et al, *Giant anomalous Hall effect in Fe-based microwires grown by focused-electron-beam-induced deposition*, J. Phys. D: Appl. Phys. 45, 035001 (2012).

[3] F. Porrati, M. Pohlit, J. Müller, S. Barth, F. Biegger, C. Gspan, H. Plank, M. Huth, *Direct writing of CoFe alloy nanostructures by focused electron beam induced deposition from a heteronuclear precursor*, Nanotechnology 26, 465701 (2015).

[4] R. Sachser, F. Porrati, C. H. Schwalb, M. Huth, *Universal Conductance Correction in a Tunable Strongly Coupled Nanogranular Metal*, Phys. Rev. Lett. 107, 206803 (2011).

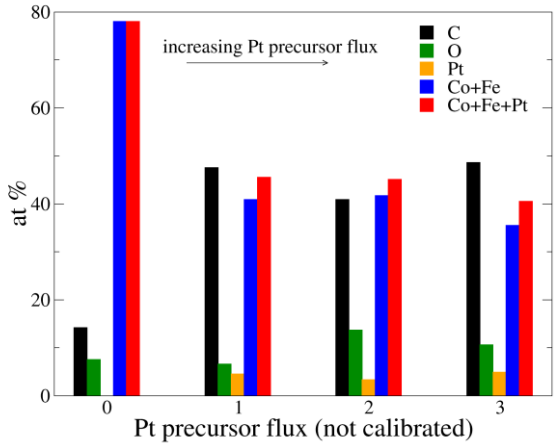

Fig. 1: Composition of four deposits obtained with different Pt precursor fluxes measured by EDX. The combined metal content is reduced from about 78 at% to 40 at%.

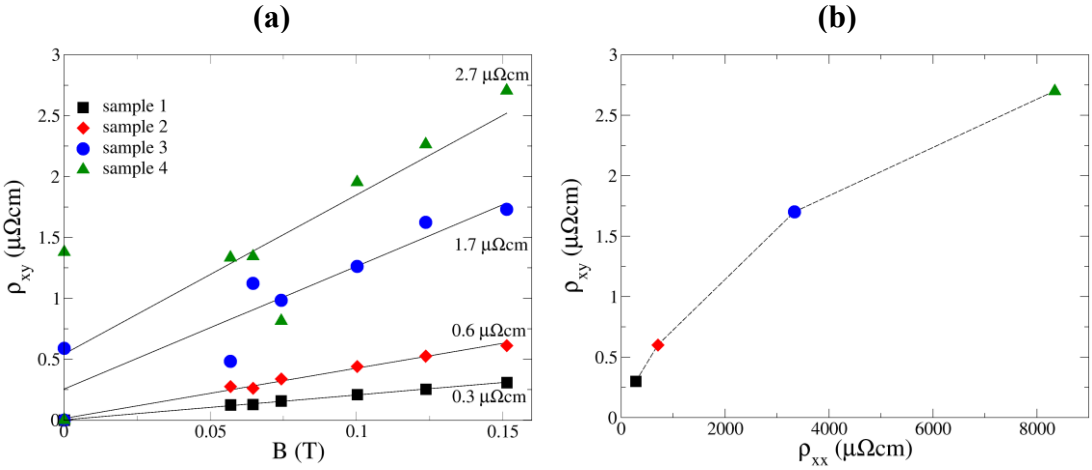

Fig. 2: **(a)** Hall resistivity as function of the magnetic field for samples with different metal content. The sample with the highest metal content shows the lowest Hall resistivity. **(b)** Hall resistivity at B=150mT plottet against resistivity. For lower metal content the resistivity and the Hall resistivity are enhanced.

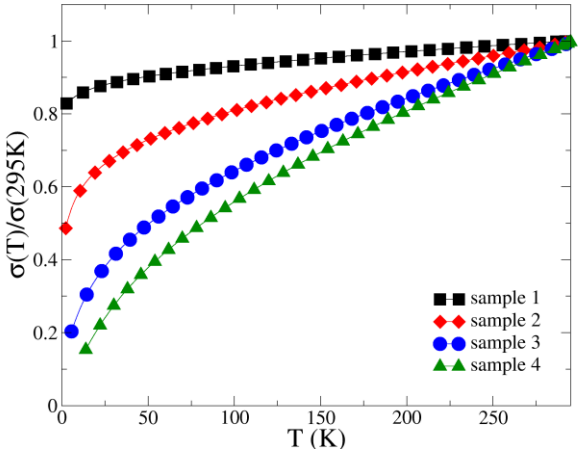

Fig. 3: Normalized conductivity for samples with different metal content. For samples with lower metal content the transport characteristics is shifted towards a metal-to-insulator transition.

Towards a simple and fast protocol for magneto-electrical properties enhancement of non-noble ferromagnetic nanocomposites grown by focused-electron-beam-induced deposition

M.V. Puydinger dos Santos[1,2]*, S. Barth[3], F. Béron[1], K.R. Pirota[1], J.A. Diniz[2], S. Moshkalev[2], and I. Utke[4]

[1] Institute of Physics Gleb Wataghin, University of Campinas, Rua Sérgio Buarque de Holanda 777 Cidade Universitária, 13083-859 Campinas-SP, Brazil

[2] Faculty of Electrical and Computing Engineering and Center for Semiconductor Components and Nanotechnologies, University of Campinas, Av. Albert Einstein 400, 13083-852 Campinas-SP, Brazil

[3] Institute of Materials Chemistry, TU Wien, Getreidemarkt 9/BC/02, A-1060 Vienna

[4] EMPA, Swiss Federal Laboratories for Material Science and Technology, Laboratory for Mechanics of Materials and Nanostructures, Feuerwerkerstrasse 39, 3602 Thun, Switzerland

* Corresponding author: puyding@ifi.unicamp.br

Nowadays, thin-films and multilayers based on magnetic materials present various applications in the fields of sensors and data storage. On the other hand, the possibilities of these applications could be pushed further by using individual magnetic nanostructures [1]. Although most of the approaches for their fabrication rely on standard lithography processes performed onto magnetic thin films, a growing interest exists on 3D magnetic nanostructures, whose fabrication remains challenging. Focused-electron-beam-induced deposition (FEBID) is a direct-write maskless technique that permits the growth of 3D nanostructures [2], in particular magnetic materials-based ones [3]. Deposition mechanism involves the dissociation of adsorbates induced by the FEB, leaving the non-volatile (metal) products. The unwanted simultaneous organic compounds co-deposition may either degrade the deposits electrical and magnetic properties, hence seriously limiting their applicability, or, when adequately controlled, generate complex systems yielding materials with enhanced properties. Here we present a postgrowth purification protocol, based on annealing under high vacuum [3,4], to deposits obtained from both $Co_2(CO)_8$ and $HFeCo_3(CO)_{12}$ carbonyl precursors in order to produce nanogranular systems with enhanced electrical and magnetic properties (Fig. 1). Our aim is to define by FEBID novel non-noble magnetic nanocomposites with improved electrical and magnetic properties. Focus is given to Co-based composites, obtained by low-cost precursors, to ultimately produce unique spin propagating medium. We achieved metallic thermal dependence, as well as more complex electronic transport processes. Remarkably, the intricate metal-C-O systems exhibited anisotropic magnetoresistance (AMR) signal up to around 1 order of magnitude larger than the few similar ones reported in literature [5,6]. It makes our material especially advantageous for future applications such as advanced scanning-probe systems, magnetic sensing and storage, and ferroelectric tunnel junction memristors. The physical basis behind the magneto-electric properties enhancement will be discussed.

References

[1] A. Fert, Nobel Lecture: *Origin, Development, and Future of Spintronics*, Rev. Mod. Phys. 80, 1517 (2008).

[2] J.D. Fowlkes et al., *High-Fidelity 3D-Nanoprinting via Focused Electron Beams: Growth Fundamentals*, ACS Appl. Nano Mater. 1 (3), 1028–1041 (2018).

[3] M.V. Puydinger dos Santos, et al., *Annealing-Based Electrical Tuning of Cobalt–Carbon Deposits Grown by Focused-Electron-Beam-Induced Deposition*, ACS Appl. Mater. Interfaces 8, 32496–32503 (2016).

[4] M.V. Puydinger dos Santos, et al., *Comparative Study of Post-Growth Annealing of $Cu(hfac)_2$, $Co_2(CO)_8$ and $Me_2Au(acac)$ Metal Precursors Deposited by FEBID*, Beilstein J. Nanotechnol. 9, 91–101 (2018).

[5] A. Fernández-Pacheco, J.M. De Teresa, R. Córdoba, M.R. Ibarra, *Magnetotransport Properties of High-Quality Cobalt Nanowires Grown by Focused-Electron-Beam-Induced Deposition*, J. Phys. D. Appl. Phys. 42 (5), 55005 (2009).

[6] F. Porrati, M. Pohlit, J. Müller, S. Barth, F. Biegger, C. Gspan, H. Plank, M. Huth, *Direct Writing of CoFe Alloy Nanostructures by Focused Electron Beam Induced Deposition from a Heteronuclear Precursor*, Nanotechnology 26 (47), 475701 (2015).

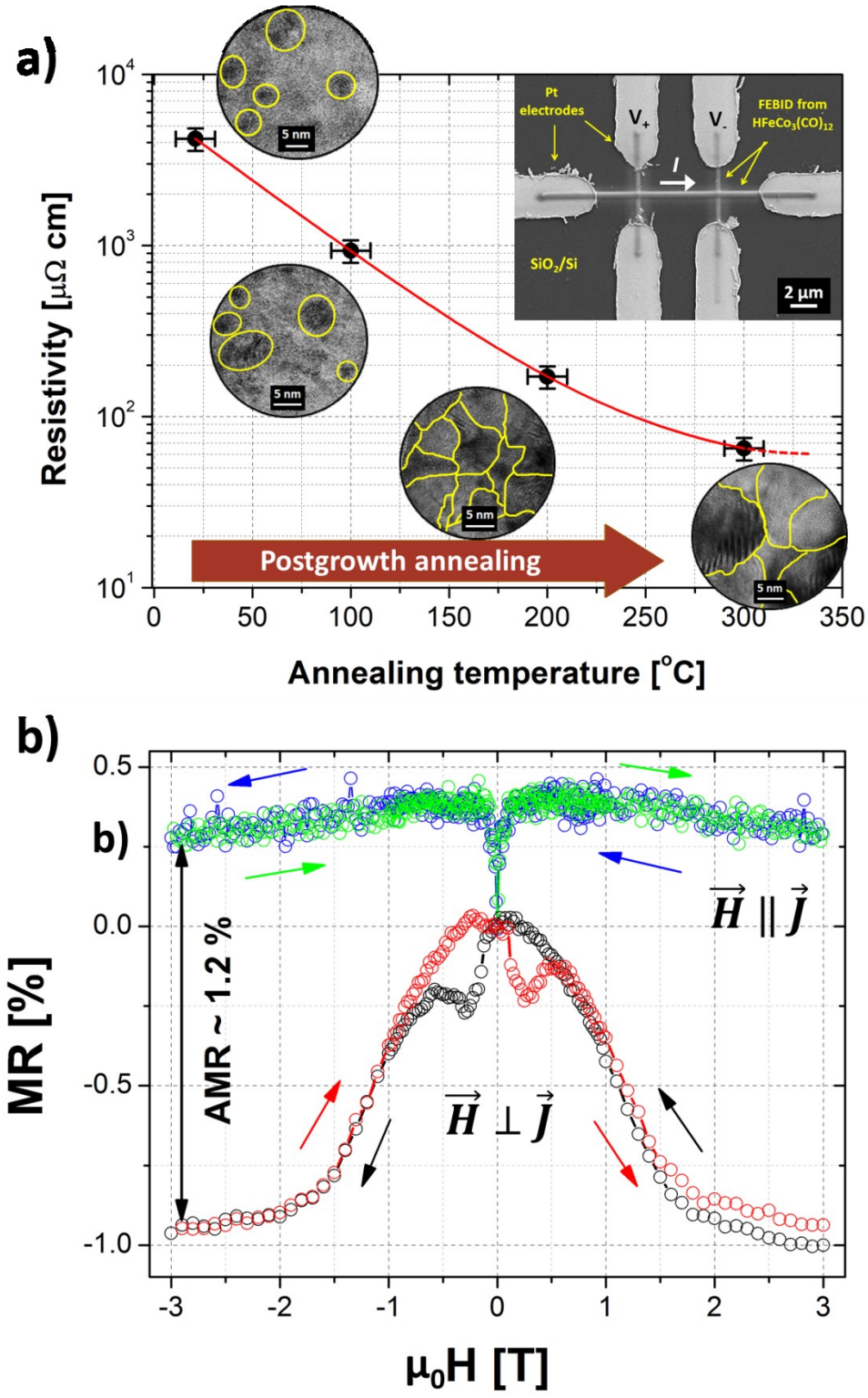

Fig. 1: Room temperature (a) resistivity and (b) magnetoresistance signal of FEBID material from $HFeCo_3(CO)_{12}$ as a function of, respectively, the postgrowth annealing temperature and the external magnetic field. Insets in (a) show top view SEM image of the FEBID structure on four point platinum electrodes taken at 5 keV and HRTEM images presenting grain percolation with the annealing temperature.

Nanomechanical Characterization of 3D FEBID Nanostructures

B.B. Lewis[1], B.A. Mound[1], B. Srijanto[2], J.D. Fowlkes[1,2] *, G.M Pharr[1,2,3], and P.D. Rack[1,2]

[1] Department of Materials Science and Engineering - University of Tennessee, Knoxville, TN 37996, USA
[2] Center for Nanophase Materials Sciences – Oak Ridge National Laboratory, Oak Ridge, TN 37831, USA
[3] Texas A&M

* Corresponding author: fowlkesjd@ornl.gov

A clear advantage of focused electron beam induced processing (FEBIP) is the ability to deposit structures on non–planar surfaces [1,2]. For this reason, focused electron beam induced processing is ideally suited for the deposition of nanoelectromechanical components, scanning probe microscopy tips and sensors; cases where suspended or sloped surfaces are often present. These applications will require the precise tuning of mechanical properties. For example, in the transduction geometry, the strain/deflection of the deposit is directly proportional to the detected electrical signal. Resonance based applications directly depend on the elastic modulus and the tuning of this property for selectivity [3]. Thus, knowledge of the mechanical properties of FEBIP structures [4,5] is a must toward realizing these potential applications.

Nanoidentation makes it possible to quantify the elastic modulus and hardness of materials deposited with nanoscale dimensions where size–dependent effects may influence material behavior. To this end, in–situ nanomechanical characterization was carried out under continuous secondary electron imaging using a Nanoflip^{TM} nanoindenter (Nanomechanics, Inc.) [6]. An elastic modulus of approximately 10 GPa was estimated for the standard deposit derived from the $MeCpPt^{IV}Me_3$ chemistry using both cantilever arm bend testing (~16 GPa) as well as compression testing (10 GPa). Experiments were conducted at a constant displacement rate of 1 nm/s and a data acquisition rate of 100 Hz to produce engineering stress versus engineering strain curves. Electron imaging occurs orthogonal to the compression axis making it possible to observe the time–dependent structural deformation. Only a qualitative estimate of the elastic modulus was achieved due to an apparent viscoelastic response, coupled with a limited number of experiments and imperfections in deposit geometry. Nonetheless, the modulus magnitude was consistent with past reports of this property and builds on the database of reported mechanical properties for FEBID deposits.

3D, mesh style objects were also studied considering the exceptional mechanical properties recently reported for symmetric, low fill factor metamaterials, at the > 100 nm length scale, achieved using two–photon lithography (TPL) [7]. The process flow extending from 3D design phase to the completion of mechanical testing will be presented. Considerable plastic deformation was observed for complex FEBID 3D mesh objects under extreme compression displacement. The degree of plastic deformation was reduced by the deposition of a ceramic Al_xO_y coating using atomic layer deposition. The coating was applied to the exterior surface of the deposit prior to compression testing and was found to strengthen the deposit where the elastic modulus increased by 30%. The non–equilibrium, metal nanoparticle/amorphous carbon composite nanostructure, typical of low temperature FEBID, was found to be stable during atomic layer deposition, at least up to an ALD temperature of roughly 200 ^{o}C. Beyond this temperature, the initial structure of the 3D mesh was deformed, presumably from carbon liberation from the deposits. Electrical measurements supported this hypothesis yielding a reduction in resistivity of the ALD coated structures at least in part explained by the increases in the metal-to-carbon ratio in the deposit.

References

[1] I. Utke, P. Hoffmann, J. Melngailis, *Gas-Assisted Focused Electron Beam and Ion Beam Processing and Fabrication,* J. Vac. Sci. Technol. B 26, 1197 (2008).

[2] M. Huth, F. Porrati, O.V. Dobrovolskiy, *Focused Electron Beam Induced Deposition meets Materials Science*, Microelec. Eng. 185-186, 9 (2018).

[3] G. Arnold, R. Winkler, M. Stermitz, A. Orthacker, J.N. Noh, J.D. Fowlkes, G. Kothleitner, M. Huth, P.D. Rack, H. Plank, *Tunable 3D Nanoresonators for Gas-Sensing Applications*, Adv. Func. Mat. 1707387 (2018).

[4] O. Satoshi et al., *Comparison of Young's Modulus Dependency on Beam Accelerating Voltage between Electron-Beam- and Focused Ion-Beam-Induced Chemical Vapor Deposition Pillars*, Jap. J. Appl. Phys. 45, 5556 (2006).

[5] V. Friedli, I. Utke, K. Molhave, J. Michler, *Dose and Energy Dependence of Mechanical Properties of Focused Electron-Beam-Induced Pillar Deposits from Cu($C_5HF_6O_2$)$_2$*, Nanotechnology 20, 385304 (2009).

[6] B.B. Lewis, B.A. Mound, B. Srijanto, J.D. Fowlkes, G.M. Pharr, P.D. Rack, *Growth and Nanomechanical Characterization of Nanoscale 3D Architectures grown via Focused Electron Beam Induced Deposition*, Nanoscale 9, 16349 (2017).

[7] L.R. Meza, A.J. Zelhofer, N. Clarke, A.J. Mateos, D.M. Kochmann, J.R. Greer, *Resilient 3D hierarchical architected metamaterials*, PNAS 112, 11502 (2015).

[8] J.D. Fowlkes et al., *High-Fidelity 3D-Nanoprinting via Focused Electron Beams: Computer-Aided Design (3BID)*, ACS Appl. Nano Mat. (2018).

[9] R. Winkler, B.B. Lewis, J.D. Fowlkes, P.D. Rack, H. Plank, *High-Fidelity 3D-Nanoprinting via Focused Electron Beams: Growth Fundamentals*, ACS Appl. Nano Mat. (2018).

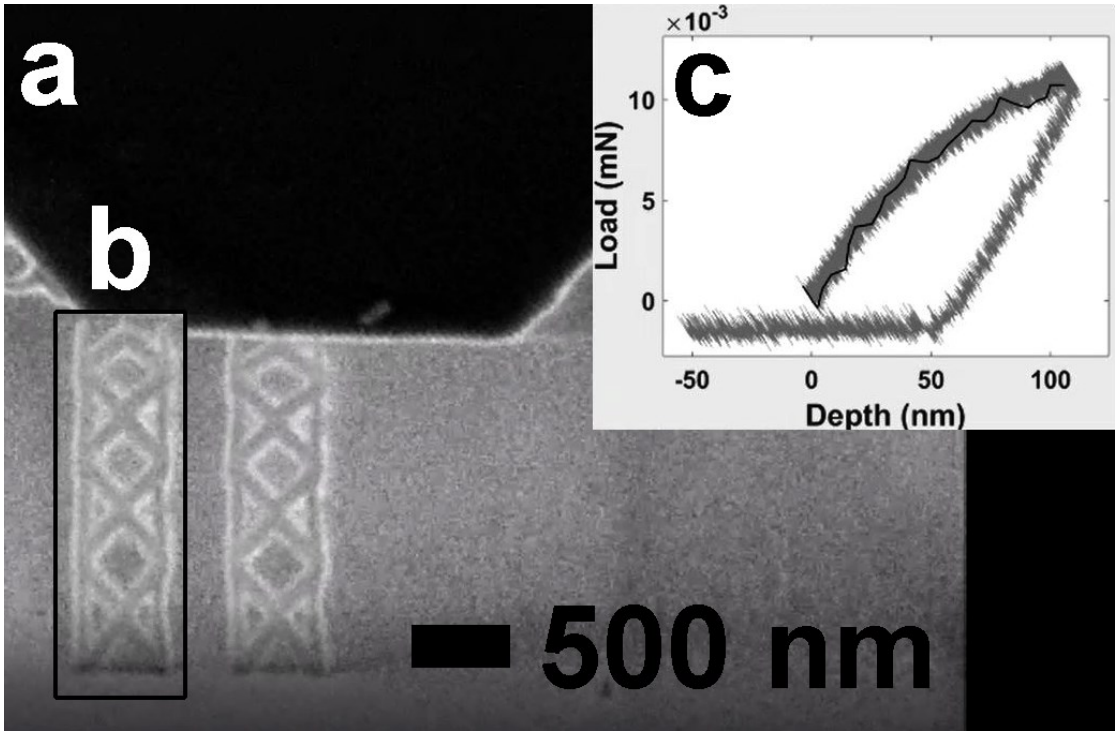

Fig. 1: (a) Secondary electron image captured during in–situ compression testing of a platinum–carbon metal matrix composite deposited by focused electron beam induced deposition and coated with 20 nm of Al_xO_y using atomic layer deposition (ALD). The secondary electron image was acquired orthogonal to the nanostructure during testing so that the time–dependent deformation can be observed. (b) The undeformed, as–deposited nanostructure prior to mechanical testing. The computer-aided design program 3BiD [8,9] was used to create the beam exposure path required to deposit the nanostructure. (c) Load–displacement data collected dynamically during compression testing makes it possible to estimate the magnitude of the elastic modulus of the deposit. The SE image shown in (a) was acquired following 100 nm of applied compression.

Mechanical Properties of 3D Nano-Architectures Fabricated via Focused Electron Beam Induced Deposition

J. Fröch[1,2], R. Winkler[1,3], J. Sattelkow[1,3], C. Schwalb[4], M. Winhold[4], E. Fantner[4], and H. Plank[1,3,5]*

[1] Institute of Electron Microscopy and Nanoanalysis, Graz University of Technology, 8010 Graz, Austria
[2] now at Institute of Biomedical Materials and Devices (IBMD), Faculty of Science, University of Technology Sydney, Ultimo, NSW, 2007, Australia
[3] Christian Doppler Laboratory – DEFINE, Graz University of Technology, 8010 Graz, Austria
[4] GETec Microscopy Inc. & SCL Sensor.Tech. Fabrication Inc., 1220 Vienna, Austria
[5] Graz Centre for Electron Microscopy, 8010 Graz, Austria

*Corresponding author: harald.plank@felmi-zfe.at

With the recent introduction of controlled 3D nano-printing via focused electron beam induced deposition [1], an entirely new range of applications such as nano-photonics [2], -mechanics [3], or -electronics comes within reach whose fabrication is extremely challenging or even impossible with alternative techniques. In this contribution, we focus on mechanical properties of freestanding 3D nano-architectures for atomic force microscopy (AFM) based application as high-resolution thermal nano-probes. During operation as such, these probes will experience relatively high pressures with respect to their nanoscale size, thus a deep understanding of the mechanical response under force load is necessary to optimize the geometry towards specific applications and to avoid eventual misinterpretation when utilized as nano-probes. A combined approach of finite element simulation, AFM based force spectroscopy and real-time imaging via scanning electron microscopy (Fig 1) is used to identify and compensate highly unwanted peculiarities and to understand the underlying mechanisms at hand. We discuss an unexpectedly strong influence of non-straight side branches as well as the consequences of fabrication mismatches on the lowest nanoscale, leading to non-linear mechanical behavior and morphological twisting (Fig 2a), respectively. Finally, after optimization, we demonstrate the basic imaging capability of the fabricated probes (Fig 2b) and overall demonstrate the high demands on nanoscale accuracy during 3D nano-printing to exploit the full potential in terms of predictable mechanical properties. In summary, we successfully derived the ideal design of FEBID based 3D nano-architectures for further application as AFM based thermal nano-probe as a central future perspective in future our research strategy.

References

[1] J.D. Fowlkes et al., *Simulation-guided 3D nanomanufacturing via focused electron beam induced deposition,* ACS nano 10.6, 6163-6172 (2016).

[2] R. Winkler et al., *Direct-write 3D nanoprinting of plasmonic structures,* ACS applied materials & interfaces 9.9, 8233-8240 (2016).

[3] G. Arnold et al., *Tunable 3D Nanoresonators for Gas-Sensing Applications,* Advanced Functional Materials 1707387 (2018).

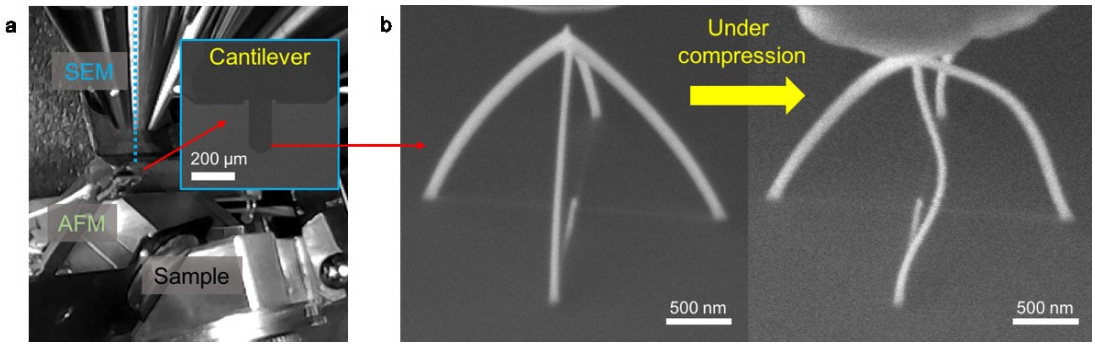

Fig. 1: Correlative *in-situ* force measurements. **a,** the combined AFM – SEM measurement setup. **b,** utilizing the combined approach 3D printed FEBID structures can be directly accessed and with a prepared cantilever the dynamic behavior of such structures can be studied under force load.

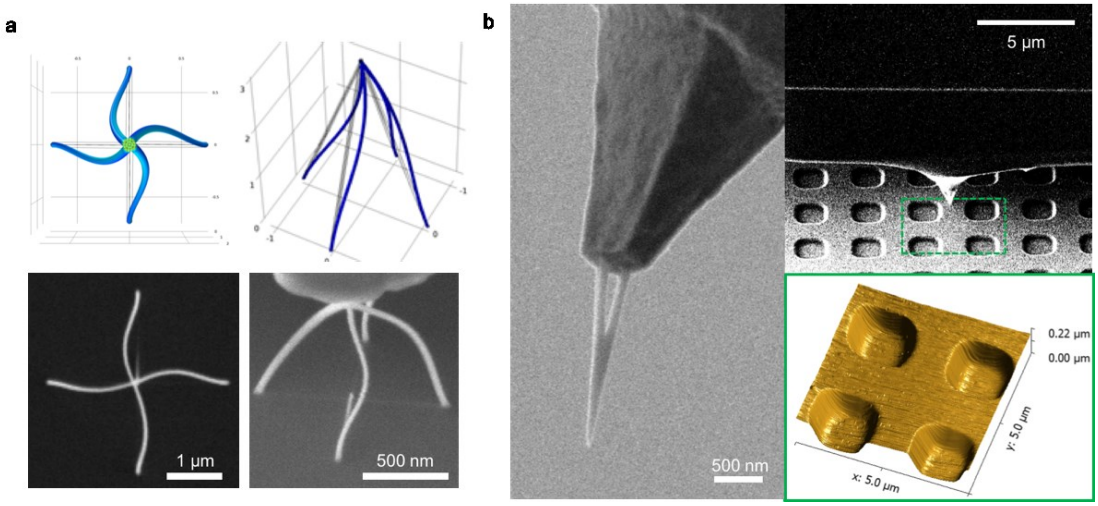

Fig. 2: Iterative adoption of our model to optimize the functionality. **(a)** by adopting our FES model, we unravel the underlying mechanical properties of these structures. **(b)** finally, we deploy optimized Pt based 3D nanoprobes on AFM cantilevers to demonstrate their imaging capability.

Direct-Write Fabrication of Electric and Thermal High-Resolution Nano-Probes on Self-Sensing AFM Cantilever

J. Sattelkow[1,2], J. Fröch[1], R. Winkler[1,2], C. Schwalb[3], M. Winhold[3], A. Deutschinger[3], T. Strunz[3], E.G. Fantner[3], V. Stavrov[4], and H. Plank[1,2,5]*

[1] Institute of Electron Microscopy and Nanoanalysis, Graz University of Technology, 8010 Graz, Austria
[2] Christian Doppler Laboratory – DEFINE, Graz University of Technology, 8010 Graz, Austria
[3] GETec Microscopy Inc. & SCL Sensor.Tech. Fabrication Inc., 1220 Vienna, Austria
[4] AMGT Inc., 2140 Botevgrad, Bulgaria
[5] Graz Centre for Electron Microscopy, 8010 Graz, Austria

* Corresponding author: harald.plank@felmi-zfe.at

Atomic Force Microscopy (AFM) has evolved into an essential part in research and development due to its quantitative 3D surface characterization capabilities on the nanoscale together with the possibility to simultaneously access laterally resolved magnetic, chemical, mechanical, optical, electric or thermal properties of the sample surface.

The recent introduction of highly compact AFM instrumentation (e.g. AFSEM™ by GETec Microscopy Inc.) for the seamless integration in Scanning Electron and / or Focused Ion Beam Microscopes (SEM / FIB) enables multi-purpose *in situ* studies which is beneficial for correlated nanoscale analyses and for situations where the vacuum should not be broken. The core element of this technology are self-sensing cantilever (SS-CL), which enable an electric readout, thereby eliminating a space consuming optical detection system. In a strong collaboration with the above-mentioned company, we develop different nano-probe concepts based Focused Electron Beam Induced Deposition (FEBID).

So far, two concepts have been realized to access electric and thermal properties on the nanoscale. For conductive-AFM, SS-CL are modified by Pt-C nano-pillars using FEBID, further transferred into pure platinum via gas assisted post-growth purification [1]. The results are highly conductive, mechanically rigid nano-probes with tip radii of about 5 nm for high-resolution conductive-AFM. Although the latter are briefly introduced, the main focus of this presentation is put on thermal probes due to their much more challenging requirements. The main idea for thermal nano-probes is the application of freestanding 3D nano-bridges as electric thermistors, which change their electric resistivity in dependency on the temperature. The recent progress in FEBID based 3D nano-printing enables the controlled and precise fabrication of 3D multi-pods [2] on pre-processed SS-CL tips as representatively shown in Fig. 1. The contribution is then structured in three parts. First, the nano-mechanical properties are accessed by a combined approach of finite-element simulation and experiments, which led to an ideal design of proper 3D nano-bridges. In the second part, we discuss unwanted implications of as-deposited material properties by means of strong wear effects of the tip apex during AFM operation. To overcome this issues, we subject the material to post-growth e-beam curing in high vacuum [3], which effectively modifies the carbon matrix leading to both, improved overall rigidity and high wear resistances of the front apex. Beside a strongly improved image quality (Fig. 2a), such optimized 3D nano-probes allow fast scan rates up to 100 µm/s and high mechanical wear resistance as indispensable required for reliable AFM operation. In the final part, we focus on the thermal response by monitoring the electric resistance through such 3D nano-bridges. In more detail, we demonstrate the quantitative and reversible temperature response together with fast response times of less than 32 ms/K (Fig. 2b) as a consequence of the very small volumes involved. The contribution closes with an outlook on currently ongoing activities, which include application of such 3D nano-probes in Scanning Thermal Microscopy (SThM) to access thermal surface properties on the nanoscale as new possibility for GETec's *in situ* AFM instrumentation.

References

[1] B. Geier et al., *Rapid and Highly Compact Purification for Focused Electron Beam Induced Deposits: A Low Temperature Approach Using Electron Stimulated H_2O Reactions*, J. Phys. Chem. C 14009-14016 (2014).

[2] R. Winkler et al., *High-Fidelity 3D-Nanoprinting via Focused Electron Beams: Growth Fundamentals*, ACS Nano Mater. 1014 – 1027 (2018).

[3] G. Arnold et al., *Tunable 3D Nanoresonators for Gas-Sensing Applications*, Adv. Funct. Mater 1707387 (2018).

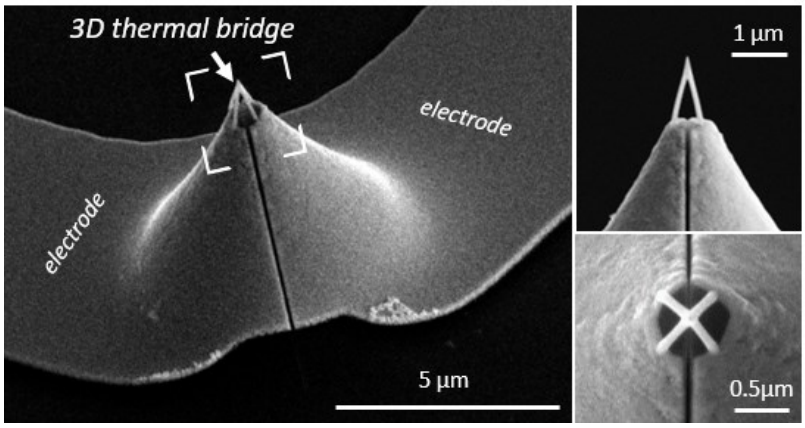

Fig. 1: SEM micrographs of a pre-processed self-sensing cantilever tip, modified by a FEBID based 3D nano-bridge for thermal nano-probing. The smaller images at the right give side and top view close-ups in which the two main electrodes are evident (left / right). When applying a low but constant electric current through the 3D nano-bridge, the according voltage drop is a function of its bridge-resistance, which changes in dependency on the temperature. While the basic concept is comparable simple, the small dimension of individual tetra-pod branches require careful adaption of the overall design to exhibit highest mechanical stability, as discussed in this contribution.

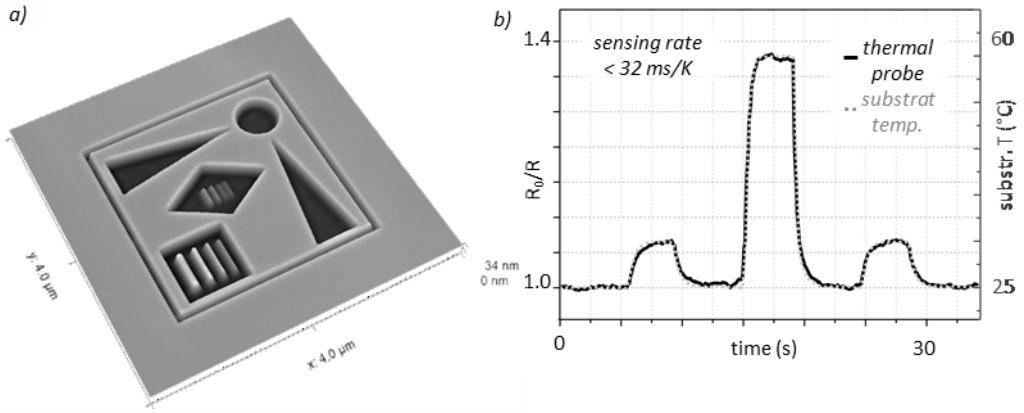

Fig. 2: (a) AFM 3D topography of a FIB processed test structure, imaged in contact mode with fully cured 3D nano-bridges at a scan speed of 100 µm/s, equivalent to 41 sec acquisition time. Comparisons to as-deposited performance and longtime stabilities are discussed in this contribution as well. (b) relative change of electric resistance (solid curve / left Y axis) in dependency on timely resolved temperature variations (dotted line / right Y axis). As evident, the 3D nano-bridges reveal a practically simultaneous response with a sensing rate of less than 32 ms/K. This not only allows dynamic characterization of surface temperatures but also is highly important for lateral resolution as the probes should not reveal cooling times on a longer time scale.

Focused Ion Beam Induced Processing of Nanosuperconductors

R. Córdoba[1,2,3]* and J.M. De Teresa[2,3,4]

[1] Laboratorio de Bajas Temperaturas, Departamento de Física de la Materia Condensada, Instituto Nicolás Cabrera and Condensed Matter Physics Center (IFIMAC), Universidad Autónoma de Madrid, 28049 Madrid, Spain
[2] Instituto de Ciencia de Materiales de Aragón (ICMA), CSIC - Universidad de Zaragoza, 50009 Zaragoza, Spain
[3] Departamento de Física de la Materia Condensada, Universidad de Zaragoza, 50009 Zaragoza, Spain
[4] Laboratorio de Microscopías Avanzadas (LMA), Instituto de Nanociencia de Aragón (INA), Universidad de Zaragoza, 50018 Zaragoza, Spain

* Corresponding author: rosa.cordoba.castillo@gmail.com

Since new physical phenomena come out when the size of a superconductor is reduced to the nanoscale, in the range of its critical superconducting coherence length [1], nanosuperconductivity is becoming a relevant research field with potential applications in quantum computing and sensing.

In this contribution, we present an inclusive scenario of Focused Ion Beam Induced Deposition by using as a primary beam, heavy ions (Ga^+ FIB) or light ions (He^+ FIB) to fabricate in-plane and out-of-plane one-dimensional (1D) nanosuperconductors.

First, we propose an unconventional route to transfer vortices as single particles through long distances (in the micrometers range), within W-C nanowires grown by Ga^+ FIBID (50 nm in width), taking profit of current-induced non-local vortex motion [2]. We measured a giant non-local electrical signal of 36 Ω at 6.3 T (see Figure 1). This value is 40 times higher than those reported for wider wires of other superconductors. Comparing the non-local electrical signal in W-C wires of different dimensions, we found that the signal for 50 nm-wide WC nanowires is nearly two orders of magnitude higher than for the 200 nm-wide WC ones. The measured giant non-local signal in the former strongly confirms that a single vortex line is more rigid than a vortex lattice in wider wires due to its quasi-1D character and its confinement potential that prevents the transversal vortex displacements.

Second, we make use of a He^+ ion microscope with resolution better than 1 nm, to fabricate out-of-plane superconducting hollow nanowires that could serve as building blocks for future three-dimensional superconducting prototypes. We demonstrate here the growth of nanowires as small as 32 nm in diameter and with an aspect ratio (length/diameter) of as much as 200 by using He^+ FIBID, which is in general impossible to achieve with other nanofabrication techniques. By means of a thorough investigation of the structural and compositional properties of the nanowires, we are able to conclude that indeed they are composed of WC_{1-x} FCC crystals of 20-30 nm in size. The magnetotransport characterization of these nanowires indicates that they become superconducting at 6.4 K and exhibit a high upper critical magnetic field and a high critical current density, up to 1.5 times larger than those reported for nanowires of similar dimensions grown by Ga^+ FIBID (see Figure 2) [3].

The fabrication of such advanced functional nanomaterials is at the cutting edge of nanofabrication methods based on focused beams of charged particles for the development of the broad field of planar (1D and 2D) and out-of-plane (3D) nanosuperconductivity.

Acknowledgement:
This project has received funding from the EU-H2020 research and innovation programme under grant agreement No 654360 NFFA-Europe.

References

[1] R. Córdoba et al., *Magnetic field-induced dissipation-free state in superconducting nanostructures,* Nature Communication 4 - 1, 1437 (2013).

[2] R. Córdoba et al., manuscript in preparation.

[3] R. Córdoba et al., *Vertical Growth of Superconducting Crystalline Hollow Nanowires by He^+ Focused Ion Beam Induced Deposition,* Nano Letters 18 - 2, 1379 - 1386 (2018).

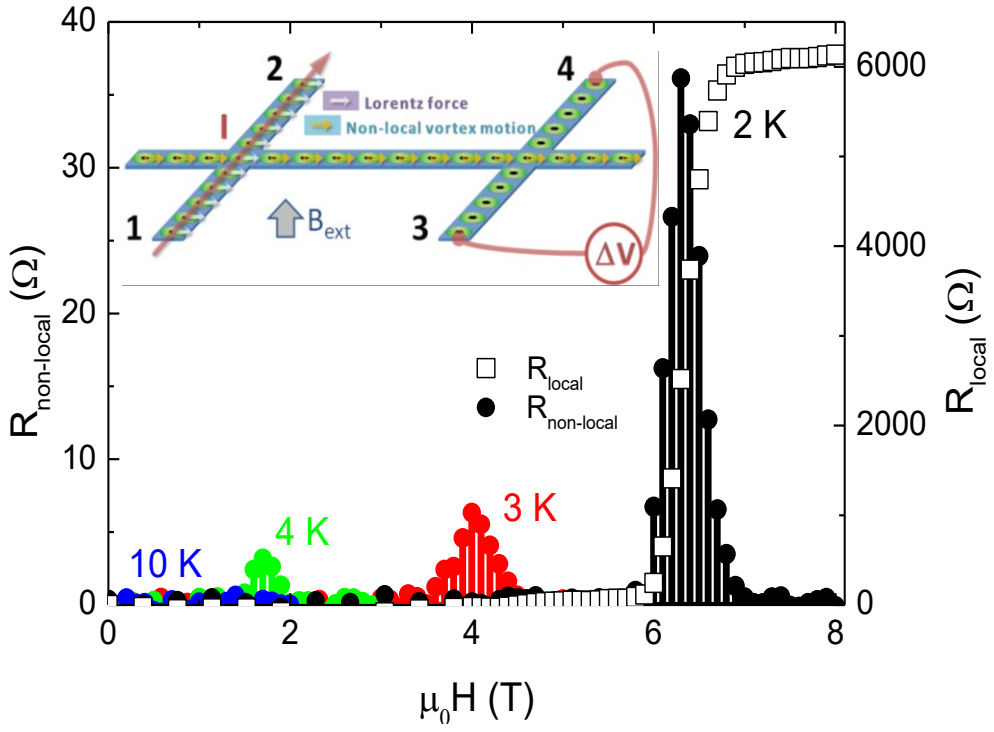

Fig. 1: Magnetic field dependence of non-local resistance (left *y*-axis) and local resistance (right *y*-axis) for the 50 nm-wide channel of 3 μm in length. Inset shows a sketch of the vortex configuration for the non-local measurements [2].

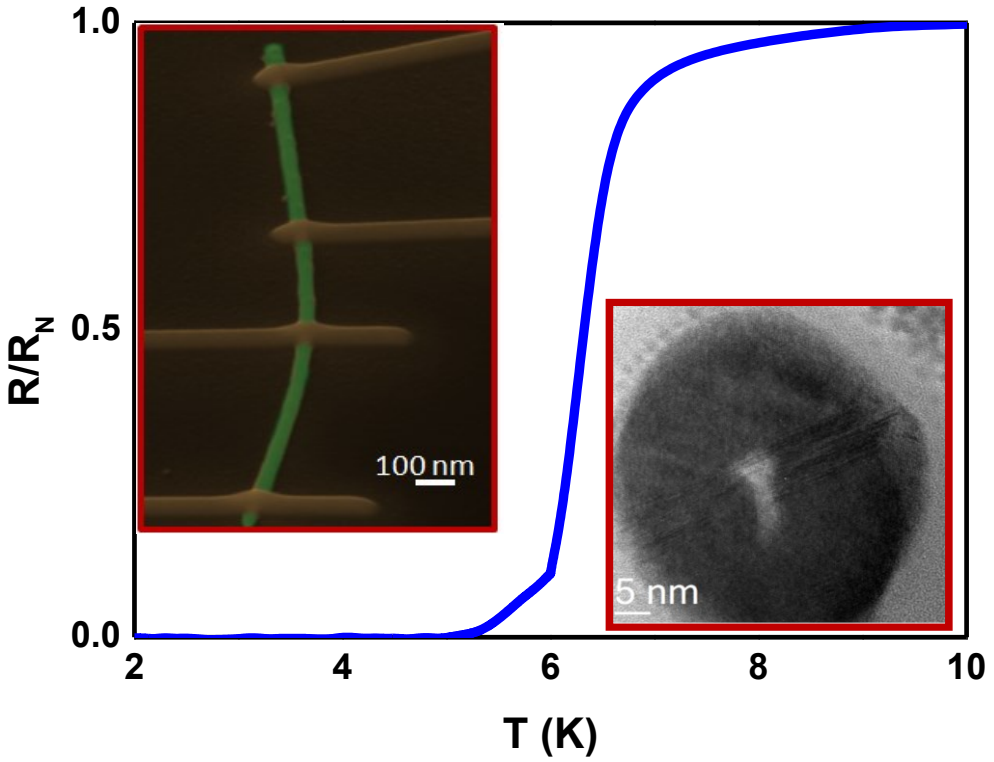

Fig. 2: Normalized resistance for a hollow nanowire as function of temperature. Insets show an SEM image of a nanowire connected by using 4 Pt FIBID contacts and a HRTEM image of its cross sectional view [3].

Ac response of nano-granular metals prepared via FEBID

M. Hanefeld* and M. Huth

Physikalisches Institut - Goethe Universität, Max-von-Laue-Str. 1, 60438 Frankfurt a. M., Germany

* Corresponding author: hanefeld@physik.uni-frankfurt.de

Granular metals are of great interest for material sciences due to their diverse electronic transport properties and can generally be described as metallic nanoparticles surrounded by a dielectric amorphous matrix. They show promising possibilities for applications in different sensing mechanisms [1] and pose a topic of ongoing research concerning their response to a time-dependent ac stimulus [2].

The main focus of current research are two different material properties present in many disordered solids, which have recently been reported in granular metals of palladium in zirconia [2]. The first of these properties, being a Universal Power Law, states that all disordered solids follow a similar conductivity-frequency dependence, when the measurement frequency surpasses a certain critical frequency, also known as the Jonscher Power Law [3]:

$$\sigma' = \sigma_{\mathrm{dc}} + A\omega^n,$$

where σ_{dc} is the conductivity at zero frequency, A a pre-exponential factor and n an exponent often between $0 < n < 1$. As the second property of interest the materials exhibit a temperature-independent scaling behaviour, where conductivity-spectra taken at different temperatures collapse into a single master curve, following a scaling law [2]:

$$\frac{\sigma'(\omega)}{\sigma_{dc}} = F\left(\frac{\omega}{\omega^\star}\right),$$

meaning that, when rescaling the measured frequency-dependent conductivities with their dc-value and rescaling the frequencies of each spectrum by a certain frequency value $\omega^\star$, all spectra follow a temperature-independent function F. These two phenomena are independently interesting to study in the nanometre regime and pose a significant topic of research when taking the temperature-independent behaviour into consideration for future applications of such nano-granular devices.

As we have previously shown, Pt(C) nano-granular metals prepared by Focused Electron Beam Induced Deposition (FEBID) exhibit a large tunability with regard to the tunnel coupling strength by means of post-growth electron irradiation (insert Fig. 2) [1,4,5,6]. As such they form an ideal model system for a systematic study on possible scaling effects in the different transport regimes of granular metals.

In Figures 1 and 2 the Pt(C)-FEBID deposit shows signs of these effects in a nano-granular metal. Fig. 1 depicts conductivity spectra taken at temperatures between 30 and 280K which show a dispersive behaviour, similar to Jonscher's Power Law, above a critical frequency. Additionally, the sample exhibits partial signs of scaling as presented above, but deviates significantly from said behaviour above 160K, as displayed in the second figure. This indicates that the occurrence of scaling may be limited to certain regions of the transport phase diagram of nano-granular metals.

We will give further insights to the state of our measurements on the ac response of such deposits and show the capabilities of FEBID to create an ideal model environment for an in depth analysis of the ac conduction characteristics of granular metals depending on their properties.

References

[1] M. Huth et al., *Focused electron beam induced deposition: A perspective*, Beilst. J. Nanotechn. 3, 597–619 (2012).

[2] H. Bakkali et al., *Universality of the electrical transport in granular metals*, Sci. Rep. 6, 29676 (2016).

[3] A.K. Jonscher, *The 'universal' dielectric response*, Nature 267, 673-679 (1977).

[4] M. Huth, F. Porrati, O.V. Dobrovolskiy, *Focused electron beam induced deposition meets materials science*, Microelect. Eng. 185-186, 9-28 (2018).

[5] F. Porrati et al., *Tuning the electrical conductivity of Pt-containing granular metals by postgrowth electron irradiation,* J. Appl. Phys. 109, 063715 (2011).

[6] R. Sachser et al., *Universal conductance correction in a tunable strongly coupled nanogranular metal,* Phys. Rev. Let. 107, 206803 (2011).

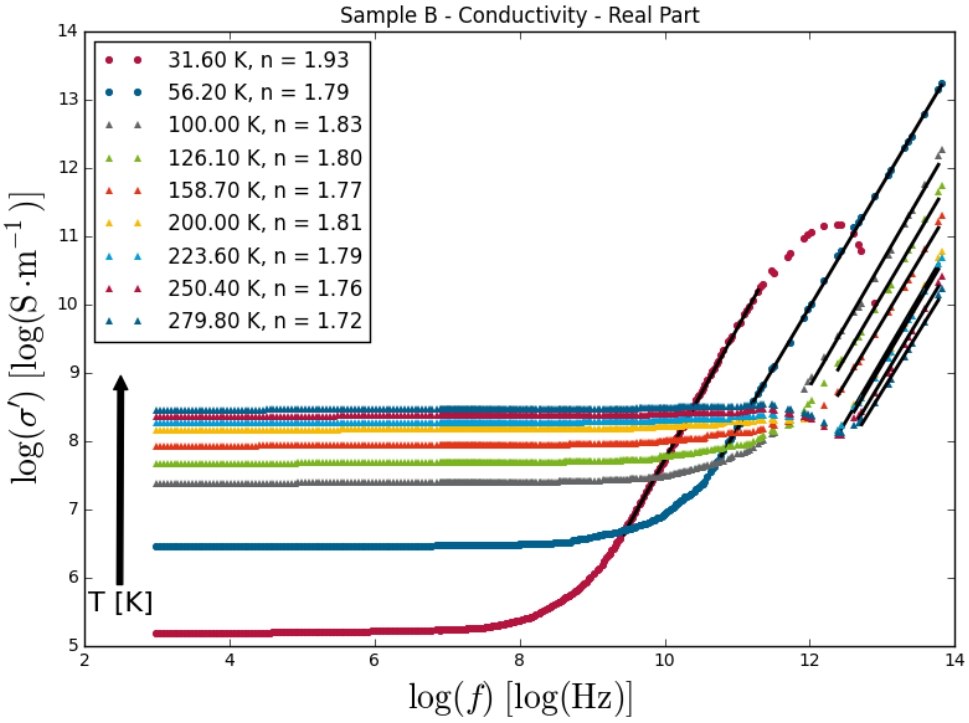

Fig. 1: Conductivity spectra taken at temperatures between 30 and 280K which show a dispersive behaviour, similar to Jonscher's Power Law, above a critical frequency. The arrow depicts the direction of rising temperature values.

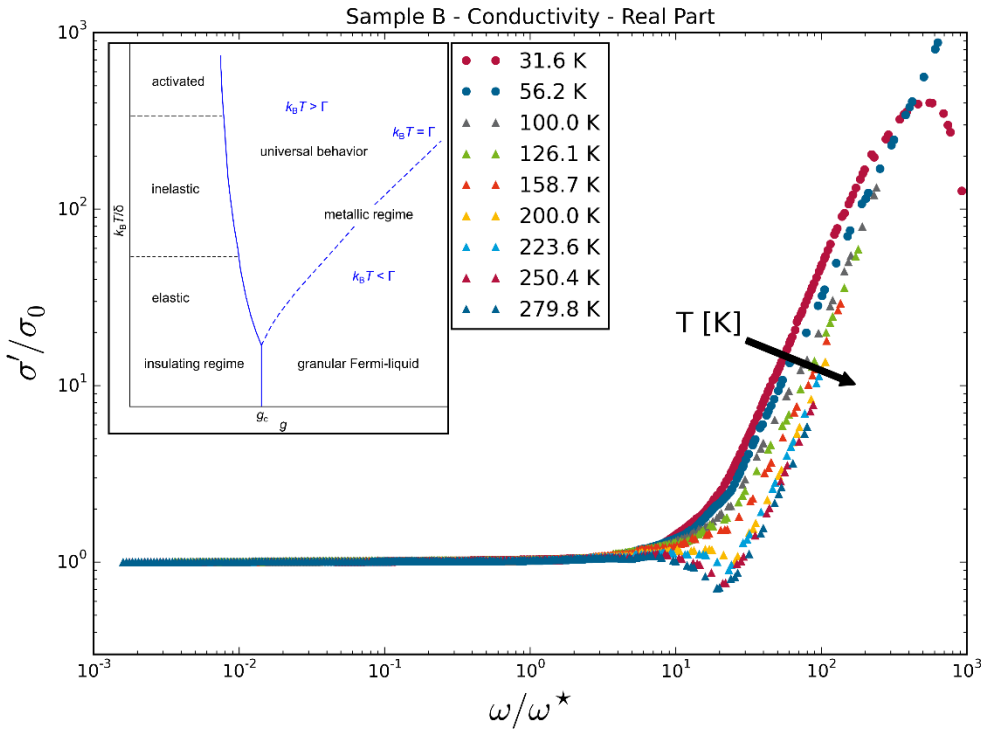

Fig. 2: Samples show signs of a temperature independent scaling behaviour, when rescaling the data of Fig. 1 like explained above. Spectra collapse into a single master curve below 100K, but deviate significantly from that behaviour above 160K. The arrow depicts the direction of rising temperature values. **Insert**: Electron irradiation is the perfect tool to tune important conduction parameters like the inter-grain coupling strength g and the volume fraction of the crystallites compared to the surrounding matrix, ultimately influencing the conductance regime of the deposits [1].

Accessing the Internal Morphology of Nano-Granular FEBID Materials in 3D Space by Electron Tomography

C. Trummer[1], R. Winkler[2], H. Plank[1,2,3], G. Kothleitner[1,3], and G. Haberfehlner[1,3]*

[1] Graz Centre for Electron Microscopy, Steyrergasse 17, 8010 Graz, Austria
[2] Christian Doppler Laboratory DEFINE – Graz University of Technology, Steyrergasse 17, 8010 Graz, Austria
[3] Institute of Electron Microscopy and Nanoanalysis, Graz University of Technology, Steyrergasse 17, 8010 Graz, Austria

* Corresponding author: georg.haberfehlner@felmi-zfe.at

Focused electron beam induced deposition (FEBID) is an additive, direct-write fabrication technique that enables controlled material deposition of nanoscale structures on virtually any given surface. Typically, organometallic precursors are used, e.g. $MeCpPtMe_3$, resulting in nano-granular materials composed of metallic nano-grains (e.g. Pt) spatially embedded in carbonaceous matrix. [1].

The distances between individual grains as well as the chemistry of the carbon matrix significantly influence electrical [2] and mechanical [3] functionalities (see Fig. 1), which form the basis for potential applications of FEBID structures, such as gas sensing via nanoscale resonators or functionalized tips for advanced atomic force microscopy (AFM). In the last decade, different processes have been developed to modify FEBID materials after initial growth by e.g. e-beam based curing in high-vacuum or full chemical purification in H_2O atmospheres. To shed light on the implications of these modification approaches and to unravel the relation between morphology, chemistry and materials' properties, conventional two-dimensional (2D) projection images of the FEBID deposits via transmission electron microscopy are often insufficient. To go beyond these limitations, three-dimensional (3D) nano-analysis of internal morphology, as well as information about chemical composition and bonding character is indispensably required. For this purpose, scanning transmission electron microscopy (STEM) based methods are a powerful characterization class as it intrinsically provides the required resolution on the nanoscale and below. The expansion into 3D space can be done by STEM tomography, which allows 3D reconstruction, derived from tilt series of 2D projections acquired with annular dark field (ADF) detectors [4]. Further coupling to electron energy-loss spectroscopy (EELS) allows correlated access to chemical information [5].

In this first approach, we investigate nano-granular Pt-C FEBID deposits before and after post-growth e-beam curing, as recently applied for tuning the Young modulus in resonant sensor applications [3]. By using STEM tomography, we reconstruct free-standing FEBID deposits in 3D space (see Fig. 2), which yields sizes, shapes and spatial distribution of Pt grains together with their inter-grain distances. EELS characterization provides highly valuable information of chemical bonding in the carbon matrix by analyzing the fine structure of the carbon K-edge. Based on the combined result, we study the implications of post-growth e-beam curing on internal grain sizes, shapes and their spatial distribution together with chemical aspects of the carbon matrix. We attempt to link this information to measured mechanical properties of FEBID materials before and after e-beam curing. By that, our work will help in understanding the processes involved in deposition and post-processing of FEBID deposits. Furthermore, the precise 3D information can serve as basis for realistic simulations of electrical, mechanical or thermal properties of nano-granular FEBID materials [6].

References

[1] M. Huth, F. Porrati, C. Schwalb, M. Winhold, R Sachser, M. Dukic, G. Fantner, *Focused electron beam induced deposition: A perspective,* Beilstein Journal of Nanotechnology 3, 597–619 (2012).

[2] H. Plank, G. Kothleitner, F. Hofer, S.G. Michelitsch, C. Gspan, A. Hohenau, J. Krenn, *Optimization of Postgrowth Electron-Beam Curing for Focused Electron-Beam-Induced Pt Deposits,* J. Vac. Sci. Technol. B 29, 51801–51807 (2011).

[3] G. Arnold, R. Winkler, M. Stermitz, A. Orthacker, J. Noh, J. Fowlkes, G. Kothleitner, M. Huth, P. Rack, H. Plank, *Tunable 3D Nano-Resonators for Gas-Sensing Applications.* Advanced Functional Materials, in press 1-16 (2018).

[4] P. Ercius, O. Alaidi, M.J. Rames, G. Ren, *Electron Tomography: A Three-Dimensional Analytic Tool for Hard and Soft Materials Research.* Advanced Materials 27, 5638–5663 (2015).

[5] R.F. Egerton, *Electron energy-loss spectroscopy in the TEM,* Reports on Progress in Physics 72, 016502 (2009).

[6] F. Porrati, R. Sachser, C.H. Schwalb, A.S. Frangakis, M. Huth, *Tuning the Electrical Conductivity of Pt-Containing Granular Metals by Postgrowth Electron Irradiation,* J. Appl. Phys. 109, 063715–063717 (2011).

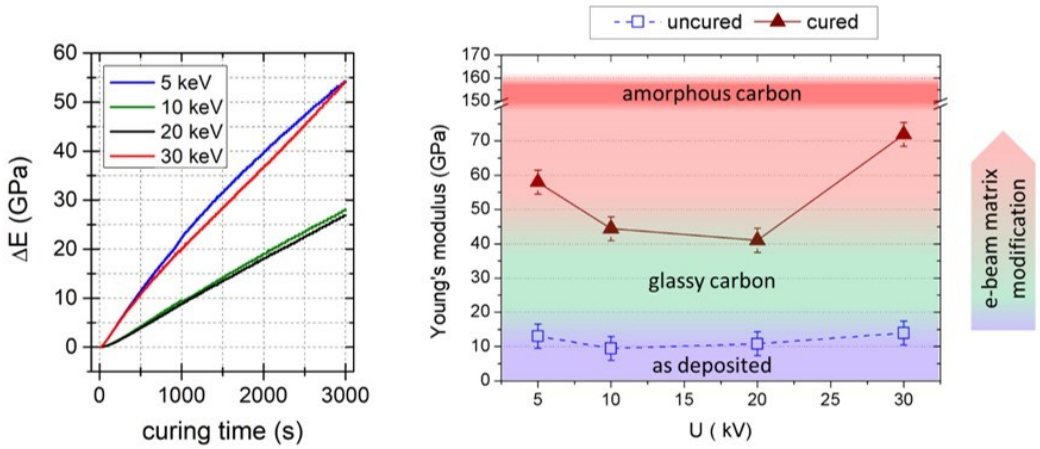

Fig. 1: Tuning the mechanical properties of freestanding Pt-C nano-pillars by post-growth e-beam curing [3]. The left graph shows the Young modulus increase during e-beam exposure for pillars prepared at different primary electron energies. The right graph gives absolute Young's modulus values for as-deposited (blue squares) and cured (red triangles) Pt-C materials in dependency on the initial fabrication energy. The shades indicate the modification from loosely bound carbon networks (blue) over glass carbon (green) towards amorphous carbon (red), while highly accurate information on Pt grain sizes, shapes and their spatial resolution was missing in the related study.

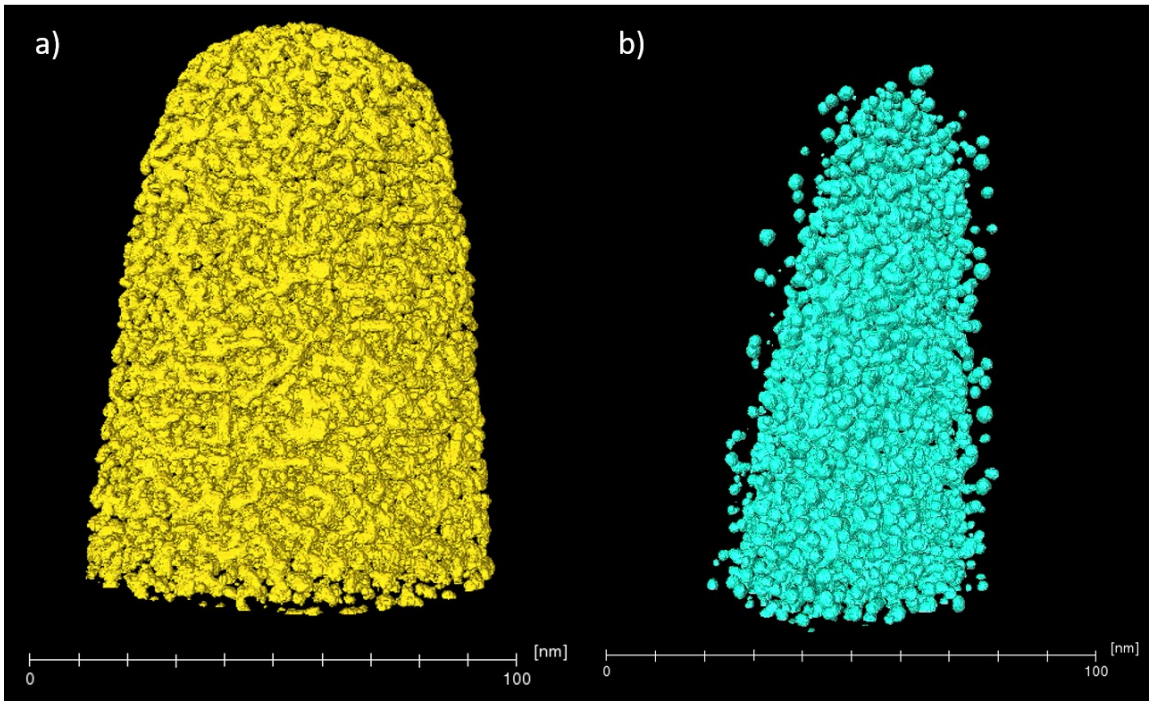

Fig. 2: Accessing the internal 3D morphology accessed by STEM tomography. The images compare the top region of freestanding Pt-C nano-pillars before (a) and after (b) e-beam curing. Grain sizes, shapes and spatial distribution changes, as discussed in detail in this contribution.

Electron Beam Induced Deposition Using Novel Platinum Precursors: $PtCl_2(CO)_2$ and $PtBr_2(CO)_2$

A. Mahgoub[1]*, C.W Hagen[1], R. Thorman[2], D.H. Fairbrother[2], H. Lu[3], and L. McElwee-White[3]

[1] Delft University of Technology, Department of ImPhys, Lorentzweg 1, 2628CJ Delft, The Netherlands
[2] Johns Hopkins, Department of Chemistry, Baltimore, MD 21218, United States
[3] University of Florida, Department of Chemistry, Gainesville, Florida 32611-7200, United States

* Corresponding author: M.I.M.A.Mahgoub-1@tudelft.nl

Properties of deposited structures using electron beam induced deposition (EBID) heavily depend on the precursor used. Thus, it is important to study different precursors, synthesize new ones with more desired properties, characterize their performance and compare them with existing commonly used precursors. In this work, two new platinum precursors were synthesized and used for EBID in a regular scanning electron microscope (SEM). The two novel precursors are $PtCl_2(CO)_2$ and $PtBr_2(CO)_2$. Their design takes advantage of the known tendency for CO and halides to dissociate from metal centers upon electron irradiation [1]. In addition, the use of four-coordinate Pt(II) centers minimizes the number of metal-ligand bonds that must be broken for complete precursor decomposition [1]. The decomposition of the $PtCl_2(CO)_2$ precursor has been studied recently, using surface science techniques, and deposits were made in an ultra-high vacuum (UHV) environment [2,3]. The second precursor, $PtBr_2(CO)_2$, is now used for EBID for the very first time in both an electron microscope and an UHV environment. Deposits obtained with both precursors in the electron microscope (FEI NovaNanoLab 600 Dual Beam System) are compared to deposits made with the commonly used Pt precursor $MeCpPtMe_3$.

In studies conducted in the electron microscope the novel precursors were inserted in regular Gas Injection Systems (GIS), which are normally used for $MeCpPtMe_3$, in a nitrogen filled glovebox. The 2 precursors are found to behave quite different from $MeCpPtMe_3$ when introduced into the SEM chamber. They require a different crucible temperature to reach a sufficient vapor pressure, and upon opening the GIS valve a sharp pressure rise is observed followed by a slow decrease. We were able to form deposits from both precursors, which is the first step towards possible use as EBID precursors (fig. 1). Several experiments were carried out to find suitable parameters for deposition and to figure out in which growth regime (precursor or current limited) the deposition occurs. Surprisingly, in the current limited regime, the growth rate of $PtCl_2(CO)_2$ is higher than for $MeCpPtMe_3$, while in the precursor limited regime it is the other way around. However, the $PtBr_2(CO)_2$ always shows a lower growth rate than the other 2 precursors.

The next important aspect of a precursor is the composition of the deposits. We deposited big squares of the 3 precursors and performed EDX on them. Deposition experiments performed using $PtCl_2(CO)_2$ [2] and $PtBr_2(CO)_2$ in UHV revealed that the deposits consisted of platinum and halogen atoms only with a stoichiometry of PtX_2 (X=Cl, Br). Surprisingly, the composition we found for deposits made in the SEM was totally different. For all three precursors there was at least 70 atomic percent of carbon in the deposits. To verify our results, we compared our EDX results for the reference precursor $MeCpPtMe_3$ to literature values and found good agreement. The high carbon content observed in the electron microscope may originate from CO associated with the precursors, or from hydrocarbons that are ubiquitous in the SEM vacuum chamber. In an attempt to better understand the origin of the differences observed in the composition, results will be presented of deposition experiments using $PtBr_2(CO)_2$ conducted in the UHV chamber in the presence of known partial pressures of CO and hydrocarbons.

Furthermore, we observed that at high beam currents, deposition from $PtCl_2(CO)_2$ changes drastically. A competing etching process of the Silicon substrate is observed (fig. 2). This may be ascribed to the formation of HCl from ever present water in the SEM chamber. To check whether water is playing a role in this, experiments were performed on a sample heated to 210°C, to remove adsorbed water from the sample surface. Indeed the etching effect disappeared completely.

In conclusion, deposition is observed from $PtCl_2(CO)_2$ and $PtBr_2(CO)_2$ precursors, for the first time used in a regular SEM. $PtCl_2(CO)_2$ could potentially be used as an EBID precursor since it is less sticky than $MeCpPtMe_3$ and under certain conditions can have higher growth rates than $MeCpPtMe_3$, but high currents should be avoided to stay away from substrate etching effects. In the UHV environment $PtCl_2(CO)_2$ or $PtBr_2(CO)_2$ form deposits that do not have any carbon contamination although significant carbon is observed in deposits created from these precursors in the electron microscope; the metal content of the deposits created from $PtCl_2(CO)_2$ or $PtBr_2(CO)_2$ in the electron microscope is only slightly better than $MeCpPtMe_3$. $PtBr_2(CO)_2$ always led to lower growth rates and a worse composition than $MeCpPtMe_3$. By varying the deposition conditions in the UHV environment the source of carbon contamination observed in deposits created in the electron microscope will be elucidated.

References

[1] J. Spencer et al., *Understanding the electron-stimulated surface reactions of organometallic complexes to enable design of precursors for electron beam-induced deposition,* Appl. Phys. A. 117, 1631-1644 (2014).

[2] J.A. Spencer et al., *Electron Induced Surface Reactions of cis-*$PtCl_2(CO)_2$*: A Route to Focused Electron Beam Induced Deposition of Pure Pt Nanostructures,* Journal of the American Chemical Society 138 (29), 9172-9182 (2016).

[3] J.A. Spencer et al., *Comparing postdeposition reactions of electrons and radicals with Pt nanostructures created by focused electron beam induced deposition,* Beilstein J. Nanotechnol. 8, 2410–2424 (2017).

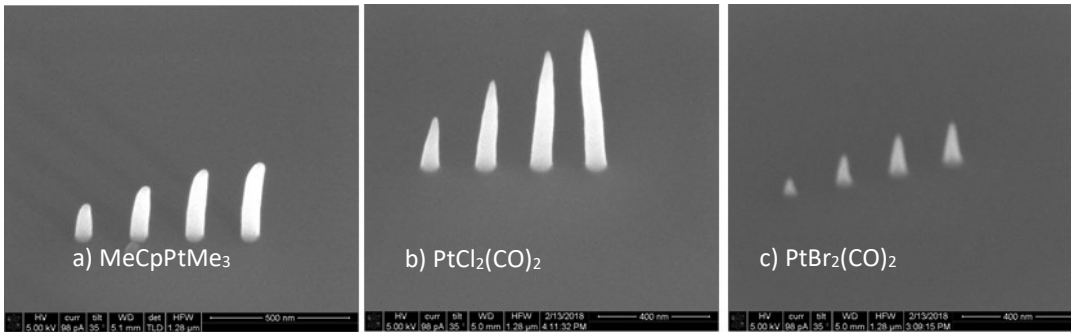

Fig. 1: Pillars deposited using 3 Pt-precursors. The pillars were deposited at 18 KV, 38pA. The writing strategy was to stay with the beam on one pillar for a certain dwell time, then blank the beam for a refresh time = 10xdwell time, then move to the next pillar. When the first pass over the 4 pillars is finished, this is repeated 200 times. The dwell time in each image increases, from left to right, from 0.5 to 2ms.

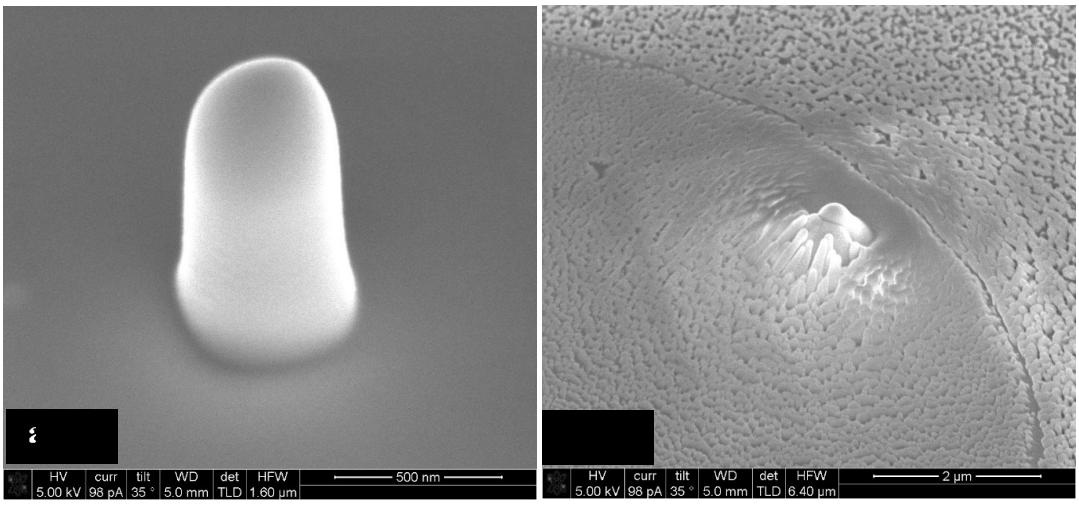

Fig. 2: a) $PtCl_2(CO)_2$ square deposited at 0.4nA, 5KV. The silicon substrate seen around the deposit is smooth and doesn't show any etching effects. **b)** Substrate etching effect observed for the $PtCl_2(CO)_2$ deposited at 6.3nA, 5KV. The substrate consists of a Silicon circular area (lower left) surrounded by black silicon (etched silicon, upper right). It is seen that after deposition the circular area looks the same as the surrounding black silicon.

Binary Mn-Si nanostructures prepared by the $SiH_3Mn(CO)_5$ precursor

F. Porrati[1]*, S. Barth[2], R. Sachser[1], F. Jungwirth[2], M. Eltsov[3], A. Frangakis[3], and M. Huth[1]

[1] Goethe-Universität, Institute of Physics, Max-von-Laue-Str. 1, D-60438 Frankfurt am Main, Germany
[2] TU Wien, Institute of Materials Chemistry, Getreidemarkt 9/BC/02, A-1060 Wien, Austria
[3] Goethe-Universität, Buchmann Institute, Max-von-Laue-Str. 15, D-60438 Frankfurt am Main, Germany

* Corresponding author: porrati@physik.uni-frankfurt.de

Heteronuclear carbonyls are a family of compounds which can be used to fabricate bimetallic nanostructures by means of focused electron beam induced deposition (FEBID), see e.g. [1-2]. In the present work, we extend the use of heteronuclear precursors to the fabrication of silicon-based FEBID nanostructures. In particular, we employ the silicon-metal carbonyl $SiH_3Mn(CO)_5$ to prepare Mn-Si binary alloys, which we characterize by compositional analysis, magnetotransport measurements and microstructural investigations.

The EDX analysis carried out on deposits prepared with 5 kV acceleration voltage and 6.3 nA electron current, revealed a composition of about 35 at% Mn, 18 at% Si, 29 at% C, 18 at% O. As shown in Fig. 1, the composition of the deposits slightly changes with the electron beam current. In particular, the sum [Mn]+[Si] increases from about 40 at% to 53 at% from 0.4 nA to 6.3 nA. Correspondingly, [C] and [O] slightly decrease. The composition is found to be independent of the acceleration voltage and of the dwell time. The [Mn]/[Si] ratio, which is expected to be equal to 1 from the stochiometry of the precursor, is consistently found to be equal to 2 in the deposits, which indicates selective loss of silyl groups.

The room temperature resistivity of as-grown samples is about $8 \cdot 10^3$ μΩcm. The resistivity decreases by means of a post-growth low-energy electron irradiation treatment. In particular, for an irradiation dose of 6250 nC/μm^2, which was the maximal used in the experiment, the resistivity drops to $6.6 \cdot 10^2$ μΩcm. In Figure 2 we plot the temperature dependence of the normalized conductivity in the range 4-285 K. The samples show a behavior typical of the quasi-metallic regime, with finite conductivity at low temperature. In Figure 3 we show the results of Hall effect measurements carried out at 4K. No anomalous Hall effect is measured, indicating that the samples are not ferromagnetic. Further, the ordinary Hall effect is characterized by a change of sign in the Hall coefficient. In particular, as-grown samples show a negative Hall coefficient, indicating an electron-like transport; while post-treated samples show a positive Hall coefficient, indicating a hole-like transport.

Microstructural investigations were carried out by transmission electron microscopy. As-grown samples do not show any well-defined ring, which is characteristic for an amorphous material. The sample irradiated with a dose of 6250 nC/μm^2 shows a diffraction pattern, as depicted in Figure 4. The analysis of the radial intensity obtained by azimuthal integration of the diffraction pattern shows five peaks, which are compatible with a novel Mn_2SiO_4 spinel phase, which, however, forms only a small volume fraction of the sample.

References

[1] F. Porrati et al., *Direct writing of CoFe alloy nanostructures by febid from a heteronuclear precursor*, Nanotechnology 26, 475701 (2015).

[2] R. Kumar et al., *Electron interactions with the heteronuclear carbonyl precursor $H_2FeRu_3(CO)_{13}$ aid comparison with $HFeCo_3(CO)_{12}$: from fundamental gas phase and surface science studies to FEBID*, Beilstein J. Nano. 9, 555 (2018).

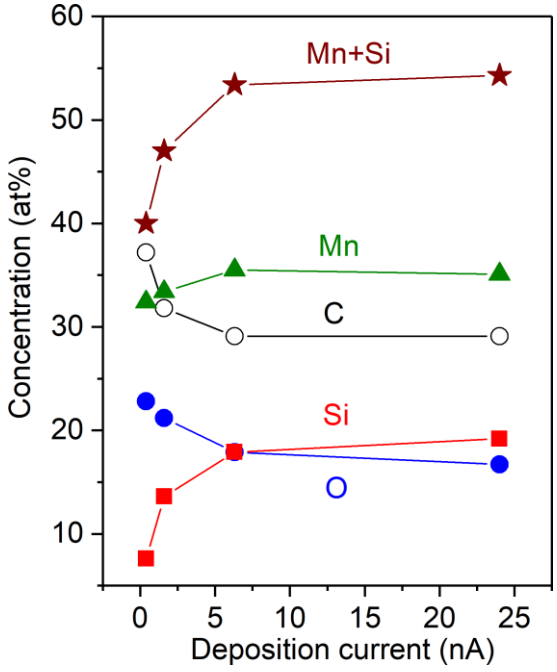

Fig. 1: EDX compositional data from samples fabricated at room temperature with 5keV electron beam by the $SiH_3Mn(CO)_5$ precursor gas.

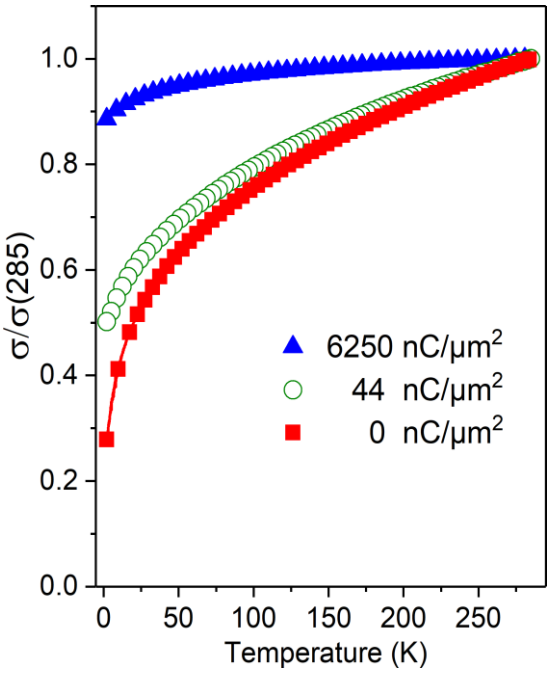

Fig. 2: Conductivity temperature dependence of the as-grown sample (squares) and of two samples treated by irradiation after-growth. The behavior of the samples is quasi-metallic.

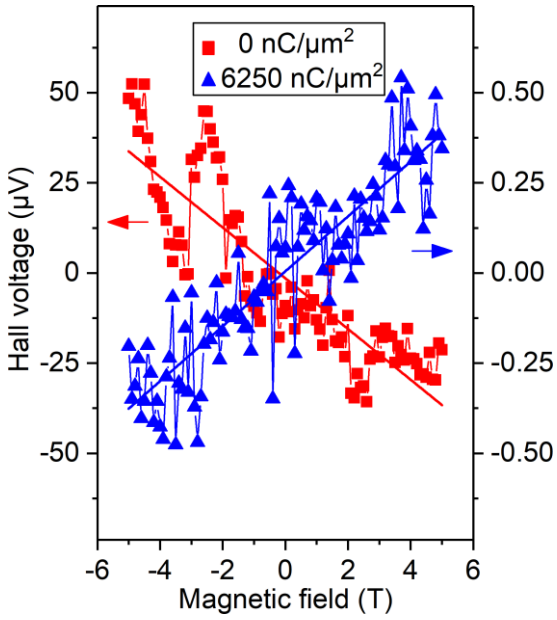

Fig. 3: Hall effect measured for the as-grown and for a sample treated by irradiation after-growth. The corresponding charge carrier densities are $2.2x10^{20}$ cm^{-3} and $1.4x10^{22}$ cm^{-3}, respectively.

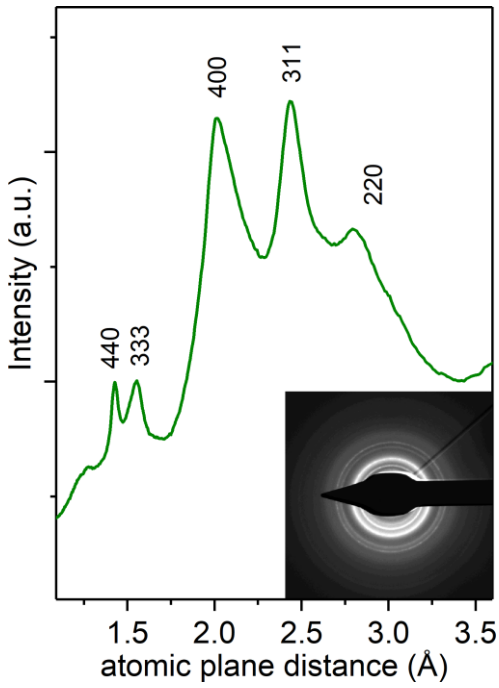

Fig. 4: Radial intensity of the diffraction pattern of the sample irradiated with 6250 nC/μm². The peaks are compatible with a novel Mn_2SiO_4 spinel phase, which is confined at the surface of the sample.

On the Role of Surface and Precursor Chemistry for Electron Beam Induced Surface Activation (EBISA)

F. Vollnhals*, M. Drost, C. Preischl, E. Bilgilisoy, and H. Marbach

Lehrstuhl für Physikalische Chemie II, Universität Erlangen-Nürnberg, Egerlandstr. 3, 91058 Erlangen, Germany

* Corresponding author: florian.vollnhals@fau.de

The world of focused electron beam induced processing encompasses techniques like electron beam induced deposition (EBID) and etching (EBIE). In the most prominent example, EBID, a focused electron beam is used to locally decompose precursor molecules on the surface to yield solid deposits, while volatile fragments are removed by the vacuum system. The use of metal-organic precursor molecules allows for a wide range of possible chemical compositions and chemical/physical properties of the resulting deposit. The use of a focused electron beam makes it possible to deposit arbitrarily shaped structures with ultimate lateral sizes in the low single digit nanometer regime without the need for multiple processing steps, making EBID a very versatile tool for rapid prototyping, circuit editing and fundamental research [1].

As an extension to EBID, we introduced the concept of Electron Beam Induced Surface Activation (EBISA) [2, 3]. In EBISA, a surface is locally modified by an electron beam under UHV conditions, i.e., in the absence of precursor, such that it becomes active towards the catalytic decomposition of precursor supplied subsequently. A number of EBID precursors have been found to exhibit this behavior on specific substrates, most prominently Iron pentacarbonyl, $Fe(CO)_5$, and Cobalt tricarbonyl nitrosyl, $Co(CO)_3NO$. In addition, these precursors exhibit autocatalytic growth in UHV conditions, i.e., local decomposition of further molecules at the initial deposit results in constant deposit growth as long as precursor is supplied. In the case of $Fe(CO)_5$, this catalytic process leads to growth of clean (>95 %at.), polycrystalline iron deposits on the surface, while $Co(CO)_3NO$ yields CoO_xN_y deposits with a composition of roughly 50 at% Co, 40 at% O, and 10 at% N.

The susceptibility to activation by the electron beam certainly depends on the chemical nature of the substrate material (more precisely: the chemistry of the immediate surface). It was found that both oxides as well as molecular films can be activated. The oxides include SiO_x-terminated silicon and silicon nitride, as well as well-defined, 1x1 and 1x2 reconstructed TiO_2(110) [4, 5]. EBISA could also be observed for molecular substrates like thin (>1 close packed layer) 2HTPP-covered surfaces (2H-tetraphenyl porphyrin) [5, 6] and more complex surface-anchored metal organic frameworks [7].

The specifics of the interaction of the precursor molecules with the active site, while still not fully understood, can be successfully exploited to improve the nanofabrication by EBISA. In this contribution, we will discuss the differences in chemistry of $Co(CO)_3NO$ and $Fe(CO)_5$ for different TiO_2 surface terminations and their influence on the deposition process as well as show how 2HTPP layers on these substrates can be used to facilitate EBISA experiments. The presented findings indicate novel routes toward the controlled fabrication of chemically well-defined nanostructures which will be discussed along with latest results.

References

[1] a) W. van Dorp, C.W. Hagen, J. Appl. Phys. 104, 081301 (2008); b) I. Utke et al., JVST B 26, 1197 (2008); c) S.J. Randolph et al., Crit. Rev. Solid State Mater. Sci. 31, 55 (2006); d) I. Utke, A. Gölzhäuser, Ang. Chem. Int. Ed., 49, 9328 (2010).

[2] H. Marbach, *Electron beam induced surface activation: a method for the lithographic fabrication of nanostructures via catalytic processes*, Applied Physics A 117, 987 (2014).

[3] M.-M. Walz et al., *Electrons as "Invisible Ink": Fabrication of Nanostructures by Local Electron Beam Induced Activation of SiOx*, Angewandte Chemie International Edition 49, 4669 (2010).

[4] F. Vollnhals et al., *Electron Beam-Induced Writing of Nanoscale Iron Wires on a Functional Metal Oxide*, The Journal of Physical Chemistry C 117, 17674 (2013).

[5] M. Drost et al., *On the Principles of Tweaking Nanostructure Fabrication via Focused Electron Beam Induced Processing Combined with Catalytic Growth Processes*, Small Methods 1, 1700095 (2017).

[6] F. Vollnhals et al., *Electron Beam Induced Surface Activation of Ultrathin Porphyrin Layers on Ag(111)*, Langmuir 29, 12290 (2013).

[7] M. Drost et al., *Surface-Anchored Metal-Organic Frameworks as Versatile Resists for Gas-Assisted E-Beam Lithography: Fabrication of Sub-10 Nanometer Structures,* ACS Nano, 12, 3825 (2018).

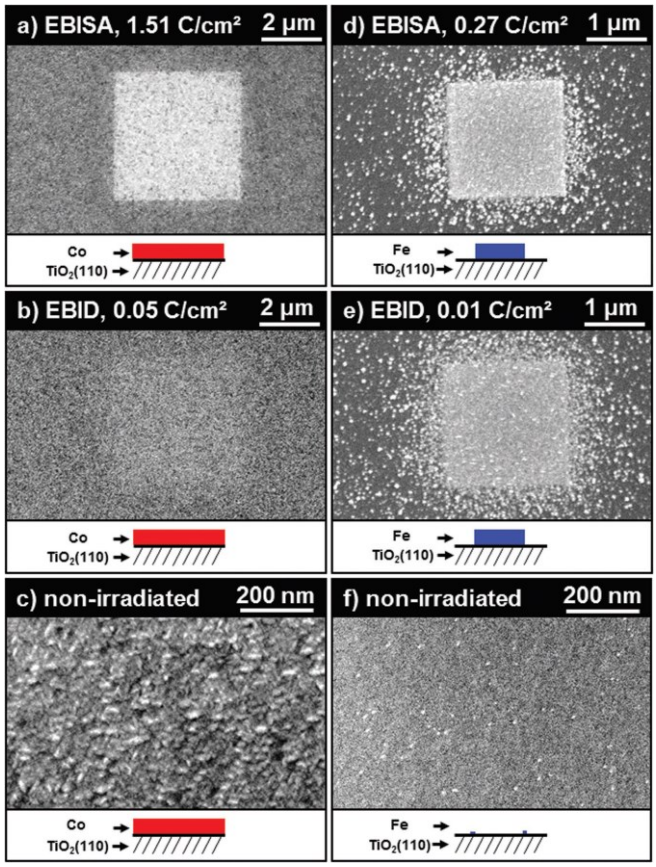

Fig. 1: FEBIP on TiO_2(110) 1 × 1. a) EBISA 4 × 4 µm² square from $Co(CO)_3NO$: a granular film has grown on the whole surface after a precursor exposure of ≈1.1 × 10^5 L: the pre-irradiated surface area appears brighter in SEM. b) EBID 4 × 4 µm² square from $Co(CO)_3NO$, autocatalytic growth time tAG = 217 min: lower contrast and less defined boundaries compared to EBISA areas. c) Blowup of the CoO_xN_y-covered, non-irradiated surface area after the experiment with $Co(CO)_3NO$. d,e) EBISA and EBID (t_{AG} = 128 min) 2 × 2 µm² square deposits from $Fe(CO)_5$: deposition and autocatalytic growth of bcc-Fe is mainly confined to irradiated areas, unselective growth is only observed at surface defects. f) Blowup of a non-irradiated surface area after the experiment with $Fe(CO)_5$, again showing only sporadic unselective growth of bcc-Fe.

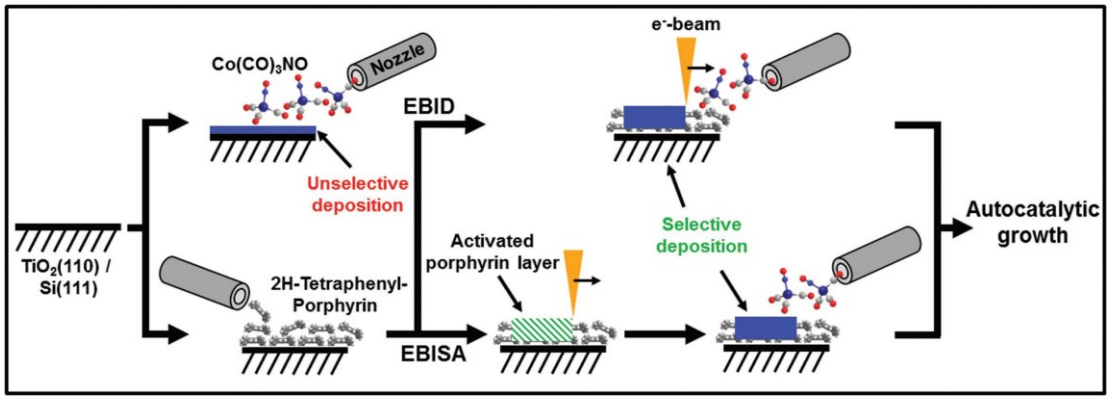

Fig. 2: Scheme of the interaction of TiO_2(110) and Si(111) surfaces with $Co(CO)_3NO$ in the presence and absence of a 2HTPP top layer. Without the 2HTPP, $Co(CO)_3NO$ decomposes without site selectivity, i.e. across the whole exposed surface. With 2HTPP present, the unselective decomposition is suppressed and EBID and EBISA become feasible. Autocatalytic growth of the initial deposits yields the final nanostructures.

Dedicated area-selective-ALD micro-reactor

P. Gruszka*, G. Di Prima, R. Sachser, and M. Huth

Department of Physics - University of Frankfurt, Max-von-Laue Str. 1, 60438 Frankfurt am Main, Germany

* Corresponding author: gruszka@physik.uni-frankfurt.de

In recent years, conventional methods of nano-structuring are slowly reaching their lower limits. Much effort is put into the investigation of optimal deposition parameters to increase the material yield which in most cases is an impossible task. A novel bottom-up approach was developed by Mackus et al. [1], which combines focused electron beam induced deposition(FEBID) and area-selective atomic layer deposition(AS-ALD).

FEBID is a serial, bottom-up and direct-write technique yielding structures with superior lateral resolution (< 10 nm), but with poor material quality. In contrast, ALD and especially AS-ALD are parallel and bottom-up approaches with exceptional thickness control resulting in high purity sub-nano films.

We successfully performed the combined FEBID-ALD process in our Nova 600 Dual Beam scanning electron microscope [2]. First, we deposited ultra-thin FEBID-Platinum structures on a silicon dioxide substrate. Afterwards, we performed a purification technique developed by Sachser et. al. to remove excess carbon and reveal the platinum crystallites for the subsequent step. The ALD experiments were conducted on purified platinum FEBID-nanostructures [3] which were monitored via in-situ conductance measurements.

For further investigation and optimization, we built a dedicated AS-ALD micro-reactor. It is capable to fit one substrate and the reaction volume is as small as 20 ml. Furthermore, this chamber enables us to monitor the ALD process via electrical in-situ measurements. First experiments in the micro-reactor show selective growth and a speed-up in the process since we are now able to use much higher pressures to run the ALD.

References

[1] A.J.M. Mackus et al., *Local deposition of high-purity Pt nanostructures by combining electron beam induced deposition and atomic layer deposition,* J. Appl. Phys. 107, 116102 (2010).

[2] G. Di Prima et al., *In situ conductance monitoring of Pt thin film growth by area-selective atomic layer deposition,* Nano Futures 1(2), 25005 (2017).

[3] R. Sachser et al., *Catalytic purification of directly written nanostructured Pt microelectrodes*, ACS Appl. Mater. Interfaces 6, 15868 (2014).

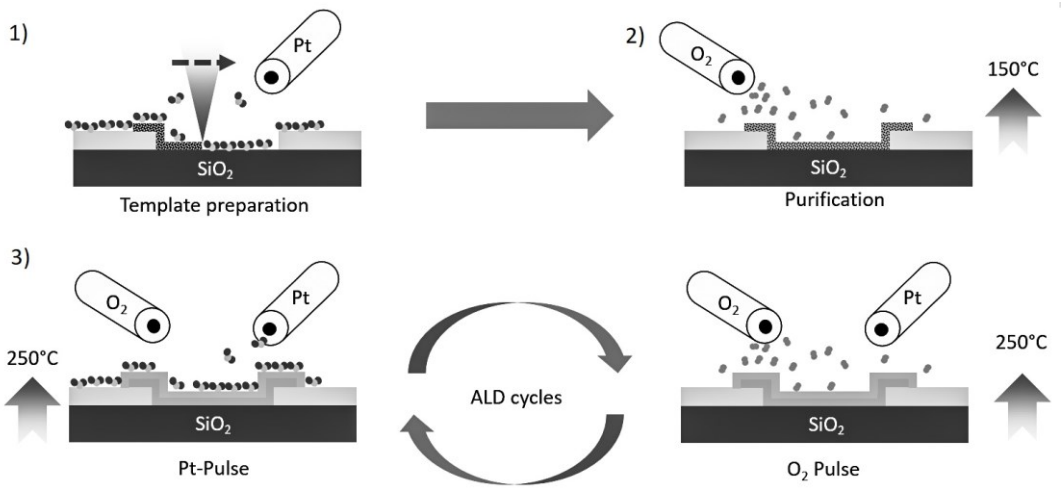

Fig. 1: Typical preparation of a Platinum AS-ALD nano-structure. 1) An ultra-thin platinum template is created using FEBID. 2) Purification of the template to remove excess carbon and to reveal the platinum crystallites. 3) Sequential ALD process to grow platinum selectively on top of the template structure.

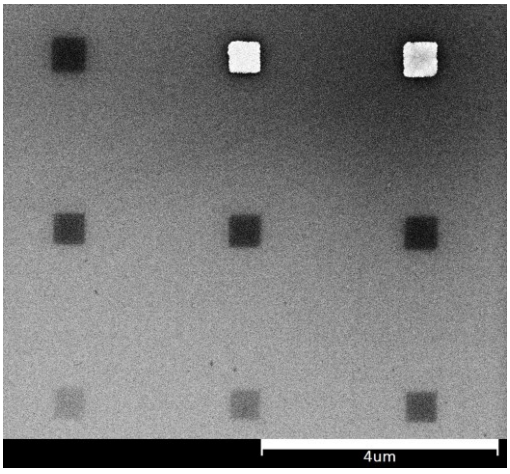

Fig. 2: Dosage test to determine the minimal charge dosage to create enough nucleation sites for the area selective ALD process.

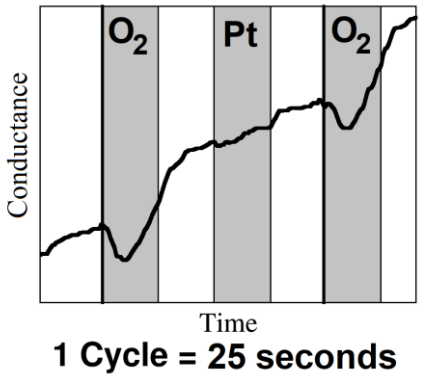

Fig. 3: Typical in-situ monitoring data of the platinum ALD process. The conductance raises linear in time in a step-like behavior as the deposit grows due to the ALD process.

Towards the Plasmonic Optical Nanopores for Single Molecule Analysis by Using Electron Beam Irradiations

S.S. Choi[1]*, M.J. Park[2], S.J. Oh[1], H.T. Kim[3], and S.J. Choi[3]

[1] Research Center for Nano-Bio Science, SunMoon University, Ahsan, Chungnam 31460, South Korea
[2] Department of Physics, Korea Military Academy, Noon Gu, Gong Reung 2 Dong, PO box 77-1, Seoul, South Korea.
[3] Department of Physics, Inchon National University, Inchon 22012, South Korea

* Corresponding author: sscphy2010@gmail.com, sscphy1982@daum.net

About 60 years ago, Coulter cell counter with an electrical detection technique was invented by Dr. Coulter. Biomolecule such as red blood cell was translocated through the micrometer size orifice in the liquid. During translocations of each molecule via the micron size orifice in the liquid, the electrical impedances would be changed and recorded [1]. Due to fast developed nanofabrication technology, the portable USB memory size nanopore device called MinION with an electrical detection technique in the liquid state was launched by Oxford Nanopore Technology a couple years ago [2]. However, the high error rates were reported even though the error rates have been reduced significantly from initial high error rates over 80% [3]. Considering the current nanobio devices including the genome sequencing instrument are utilizing optical detection technique, optical nanopore devices can be excellent candidates for next generation single molecule sensor. However, the tiny nano-aperture with its diameter of ~ 10 nm or less would have negligible optical transmission from Bethe's law; $T \sim (d/\lambda)^4$. Optical transmission through the tiny nano-aperture can be enhanced either by providing the groove patterns or periodic arrays [4].

We fabricated Au aperture array on the nanometer thick Au membrane by using focused ion beam (FIB) technique, and the high energy electron beam irradiations by using TEM (transmission electron microscopy) on the Au film were carried out. When the high energy electron beam irradiates on the Au film, the irradiated specimen area become viscous, the Au atoms along with C atoms would diffuse and forms the pore membrane, when the drilled aperture diameter is smaller than the thickness of the Au film. A (5 x 5) aperture array on a 200 nm thick Au film is presented in Figure 1. The diameter and the pitch of the fabricated aperture array is ~ 120 nm diameter and 0.5 micron, respectively. The electron beam irradiations at 200 keV inside the yellow circle with ~a 400 nm radius were performed. The temperature rise on the nanoscale irradiated region would be very high due to electron beam induced thermal spike. Figure 2 presents the Au-C diffused membrane inside the B2 aperture as in Fig 2 (b). The electron beam irradiation was carried out with 2 pA at 200 keV for 10 minutes. No diffused membrane was observed other than B2 aperture [5].

We also utilized the field emission scanning electron microscopy technique to form the Au-C diffused membrane in Figure 3. A 1.4 nA electron beam current at 2 keV was irradiated on ~ a 270 nm diameter Au aperture for 1 min, 3 min, and 5 min. With increasing the irradiation time, the pore diameter was reduced from 266.3 nm to 38.7 nm, and 10 nm, respectively. This diffusion phenomenon may be attributed to the concentration-dependent atomic diffusion. The detailed diffusion mechanisms related to TEM and FESEM electron beam irradiation is still under investigation.

References

[1] M. Muthukumar, C. Plesa, C. Dekker, *Single-molecule sensing with nanopores*, Physics Today 68, 40 (2015).

[2] E.C. Hayden, *Pint-sized DNA sequencer impresses first users*, Nature 521, 15 (2015).

[3] A. Mikheyev, M.M.Y. Tin, *A first look at the Oxford Nanopore MinION sequencer*, Mol. Ecol. Resour. 14, 1097 (2014).

[4] T.W. Ebbesen, H.J. Lezec, H.F. Ghaemi, T. Thio, P.A. Wolff, *Extraordinary optical transmission through sub-wavelength hole arrays*, Nature 391, 667 (1998).

[5] S.S. Choi, S.J. Oh, C.H. Han, D.J. Park, S.B. Choi, Y.S. Kim, N.K. Park, *Au cluster formation on a pore-containing membrane under various surface treatments*, J. Vac. Sci. Technol B. 35, 04F107 (2017).

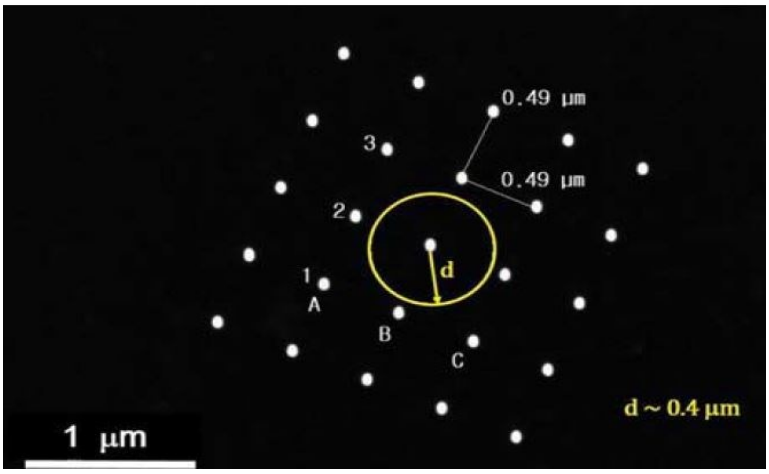

Fig. 1: A TEM image of the aperture array on the 200 nm Au free standing film. The aperture array with its diameters of ~120 nm was drilled by using 30 keV FIB. The pitch was measured to be 0.49 μm. The yellow circle with 400 nm diameter indicates the illumination area of 300 keV electron beam.

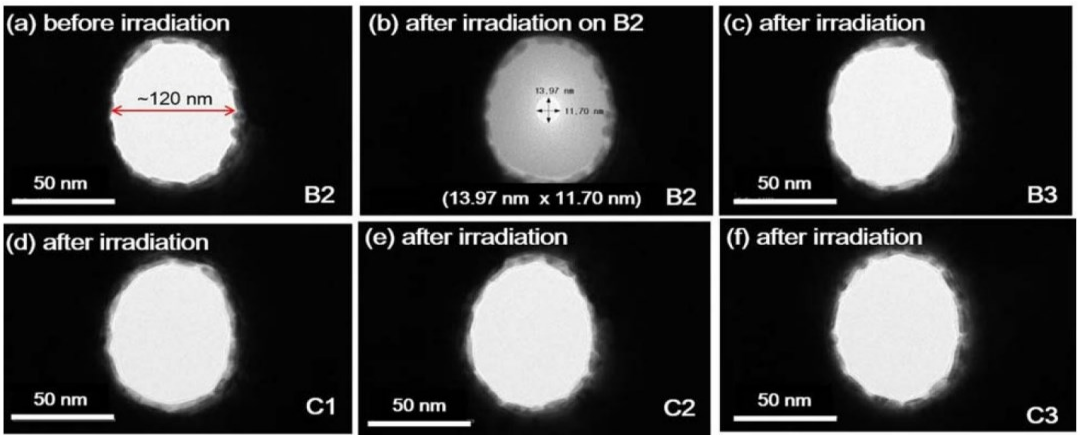

Fig. 2: TEM images of the Au apertures before and after the electron beam irradiations. The irradiated aperture is noted as B2, other apertures close to the center aperture B2 are noted as B3, C1, C2, and C3. After a 2 pA electron beam irradiation at 200 keV for 10 minutes on the Au aperture (B2), the (13.97 nm x 11.70 nm) size pore was formed as shown in (b). However, no pore membranes except B2 aperture were formed as shown in (c), (d), (e), and (f).

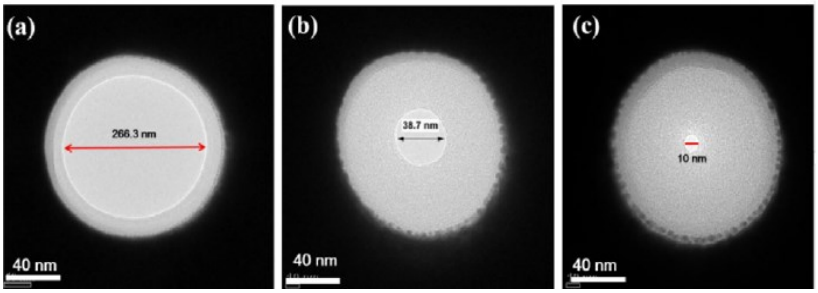

Fig. 3. TEM images of the formed pore membranes inside the Au apertures. Under FESEM electron beam irradiations with 1.4 nA at 2 keV for 1 min (a), 3 min (b), and 5 min (c), the pore diameters are getting smaller to be 266.3 nm, 38.7 nm, 10 nm diameter, respectively.

POSTER PRESENTATIONS

P 1	**Stefano Frabboni** (CNR NANO S3 and FIM Department UNIMORE, Modena, Italy) *Magnetic characterization of Cobalt Nanowires and Square Nanorings fabricated by Focused Electron Beam Induced Deposition (p. 88)*
P 2	**Yuki Katori** (Shibaura Institute of Technology, Tokyo, Japan) *Micro-patterning of electrochromic Prussian Blue particles using focused electron beam irradiation (p. 90)*
P 3	**Marcus Rohdenburg** (University of Bremen, Germany) *Cisplatin Revisited: On the Strong Electron-Induced Reducing Ability of NH3 Ligands in Ammine Precursors (p. 92)*
P 4	**Kai Ahlenhoff** (University of Bremen, Germany) *Electron-induced decomposition of silver(I) carboxylates: Role of the alkyl chain (p. 93)*
P 5	**Cristiano Glessi** (University of Oslo, Norway) *Thermal Evaluation of Potential FEBID Precursors (p. 94)*
P 6	**Ding Zhao** (Danchip/CEN, Technical University of Denmark, Lyngby, Denmark) *Ice Resists for 3D Electron Beam Processing: Instruments in Denmark and China (p. 96)*
P 7	**Nicole Auth** (ZEISS SMT, Rossdorf, Germany) *New mask absorber materials addressed by FEBIP based Mask Repair (p. 98)*
P 8	**Luka Skoric** (Cavendish Laboratory, University of Cambridge, UK) *Investigating the limits of Dark-Field magneto-optical Kerr effect for the characterization of three-dimensional magnetic FEBID nanowires (p. 99)*
P 9	**Gaudhaman Jeevanandam** (Delft University of Technology, The Netherlands) *Towards Cleanroom in an SEM (p. 101)*
P 10	**Maria Pintea** (The Open University, Milton Keynes, UK) *Velocity Map Imaging Applied to Dissociative Electron Attachment for FEBID Precursors (p. 103)*
P 11	**Reza Tafrishi** (University of Iceland, Reykjavik, Iceland) *Low Energy Electron Dissociation of Model Compounds for EUVL Resist Materials (p. 104)*
P 12	**Ali Kamali** (University of Iceland, Reykjavik, Iceland) *Low Energy Electron Induced Dissociation of potential Au(I) Precursors for Focused Electron Beam Induced Deposition Technique (p. 106)*
P 13	**Maicol Cipriani** (University of Iceland, Reykjavik, Iceland) *Potential means for enhanced cross-linking efficiency of SAMs for the production of carbon nano-membranes; project and perspectives (p. 107)*
P 14	**Heinz Wanzenboeck** (Vienna University of Technology, Austria) *Magnetic Nanorings made by FEBID (p. 109)*
P 15	**Daniel Rhinow** ((ZEISS SMT, Rossdorf, Germany) *Multicomponent patterned ultrathin carbon nanomembranes by laser ablation (p. 111)*
P 16	**Po Yuan Shih** (ZEISS SMT, Rossdorf, Germany) *Focused Electron Beam Induced Deposition resolution study on EUV masks (p. 112)*

P 1. Magnetic characterization of Cobalt Nanowires and Square Nanorings fabricated by Focused Electron Beam Induced Deposition

F. Venturi[1,2]*, G.C. Gazzadi[2], A.H. Tavabi[3], A. Rota[4], R.E. Dunin-Borkowski[3], and S. Frabboni[1,2]

[1] FIM Department, University of Modena and Reggio Emilia, Via G. Campi 213/a, Modena I-41125, Italy
[2] CNR Institute Nanoscience, S3 Center, Via G. Campi 213/a, Modena I-41125, Italy
[3] Ernst Ruska-Centre for Microscopy and Spectroscopy with Electrons and Peter Grünberg Institute, Forschungszentrum Jülich, 52425 Jülich, Germany
[4] Intermech-Mo.Re. Center, University of Modena and Reggio Emilia, Via Vignolese 905/b, Modena I-41125, Italy

* Corresponding author: federico.venturi@unimore.it

The research on magnetic nanostructures is driven by their promising applications in magnetic random-access memory, magnetic logic nanodevices, and high-density data storage [1]. Focused electron beam induced deposition (FEBID) is a versatile technique for the deposition of nanostructures of the desired shape and size. The shape has an important role in determining the magnetic anisotropy of the nanostructures, which is critical for storing magnetic information in a stable and reliable way. In this work, we deposited nanowires (NWs) and square nanorings by FEBID of Co-carbonyl precursor ($Co_2(CO)_8$), and analyzed their magnetic properties using off-axis electron holography (EH), Lorentz transmission electron microscopy (L-TEM) and magnetic force microscopy (MFM).

EH measurements on as-deposited NWs are presented in Figure 1. They reveal single-domain magnetic states, with a higher phase shift, then a higher magnetization [2], for 5 keV deposition than for 15 keV deposition. This results from the higher number of contour lines around the NW. This difference may result both from a greater relative Co content (by 5–10% for the 5 keV deposition than for the 15 keV deposition) and from a difference in NW width, as the 5 keV ones are wider than those grown at 15 keV. Also, a longer deposition time results in a higher magnetic signal, due to the higher amount of material deposited.

L-TEM was used to image magnetic domain walls in NWs and nanorings and their motion as a function of applied magnetic field [3]. The domain walls manifested as a "kink" when observed with L-TEM, allowing for the measurement of the domain wall length that could be used for investigating the nanowire magnetic hysteresis. The NWs exhibit almost square hysteresis loops, with coercivities of approx. 10 mT. The nanorings show two different magnetization states: for low values of the applied in-plane field (0.02 T) a horseshoe was found [4], as shown in Figure 2. The horseshoe state could be changed to an opposite horseshoe state by reversing the magnetic field. An onion state [4] is observed at remanence for higher values of the applied in-plane field (0.3 T) both using L-TEM and MFM. An MFM image of a square nanoring exhibiting an onion state is presented in Figure 3.

Our results confirm the suitability of FEBID for nanofabrication of magnetic structures with tailored geometries and demonstrate the versatility of TEM techniques for the study and manipulation of magnetic domain walls in nanostructures. Altogether, EH, L-TEM and MFM provide complementary information about their static and dynamic magnetic properties.

References

[1] S.Y. Chou, M.S. Wei, P.R. Krauss, P.B. Fischer, *Single-domain magnetic pillar array of 35 nm diameter and 65 Gbits/in^2 density for ultrahigh density quantum magnetic storage*, J. Appl. Phys 76, 6673 (1994).

[2] R.E. Dunin-Borkowski, T. Kasama, A. Wei, S. L. Tripp, M.J. Hytch, E. Snoeck, R. J. Harrison, A. Putnis, *Off-axis electron holography of magnetic nanowires and chains, rings, and planar arrays of magnetic nanoparticles*, Microsc. Res. Tech. 64, 390–402 (2004).

[3] L.A. Rodríguez, C. Magén, E. Snoeck, L. Serrano-Ramón, C. Gatel, R. Córdoba, E. Martínez-Vecino, L. Torres, J.M. De Teresa, M.R. Ibarra, *Optimized cobalt nanowires for domain wall manipulation imaged by in situ Lorentz microscopy*, Appl. Phys. Lett. 102, 022418 (2013).

[4] P. Vavassori, M. Grimsditch, V. Novosad, V. Metlushko, B. Ilic, *Metastable states during magnetization reversal in square permalloy rings*, Phys. Rev. B 67, 134429 (2003).

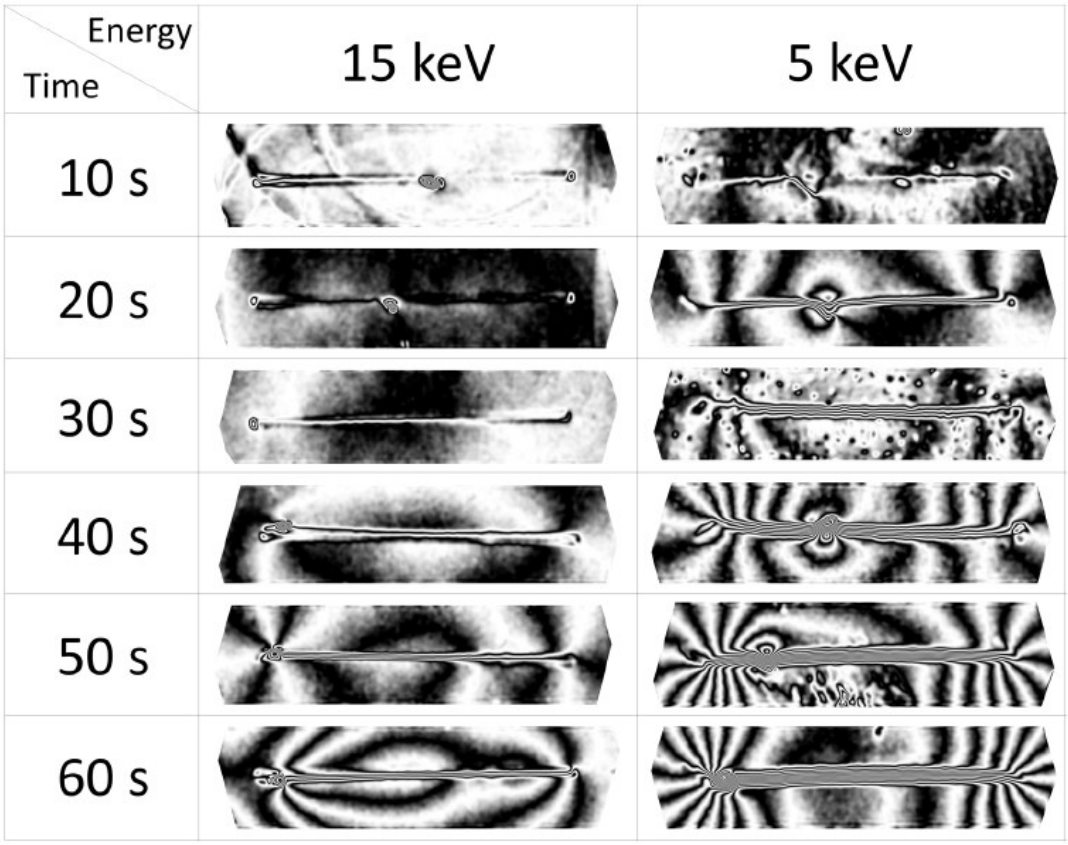

Fig. 1: Cosine of 18 times the magnetic phase shift recorded using EH from Co NWs deposited at electron beam energies of 15 and 5 keV for increasing deposition times (from 10 to 60 s). The black equiphase contours have a dipolar form, in particular for longer deposition times and for deposition at 5 keV, leaving one vertex of each NW and entering the opposite one.

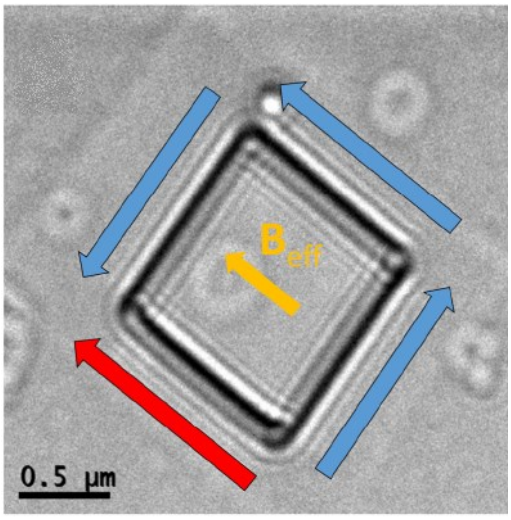

Fig. 2: L-TEM image of a square ring, showing the magnetization direction of each of the composing NWs under an applied magnetic field B_{eff} = 0.02 T. The micrograph shows a saturated horseshoe state.

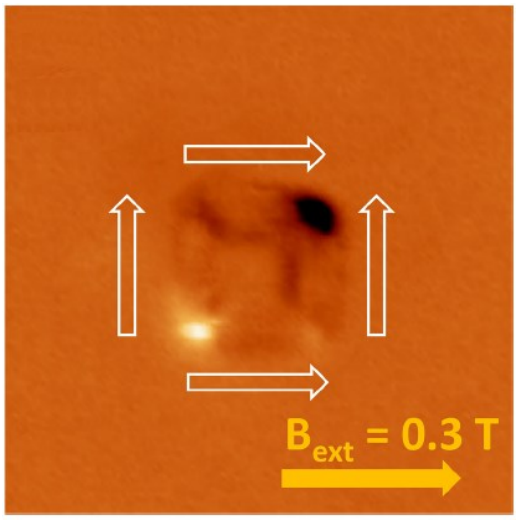

Fig. 3: MFM image of the square ring after applying a 0.3 T external field oriented along the side towards the right. This domain arrangement, with bright and dark spots at the vertices of the diagonal, provides evidence for a magnetic onion state, as indicated by the white arrows.

P 2. Micro-patterning of electrochromic Prussian Blue particles using focused electron beam irradiation

Y. Katori, Y. Suzaka, and M. Shimojo*

Department of Materials Science and Engineering, Shibaura Institute of Technology, 3-7-5 Toyosu, Koto, Tokyo, 135-8548, Japan

* Corresponding author: mshimojo@shibaura-it.ac.jp

Electrochromic (EC) materials can reversibly change their optical properties under an applied voltage as a result of electrochemical redox reaction. Prussian Blue (PB) is a well-known EC material that changes the colour form blue to colourless and transparent. When voltage is applied in the presence of K^+ ions, PB shows EC characteristics by removing and inserting K^+. The colour changes from blue to transparent by reduction and returns to blue by oxidation [1, 2].

Recently, PB is used as display elements. The fine patterning of PB particles on a transparent substrate would lead to the development of high-quality display elements. Thus, a patterning technique was developed and the effects of electron dose were investigated in this research.

Figure 1 shows a schematic illustration of this patterning method. This method consists of three steps. Firstly, PB particles, the diameter of which was in a range of 10-20 nm, were placed over the entire surface of an ITO substrate. Secondly, focused electron beams, the acceleration voltage of which was 20kV, were irradiated on the PB particles in a hollow rectangle, as a target shape, on the surface using a scanning electron microscope at electron doses of 50 and 1500 C/m^2. Finally, the unfixed particles were removed using ultrasonication in pure water for 10 s. In the second step, some decomposition products formed by the electron beam irradiation are considered to fix the PB particles, as a similar mechanism described elsewhere [3]. EC characteristics were then investigated by applying either +1.5 V or -1.5 V to the substrate in an aqueous KCl solution adjusted to pH 4.

Figure 2 shows optical microscope (OM) images of the PB particles fixed on the ITO substrate at electron doses of 50 and 1500 C/m^2. PB particles were fixed in the targeted hollow rectangle at an electron dose of 50 C/m^2. While at a dose of 1500 C/m^2, PB particles were fixed in a solid rectangle. At a high dose, a large number of back-scattered electrons from the substrate, which are ranged in the order of a few microns [4], may contribute to the fixation even at the central region of the rectangle.

Figure 3 shows OM images of the patterned PB particles fixed at a dose of 50 C/m^2 and at oxidized and reduced states. The PB can be changed in colour reversibly between blue and colourless transparent. Figure 4 shows the PB particles arranged in the form of our university emblem at an electron dose of 50 C/m^2, indicating a change in colour. This proves that this method can be used for complex patterning at a resolution of less than 1 µm.

References

[1] L.M.N. Assis, R. Leones, J. Kanicki, A. Pawlicka, M.N. Silva, *Prussian Blue for electrochromic devices,* J. Electroanal Chem. 777, 33-39 (2016).

[2] S. Hara, H. Tanaka, T. Kawamoto, M. Tokumoto, M. Yamada, A. Gotoh, H. Uchida, M. Kurihara, M. Sakamoto, *Electrochromic Thin Film of Prussian Blue Nanoparticles Fabricated using Wet Process,* Jpn. J. Appl. Phys. 46, 945-947 (2007).

[3] T. Noriki, S. Abe, K. Kajikawa, M. Shimojo, *Patterning technique for gold nanoparticles on substrates using a focused electron beam,* Beilstein J. Nanotechnol. 6, 1010-1015 (2015).

[4] D. Morioka, T. Nose, T. Chikuta, K. Mitsuishi, M. Shimojo, *Fixation mechanisms of nanoparticles on substrates by electron beam irradiation,* Beilstein J. Nanotechnol. 8, 1523-1529 (2017).

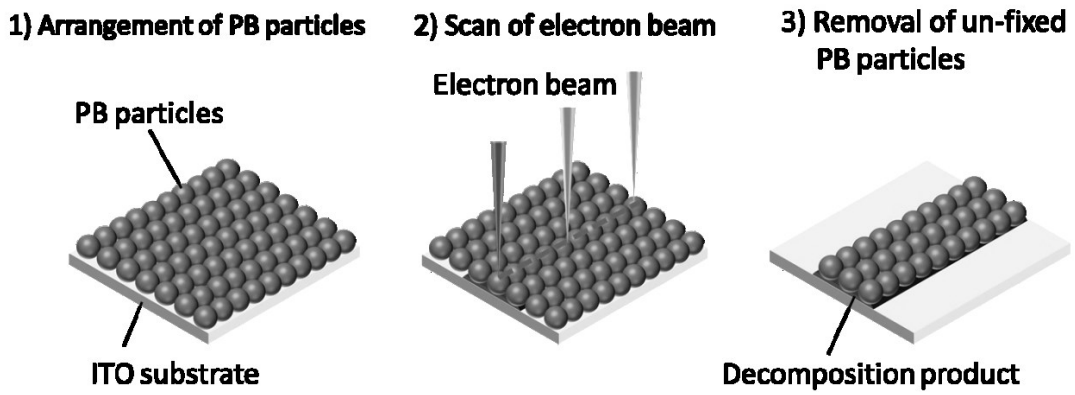

Fig. 1: Schematic illustration of experimental procedure

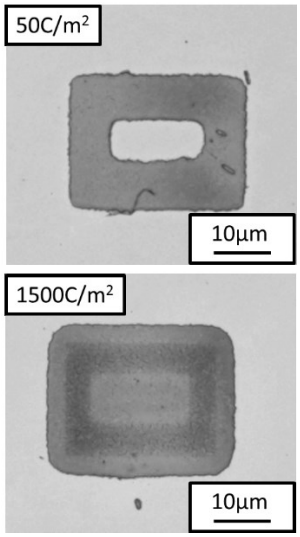

Fig. 2: OM images of PB particles fixed on an ITO substrate, at electron doses of 50 C/m^2 and 1500 C/m^2.

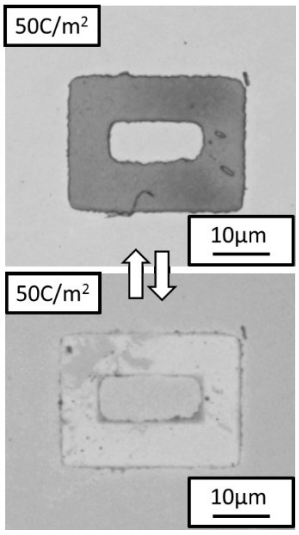

Fig. 3: OM images indicating a change in colour of patterned PB particles fixed at an electron dose of 50 C/m^2.

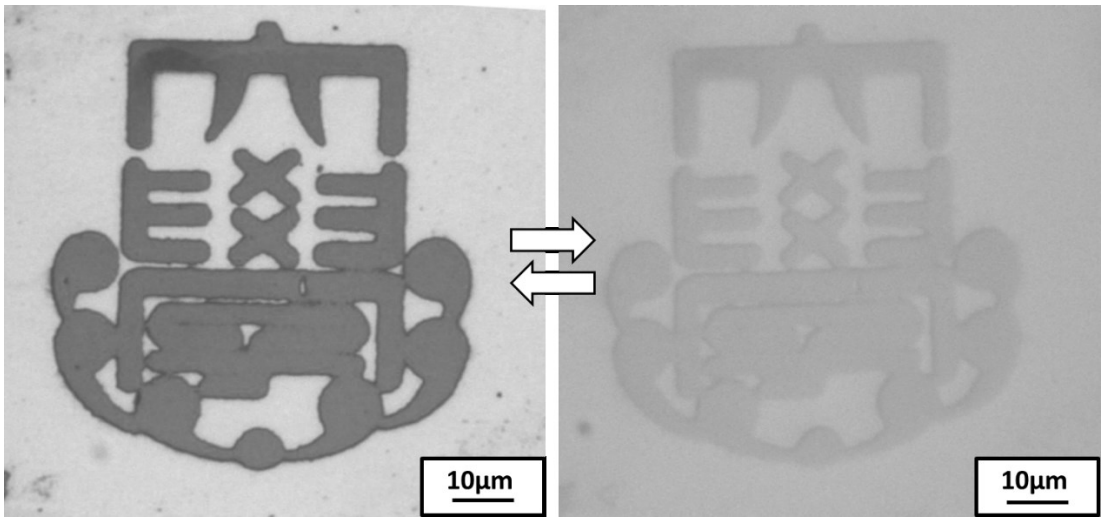

Fig. 4: PB particles were arranged in the form of our university emblem, indicating a change in colour.

P 3. Cisplatin Revisited: On the Strong Electron-Induced Reducing Ability of NH_3 Ligands in Ammine Precursors

M. Rohdenburg*, K. Ahlenhoff, and P. Swiderek

University of Bremen, Fachbereich 2 (Chemie/Biologie), Institute of Applied and Physical Chemistry, Leobener Straße 5, PO Box 330440, 28334 Bremen, Germany

* Corresponding author: m.rohdenburg@uni-bremen.de

Cisplatin (*cis*-$Pt(NH_3)_2Cl_2$ = *cis*-diamminedichloroplatinum(II), CDDP) has recently been tested as a precursor for FEBID of Pt but instead of yielding pure deposits, high chlorine contents were obtained [1]. This observation contrasted with electron exposure experiments conducted on CDDP crystals which nicely decompose under the electron beam to yield pure metallic Pt. This discrepancy was explained by the different trapping capabilities of a bulk crystal and a thin surface adsorbate. While NH_3 ligands can simply desorb from a thin deposit, they remain trapped in a large crystal and can thus unfold their known capability to act as a reducing agent under electron irradiation [2] and, therefore, to fully reduce the Pt in the crystal.

In the case of the structurally similar *cis*-$Pt(CO)_2Cl_2$, a high chlorine content of the primary deposit was confirmed in accordance with our CDDP results [3]. An electron-stimulated purification procedure involving high electron doses of up to $1.5x10^{19}$ e^-/cm^2 was then successfully applied to remove the chlorine content by an electron-stimulated desorption (ESD) type process.

Herein, we revisit CDDP in light of the results obtained from the *cis*-$Pt(CO)_2Cl_2$ study. We have grown crystalline CDDP surface layers on gold via a low-pressure sublimation approach and characterized them by Reflection-Absorption Infrared Spectroscopy (RAIRS). ESD from these CDDP films was then observed during exposure to 500 eV electrons. The results confirm that NH_3 in fact enhances the removal of chlorine from the deposit. An electron-induced reaction of the NH_3 ligands supplies hydrogen that enables the conversion of chlorine ligands to HCl as seen in the ESD mass spectrum. These results also imply that post-deposition purification of chlorine-containing FEBID deposits using NH_3 as process gas should be a promising approach.

References

[1] J. Warneke, M. Rohdenburg, Y. Zhang, J. Orszagh, A. Vaz, I. Utke, J.Th.M. De Hosson, W.F. van Dorp, P. Swiderek, *Role of NH_3 in the Electron-Induced Reactions of Adsorbed and Solid Cisplatin*, J. Phys. Chem. C 120, 4112 (2016).

[2] T. Hamann, L. Kankate, E. Böhler, J.H. Bredehöft, F.M. Zhang, A. Gölzhäuser, P. Swiderek, *Functionalization of a Self-Assembled Monolayer Driven by Low-Energy Electron Exposure*, Langmuir 28, 367 (2012).

[3] J.A. Spencer, Y.-C. Wu, L. McElwee-White, D.H. Fairbrother, *Electron Induced Surface Reactions of* cis-*$Pt(CO)_2Cl_2$: A Route to Focused Electron Beam Induced Deposition of Pure Pt Nanostructures*, J. Am. Chem. Soc. 138, 9172 (2016).

P 4. Electron-induced decomposition of silver(I) carboxylates: Role of the alkyl chain

K. Ahlenhoff* and P. Swiderek

University of Bremen, Fachbereich 2 (Chemie/Biologie), Institute of Applied and Physical Chemistry, Leobener Straße 5, PO Box 330440, 28334 Bremen, Germany

* Corresponding author: kai.ahlenhoff@uni-bremen.de

Focused electron beam induced deposition (FEBID) of silver precursors has recently gained increasing attention because silver nanostructures are desired for plasmonic applications [1]. The most promising precursors studied so far are complexes with carboxylate ligands. Even though such compounds exhibit only very low vapor pressures, recent developments in the field of gas injection systems make them suitable for FEBID applications [2]. However, relatively little is known about their decomposition behavior upon electron irradiation. From a chemical point of view it is expected that α-cleavage of the carboxylate group would be the dominant decomposition channel leading to a formation of gaseous CO_2 and an alkyl radical. The stability of this radical should then play an essential role for the subsequent chemical processes. While highly reactive radicals would react rapidly with other surface species and thus become integrated in the deposit, more stable radicals with longer lifetimes might be able to desorb and would thus not contribute to the carbon contamination.

Here we report an electron stimulated desorption (ESD) study of two silver(I) carboxylate compounds with varying alkyl chains (Fig. 1) to investigate this dependency of the reaction on the structure of the radical. The first precursor is silver(I)-2,2-dimethylbutyrate that has recently been applied in FEBID [1]. According to our hypothesis explained above, this compound would form a stable tertiary alkyl radical. The second precursor, silver(I) heptanoate, has a similar number of carbon atoms but a linear alkyl chain so that the presumably resulting primary radical is highly reactive. The comparison of ESD mass spectra from both precursors reveals in fact that, upon electron irradiation, only silver(I)-2,2-dimethylbutyrate generates large volatile fragments that can be related to desorption of the intact radical.

References

[1] K. Höflich, J. Jurczyk, Y. Zhang, M. Puydinger dos Santos, M. Götz, C. Guerra-Nuñez, J. Best, C. Kapusta, I. Utke, *Direct Electron Beam Writing of Silver-Based Nanostructures*, ACS Appl. Mater. Interfaces 9, 24071 (2017).

[2] L. Berger, K. Madajska, I.B. Szymanska, K. Höflich, M.N. Polyakov, J. Jurczyk, C. Guerra-Nuñez, I. Utke, *Gas-assisted silver deposition with a focused electron beam*, Phys. Appl. Lett. 94, 54321 (2009).

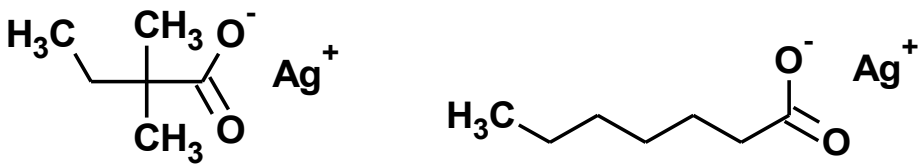

Fig. 1: Molecular structure of silver(I)-2,2-dimethylbutyrate (left) and silver(I) heptanoate (right).

P 5. Thermal Evaluation of Potential FEBID Precursors

C. Glessi[1]*, J. Jurczyk[2,3]*, K. Madajska[3], I. Szymanska[3], I. Utke[2], and M. Tilset[1]

[1] Department of Chemistry - University of Oslo, Sem Sælands vei 26, 0371 Oslo, Norway
[2] EMPA, Swiss Federal Laboratories for Materials Science and Technology, Feuerwerkerstrasse 39, 3602 Thun, Switzerland
[3] Faculty of Physics and Applied Computer Sciences, AGH University of Science and Technology Krakow, Al. Mickiewicza 30, 30-059 Kraków, Poland
[4] Department of Chemistry, Nicolaus Copernicus University, Gagarina 7, 87100 Toruń, Poland

* Corresponding authors: cristiano.glessi@smn.uio.no, Jakub.Jurczyk@empa.ch

The development of compounds specifically designed to be applied as FEBID precursors is of focal importance for the progress of this field. One of the key properties of the potential precursors is that they have to be stable in gas phase and volatile at moderate temperatures. Different methods have been applied to investigate the physical properties of the precursors, ranging from sublimation to thermogravimetric analysis (TGA).

This last technique has so far proved limited applicability for real FEBID process. The data obtained from the TGA experiments and from the actual evaporation of the precursor in vacuum chamber of FEBID equipment did not always match, due to a staggering difference in experimental conditions. [1][2]

The use of TGA under vacuum (10^{-2} mbar) led instead to results that match the ones obtained from the FEBID experiments (Figure 1). Using *vacuum*-TGA gives quantitative information not only about the thermal stability and volatility of the precursor, but eventually, its vapor pressure. [3] *Vacuum*-TGA experiments at a constant temperature made it also possible to obtain the perfect evaporation temperature to achieve a constant precursor flow in vacuum. *Vacuum*-TGA has been applied to several gold and silver containing precursors that present a great chemical difference (Figure 2 and Figure 3).

The development of a more suitable method of thermodynamical evaluation for FEBID precursors could lead finally to establish a standard procedure to fully characterize, chemically and physically, potential organometallic precursors.

References

[1] E. Szłyk, P. Piszczek, M. Chanerski, A. Golinski, *Studies of thermal decomposition process of Ag(I) perfluorinated carboxylates with temperature variable IR and MS*, Polyhedron 20, 2853 (2001).

[2] K. Höflich, J. Jurczyk, Y. Zhang, M.V. Puydinger dos Santos, M. Götz, C. Guerra-Nuñez, J.P. Best, C. Kapusta, I. Utke, *Direct Electron Beam Writing of Silver-Based Nanostructures,* ACS Appl. Mater. Interfaces 9, 24071 (2017).

[3] G.V. Kunte, S.A. Shivashankar, A.M. Umarji, *Thermogravimetric evaluation of the suitability of precursors for MOCVD*, Meas. Sci. Technol. 19, 025704 (2008).

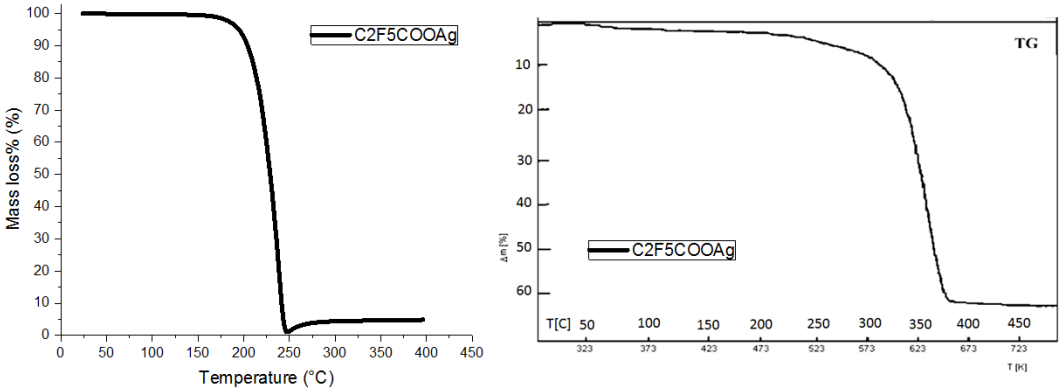

Fig. 1: Comparison between results obtained with *vacuum*-TGA for C_2F_5COOAg (sx) and the previously reported TGA (dx).

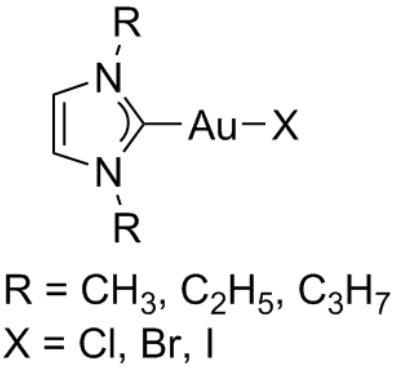

Fig. 2: Generic structure of the gold complexes.

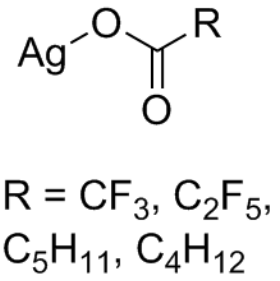

Fig. 3: Generic structure of the silver complexes.

P 6. Ice Resists for 3D Electron Beam Processing: Instruments in Denmark and China

D. Zhao[1], Y. Hong[2], W. Tiddi[1], A. Elsukova[1], M. Beleggia[1], M. Qiu[2,3]*, and A. Han[1]*

[1] Danchip/CEN, Technical University of Denmark, 2800 Kgs. Lyngby, Denmark
[2] College of Optical Science and Engineering, Zhejiang University, 310027 Hangzhou, China
[3] Westlake University, 310030 Hangzhou, China

* Corresponding author: minqiu@zju.edu.cn, anph@dtu.dk

3D printing has had a revolutionary impact in mechanical engineering, and downscaling efforts has made significant progress. Most noticeable is two photon polymerization that allows fabrication of 3D structures down to 200 nm [1]. Unfortunately, this technology is inherently slow because of the nature of the unlikely 2 photon reaction which must be enhanced with a well-controlled localized polymerization process. Scalability is also difficult.

For 3D nanoscale patterning, electron beam processing, such as focused electron beam induced deposition (FEBID) is well known and enables beautiful and highly complex nanoscale 3D structures in a few nanometer sizes. Another newer but fundamentally different electron beam processing method towards 3D nanofabrication is ice lithography (IL), where ice serves as a resist for electron beam lithography. While FEBID is an electron-gas-surface interaction, IL is an electron-solid-surface interaction. The first dedicated IL instrument was reported in 2011 [2], which could be used to fabricate 3D nanostructures on fragile freely hanging single-walled carbon nanotubes [3]. Since the IL instrument is not available commercially, it usually takes a very long time to build up a dedicated system.

As collaborating groups, we report the design, material choice, implementation and operation of two IL instruments; one at Technical University of Denmark (DTU), Denmark, and one at Zhejiang University (ZJU), China. They are maybe the only two IL instruments that work well in the world. As shown in Figure 1, the Danchip's research group at DTU has repurposed a Zeiss LEO SEM equipped with a Raith Elphy Quantum EBL module [4,5]. The SEM vacuum chamber was fitted with a liquid nitrogen cooled cryostage for sample cooling and cold finger to condense vacuum contaminants. Through a custom gas injection system (GIS) organic molecule, e.g. anisole, is injected into the SEM chamber and condensed onto the sample. The GIS controls the deposition rate and final ice film thickness. A load-lock allows fast sample transfer and exchange while maintaining cryogenic conditions in the process environment. By stacking nanoscale patterns made in organic ice, 3D nanostructures are created through complementary cyclic condensation, exposure and sublimation processes (Fig. 1). Here, organic ice is usually a negative resist and the patterns after exposure are hardly removed even when placed in mild acids and bases. Additional etching process is necessary to realize pattern transfer for organic ice.

Prof. Qiu's group at ZJU has modified a Zeiss Sigma SEM (Fig. 2). The instrument is similar in principle to that at DTU, which is equipped with a gas injection system, liquid nitrogen cooled cryostages, and a load-lock chamber. In ZJU instrument, water ice is formed onto the sample and acts as a positive resist. It can also deposit metals at cryogenic temperature for pattern transfer. Due to the very low sensitivity of water ice resist, a bridge-like nanostructure could be obtained by modulating the dose during onetime exposure.

References

[1] X. Zhou, Y. Hou, J. Lin, *A review on the processing accuracy of two-photon polymerization*, AIP Adv. 5, 030701 (2015).

[2] A. Han, J. Chervinsky, D. Branton, J. Golovchenko, *An ice lithography instrument*, Rev. Sci. Instru. 82, 065110 (2011).

[3] A. Han, A. Kuan, J. Golovchenko, D. Branton, *Nanopatterning on nonplanar and fragile substrates with ice resists*, Nano Lett. 12, 1018–1021 (2012).

[4] W. Tiddi, A. Elsukova, H.T. Le, P. Liu, M. Beleggia, A. Han, *Organic Ice Resists*, Nano Lett. 17, 7886-7891 (2017).

[5] W. Tiddi, A. Eluskova, M. Beleggia, A. Han, *Organic ice resists for 3D electron beamprocessing: instrumentation and operation*, Microelectron. Eng. 192, 38-43 (2018).

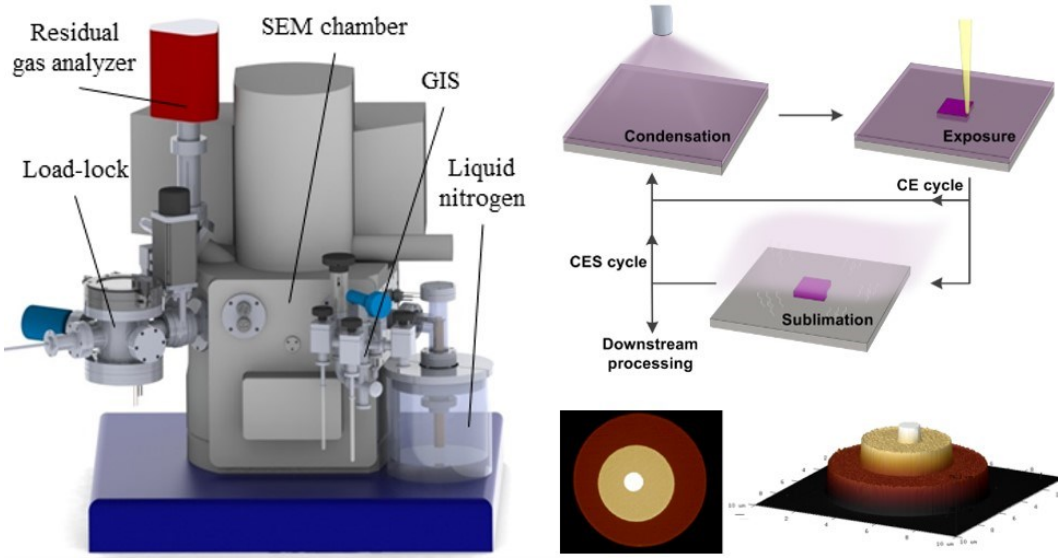

Fig. 1: DTU IL instrument (left) and organic ice resist processing sequence and AFM images of fabricated 3D structures (right).

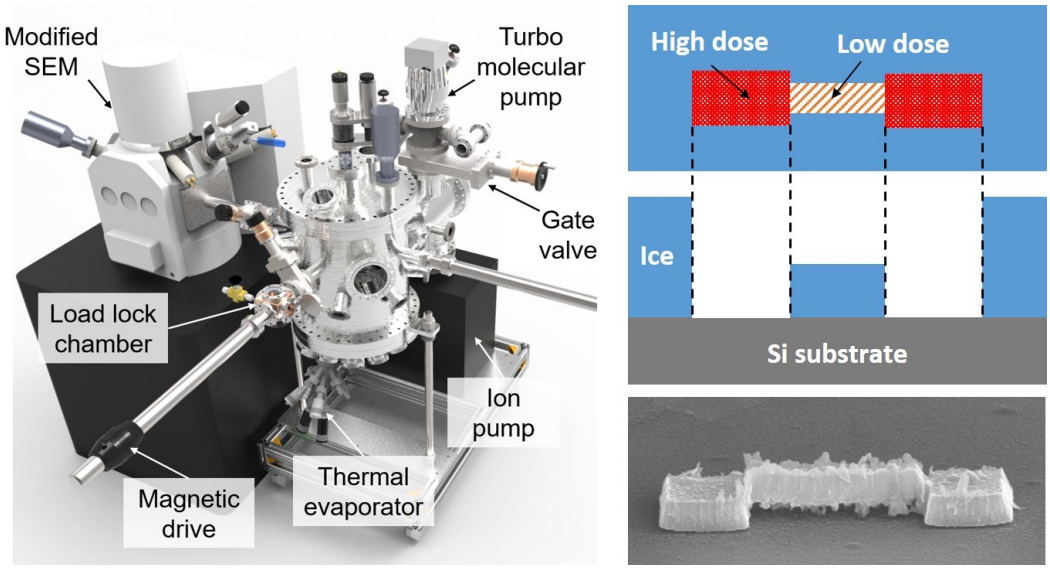

Fig. 2: ZJU IL instrument (left) and water ice resist under dose-modulated exposure and SEM image of fabricated 3D bridge-like structures (right).

P 7. New mask absorber materials addressed by FEBIP based Mask Repair

N. Auth*, D. Rhinow, P. Spies, and T. Hofmann

Carl Zeiss SMT GmbH - ZEISS Group, Industriestr. 1, 64380 Rossdorf, Germany

* Corresponding author: nicole.auth@zeiss.com

Focused electron beam tools are widely used by the semiconductor industry. Despite its unique properties, the FEBIP technology is still a niche in industrial application. However, it has proven to be the key technology for semiconductor mask repair, an indispensable step in the mask fabrication process.

In contrast to ion tools with their physical sputtering contribution, the chemical nature of the FEB process gives rise to the main merit of the technology and at the same time causes one of its main challenges – a (potentially) highly selective, non-invasive process requiring an etching chemistry which is unique for each material that has to be processed.

Driven by shrinking features sizes, highly durable materials have been introduced and the customization of mask materials fitting the needs of specific customers has led to a steep increase in mask types on the market. Another example is the emerging EUV technology (Fig. 1) calling for a bunch of new materials as candidates for EUV mask fabrication. Especially the absorber layer still does not fully meet the requirements of the industry, therefore new materials, such as Ni, Ni oxides and alloys, etc. are discussed [1-3].

In order to keep up pace with the ongoing development significant effort is required. This opens a wide field for potential basic research activities, ranging from chemistry screening for specific materials, building a more general theoretical understanding of the chemical processes as well as tailoring of new precursors fitting the unique properties of the FEBIP technology. We will give insight into the current status of FEBIP mask repair technology with respect to the emerging challenges we are facing.

References

[1] V. Luong, V. Philipsen, E. Hendrickx, K. Opsomer, Ch. Detavernier, Ch. Laubis, F. Scholze, M. Heyns, *Ni-Al Alloys as Alternative EUV Mask Absorber*, Appl. Sci. 8(4), 521 (2018).

[2] D. Hay, P. Bagge, I. Khaw, L. Sun, O. Wood, Y. Chen, R.-H. Kim, Z. J. Qi, Z. Shi*, Thin absorber extreme ultraviolet photomask based on Ni–TaN nanocomposite material*, Opt. Lett. 41, 3791 (2016).

[3] D.G. Woo, J.H. Kim, J.S. Kim, S.l. Hong, J. Ahn, *Study of Novel EUV Absorber: Nickel & Nickel Oxide*, Korean J. Met. Mater. 55, 198 (2017).

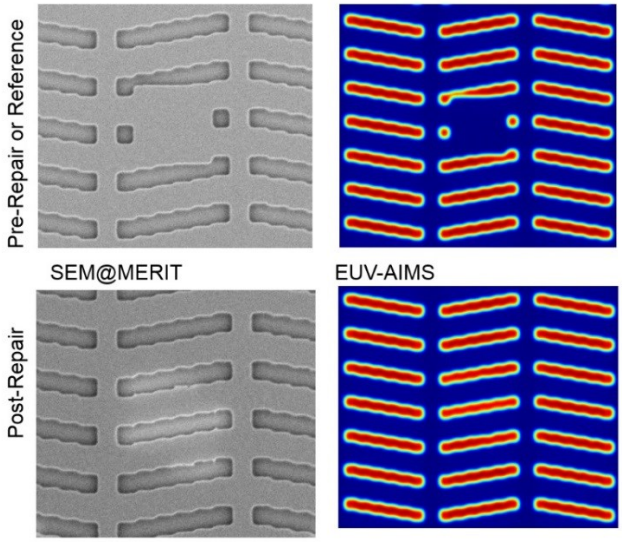

Fig. 1: Ebeam repair of a EUV photomask with a MeRiT® tool. (left) SEM images of a EUV mask with an opaque defect before (top) and after repair (bottom). (right) Acquisition of aerial images with AIMS™ EUV confirms successful repair.

P 8. Investigating the limits of Dark-Field magneto-optical Kerr effect for the characterization of three-dimensional magnetic FEBID nanowires

L. Skoric[1]*, D. Sanz-Hernandez[1], J.D. Fowlkes[2], P.D. Rack[2], and A. Fernández-Pacheco[1]

[1] Cavendish Laboratory, University of Cambridge, JJ Thomson Avenue, CB3 0HE, UK
[2] Nanofabrication Research Laboratory, Center for Nanophase Materials Sciences, Oak Ridge National Laboratory, Oak Ridge, Tennessee 37831, United States

* Corresponding author: ls604@cam.ac.uk

Three-dimensional spintronics is a newly emerging area of research, where 3D magnetic nanostructures are block elements where data is stored and processed along the whole space. These devices have a potential to become a disruptive technology, outperforming CMOS by having storage capacities reaching Tbit/in^2, non-volatility, low power consumption during operation, and with the ability of performing logic operations. Simulations of three-dimensional spintronic systems such as spirals, tubes and spheres suggest the emergence of unexplored physics [1,2].

However, so far, very few of such systems have been experimentally realised due to huge challenges regarding fabrication and characterization of three-dimensional nanostructures. This has been restricting the memory density of spintronic devices when compared to modern CMOS architectures, limiting their technological applicability. New Focused Electron Beam Induced Deposition (FEBID) nanoprinting methods [3, 4] make now possible, for the first time, the development of 3D magnetic nanostructures. The study of magnetic properties of such systems is far from trivial and requires new characterisation methods. Previously, methods such as transmission electron microscopies (TEM) and X-ray microscopy (XM) have been used for that purpose [5]. More recently, Mamoori *etal d*emonstrated the use of high-resolution micro-Hall magnetometry for characterisation of freestanding CoFe 3D nano-architectures [6]. Moreover, dark field Magneto-Optical Kerr effect (DFMOKE) method of characterization of 3D magnetic structures has recently been developed by our group [7]. In MOKE, the change of polarization of light reflected from a magnetic sample is exploited to deduce the magnetic moment with high sensitivity, going as low as $\mu \sim 6 \times 10^{-15} Am^2$ [8]. In the setup similar to the diffraction MOKE [9] where a detector is measuring light reflected under different angles with respect to the substrate plane, DFMOKE separates the substrate and nanostructure signals for simultaneous imaging. In the previous study, DFMOKE has been used to probe 300nm wide nanowires (NWs) and characterize substrate-to-nanowire domain wall injection [7].

However, the DFMOKE measurements are very sensitive to deviations in geometry and roughness of the sample. Therefore, the objective of this study has been investigating the limits of DFMOKE, how it can be extended to smaller magnetic volumes, and applied to nanowires with varying lengths and widths. Pt-C NWs were fabricated 30° to the substrate using FEBID with the widths ranging from 300nm down to 60nm (Fig. 2). Curvature at the substrate-to-nanowire interconnect introduces a pinning potential for domain walls. To reduce this effect, a smooth transition was fabricated by continuous variation of FEBID dwell times in the first 300nm of the structures. The structures were used as a scaffold for evaporation of 50nm thick layer of permalloy, making the magnetic volume between $5.2 \times 10^{-14} Am^2 - 1.0 \times 10^{-14} Am^2$. The resolution limit of the dark-field MOKE for characterization of 3D nanostructures was tested (Fig. 3). We investigated the effect of width on domain wall motion and pinning. The evolution of transmission fields with geometry will be discussed in the framework of local roughness in the wires, which depends on the details of the FEBID scanning strategy. This work will serve as a basis for further investigation of 3D domain wall conduits of more complex geometries.

References

[1] A. Fernández-Pacheco, R. Streubel, O. Fruchart, R. Hertel, P. Fischer, R.P. Cowburn, T*hree-dimensional nanomagnetism,* Nat. Commun. 8, (2017).

[2] R. Streubel et al., *Magnetism in curved geometries*, J. Phys. Appl. Phys., vol. 49, no. 36, p. 363001 (2016).

[3] A. Fernández-Pacheco et al., *Three dimensional magnetic nanowires grown by focused electron-beam induced deposition*, Sci. Rep. 3 (2013).

[4] J. Pablo-Navarro et al., T*uning shape, composition and magnetization of 3D cobalt nanowires grown by focused electron beam induced deposition (FEBID)*, J. Phys. Appl. Phys. 50, 18, 18LT01 (2017).

[5] P. Fischer, *X-Ray Imaging of Magnetic Structures*, IEEE Trans. Magn. 51, 2, 1–31 (2015).

[6] M.K.I. Al Mamoori et al., *Magnetic Characterization of Direct-Write Free-Form Building Blocks for Artificial Magnetic 3D Lattices*, Materials 11, 2, 289 (2018).

[7] D. Sanz-Hernández, R.F. Hamans, J.-W. Liao, A. Welbourne, R. Lavrijsen, A. Fernández-Pacheco, *Fabrication, Detection, and Operation of a Three-Dimensional Nanomagnetic Conduit*, ACS Nano (2017).

[8] D.A. Allwood, G. Xiong, M.D. Cooke, R.P. Cowburn, *Magneto-optical Kerr effect analysis of magnetic nanostructures*, J. Phys. Appl. Phys. 36, 18, 2175 (2003).

[9] M. Grimsditch, P. Vavassori, *The diffracted magneto-optic Kerr effect: what does it tell you?*, J. Phys. Condens. Matter 16, 9, R275 (2004).

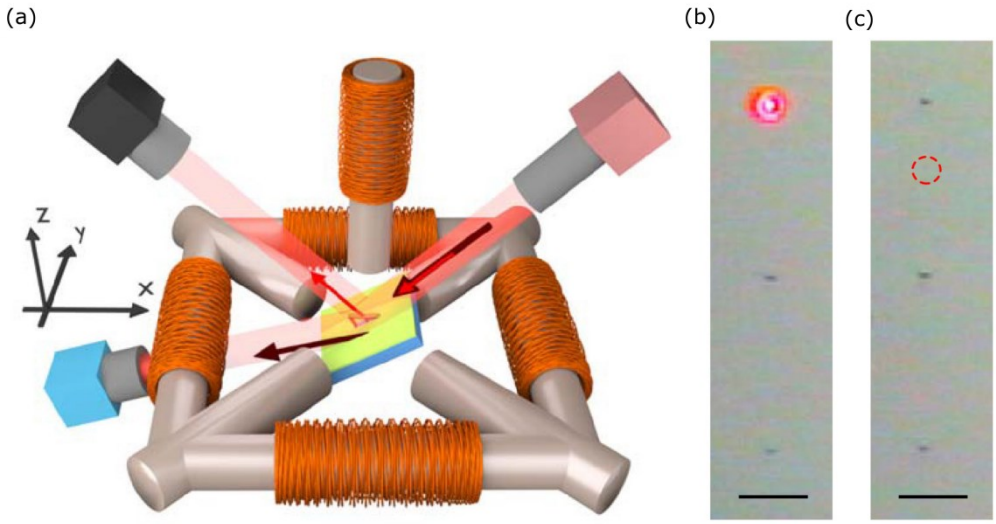

Fig. 1: Dark-field magneto-optical Kerr effect microscope configuration. (a) Substrate and sample reflect incident polarized laser light under different angles allowing independent magnetization measurements. (b) and (c) Image obtained with a CCD camera positioned at the same angle as black detector. Three NWs are observed as black dots on the image. The laser light is observed by the camera only when it is aligned with the structure (laser position in the second image marked with dotted circle). Adapted from [7].

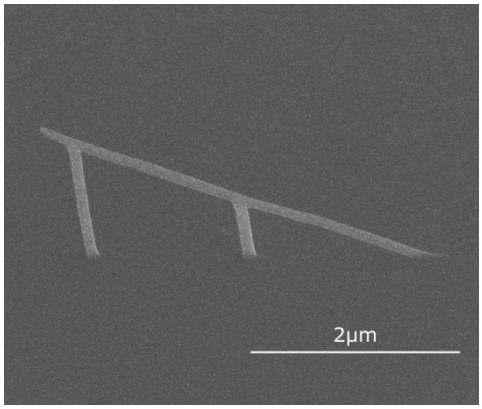

Fig. 2: 70nm wide NW built out of Pt-C. These are used as a scaffold for permalloy evaporation and are then characterized with dark-field MOKE.

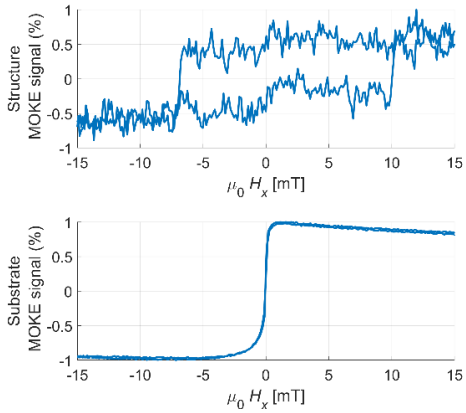

Fig. 3: Dark-field MOKE measurements of the 70nm wide NW (Fig. 2b). Substrate and structure signals are visibly separated. The switching fields of the structure are -6.8mT and 10.0mT.

P 9. Towards Cleanroom in an SEM

G. Jeevanandam*, V. van der Meijden, C.W. Hagen, and P. Kruit

Department of Imaging Physics, Delft University of Technology, Lorentzweg 1, 2628 CJ Delft, The Netherlands

* Corresponding author: G.Jeevanandam@tudelft.nl

A cleanroom is a necessity to fabricate nano-scale devices, because it protects the substrate from contamination as much as possible between the different steps in a fabrication process. A typical cleanroom fabrication process involves: substrate cleaning, deposition (evaporation or sputter), lithography and etching (dry etch or wet etch). All these steps require dedicated instruments in a cleanroom which is expensive to run. Furthermore, it is time consuming to manually switch from one tool to another for the subsequent process. Also, the fabrication area of interest for research is typically small, unlike the wafer-scale fabrication processes in cleanrooms. We envision fabricating an entire device inside a scanning electron microscope (SEM) i.e., "a cleanroom in an SEM". Our goal is to bring in a substrate inside the microscope and do the required steps to fabricate a device, including its inspection, in the same tool. This way, the vacuum is maintained between the different processes and, therefore, an expensive cleanroom will not be needed. We will achieve this by developing additional miniaturized standard nanofabrication tools as add-on's to an SEM. For this work, we are going to upgrade a dual beam instrument which combines an SEM and a focused ion beam (FIB) in a single instrument such that we already have the functionality of high resolution imaging along with milling of the sample and focused electron/ion beam induced deposition (EBID/IBID) and etching (EBIE).

To realize a cleanroom in an SEM, we are developing the following miniaturized tools. i) A heater that can be used in any SEM, as it is manufactured on top of a standard SEM stub. The heater can be used to clean the surface of the substrate and to remove adsorbed water vapor. ii) A novel miniature sputter tool, based on a DC micro-plasma source [1]. The schematic of the micro-plasma source, along with its measured Paschen curve is shown in Fig. 1. iii) A miniature deposition tool using thermal evaporation of materials. We are using the Philips cathodes from a cathode ray tube as a heating source. An image of the miniature evaporator along with a deposited Au layer is shown in Fig. 2. And iv), we are working on the integration of atomic layer deposition (ALD) in the SEM by modifying an existing gas insertion system (GIS). Here, we aim at thermal ALD processing using our homemade heater and using Pt EBID as a seed layer [2].

We envision the following example process flow for pattern transfer inside the SEM. We start with a clean substrate. Then, we deposit material (e.g. Au) on the substrate using the miniaturized evaporator. We pattern a desired shape using EBID (C-deposit) which acts as a mask [3]. Then, we transfer the EBID structure into the underlying deposited layer using the miniature sputter etch tool. Any remaining C-deposit can be removed by using EBIE using H2O vapor. We will present the ongoing developments in the poster.

References

[1] K.H. Schoenbach, K. Becker, *20 years of microplasma research: a status report*, Eur. Phys. J. D 70, 29 (2016).

[2] A.J.M. Mackus, S.A.F. Dielissen, J.J.L. Mulders, W.M.M. Kessels, *Nanopatterning by direct-write atomic layer deposition*, Nanoscale 4, 4477 (2012).

[3] M. Scotuzzi, M.J. Kamerbeek, A. Goodyear, M. Cooke, C.W. Hagen, *Pattern transfer into silicon using sub-10 nm masks made by electron beam induced deposition*, J. Micro/Nanolith. MEMS MOEMS 14, 031206 (2015).

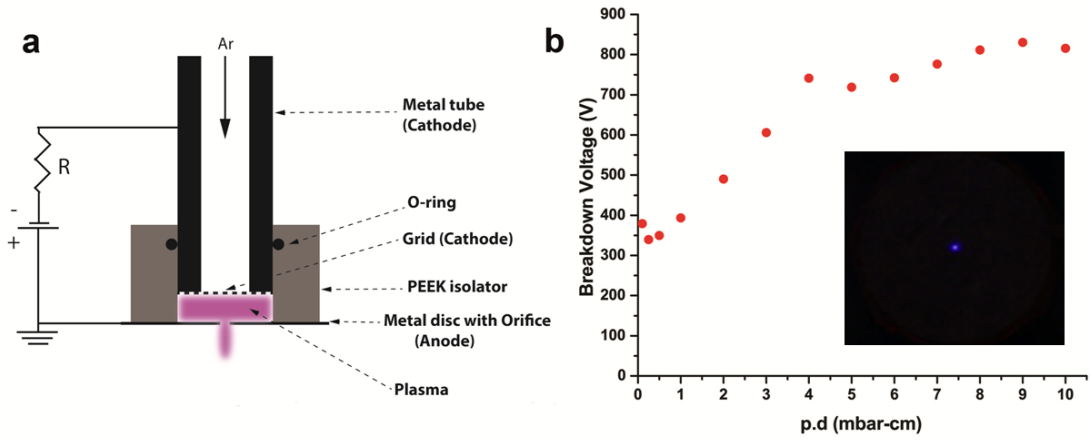

Fig. 1: a) Schematic of the DC microplasma source. b) Graph showing the Paschen curve measured for the microplasma source. Inset photograph showing the observed Ar plasma.

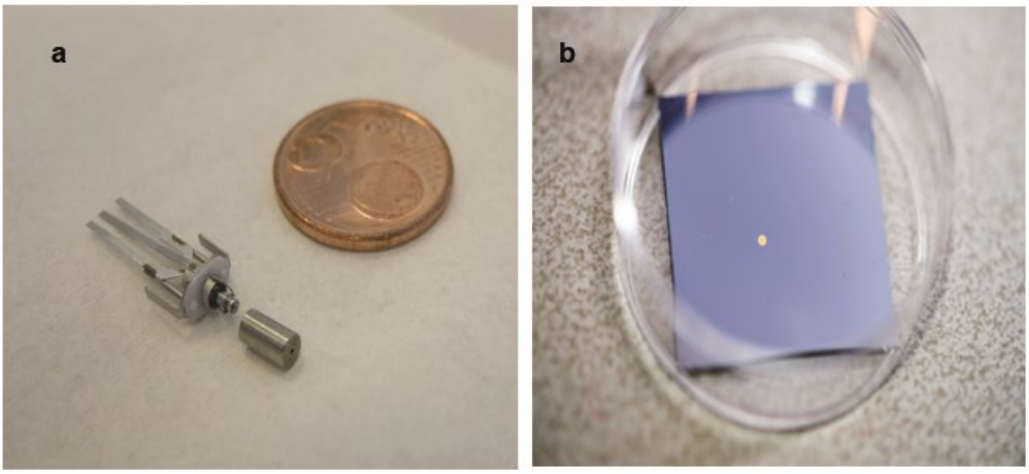

Fig. 2: a) Photograph showing the miniature evaporator source with a 5 Euro cent coin as a reference. b) Photograph of a 23x23 mm silicon sample with the deposited gold from the miniature evaporator.

P 10. Velocity Map Imaging Applied to Dissociative Electron Attachment for FEBID Precursors

M. Pintea* and N.J. Mason

School of Physical Sciences, The Open University, Milton Keynes, Walton Hall, MK7 6AA, United Kingdom

*Corresponding author: Maria.pintea@open.ac.uk

Developed less than a decade ago, the velocity map imaging technique can provide new insights into the spectroscopy and dissociation dynamics of the molecular states of precursors for FEBID. As part of the ELENA EU Horizon 2020 Training network, https://elena-eu.org. We will use velocity map imaging (VMI) to study Dissociative Electron Attachment (DEA) to FEBID precursor molecules and provide answers to the question of "How and where does DEA break ligands?" The efficiency of ligand fragmentation determines the final purity of the deposited metal elements on the substrate.

Preliminary experiments to explore VMI methodology have been performed on O_2 and NH_3, exploring DEA through 'resonances' at 6.5 eV and 11.5 eV. At higher energy we have repeated studies of Nag and Nandi, 2017 at energies of 21-35 eV to explore dissociation of molecular oxygen, by passing through a Rydberg state or by direct excitation dissociate in formation of a cation - anion pair:

$$O_2 + e^- \rightarrow O_2^* + e^- \rightarrow O^+ + O^- + e^-$$

We will now extend this methodology to study compounds used in FEBID such as $MeCpPtMe_3$, $W(CO)_6$, $Co_2(CO)_8$, $MeCpPtMe_3$, $Me_2Au(acac)$, $Pt(PF_3)_4$, $Co(CO)_3NO$ and $Si(OC_2H_5)_4$.

References

[1] R.N. Bhargava, V.S. Prabhudesai, E. Krishnakumar, *Resonances in dissociative electron attachment to water*, J. Phys. B: At. Mol. Opt. Phys. 42, 225203 (2009).

[2] C. Hauchard, P.A. Rowntree, *Low-energy electron-induced decarbonylation of $Fe(CO)_5$ films adsorbed on Au(111) surfaces*, Can. J. Chem. 89, 1163–1173 (2011).

[3] B. Omarsson, E.H. Bjarnason, S.A. Haughey, T.A. Field, A. Abramov, P. Klupfel, H. Jonssona, O. Ingolfsson, *Molecular rearrangement reactions in the gas phase triggered by electron attachment*, Phys. Chem. Chem. Phys. 15, 4754 (2013).

[4] R.N Bhargava, V.S. Prabhudesai, G. Aravind, P. Rawat, E. Krishnakumar, *Velocity Map Imaging of H^- Ions from Dissociative Electron Attachment to H_2O*, Journal of Physics: Conference Series, Molecular (2007).

[5] E. Szymanska Vaibhav, S. Prabhudesai, N. J. Mason, E. Krishnakumar, *Dissociative electron attachment to acetaldehyde, CH_3CHO. A laboratory study using the velocity map imaging technique*, Phys.Chem. Chem. Phys. 15, 998 (2013).

[6] E. Krishnakumar, S. Denifl, I. Cadze, S. Markelj, N.J. Mason, *Dissociative Electron Attachment Cross Sections for H2 and D2*, PRL 106, 243201 (2011).

P 11. Low Energy Electron Dissociation of Model Compounds for EUVL Resist Materials

R. Tafrishi* and O. Ingólfsson

Department of Chemistry, Science institute - University of Iceland, Dunhagi 3, 107 Reykjavik, Iceland

* Corresponding author: ret1@hi.is

One of the most important components of EUVL is the technological advancement of photoresists. The current project aims to establish gas phase branching ratios and cross sections for low energy electron induced fragmentation for monomer units as model compounds for typical EUVL resist materials. The initial target molecules will be Tert-butyl acrylate ($C_7H_{12}O_2$) and 4-ethenylphenol (C_8H_8O) as shown in figure two and three. The reactions of these molecules with low energy electrons will be studied in the gas phase through sublimation in to high vacuum where they are exposed to low energy electrons generated by a trochoidal electron monochromator and the influence of incident electron energy on fragmentation is studied by means of mass spectroscopy. Special emphasis will be on halogenated derivatives to study possible means of activating local radical reactions in such resists materials. The energy range explored will be 0-150 eV with an achievable resolution better than 100 meV [1].

In the future, resists must show considerable improvement in resolution, line edge roughness (LER), and sensitivity. Unfortunately, these three resist properties are in opposition to each other and have been described as the RLS (resolution, LER, and sensitivity), there are currently no resists that can meet all three requirements at once [2]. Now, we hereby study the reactions between model compounds representing typical resist materials and low energy electrons to understand the role of secondary electrons in EUVL resist material and eventually to activate local radical reaction in them.

Currently significant effort is committed to search for suitable EUVL resist materials that meet the RLS requirements for sub 7 nm lithography [3-5]. Our main objective is to aid understanding of the role of low energy (0-50 eV) secondary electrons in EUVL to eventually use that knowledge to have better control in case of chemistry in resist materials. In the long run, we hope that such studies help to obtain rational models for electron controlled chemistry in EUVL resist material.

Acknowledgment: This project is an integral part of the MSC ITN Low Energy Electron driven chemistry for the advantage of emerging Nano-fabrication methods; ELENA and has received funding from the European Union's Framework Programme for Research and Innovation Horizon 2020 (2014-2020) under the Marie Skłodowska-Curie Grant Agreement No. 722149.

References

[1] E.H. Bjarnason et al., *Dissociative electron attachment to titatinum tetrachloride and titanium tetra isopropoxide,* The European Physical Journal D 68:121 (2014).

[2] Li Li et al., *Extreme ultraviolet resist materials for sub-7 nm patterning*, The Royal Society of Chemistry 46 4855-4866 (2017).

[3] V.S.V. Satyanarayana et al., *Design and Synthesis of Novel Resist Materials for EUVL*, Proc. of SPIE 9048 90481W-1 (2016).

[4] D. De Simone et al., *Photoresists in extreme ultraviolet lithography (EUVL)*, Adv. Opt. Techn. 1-10 (2017).

[5] I. Aratani et al., *Evaluation of Novel Resist Materials for EUV Lithography*, Proc. of SPIE 7273 (2009).

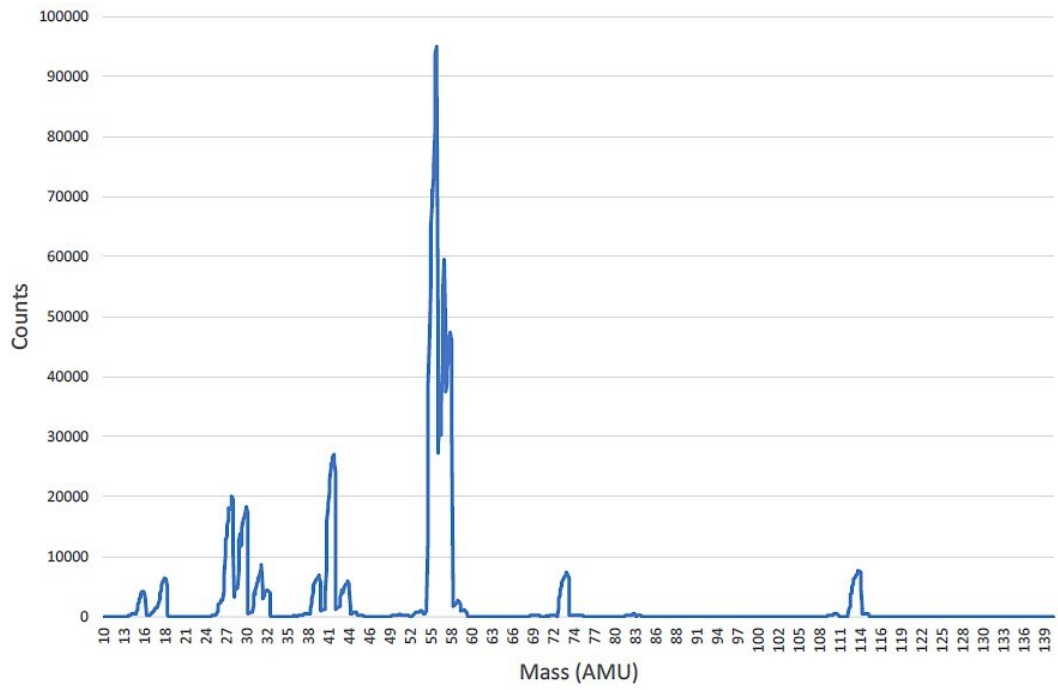

Fig. 1: Mass diagram of tert-butyl acrylate as a common EUVL resist monomers.

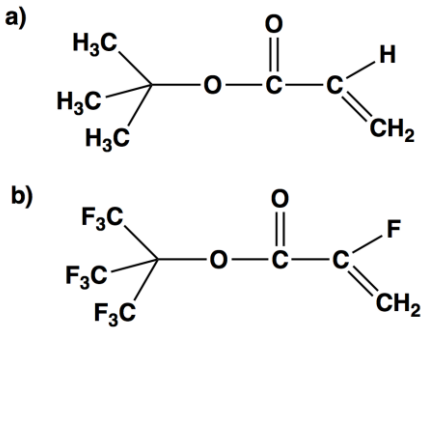

Fig. 2: Tert-butyl acrylate as a common EUVL resist monomers a) non-fluorinated b) fluorinated.

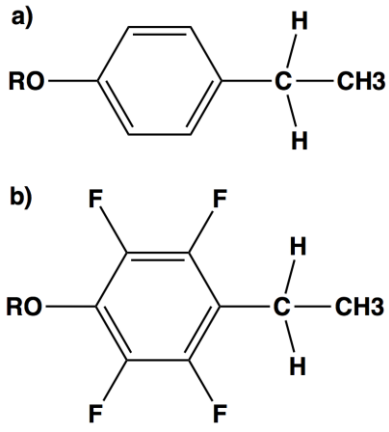

Fig. 3: 4-ethenylphenol as a common EUVL resist monomers a) non-fluorinated b) fluorinated.

P 12. Low Energy Electron Induced Dissociation of potential Au(I) Precursors for Focused Electron Beam Induced Deposition Technique

A. Kamali[1]*, W. Carden[2], L. McElwee-White[2], and O. Ingólfsson[1]

[1] Department of Chemistry and Science Institute - University of Iceland, Dunhagi 3, 107 Reykjavik, Iceland
[2] Department of Chemistry - University of Florida, Gainesville, 32611 Florida, United States

* Corresponding author: alk31@hi.is

Gold nanostructures have been widely used in electronics, biomedical, and catalysis applications due to their superb electrical properties, biocompatibility and large surface to volume ratio. Heretofore, different fabrication techniques such as photolithography, electron beam lithography, and metal layer deposition have been employed in order to build highly pure and conductive gold nanostructures. However, these techniques are restricted by the required use of photoresists, their multi-step nature, and are generally confined to flat surfaces. To cope with these challenges, a single-step, direct write nanofabrication technique capable of writing 3D nanostructures on uneven surfaces would be advantageous.

Focused Electron Beam Induced Deposition (FEBID) is such a single step, direct-write nanofabrication technique that can write 3D nanostructures with different geometries on even or uneven surfaces [1]. In this approach, a focused high-energy electron beam is applied to a substrates surface under continuous feed of gaseous, molecular precursors that typically constitute organometallic compounds. These compounds decompose through electron molecule interaction leaving a nonvolatile deposit while volatile fragments are pumped away. However, broadening of the deposits beyond the diameter of the primary beam and low metal purity, due to incomplete precursor decomposition and co-deposition of background gas, still hamper the widespread adoption of this method. These effects are largely attributed to the interaction of the precursor molecules with backscattered and low energy secondary electrons, which are unavoidably generated when high-energy irradiation impinges on surfaces (see e.g. refs 1 and 2 and refs therein).

Currently, the most promising gold precursor is Cl-Au-CO, which has been applied for the fabrication of gold nanostructures with better than 90% purity, both in in direct FEBID [2] and in combination with water as oxidative enhancer during deposition [3]. However, this compound is very difficult to handle due to facile loss of the carbonyl ligand and water-sensitivity, limiting its practical applicability.

Motivated by the high purity deposition achievable with this gold(I) precursor molecule, we are currently systematically comparing the fundamental electron induced dissociation processes of different gold(I) complexes, seeking thermally stable compounds that still decompose effectively upon low energy electron interaction. Our current target molecules are gold (I) complexes with different halogen ligands and where the CO-group has been replaced with a more strongly bound ligand.

Here we present preliminary results of the thermal stability and the gas phase decomposition of such novel gold(I) complexes, provided by the group of Lisa McElwee-White at the University of Florida. Specifically, we focus on the decomposition of these compounds through dissociative electron attachment, dissociative ionization and dipolar dissociation in the electron incident energy range from about 0-70 eV.

Acknowledgment: This project is an integral part of the MSC ITN Low energy ELEctron driven chemistry for the advantage of emerging NAno-fabrication methods; ELENA and has received funding from the European Union's Framework Programme for Research and Innovation Horizon 2020 (2014-2020) under the Marie Skłodowska-Curie Grant Agreement No. 722149.

References

[1] I. Utke, P. Hoffman, et al., *Gas-assisted focused electron beam and ion beam processing and fabrication*, J. Vac. Sci. Technol. 26, 1197-1276 (2008).

[2] R.M. Thorman, R.T.P. Kumar, D.H. Fairbrother, O. Ingólfsson, *The role of low-energy electrons in focused electron beam induced deposition: four case studies of representative precursors*, Beilstein J Nanotechnol. 6, 1904–1926 (2015).

[3] J.J.L. Mulders, J.M. Veerhoek, E.G.T Bosch, P.H.F Trompenaars, *Fabrication of pure gold nanostructures by electron beam induced deposition with Au(CO)Cl precursor: deposition characteristics and primary beam scattering effects,* J. Phys. D: Appl. Phys. 45, 475301 (2012).

[4] M.M. Shawrav, P. Taus, H.D. Wanzenboeck, M. Schinnerl, M. Stöger-Pollach, S. Schwarz, A. Steiger-Thirsfeld, E. Bertagnolli, *Highly conductive and pure gold nanostructures grown by electron beam induced deposition,* Sci. Rep. 6, 4003 (2016).

P 13. Potential means for enhanced cross-linking efficiency of SAMs for the production of carbon nano-membranes; project and perspectives

M. Cipriani[1]*, A. Terfort[2], S. Koch, A. Gölzhäuser[3], and O. Ingólfsson[1]

[1] Department of Chemistry and Science Institute - University of Iceland, Dunhagi 3, 107 Reykjavik, Iceland.
[2] Department of Chemistry, Institute of Inorganic and Analytical Chemistry, Goethe- University, 60438 Frankfurt, Germany.
[3] Physics of Supramolecular Systems and Surfaces, Bielefeld University, 33613 Bielefeld, Germany.

* Corresponding author: mac31@hi.is

Carbon nano-membranes (CNMs) are molecular membranes with thicknesses of 1 to few nm, high thermal stability and mechanical strength [1,2]. In recent years, the Gölzhäuser group (University of Bielefeld) has developed protocols to produce functional CNMs by electron induced cross-linking of aromatic SAMs [2], a process where the cross-linking is mainly attributed to electron induced C-H bond rupture through dissociative ionization [3]. Low energy electron induced bond rupture can, however, also proceed through neutral or dipolar dissociation up on electronic excitation or through dissociative electron attachment (DEA)) [4-6]. It is thus advantageous to better understand the role of these processes in the cross-linking step and eventually use that to enhance the cross-linking efficiency and/or selectivity.
First experiments in this direction were recently conducted on the halogenated biphenyls: 2-iodo-biphenyl, 2-bromo-biphenyl and 2-chloro-biphenyl, showing significantly enhanced cross-linking efficiency for 2-iodo-biphenyl - an effect that was attributed to the comparably high efficiency of iodine loss from this compound through DEA at threshold [7].

Inspired by these results we are currently focusing on means to further enhance the electron induced cross-linking of SAMs precursors through efficient DEA processes. In this context we seek to functionalize biphenyls to promote DEA through intermolecular hydrogen bond formation, an approach that enables exothermic formation of HF up on DEA at 0 eV and significantly enhancing its efficiency at threshold [8,9].

Currently we are investigating the influence of intramolecular -O···H···F bond formation on DEA to potential SAMs precursors, aiming to enable this route intermolecularly in the cross linking process. Figure 1 shows potential monomers to be studied in the gas phase for proof of concept of this approach, Figure 2 the anticipated translation of this process to the cross-linking step in the production of CNMs.

Acknowledgments: MC acknowledges a PhD grant from the University of Iceland Research Fund.

References

[1] P. Angelova et al., *A Universal Scheme to Convert Aromatic Molecular Monolayers into Functional Carbon Nanomembranes*, Acs Nano 7(8), 6489-6497 (2013).

[2] A. Turchanin et al., *One Nanometer Thin Carbon Nanosheets with Tunable Conductivity and Stiffness,* Adv. Mat. 21, 1233 (2009).

[3] L. Amiaud et al., *Low-energy electron induced resonant loss of aromaticity: consequences on cross-linking in terphenylthiol SAMs*, Phys. Chem. Chem. Phys. 16(3), 1050-1059 (2014).

[4] C.R. Arumainayagam et al., *Low-energy electron-induced reactions in condensed matter*, Surf. Sci. Rep. 65 (1), 1-44 (2010).

[5] E. Böhler et al., *Control of chemical reactions and synthesis by low-energy electrons*, Chem.l Soc. Rev. 42(24), 9219-9231 (2013).

[6] I. Bald et al., *From isolated molecules through clusters and condensates to the building blocks of life*, Int. J. Mass Spectrom. 277(1–3), 4-25 (2008).

[7] S. Koch et al., *Amplified cross-linking efficiency of self-assembled monolayers through targeted dissociative electron attachment for the production of carbon nanomembranes,* Beilstein J Nanotechnol. 30(8), 2562-2571 (2017).

[8] B. Omarsson et al., *Chemical control through dissociative electron attachment - A study on pentafluorotoluene, pentafluoroaniline and pentafluoropheno,* Chemical Physics Letters 539, 7-10 (2012).

[9] B. Omarsson et al., *Molecular rearrangement reactions in the gas phase triggered by electron attachment*, Phys. Chem. Chem. Phys.15, 4754 (2013).

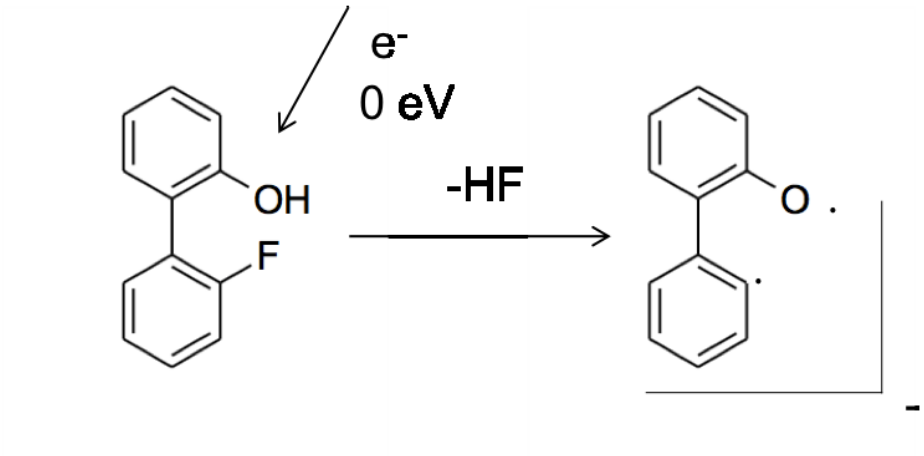

Fig. 1: Potential monomer to be studied as model compounds in the gas phase.

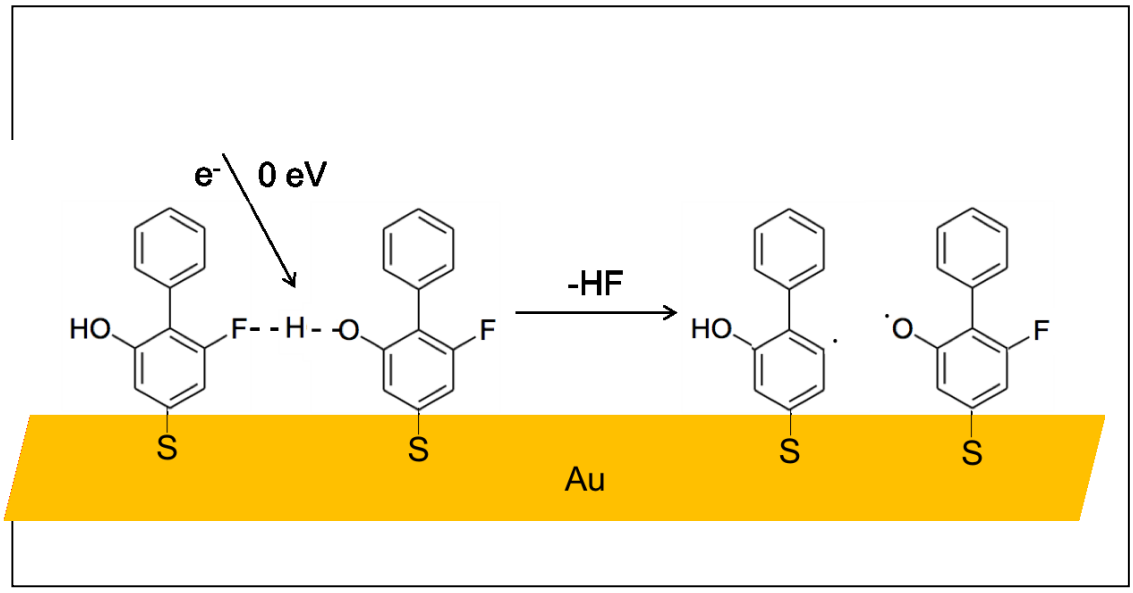

Fig. 2: Enhancement of the DEA efficiency through enabling of intra-molecular HF formation has been demonstrated in the gas phase under single collision condition. Here we plan to transfer that approach to inter-molecular HF formation to eventually promote cross-linking of SAMs through effective radical generation in the initial step.

P 14. Magnetic Nanorings made by FEBID

H.D. Wanzenboeck[1]*, M. Reichenpfader[1], E. Bertagnolli[1], M.M Shawrav[2], and M. Stoeger-Pollach[3]

[1] Institute for Solid State Electronics – Vienna University of Technology (TU Wien), Floragasse 7/1, 1040 Vienna, Austria
[2] Institute for Sensors and Actuators – Vienna University of Technology (TU Wien), Gusshausstrasse 25-29, 1040 Vienna, Austria
[3] University Center for Transmission Electron Microscopy (USTEM) – Vienna University of Technology (TU Wien), Wiedner Hauptstrasse 5-9, 1040 Vienna, AUSTIRA

* Corresponding author: Heinz.wanzenboeck@tuwien.ac.at

Nanomagnet logic (NML) is a current-free, voltage-free logic processing technology that relies on information transfer and information processing via coupling of magnetic fields between single-domain nanomagnets. The NML majority gate structure first described in 2006 [1] allows to perform logic "AND" as well as "OR" functions. However, already in the early 1960s the magnetic core technology used magnetic fields in a magnetic ring for logic operations. In this work we report on the fabrication and magnetic characterization of circular and ellipsoidal nanorings of magnetic material. The application of magnetic nanorings for magnetic data processing will be discussed.

The first nanomagnet logic circuits were realized by conventional lithography and deposition of magnetic layers. Several studies have demonstrated that FEBID is a powerful prototyping method for nanomagnetic devices. Magnetic nanostructures of iron [2] and of cobalt [3,4] have been successfully deposited by FEBID. By post-processing the magnetic properties could even be tuned [5] and since then many applications of FEBID nanomagnet structures have been developed [6]. Even 3-dimensional magnetic nanostructures [7] have been fabricated by FEBID that are not feasible by any other fabrication technology. In this work we evaluate magnetic nanoring structures as building blocks for nanomagent logic devices. A finely focused electron beam was used to induce the chemical vapour deposition of Fe(CO)5 to deposit iron nanorings in various geometries at room temperature (Fig. 1).

In previous studies we have observed that the shape of iron nanomagnets influences the magnetic domain state and that the thickness of iron nanowires allows to control the magnetic coercivity of FEBID-mafe structures. In principle rings of magnetic material offer several magnetic configurations (Fig, 2) including both in-plane and out-of-plane magnetic configurations. By FEBID iron nanorings with varying diameters in the range of 300 nm to 2 µm and varying thickness in the range from 20 nm up to 100 nm have been deposited. Also elliptical geometries with different axis ratios have been deposited. The fabricated iron structures were exposed to an external magnetic field for initialization of the magnetic orientation. The magnetic properties were characterized by magnetic force microscopy (MFM) using a self.made MFM probe, where the magnetic tip consisted of an iron nanopillar deposited on a commercial AFM cantilever. The function of these self-made MFM probes was tested and confirmed by measurement of the magnetic domains of a magnetic hard disc. The structure and chemical composition of the deposited iron nanorings was investigated by transmission electron microscopy (TEM) and X-ray spectroscopy. The results indicate that an axial magnetization, that generates an out-of-plane magnetic field, can be achieved for selected, advantageous nanoring geometries (Fig. 3). In addition, diametrical orientations featuring in-plane magnetic fields can be obtained. We propose that nanorings can be used as magnetic elements that can provide in-plane as well as out-of-plane magnetic fields.

In a final phase, also the magnetic coupling between linear nanowires and circular nanorings was investigated. This is relevant for combining magnetic nanorings with linear nanomagnets as used now. We will discuss new complex circuitry with magnetic nanorings that enhances the functionality of nanomagnet logic. An outlook on potential future applications will be given.

References

[1] A. Imre, G. Csaba, L. Ji, A. Orlov, G. H. Bernstein, W. Porod, Science 311 (5758), 205 (2006).

[2] M. Takeguchi, M. Shimojo, K. Furuya, Nanotechnology 16 (8), 1321 (2005).

[3] G. Boero, I. Utke, T. Bret, N. Quack, M. Todorova, S. Mouaziz, P. Kejik, J. Brugger, R.S. Popovic, P. Hoffmann, Applied Physics Letters 86 (4), 042503 (2005).

[4] A. Fernandez-Pacheco, J.M. De Teresa, R. Córdoba, M.R. Ibarra, Journal of Physics D 42 (5), 055005 (2009).

[5] O.V. Dobrovolskiy, M. Kompaniiets, R. Sachser, F. Porrati, C. Gspan, H. Plank, M. Huth, Beilstein Journal of Nanotechnology 6(1), 1082 (2015).

[6] J.M. De Teresa and A. Fernández-Pacheco, Applied Physics A 117 (4), 1645 (2014).

[7] L. Keller, M. Al Mamoori, J. Pieper, C. Gspan, I. Stockem, C. Schröder, S. Barth, R. Winkler, H. Plank, M. Pohlit, J. Müller, M. Huth, Scientific Reports 8, 6160 (2018).

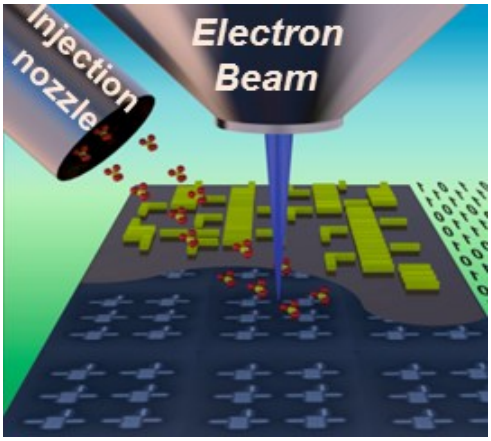

Fig. 1: Schematic illustration of additive direct write lithography of nanomagnets by focused electron beam induced deposition.

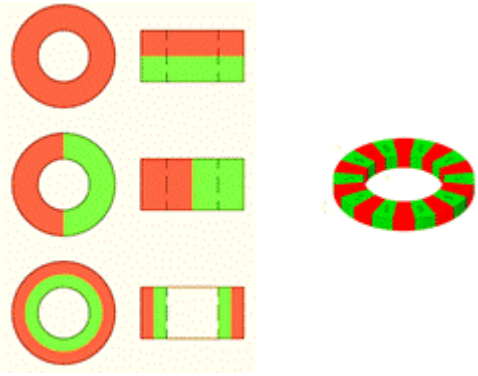

Fig. 2:. Possible magnetic orientation in a magnetic nanoring structure: axial (out-of-plane), diametrical (in-plane), radial (in-plane), multipole (circular in-plane).

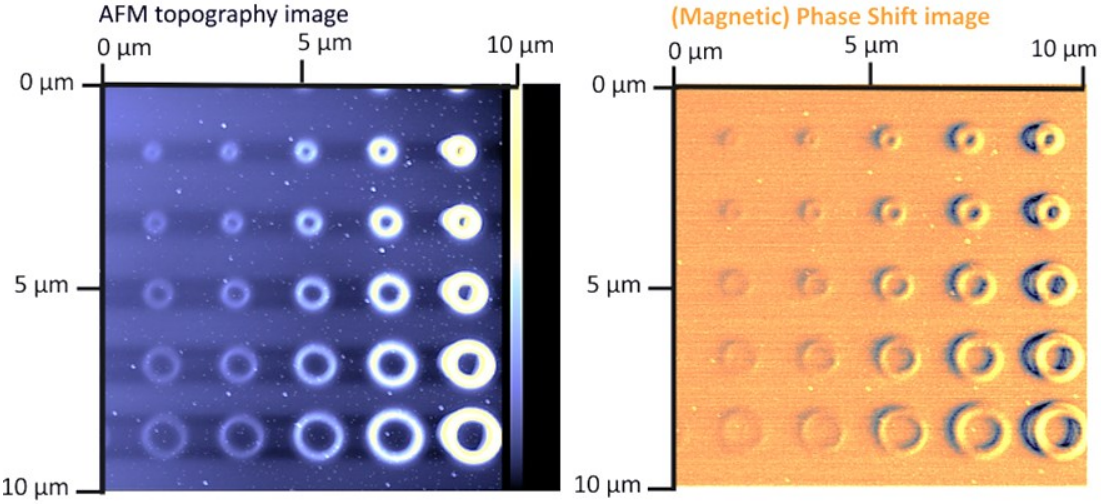

Fig. 3: AFM and MFM of a magnetic iron ring structures. The iron rings have a diameter in the range from 300 nm to 2 µm. MFM data suggest a permanenet magnetization.

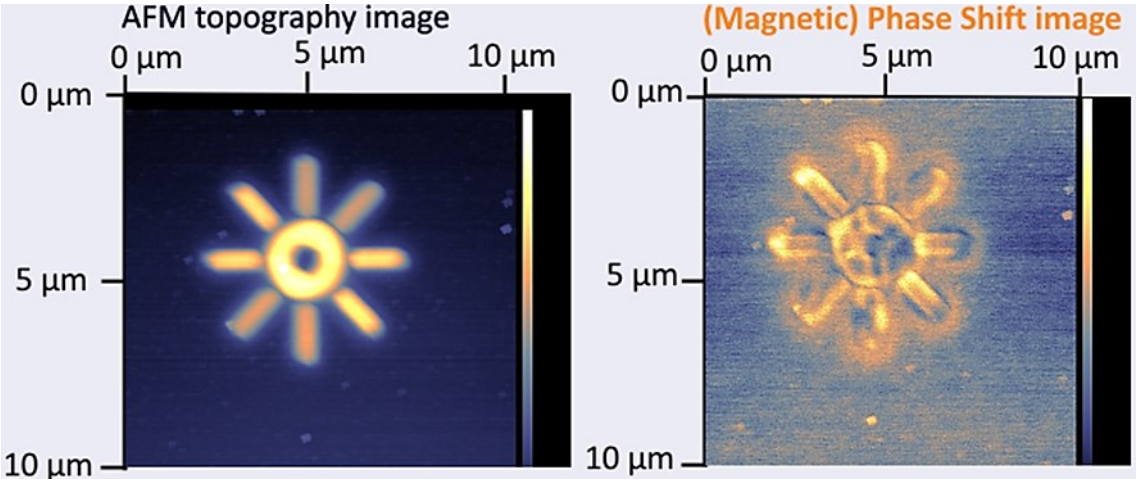

Fig. 4: AFM and MFM of a magnetic iron ring with linear inputs. Linear inputs are a potential way to pin magnetic orientation of the magnetic nanorings.

P 15. Multicomponent patterned ultrathin carbon nanomembranes by laser ablation

D. Rhinow[1]*, N. Frese[2], J. Scherr[3], A. Beyer[2], A. Terfort[3], A. Gölzhäuser[2], and N. Hampp[4]

[1] Carl Zeiss SMT GmbH - ZEISS Group, Industriestr. 1, 64380 Rossdorf, Germany
[2] University of Bielefeld, Faculty of Physics, Universitätsstr. 25, 33615 Bielefeld, Germany
[3] Goethe-University Frankfurt, Department of Chemistry, Max-von-Laue-Str. 9, 60438 Frankfurt, Germany
[4] Philipps-University Marburg, Department of Chemistry, Hans-Meerwein-Str. 4, 35032 Marburg, Germany

* Corresponding author: daniel.rhinow@zeiss.com

Carbon nanomembranes (CNMs) are obtained by electron beam-induced crosslinking of aromatic self-assembled monolayers (SAMs) on solid substrates [1]. CNMs made from a single type of precursor molecule are uniform with homogeneous chemical and physical properties.

We have developed a method for the fabrication of internally pattern CNMs. Aromatic SAMs are patterned by photothermal desorption of thiols using a focused laser beam [2-3], which are subsequently crosslinked using low-energy electron irradiation.

The structure of multicomponent patterned CNMs is preserved upon transfer to different substrates. Internally patterned CNMs were analyzed by scanning electron microscopy, helium ion microscopy, and X-ray photoelectron spectroscopy [4] (Fig. 1). The methods enable the fabrication of patterned two-dimensional materials with local variation in chemical and physical properties on the micrometer to centimeter scale.

References

[1] A. Turchanin, A. Gölzhäuser, *Carbon nanomembranes from self-assembled monolayers: Functional surfaces without bulk*. Prog. Surf. Sci. 87, 108-162 (2012).

[2] D. Rhinow, N.A. Hampp, *Forming alkanethiol microstructured self-assembled monolayers on gold by laser ablation*. IEEE Trans. Nanobiosci. 5, 188-192 (2006).

[3] D. Rhinow, N. Hampp, *Solid-supported multicomponent patterned monolayers*, Adv. Mater. 19, 1967-1972 (2007).

[4] N. Frese, J. Scherr, A. Beyer, A. Terfort, A. Gölzhäuser, N. Hampp, D. Rhinow, *Multicomponent patterned ultrathin carbon nanomembranes by laser ablation*, Appl. Surf. Sci. 126-130 (2018).

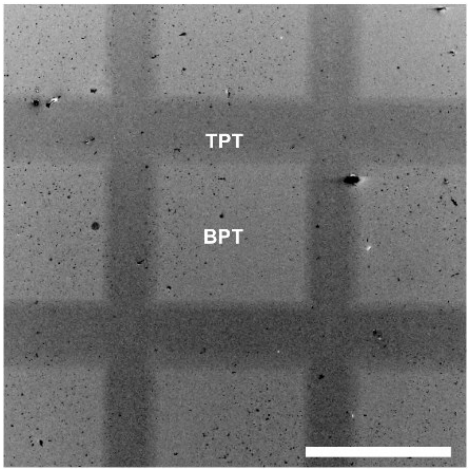

Fig. 1: Analysis of internally patterned CNMs by scanning electron microscopy. Shown is a patterned CNM consisting of terphenylthiol (TPT) and biphenylthiol (BPT).

P 16. Focused Electron Beam Induced Deposition resolution study on EUV masks

P.Y. Shih, Ch.F. Hermanns, J. Oster, and K. Edinger*

Carl Zeiss SMT GmbH - ZEISS Group, Industriestr. 1, 64380 Rossdorf, Germany

* Corresponding author: klaus.edinger@zeiss.com

For lithography processes in the semiconductor production, photomasks, opaque plates with transparent regions, are used to create defined patterns on wafers. Their tremendous production cost in case of high-end masks makes it mandatory to optimize their fabrication by repairing their defects. In order to do so, focused electron beam induced processing is the standard technique.

For EUV lithography a new class of mask with smaller structures enter the stage, that drives mask complexity and cost. In order to achieve a high mask repair yield, the nanometer-accurate deposition of missing material of the absorber layer is essential. So a high repair resolution at the finite height of the latter one is mandatory.

The increase of the deposition height leads to a significant broadening at the deposition base. Among the different process parameters, the energy of the electrons of the primary beam can be used to tune this effect. In figure 1 a and b, line cross section profiles obtained from AFM images are displayed. They belong to deposited single lines that were written with a high (fig. 1a) and low (fig. 1b) energy of the primary electrons on EUV masks, respectively, while other process parameters are identical. For different primary electrons, the development of the line cross section profile for varying exposure times is shown. For comparable deposition heights of these two cases, the lateral broadening behaves different. For electrons with a higher primary energy it is bigger. This clearly reveals the possibility to achieve a higher resolution by applying a lower energy of primary electrons.

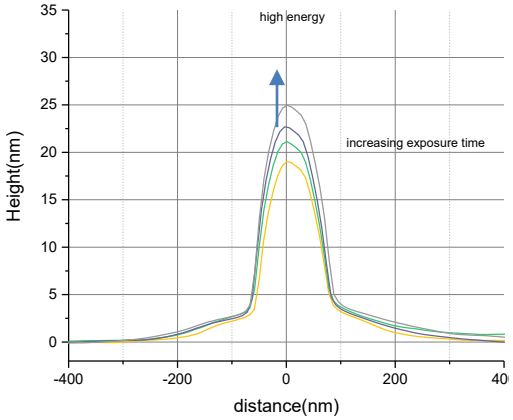

Fig. 1a: AFM line cross section profile of a single line deposition obtained by using a high energy of primary electrons.

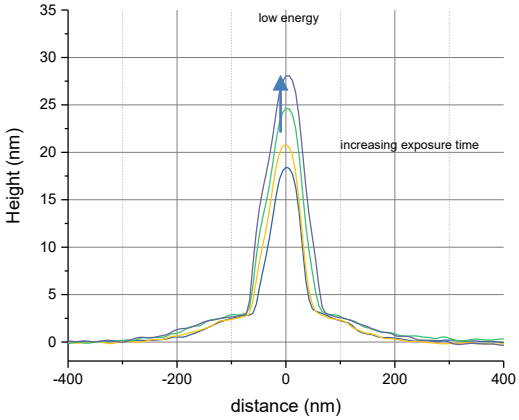

Fig. 1b: AFM line cross section profile of a single line deposition obtained by using a low energy of primary electrons.

SPONSOR PRESENTATIONS

Getting more Control over Process Rate and finding appropriate Process Strategy

A. Rudzinski* and F. Nouvertne

Raith GmbH, Konrad-Adenauer Alle 8, 44263 Dortmund, Germany

* Corresponding author: axel.rudzinski@raith.de

Control position and growth of 3D-deposits or freely suspended nano-devices by Marker recognition and dedicated design tools for 3d-deposits.

In-situ EBIP -rate determination by probing for etching and deposit rate determination and probing for milling strategies comparison.

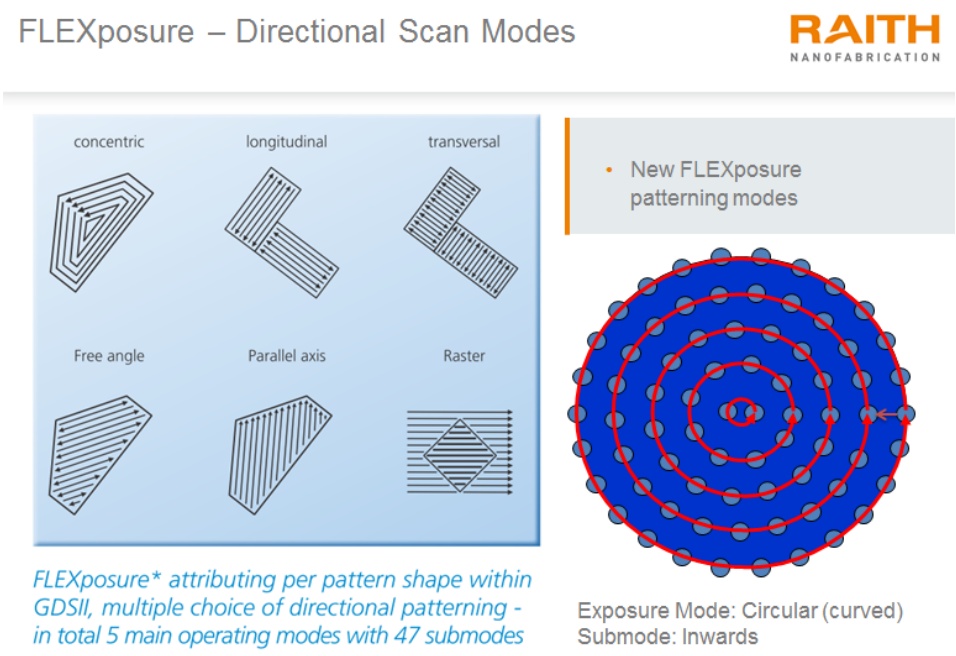

Fig. 1: multiple area filling strategies for process control.

Fig. 2: Probing tool for in-situ process control.

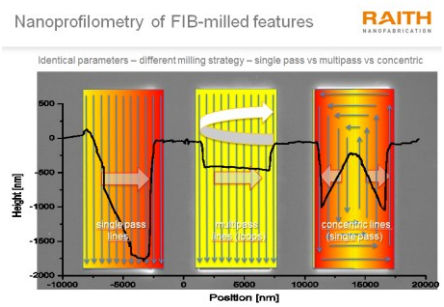

Fig. 3: probing for process strategy optimization.

The AFSEM™ -Correlative In-Situ Characterization of 3D Nanostructures by Combining SEM and AFM

C. H. Schwalb[1]*, P. Frank[1], S. Hummel[1], R. Sachser[2], M. Huth[2], J. Sattelkow[3], R. Winkler[3], and H. Plank[3]

[1] GETec Microscopy GmbH, Seestadtstr. 27, A-1220 Vienna, Austria
[2] Physikalisches Institut, Goethe University Frankfurt, Max-von-Laue-Str. 1, 60438 Frankfurt, Germany
[3] Institute of Electron Microscopy and Nanoanalysis, Graz University of Technology, Steyrergasse 17, 8010 Graz, Austria

* Corresponding author: chris.schwalb@getec-afm.com

Focused electron-beam-induced processing (FEBIP) represents one of the most flexible approaches for functional nanostructure fabrication. During and after the growth process, e.g., electrical in-situ measurements as well as energy-dispersive X-ray spectroscopy are commonly employed to characterize electrical and chemical properties of fabricated structures. However, one major drawback is the lack of further in-situ analysis tools which grants access to real 3D topographic information, laterally resolved conductance maps, local magnetic or mechanical properties.

We present a novel AFM – the AFSEM™ – that allows correlative in-situ analysis by combining the full SEM and AFM capability [1,2]. The AFM measurement takes place in the field of view of the electron beam and thus allows for non-destructive and non-contaminating analyses of FEBID structures directly after fabrication. This is rendered possible by eliminating the need for optical detection and implementing novel low-noise self-sensing cantilever probes [3]. These cantilevers are equipped with a deflection sensor that directly measures the cantilever signal electrically, therefore removing the space consuming requirement for optical readout. In addition, we make use of FEBIP for a variable tip modification of the cantilever structures by 3D nanoprinting of sharp purified metallic or magnetic tips.

We present a broad variety of case studies for correlative in-situ analysis of nanostructured materials. We demonstrate the results for in-situ electrical characterization for nanoscale dose-dependent conductivity measurements of nanogranular Pt(C) structures after FEBIP. In addition, we show correlative in-situ SEM and MFM characterization of magnetic FEBID structures. Finally, we investigate nanostructured samples treated by helium ion treatment and discuss future applications.

References

[1] J. Kreith, T. Strunz, E.J. Fantner, G.E. Fantner, M. Cordill, *A versatile atomic force microscope integrated into a scanning electron microscope*, Rev. Sci. Instr. 88, 053704 (2017).

[2] D. Yablon, P. Werten, M. Winhold, C.H. Schwalb, *Inproved Understanding of Material Behavior using Correlative In-Situ Techniques*, Microscopy and Microanalysis 23, 792-793 (2017).

[3] M. Dukic, J.D. Adams, G.E. Fantner, *Piezoresistive AFM cantilevers surpassing standard optical beam deflection in low noise topography imaging*, Scientific Reports 5, 16393 (2015).

Fig. 1: The AFSEM™ - Designed to fit into your hand and your SEM or Dual-beam Microscope.

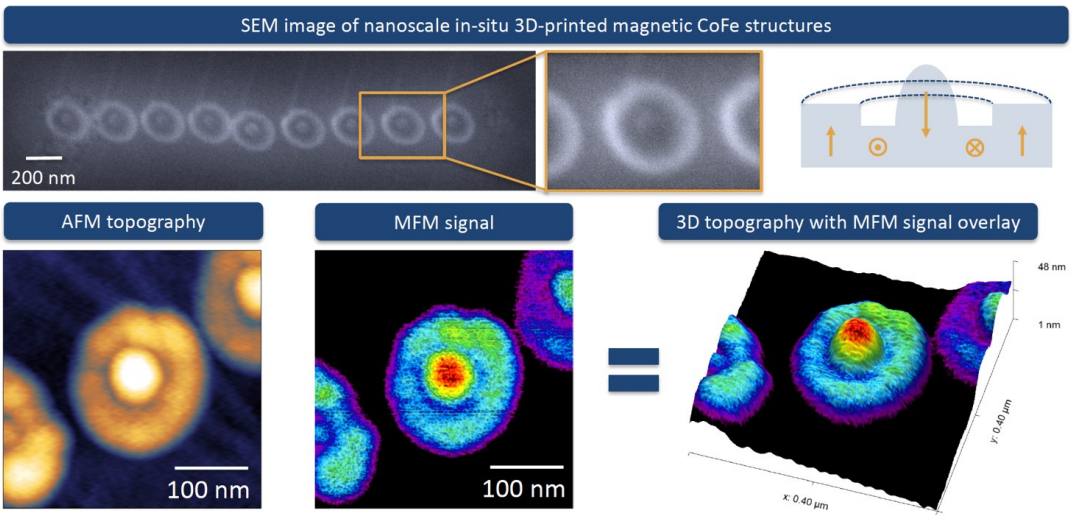

Fig. 2: Correlative in-situ characterization of CoFe magnetic nanostructures fabricated by FEBID. The SEM can be used to find the FEBID structures of interest and the AFM provides real 3D topography information in combination with the magnetic properties of the nanostructures, without the need to expose the sample to air.

SEM and GIS Instrumentation for FEBIP

J. Jiruše and T. Hrnčíř

R&D Physics – TESCAN Brno, Libušina třída 1, 623 00 Brno, Czech Republic

* Corresponding author: jaroslav.jiruse@tescan.com

Focused Electron Beam Induced Processing (FEBIP) is a well-known method of direct nanofabrication of materials. It combines the Gas Injection System (GIS) and the electron beam, usually from Scanning Electron Microscope (SEM). Here we present an overview of the instrumentation possibilities of Tescan-Orsay microscopes.

There are 3 types of electron optics used in field-emission SEM. The conventional SEM column is based on magnetic lenses. The resolving power is 1 nm at high acceleration voltage but worsens 3 times at low voltage around 1 keV. The imaging is formed by traditional secondary electron (SE) and back-scattered electron (BSE) detectors which accept integral signals and do not offer angular or energy filtration.

Recently introduced BrightBeam™ SEM column [1] combines a high-potential tube with a magnetic-electrostatic objective lens delivering ultra-high resolving power (1.7 nm at 1 keV) when the specimen is in the magnetic-field-free mode. Specialized detectors inside the column enable angular as well as energy selection of both SE and BSE signals, thus providing various contrasts of the images.

Triglav™ SEM column [2] is equipped with the TriLens™ triple objective lens system to enable ultra-high resolving power down to 0.7 nm when the specimen is immersed in the magnetic field, analysis in field-free mode and multiple display modes combining all three lenses. The detection system includes a triplet of complementary BSE detectors for angular and energy selection of electrons and a triplet of SE detectors. Subtle differences between electron columns may be very important for specific applications.

Both BrightBeam™ and Triglav™ columns contain an important function for spot shape optimization which is especially useful at high beam currents where beam tails may deteriorate FEBIP results.

The GIS brings a gaseous form of a selected precursor in the vacuum chamber. The interaction between the charged particle beam and the gas molecules lead to the decomposition/recombination of the injected molecules to form local decomposition or deposition on a substrate. 5-GIS merges five nozzles with 5 independent precursors. It is moved by motorized stage with safety touch alarm. It occupies just one port on the chamber, which is a big advantage especially for complex configurations. MonoGIS offers one nozzle with one precursor. It is moved by fast pneumatic actuator.

Recently developed OptiGIS is a new generation of the single nozzle system with significantly reduced dimensions out of the chamber, faster run-up time and reduced remanence effect of the injection pressure. It allows exchanging the reservoir without venting the chamber and contains an automated detection of the installed precursor type.

The instrumentation may be advantageously combined with focused ion beam (FIB) columns. The Ga ions column Orage aims at high resolving power 2.5 nm while Xe ions column i-FIB delivers high beam current 2.5 µA. Combinations of 2 FIBs and 3 SEMs give rise to 6 FIB-SEM workstations. Then GIS may be used for ion etching or ion deposition as well. In all cases of electron/ion etching/deposition, a special gas chemistry may be applied.

References

[1] P. Sytař, J. Jiruše, A. Závodný, *A New SEM Column Combining Ultra-High Resolution and Flexible Scanning*, Microsc. Microanal. 23 (Suppl 1), 38-39 (2017).

[2] J. Jiruše, M. Havelka, J. Polster, *Design of an Ultra-High Resolution SEM for Enhanced Analysis*, Microsc. Microanal. 22 (Suppl 3), 578-579 (2016).

High resolution imaging and sub 10nm nano-structuring with He and Ne Ions

P. Gnauck*

Carl Zeiss Microscopy, Carl Zeiss Str. 22, 73447 Oberkochen, Germany

* Corresponding author: peter.gnauck@zeiss.com

The Helium Ion Microscope has been described as an impact technology offering new insights into the structure and function of nanomaterials. Combining a high brightness Gas Field Ion Source (GFIS) with unique sample interaction dynamics, the helium ion microscope provides images offering unique contrast and complementary information to existing charged particle imaging instruments such as the SEM and TEM. Formed by a single atom at the emitter tip, the helium probe can be focused to below 0.25nm offering the highest recorded resolution for secondary electron images. The small interaction volume between the helium beam and the sample also results in images with stunning surface detail.

Besides imaging, the helium ion beam can be used for fabricating nanostructures at the sub-10nm length scale. Researchers have used the helium ion beam for exposing resist and features as small as 4nm have been reported. The main advantage of helium ion lithography over electron beam lithography is the minimal proximity effect. The helium ion beam has also been used for deposition and etching in conjunction with appropriate chemistries. Helium induced deposition results in higher quality deposits than with Ga-FIB or EBID (Electron Beam Induced Deposition). Finally, the helium ion beam can be used for direct sputtering of different materials. Patterning of graphene has resulted in 5nm wide nanoribbons and 3.5nm holes in silicon nitride membranes have been demonstrated. However, due to its lower mass, the helium sputter rate is significantly lower than with gallium. To overcome this issue, the GFIS can also be operated with Ne. This also enhances the capabilities of the HIM towards high resolution analytical techniques like SIMS.

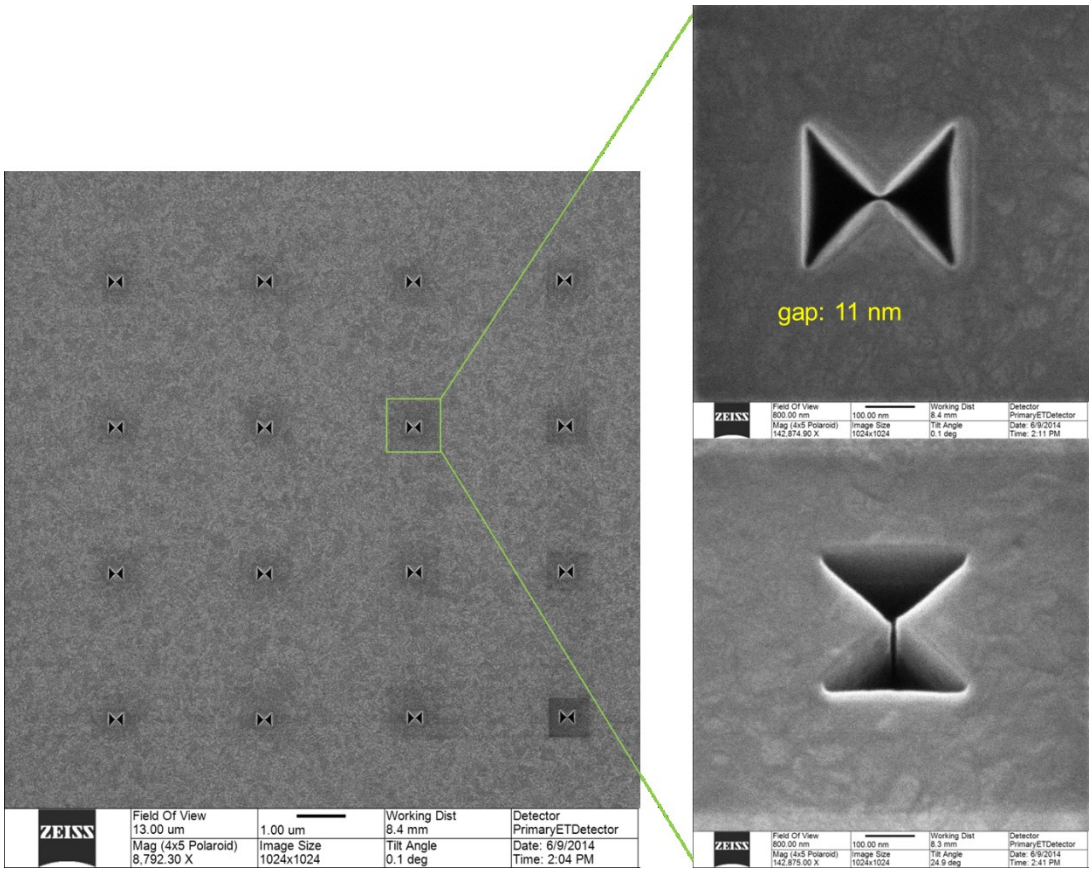

Fig. 1: Bowtie shaped plasmonic antennas created with the Neon ion beam. The sidewalls of the structure are almost perfectly vertical.

The Xe PlasmaFIB

H. Mulders*

ThermoFisherScientific, MSD, Business Unit Material Science, Eindhoven, The Netherlands

* Corresponding author: hans.mulders@thermofisher.com

ThermoFisher Scientific provides tools for nano-technology such as SEM, TEM and FIB and is known formerly as FEI Company, that introduced the FIB to the material science community in 1996. So the Ga+ FIB has been around for many years and found its way into many different applications. Over time, the beam has been optimized in two directions: higher resolution and lower kV. With the development of the many new applications, the limitations of Ga also became apparent: embedding of the beam particle in the sample material, the residual damage to the sample top surface and practical limitations in mill-sizes of the sample. Especially for 3D imaging and analysis (EBSD and EDX), the process-time scales as the third power of the linear dimension. A practical limit for Ga is 20 x20 x5 µm. In many steel and mineral based samples however, the grain size is bigger and hence it is requiring a 3D analysis of typically 100 x 100 x 50 µm. With a Ga FIB this would lead to unacceptably long milling times.

The search for higher milling speeds, results in the application of femto-second laser ablation or in the search of a different ion source, such as a plasma based Xe^+ beam. The source has a high-enough brightness to still allow a small beam diameter at low current, while at high current the 1 µA limit can easily be exceeded. In addition to the higher current, the milling capability of the Xe ion (at/ion) is higher for most materials compared to Ga. Therefore, it brings the sample dimensions for 3D analysis to a higher level and it increases the process speed for lower dimensions (compared to Ga). The Xe FIB also preserves the milled surface in high quality, directly ready for EBSD indexing with high reliability.

Also for FEBID type work, the Xe may offer additional benefits as the atom is not embedded in the deposition. However, many deposition and etching processes will need an adjustment of their process parameters because the dynamics are very different. In addition, the new systems will be able to run other gases as well: O_2 being one of the most interesting ones due to the inherent capability of in-situ purification and avoiding Ga deposition, which is favorable for the resistivity of oxide based materials such as SiO_2. Therefore, it is expected that depositions with an oxygen beam will have a higher resistivity and break down voltage: so material with a better quality.

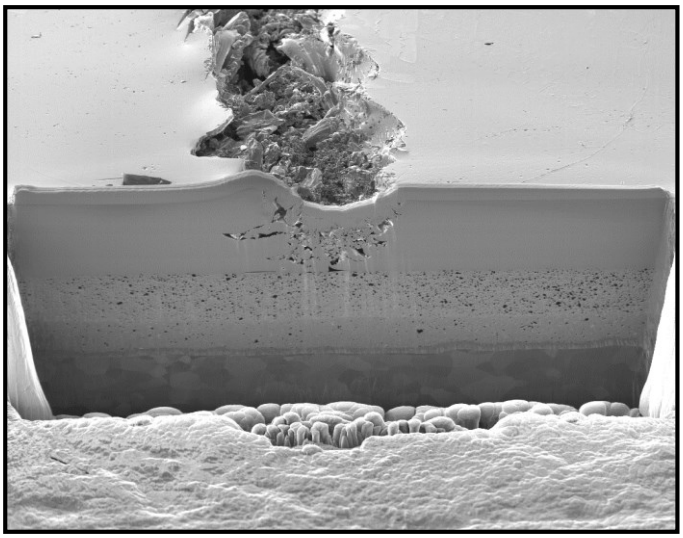

Fig. 1: Site specific cross-sections for scratch testing and adhesion in paint coatings. Sample Courtesy: Audi AG. HFW = 500 µm. Xe^+ mill time = 3 hrs 45 min. Equivalent Ga^+ time > 3 days

LIST OF AUTHORS

LIST OF PARTICIPANTS

Surname, N. (e-mail)	**Surname, N. (e-mail)**
Ahlenhoff, K. (kai.ahlenhoff@uni-bremen.de)	Le Gal, P. (Pierre.LEGAL@orsayphysics.com)
Aprile, G. (g.aprile@inrim.it)	Mahgoub, A. (M.I.M.A.Mahgoub-1@tudelft.nl)
Auth, N. (nicole.auth@zeiss.com)	Markò, D. (dominik.marko@tescan.com)
Berger, L. (Luisa.Berger@empa.ch)	Matsui, S. (shinjimatsui1@gmail.com)
Bishop, J. (jamesdbishop1@gmail.com)	McElwee-White, L. (lmwhite@chem.ufl.edu)
Choi, S.S. (sscphy2010@gmail.com)	Morandi, V. (morandi@bo.imm.cnr.it)
Cipriani, M. (mac31@hi.is)	Mulders, H. (hans.mulders@thermofisher.com)
Cordoba, R. (rocorcas@unizar.es)	Ortolani, L. (ortolani@bo.imm.cnr.it)
De Teresa Nogueras, J.M. (deteresa@unizar.es)	Pablo-Navarro, J. (javpablo@unizar.es)
Di Prima, G. (diprima@physik.uni-frankfurt.de)	Pintea, M. (maria.pintea@open.ac.uk)
Edinger, K. (klaus.edinger@zeiss.com)	Plank, H. (harald.plank@felmi-zfe.at)
Fernàndez-Pacheco, A. (af457@cam.ac.uk)	Porrati, F. (porrati@physik.uni-frankfurt.de)
Fowlkes, J. (jfowlkes@utk.edu)	Preischl, C. (Christian.Preischl@fau.de)
Frabboni, S. (stefano.frabboni@unimore.it)	Puydinger dos Santos, M. (puyding@ifi.unicamp.br)
Fröch, J. (Johannes.E.Frch@student.uts.edu.au)	Rhinow, D. (daniel.rhinow@zeiss.com)
Gazzadi, G.C. (giancarlo.gazzadi@nano.cnr.it)	Rohdenburg, M. (m.rohdenburg@uni-bremen.de)
Glessi, C. (cristiano.glessi@smn.uio.no)	Rosi, P. (paolo.rosi@unimore.it)
Goupil, G. (Gregory.GOUPIL@orsayphysics.com)	Sachser, R. (sachser@physik.uni-frankfurt.de)
Gruszka, P. (gruszka@physik.uni-frankfurt.de)	Sanz-Hernandez, D. (dsh41@cam.ac.uk)
Hagen, C.W. (C.W.Hagen@tudelft.nl)	Sattelkow, J. (juergen.sattelkow@felmi-zfe.at)
Hanefeld, M. (hanefeld@physik.uni-frankfurt.de)	Scotuzzi, M. (marijke.scotuzzi@phenom-world.com)
Hastings, J.T. (todd.hastings@uky.edu)	Sellmair, J. (sellmair@nanoelectrotec.com)
Hermanns, Ch.F. (felix.hermanns@zeiss.com)	Shih, P.Y. (po-yuan.shih@zeiss.com)
Höflich, K. (katja.hoeflich@helmholtz-berlin.de)	Shimojo, M. (mshimojo@shibaura-it.ac.jp)
Hofmann, T. (thorsten.hofmann@zeiss.com)	Skoric, L. (ls604@cam.ac.uk)
Huth, M. (michael.huth@physik.uni-frankfurt.de)	Swiderek, P. (swiderek@uni-bremen.de)
Ingólfsson, O. (odduring@hi.is)	Tafrishi, R. (ret1@hi.is)
Irmer, B. (bernd.irmer@nanotools.com)	Trummer, C. (cornelia.trummer@felmi-zfe.at)
Jeevanandam, G. (G.Jeevanandam@tudelft.nl)	Utke, I. (Ivo.Utke@empa.ch)
Jiruše, J. (jaroslav.jiruse@tescan.com)	Vavassori, P. (p.vavassori@nanogune.eu)
Jurczyk, J. (Jakub.Jurczyk@empa.ch)	Vollnhals, F. (florian.vollnhals@fau.de)
Kamali, A. (alikamaali@gmail.com)	Wanzenboeck, H. (heinz.wanzenboeck@tuwien.ac.at)
Katori, Y. (ac13027@shibaura-it.ac.jp)	Winkler, R. (robert.winkler@felmi-zfe.at)
Keller, L. (L.Keller@Physik.uni-frankfurt.de)	Zhao, D. (dizhao@dtu.dk)

“FEBIP 2018” Image on backcover courtesy of Robert Winkler

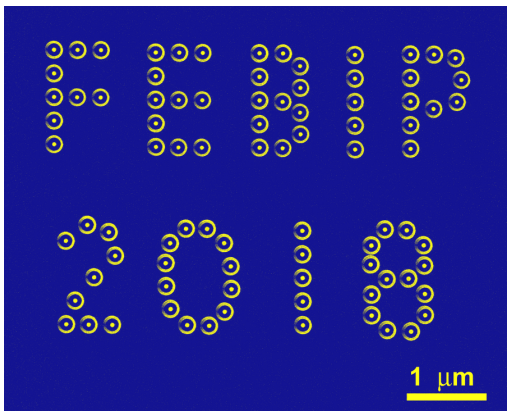

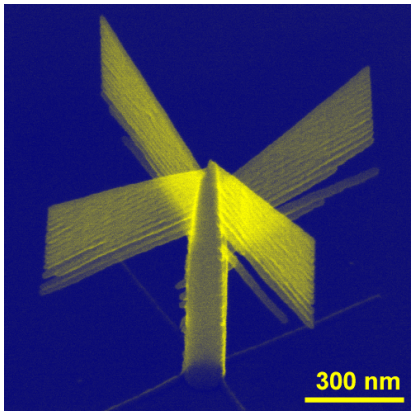

TOPICS

e-/molecule interaction process
New gas precursors' design
Modeling of deposition&etching process
Deposition&etching fundamentals: new materials and methods, purification, characterization
FEBIP applications in Magnetism, Photonics and Electronics
3D FEBID: fundamentals & applications
Focused Ion beam (Ga, He) deposition

web.nano.cnr.it/FEBIP2018-Modena/

CNRNANO MODENA S3

Edited by Cnr Istituto Nanoscienze
via Campi 213/A
I-41125 Modena
www.nano.cnr.it